University of St Andrews

Full metadata for this thesis is available in
St Andrews Research Repository
at:
http://research-repository.st-andrews.ac.uk/

University of St Andrews

Silsesquioxane Dendrimers as Catalysts – Synthesis and Molecular Modelling

Katherine J. Haxton

Thesis for PhD Degree

September 2004

Th_{E771}

Declaration

I, Katherine Jane Haxton, hereby certify that this thesis, which is approximately 65,000 words in length, has been written by me, that it is the record of work carried out by me and that it has not been submitted in any previous application for a higher degree.

date .15|12|04...   signature of candidate

I was admitted as a research student in September 2001 and as a candidate for the degree of PhD in August 2002; the higher study for which this is a record was carried out in the University of St Andrews between 2001 and 2004.

date .15|12|04...   signature of candidate

I hereby certify that the candidate has fulfilled the conditions of the Resolution and Regulations appropriate for the degree of PhD in the University of St Andrews and that the candidate is qualified to submit this thesis in application for that degree.

date .18/1/05.   signature of supervisor

Abstract

This thesis reports several molecular modelling investigations of Polyhedral Oligomeric Silsesquioxane (POSS) dendrimers. Dendritic alcohols and diphenylphosphines were studied and in the case of the latter, the bite angle for a series of POSS dendrimers was calculated in an attempt to explain catalytic data from the hydroformylation of oct-1-ene. A small rhodium complex was also studied attached to the dendrimer to investigate the influence of the dendritic structure on metal complexes.

Several synthetic investigations into the convergent synthesis of POSS dendrimers using Fréchet type wedges and PAMAM branches have been carried out, indicating that PAMAM dendrons show the most potential for attachment to the POSS core and subsequent functionalisation and several new compounds have been synthesised. A number of POSS and related silicate molecules have been synthesised and two crystal structures are reported.

Acknowledgements

"Every Silver Lining Has A Cloud..."

Table of Contents

Contents

Contents

Contents

Contents

Contents

Contents

Contents

Chapter 1. Introduction, Aims and Objectives

1.1 Materials Research

Financial, environmental and technological needs provide a driving force for modern scientific research. The need for high performance materials obtained cheaply, at lower cost to the environment encourages research into novel materials with well-defined structures and tailored for specific properties. Such materials include polymers, micro- and mesoporous- materials[1] and catalysts, both homogeneous and heterogeneous. The class of materials known as molecular sieves provides an excellent example of substances where structure specifically influences function.
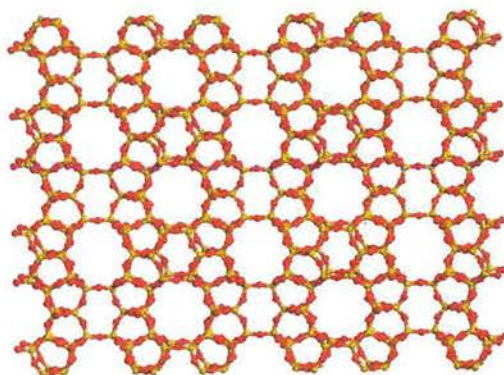
Figure 1.1: Molecular Sieve Structure, Si-0-Si framework, Si: yellow, Oxygen: Red

Molecular sieves include zeolites and other inorganic oxides and are porous materials with well-defined crystalline structures, usually microporous. The term sieves arises from their ability to separate atoms or molecules by their size, charge or shape. Silica molecular sieves include zeolites, usually aluminosilicates containing silicon and aluminium oxides. It is from zeolites that we can take inspiration for many new types of materials. Zeolites consist of primary building units (PBUs) comprising linked TO_4 tetrahedra. These link together to form secondary building units (SBUs) that form cage-like structures. Of particular interest are the SBUs illustrated below:
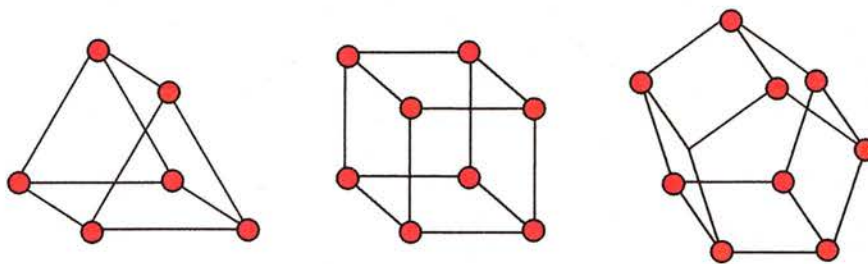
Figure 1.2: 3-3 double ring (double 3 ring, D3R), 4-4 double ring (double 4 ring, D4R) and 5-5 double ring (double 5 ring, D5R). D3R is not found in zeolites but has been identified in other molecular sieves[2].

These structures provide interesting starting points for new materials, inorganic-organic hybrids such as polymers or metal-organic frameworks.

Zeolites and other types of molecular sieves are traditionally synthesised by hydrothermal means, requiring specific conditions (high temperature and pressure) and precise ratios of reagents[2]. While there is a great deal of variety in the structures and composition of molecular sieves, both through altering the framework and the addition of organic species as templates or adsorbates, there are limits to how far the structure can be controlled.

Inorganic – organic hybrid materials offer a new route to functional materials and the inclusion of a greater degree of organic functionality allows for greater control of the structures and, therefore, increases the potential applications. These can take the form of random or well defined polymers, framework structures and related monomeric precursors.

1.2 Silsesquioxanes

1.2.1 Introduction

Molecules with the general formula $[RSiO_{x/2}]$ are known as siloxanes where R maybe H, alkyl, alkenyl or some other organic derivative. The various types are detailed in table 1.1. The siloxane linkage, Si-O-Si is formed when different groups join to form larger molecules.

Silicon Species	General Formula	Nomenclature
Siloxy	$[R_3SiO_{1/2}]$	M
Siloxane	$[R_2SiO_{2/2}]$	D
Silsesquioxane	$[RSiO_{3/2}]$	T
Silicate	$[SiO_{4/2}]$	Q

Table 1.1: Table summarising the types of silicon-oxygen species being discussed and their simplified letter nomenclature[3].

Siloxy groups are good terminal groups because they halt formation of larger siloxane networks, siloxane groups are ideal candidates for forming large chain-like molecules while silsesquioxanes and silicates are most commonly found forming three-dimensional structures, both random polymers and oligomers due to the number of siloxane linkages that can be created. In all cases, a large number of structures with a large number of functionalities have been reported.

Silsesquioxanes and silicates are of particular interest because they are capable of forming species analogous to the SBUs from zeolites, most commonly D4R but D3R and D5R have been reported along with larger cages and rings[4].
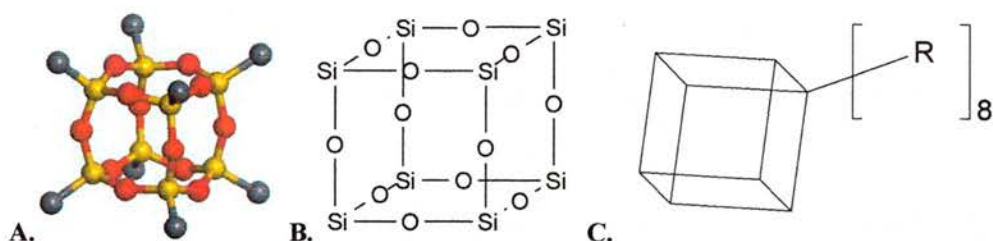
Figure 1.3: POSS framework, T8 Cage. Representation **A** Silicon – yellow, Oxygen – Red and Generic substituents – grey; Representation **B** shows cubic framework; Representation **C** shows simplified structure with one substituent that will be used henceforth.

The shorthand notation for silicates and polyhedral silsesquioxanes uses letters to denote the silicon type as well as numbers and superscripts to denote functional groups. These are summarised in table 1.2.

R Group	Formula	Formula	Notation
H-	$[HSiO_{3/2}]_8$	$H_8Si_8O_{12}$	H_8T_8
CH_2CH-	$[CH_2CHSiO_{3/2}]_8$	$C_{16}H_{40}Si_8O_{12}$	Vinyl $_8T_8$
$(CH_3)_3SiO-$	$[(CH_3)_3SiOSiO_{4/2}]_8$	$C_{24}H_{72}Si_{16}O_{28}$	Q_8M_8
$CH_2CH(CH_3)_2SiO-$	$[CH_2CH(CH_3)_2SiOSiO_{4/2}]_8$	$C_{32}H_{88}Si_{16}O_{28}$	$Q_8M_8^{Vi}$
$H(CH_3)_2)SiO-$	$[H(CH_3)_2SiOSiO_{4/2}]_8$	$C_{16}H_{56}Si_{16}O_{28}$	$Q_8M_8^{H}$

Table 1.2: Silsesquioxanes and Silicates of relevance, R group refers to diagram in figure 1.3C

Polyhedral Oligomeric Silsesquioxane (POSS) is the name given to molecules with the general formula $[RSiO_{3/2}]_n$ where n ranges from 6 (D3R) to 18 with a three-dimensional cage-like structure. The name silsesquioxane derives from the term *siloxane* (Si-O-Si) and *silses*, meaning one and a half. There have also been a number of alternative names proposed for these and related molecules such as *spherosiloxanes* [5,6] referring to the pseudospherical shape of the molecules and correspondingly silicate derivatives, eg $Q_8M_8^{H}$ have been named *siloxysilsesquioxanes* or *spheriosilicates* [7].
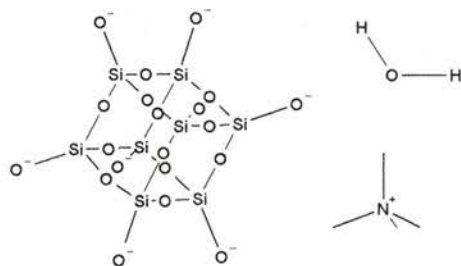
Figure 1.4: Tetramethylammoniumsilicate (TMAsilicate) molecule shown with one tetramethylammonium cation and one water molecule for clarity, $(NMe_4)_8^{8+} [SiO_{4/2}]_8^{8-}$. XH_2O

The cubic D4R analogue has the formula $[RSiO_{3/2}]_8$ and is the preferred product of many silsesquioxane syntheses. The silicate analogue of this, $[SiO_{4/2}]_8$ is also approximately cubic and can be functionalised with siloxy groups giving species of the form $[R_3SiOSiO_{4/2}]_8$.

1.2.2 Synthesis

Polyhedral silsesquioxanes are commonly synthesised by hydrolytic condensation of trichloro- or triethoxy- silanes. The structure of the species formed in the reaction is highly dependent on the reaction conditions especially the concentration of reactants (particularly the silane monomers), solvent, pH, temperature, availability of water, base or acid catalysis (or 'self-catalysis') and the solubility of the product. Sol-gels and silsesquioxane gels are often synthesised from the same monomers as POSS species and so the reaction conditions must be carefully controlled to avoid the irreversible formation of such gels[8].

Trichloro- or trialkoxy- silanes are typical monomers for these processes with the fourth substituent consisting of a small group such as H, vinyl, allyl, propylamine, alkyl or aryl.

Monomer	Reported Products	Reference
Cl_3Si-H	T8, T10, T12, T14	3, 9, 10
$(EtO)_3Si-H$	T8	9
$Cl_3Si-CHCH_2$	T8	11
$Cl_3Si-CH_2CH_2CH_2Br$	T8	12,13
$(EtO)_3Si-CH_2CH_2CH_2NH_2$	T8	14
$Cl_3Si-C_6H_5$	T8	15-18
$Cl_3Si-C_6H_4CH_2Cl$	T8	19
$Cl_3Si-CH_2CH_2CH_2C_6H_4OCH_3$	T6	20
$MeSi(OMe)_2CH_2$ (2,2,6,6,-tetramethylpiperidino)	T8	21

Table 1.3: Monomers and typical silsesquioxane cages synthesised by condensation

More exotic monomers can be prepared through hydrosilation reaction of trichloro- or triethoxy- silane with unsaturated species to form larger molecules. Condensation reactions produce a range of products including various rings and cages although T8 cages are often formed preferentially due to being less soluble in common organic solvents than T10 or T6 analogues. None the less, low yields are often obtained and so most work on POSS molecules involves the synthesis of vinyl or hydrido POSS and subsequent reactions to attach a variety of functional groups.
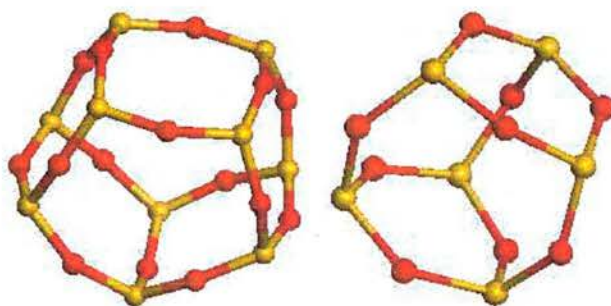
Figure 1.5: T10 and T6 silicon-oxygen cages with substituent groups removed for simplicity. Silicon – yellow and oxygen – red.

POSS molecules were first isolated in 1946 by Scott[22] and Barry[18] and soon followed by the first hydridosilsesquioxanes in 1959 by Muller *et al.*[23]. Initial yields were less than 1 % but definitely proven to be H_8T_8. Later, Frye and Collins[24] synthesised H_8T_8 in higher yields (13 %) from trimethoxysilane, acetic and hydrochloric acids in cyclohexane and improved methods by Agaskar *et al.*[4,10] and Nyman *et al.*[25] involved slow addition of trichlorosilane solution (in hexane or pentane) to a biphasic system

of solvent (hexane/toluene or pentane), hydrochloric acid, methanol and iron (III)

chloride. This has lead to reported yields of between 20 and 30 % and often a

mixture of T8 and T10 cages is formed. It is possible to use fractional crystallisation

to separate the H_8T_8 and $H_{10}T_{10}$ species, as T8 cages are less soluble and isolated

yields of T10 cages are usually lower than T8. The solvent mixtures used are known

to affect the major product formed and Bolln[9] reported the use of petroleum ether in

place of methanol and other organic solvents.

The earliest reported vinyl POSS molecules were by Voronkov *et al.*[26] synthesised

from the hydrolysis and condensation of vinyltrichlorosilane. A related structure,

allyl POSS, can be produced by the hydrolysis and condensation of

allyltrichlorosilane[27].

Feher *et al.* reported the synthesis of an octamer (γ-aminopropyl) silsesquioxane[14]

by acid catalysed hydrolysis and condensation of (γ-aminopropyl) triethoxysilane.

The product was obtained as an octahydrochloride salt and was found to be highly

soluble in water but prone to decomposition possibly due to the tendency of the

POSS cube to undergo base-catalysed rearrangements. The related aminopropyl

POSS obtained by ion exchange is highly unstable at room temperature. Despite the

difficulties of dealing with aminopropylPOSS, it remains a very useful building

block on the way to large POSS networks. This versatility is demonstrated by Feher

et al. where the amine cube has been used to create POSS based PAMAM

dendrimers and a myriad of other useful functionalised molecules including peptidyl

silsesquioxanes[28].

Various polymeric silsesquioxanes have been synthesised by hydrolysis of other

trichloro- or trialkoxy- functionalised silanes. With a view to silsesquioxane based

catalysts (dendrimeric or otherwise), the most interesting of these are

polyfluoroalkylsilsesquioxanes as reported by Kobayashi[29]. While these are random

polymers such as poly (3,3,3-trifluoropropyl) silsesquioxane or poly

(3,3,4,4,5,5,6,6,6-nonafluorohexyl) silsesquioxane synthesised by the hydrolysis of

the relevant trichlorosilane in THF or suitable fluorous solvent, controlled hydrolysis

could lead to oligomeric species such as T8 cages.
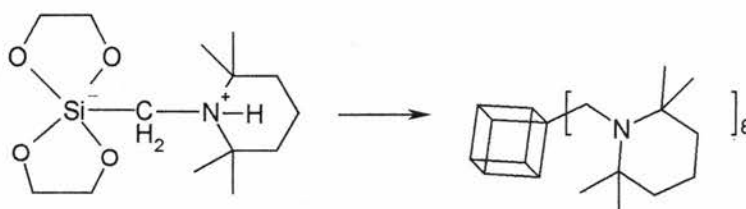
Figure 1.6: Zwitter ion synthesis of T8 POSS cage[21].

A very unusual route to a T8 cage was reported by Richter *et al.* via hydrolysis of a

zwitter ion pentacoordinate silicate species (figure 1.6)[21]. The product was

confirmed by single crystal x-ray diffraction and solid state NMR and offers a novel

route to POSS cubes.

Recently methods of synthesising the D3R analogue R_6T_6 have been reported using

non-aqueous methods, with DMSO as the oxygen source. Again functionalised

trichlorosilanes were used but yields were generally low with most reactions giving a

range of products requiring separation by column chromatography.

1.2.2.1 Functionalised POSS cubes

POSS molecules can be functionalised by a variety of methods, mainly hydrosilation

for H_8T_8 although a radical reaction has been reported leading to Cl_8T_8. Vinyl

functionalised silsesquioxane cages are extremely useful synthetically as they can

undergo hydrosilation with Si-H, hydrobromination, and bromination, cross

metathesis and other reactions typical of unsaturated groups.

Hydrosilation (hydrosilylation) is the addition of Si-H to multiple bonds, typically

alkenes, alkynes, nitriles or carbonyls. It can be catalysed by transition metals,

Chapter 1. *Introduction, Aims and Objectives*

Lewis acids or by radical or nucleophilic (tertiary amine) means. Two common catalysts for hydrosilation are platinum-based and are Speier's and Karstedt's catalysts respectively. Speier's catalyst is a solution of hydrogen hexachloroplatinic acid first reported in 1957 and is the most widely used platinum catalyst[30], while Karstedt's catalyst is a platinum complex of divinyltetramethyldisiloxane, discovered in 1973[31]. There have been some reports of the advantage of co-catalysts to enhance the catalytic activity and selectivity of the hydrosilation reaction. Most commonly this is in the form of oxygen, and thought to act as a promoting agent in the reaction and also to prevent the deactivation of the platinum complexes.

There are, as with all catalytic processes, a number of competing reactions that can occur but with careful choice of catalyst and reaction conditions any tendency for side reactions can be overcome. For example, silanes bearing electron-donating substituents such as alkyl groups are more suitable for hydrosilation with Lewis acid type catalysts, the most active of which is aluminium tribromide.
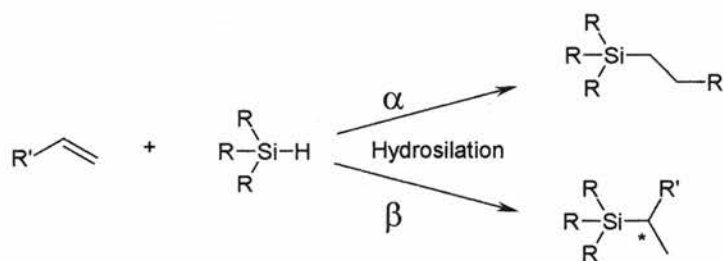
Figure 1.7: Two main competing reactions in Hydrosilation – α and β addition, β addition resulting in production of a stereogenic centre*

Addition across the double bond can occur in two ways giving two products. It is generally favourable for Si-C bond formation to occur at the terminal carbon of the alkene. This is usually termed α-addition (and will be throughout) as it occurs at the α-carbon although in the case of molecules of the form XCH_2CHCH_2 it has been reported as γ-addition where X is attached to the α-carbon. β-addition creates a branched product. Dittmar *et al.* reported that hydrosilation reactions (using Speier's catalyst) of small molecules containing the allyl functionality to H_8T_8 resulted in a

mixture of isomers depending on the constitution of the small molecules[32]. It was

found that α-addition was preferred when R (Figures 1.7 and 1.8) was a weak

electron withdrawing group.
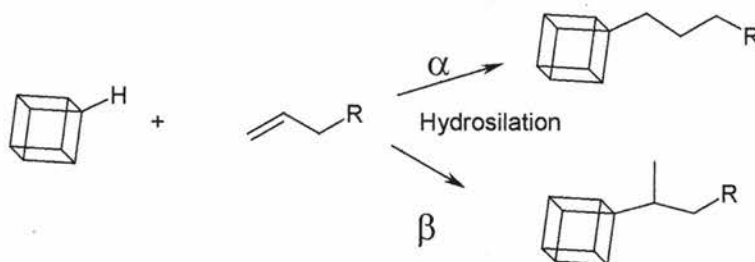
Figure1.8: α and β addition to H_8T_8 as predicted by Dittmar *et al.*[32].

A strong electron-withdrawing group (e.g. ether, ester, and cyanides) would create a

greater tendency to take part in side reactions, perhaps due to the isomerism of the

allyl groups to an internal double bond, favouring β-addition. It is also thought that

lower reaction temperatures and careful choice of solvents favour α- addition.

Radical reactions have also been used to functionalise POSS molecules. Lücke

reported a dimethylphosphine POSS, closely related to the diphenylphosphine POSS

derivatives reported by Hong *et al.*[33,34] where vinyl POSS or allyl POSS had been

functionalised with phosphines by radical reactions.

Klemperer *et al.* prepared a D4R silicate equivalent from H_8T_8 by chlorination to

form Cl_8T_8 followed by reaction with CH_3ONO to form $(CH_3O)_8[Si_8O_{12}]^4$. Other

reactions that have been used to functionalise POSS cubes include cross metathesis[35].

This was carried out successfully on both vinyl POSS and $Q_8M_8^{Vi}$ with a range of

unsaturated compounds including pent-1-ene and styrene, offering a catalytic route

towards new POSS molecules.

1.2.2.2 Corner Capping of POSS Molecules

Partially condensed POSS cubes (7 corners, 3 Si-OH groups, figure 1.9) can be prepared by condensation[36,37] or base catalysed ring opening of a complete molecule[38-40]. Typically these molecules have cyclohexyl or cyclopentyl substituents and the condensation of cyclohexyl POSS takes three years, producing the partially condensed species in reasonable yields. The vacant corner is 'capped' by adding a trichlorosilane moiety creating a 1:7 ratio of substituents.

Extensive research has been conducted into 'corner-capping' of silsesquioxanes.
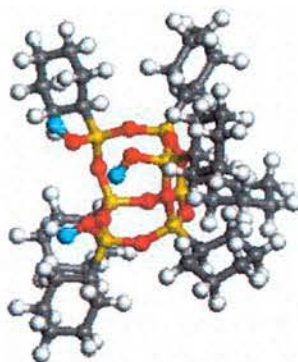
Figure1.9: Partially condensed POSS cube for corner capping with 7 cyclohexane substituents and one missing corner forming a trisilanol. The protons of the silanols have been coloured blue for emphasis. Silicon – yellow, oxygen – red, carbon – grey, hydrogen – white.

In this way a number of commercially available silsesquioxanes have been manufactured, having the general formula $R_1Cy_7Si_8O_{12}$ where R can be vinyl, diphenylphosphinoethyl-, etc.

1.2.2.3 Heterosilsesquioxanes[41]

Cubic silsesquioxane type molecules have been reported with a variety of different atoms present within the structure. The inclusion of metal groups such as titanium or aluminium can be accomplished in two main ways. Firstly, by reaction of appropriate silicon and metal containing precursors, producing a cubic molecule

where alternate corners are silicon and metal bridged by oxygen, for example titanium and aluminium[42,43] and secondly by corner capping (Section 1.2.2.2 above) where a metal compound is used to fill the open corner, completing the D4R structure. Feher's work in this area explored the utility of POSS cubes as models for silica surfaces[44-46]. Many heterogeneous catalysts used in industrially important processes rely on silica bound metal complexes and it was found that corner capping of a POSS cube created species that resemble, structurally, the sites found within these catalysts. Of course, this creates soluble, homogeneous analogues. This allowed germanium, tin and zirconium molecules to be prepared.
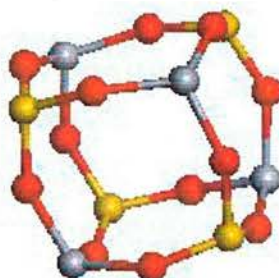
Figure 1.10: T8 cube with alternate corners of silicon (orange) and titanium (silver) bridged by oxygen (red). The substituents have been omitted for clarity[47].

Duchateau *et al.* have synthesised a number of metal containing derivatives using corner capping reactions to insert fluorene groups capable of forming zirconocene derivatives, boron and trimethyltin species[48-51]. Smet used tungsten to link two cages together, creating corner linked metal-POSS dimers[52]. Cyclohexyltrichlorosilane can be used to produce an analogous partially condensed cage and Maschmeyer has created a POSS dimer linked by titanium-oxygen bridges in this way[53].

A series of open cage POSS crystal structures have been reported in literature, mainly incorporating metals like osmium, thallium, copper, cerium or zirconium. The structures of these molecules are unusual and show the benefits of crystallography in full structure determination of POSS molecules.

1.2.2.4 Silicates

Silicate cages are readily formed by reaction of a silica source (silicic acid or tetraethoxysilane) and a quaternary ammonium hydroxide[54,55]. The size of the substituents define the size of the cage produced (table 1.4) and this has lead to the synthesis of D3R, D4R and D5R molecules as well as some larger species. The silicate anion is rarely characterised as it is most often left in solution and reacted further with a chlorosilane to produce a silylsilicate of the form $[R_3SiOSiO_{4/2}]_X$ where $X = 6, 8, 10$ etc.

R'R$_3$NOH		Cage Formed
R'	R	
2-hydroxyethyl	Methyl	D4R, $Si_8O_{20}^{8-}$
Phenyl	Methyl	D4R
Benzyl	Methyl	D4R
R' = R	Methyl	D4R
R' = R	Ethyl	D3R, $Si_6O_{15}^{6-}$
R' = R	Propyl	Unknown
R' = R	Butyl	D5R, $Si_{10}O_{25}^{10-}$

Table 1.4: Organic bases and cages formed.

Various small chlorosilanes have been used to form equivalents of both the octavinyl and octahydrido POSS as well as others detailed below.

Q_8M_8 $Q_8M_8{}^H$ $Q_8M_8{}^{Vi}$
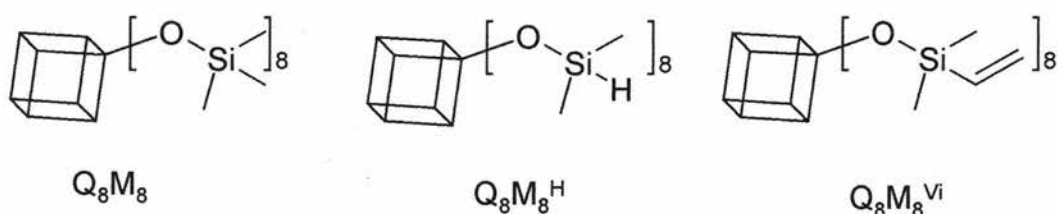
Figure 1.11: Various functionalised silicate cubes.

Auner and co workers produced a series of silicate structures in 1999 and managed to obtain crystal structures and solid state NMR data[7]. Both the vinyl and hydrido derivatives of Q_8M_8 were synthesised as well as the D5R analogue $Q_{10}M_{10}$ and its hydrido derivative. $Q_8M_8{}^H$ and $Q_8M_8{}^{Vi}$ are excellent hydrido and vinyl POSS

alternatives, synthesised from tetramethylammoniumsilicate solutions and produced in crystalline forms.

$Q_8M_8^H$ and $Q_8M_8^{Vi}$ can be used in a similar manner to the octahydrido and octavinyl POSS and participate in hydrosilation reactions although there is some debate about the $Q_8M_8^H$ Si-H bond being potentially less reactive. The main advantage of these molecules is the typical yield over two reaction steps is in the region of 80 %, compared to 20 % for silsesquioxanes.

Research by Hoebbel has involved extensive investigation into the rates of formation of silicate cubes, analysis of the products and the subsequent reactions they can take part in[56-58]. A summary of functionalised silica D4R cubes reported in literature included 36 different molecules of the form $R_8Si_8O_{20}$ where R is purely organic through to ferrocene, Sn, Co and Sb species

1.2.3 Characterisation of POSS molecules

Silsesquioxanes and silicates are generally characterised using standard analytical techniques such as multinuclear solution NMR(^{29}Si, ^{13}C, ^{1}H), Magic Angle Spinning (MAS) solid state NMR, IR etc. to name but a few. The size and symmetry of POSS molecules creates many challenges for characterisation by these methods, especially NMR. Matrix Assisted Laser Desorption Ionisation Time Of Flight (MALDI-TOF) is the most commonly used mass spectrometry technique generally due the large size of POSS macromolecules.

Small POSS molecules are generally solids and make ideal candidates for both crystallography[12,32] and MAS NMR[7,59]. A search for the word silsesquioxane in the Cambridge Structural Database give 45 hits from 1955 to the present giving crystal structures for a variety of POSS derivatives. While a number are conventional R_8T_8

type structures, there are few examples of R_6T_6 structures (including one where R is 1,1,2-trimethyl n-propyl silsesquioxane) and a number of examples of cage silsesquioxanes and metal bridged cage structures.
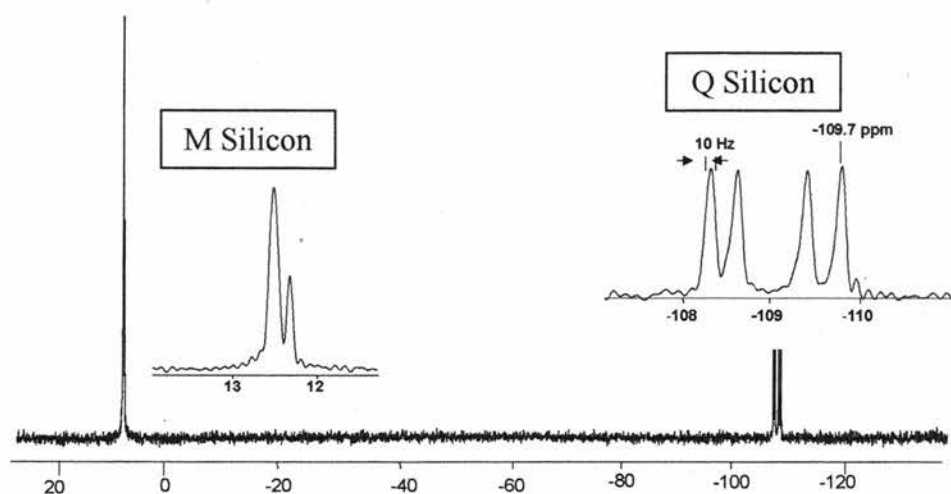
Figure 1.12: $^1H - {}^{29}Si$ Cross-Polarisation Magic Angle Spinning (CP-MAS) Solid State NMR spectra of Q_8M_8. Insert regions show peaks in more detail[60].

In addition to POSS molecules, silicate derivatives such as Q_8M_8 and related structures are also available. Q_8M_8 has found application as a standard for solid state NMR, giving two silicon signals enabling spectra to be referenced[7,59]. Photoluminescence, UV light induced emission; UV absorption and photoluminescence light excitation spectra of H_8T_8 and R_8T_8 molecules were studied by Azinovic *et al.*[61]. This systematic study of H_8T_8 and a family of R_8T_8 where R = methyl – decyl groups showed that all the molecules showed similar spectral structure and provides useful information to prove the formation of the T8 cube from standard synthetic methods.

POSS based nanoscience is a rapidly expanding area of research with the number of annual journal publications increasing nearly ten fold in the last decade. The key is the ability of silsesquioxanes and derivatives to take excellent physical properties from ceramics and combine them with versatile chemical reactivity usually only found in organic molecules. Polymeric materials containing silsesquioxanes have been found to have many improved properties and have been reported as nanocomposites, mesoporous networks, highly porous random polymers through to periodic organosilica species that have silsesquioxane stoichiometry.

Nanocomposites in particular, have been reported as dental adhesives and are showing great potential as space-survivable self healing polymers due to strong silicon-oxygen bonds (stronger than organic bonds and more resistant to ultraviolet radiation and atomic oxygen collision), and the ability to form SiO_2 films when the organic substituents have been degraded thus protecting the bulk material[62].

Silsesquioxane hybrid materials have been reported with enhanced properties such as solubility, thermal stability, greater mechanical toughness, fire retardancy, gas permeability, optical transparency and thermomechanical stability.

These advanced properties are highly tuneable due to the ease of creating multifunctionalised POSS building blocks with great chemical versatility allowing precise variation of structure and hence function.

1.3 Dendrimers

1.3.1 Overview

Dendrimers are a class of polymers that were discovered in the late 1970s realising the concept of creating ordered polymers with precisely defined size, dimensions and composition that had long been a dream of many polymer chemists. The synthetic procedures necessary to make such a dream a reality had proved elusive. Out of the many types of polymers, dendrimers and hyperbranched polymers consist of branched rather than linear repeat units although hyperbranched polymers are random, polydisperse species. Dendrimers have precisely defined size and composition, and are monodisperse.
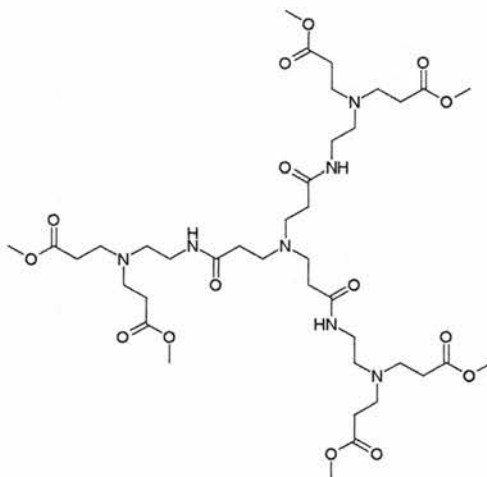
Figure 1.13: First generation PAMAM dendrimer with methyl ester terminal groups and ammonia core.

A chance discovery in 1979 by Tomalia lead to the synthesis of the first dendrimer, poly (amidoamine) through reaction of methyl acrylate and 1,2-diaminoethane in methanol[63,64]. Reaction of these two monomers without solvent produced linear random polymers of varying lengths but with alternating methyl acrylate and diaminoethane units. In this case, smaller molecules had been produced with two methyl acrylate monomers attached to each nitrogen in diaminoethane. Methanol

appeared to aid the replacement of hydrogen in diaminoethane with methylacrylate units.

It has subsequently been shown that as long as just enough methanol is added, these polymers can be created through the stepwise addition and removal of the monomers. Since this initial discovery, poly (amidoamine) dendrimers (hereafter known as PAMAM) have been widely used for a great number of applications worldwide and are commercially available through the Aldrich chemical suppliers. Dendrimer chemistry has not been limited to just one type of polymer from two monomers, and a vast number of chemical reactions have been exploited to form dendrimers.

1.3.2 Structure of Dendrimers

The primary difference between dendrimers and other polymers is the clearly defined architecture and structure that they possess. Dendrimers have a core and branched molecules, often referred to as dendrons, radiating from it. Growth of dendrimers is generally thought of as being a two step process, growth (the addition of monomers) and activation (conversion of the end groups in to a species capable of reacting with the next monomer). This builds the molecule up in layers known as generations and, as long as the reactions used are high yielding, should create perfect structures.
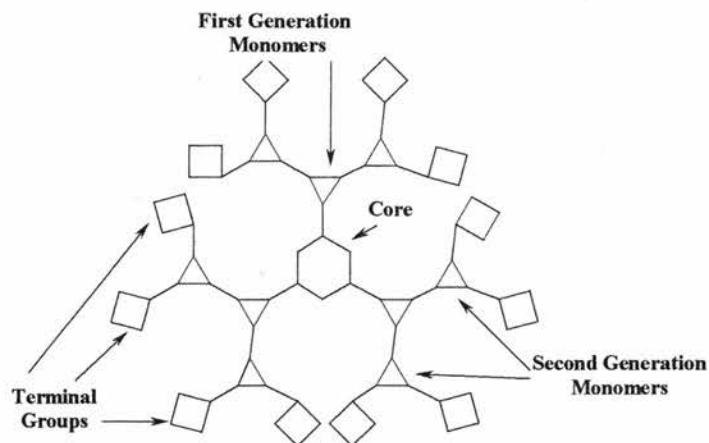
Figure 1.14: Schematic representation of a dendrimer showing core, monomer units and terminal groups.

The end groups of individual dendrons, often referred to as terminal groups are either the site of growth of higher generations or may be functionalised with other monomers to inhibit further growth, or impart different functionality. This all adds to a picture of molecules with a core, branches and terminal groups and perhaps globular in shape. What has been commonly found is that the shape of the dendrimer amplifies the shape of the core molecule up to a certain point. For example, a tetrahedral core such as silicon or carbon might impart a tetrahedral configuration of branches in low generations, while a more elongated core like 1,4-diaminobutane might create cylindrical molecules with greater density at either end. As the branches get larger, the structures become more sterically congested leading to relocation of the terminal groups and the structures become more spherical. This is known as back folding and simply describes the terminal groups curling into the interior of the molecule rather than sitting on the surface. This has implications for both dendritic growth and function, as these groups may no longer be accessible for reaction.

The notion of a two step dendrimer synthesis is true of many cases, notable PAMAM and poly (propyleneimine) but is not the only method of synthesis. Two general methods exist, divergent and convergent. The divergent synthesis begins with the

core and adds, in generations, monomers to form the completed structure whereas the convergent synthesis involves the creation of dendrons and in the final reaction step attaches them to the core. There are advantages and disadvantages to each method and these will be discussed in detail below.

1.3.3 Divergent Synthesis

The divergent synthesis requires high yielding reactions to ensure that each generation of monomers reacts at all available sites to create defect free structures. Defects are most commonly caused by incomplete reaction or side reactions. Side reactions usually cause termination of the branch through the formation of an unreactive species. Incomplete reaction occurs when either the monomers cannot gain access to the reactive sites or the reaction is too low yielding to effect full functionalisation of the dendrimer. In either case, the molecules produced no longer have precisely defined architectures and are not perfect structures. One of the interesting discoveries made in dendrimer theory is the implication of a limiting generation[65]. As dendrimers get larger, the number of terminal groups increases as a function of the degree of branching of the monomers. It has been found that there is a limit to how big a dendrimer can grow and still retain a perfect structure. This is often referred to as the starburst limit, and is caused by the surface of the molecule becoming packed with terminal groups creating an environment where further reaction is hindered, sterically or the terminal groups back fold into the interior and are shielded from the reaction.
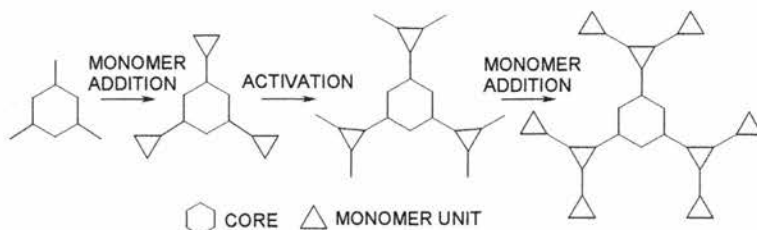
Figure 1.15: Schematic representation of divergent synthesis leading to a second-generation molecule.

Poly (propyleneimine) dendrimers were first synthesised by Vögtle *et al.* at around the same time of Tomalia's discovery of PAMAM dendrimers[66]. These were synthesised through a Michael type addition of acrylonitrile to an amine, followed by the reduction of the nitrile to a primary amine, ready for reaction with acrylonitrile again. The use of a monoamine for this synthesis (e.g. benzylamine) created branched molecules that more resemble dendrons than dendrimers.
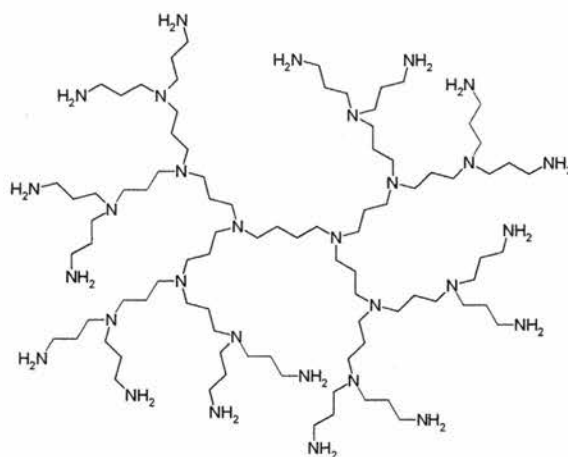
Figure 1.16: Poly (propylene imine) dendrimer with 1,4-diaminobutane core and 16 terminal amine groups.

Initially, the syntheses of high generations were inhibited by the need for metal catalysts in the reduction step due to the strong metal complexing ability of the molecules but this was soon resolved and poly (propyleneimine) dendrimers are now available with terminal amine or nitrile groups and different cores 'off the shelf'.

Newkome *et al.* reported the synthesis of highly branched molecules that were christened arborols (from the Greek, *arbor* – branch) through the formation of peptide linkages and reaction with molecules such as pentaerythritol[67,68].

Since then, divergent dendrimer synthesis has become a very common way to synthesise large dendrimers. The main advantages of this method are that large molecules can be made swiftly. If the monomers and solvents involved are volatile, it is possible to distil the excess off before the next reaction step takes place, a very easy way of purifying that works well for low generations. Beyond a certain generation, purification is not only to remove unreacted monomers, but also to remove impure products. This is very difficult to do and often a small distribution of products is considered acceptable. The disadvantages come in the form of the reactions that are used for the divergent synthesis. If they are not close to quantitative at every step, the problem of removing impure dendrimers is multiplied. Additionally, many uses of dendrimers require the dendrimers to have functionalised terminal groups, and these reactions are rarely quantitative, especially when the larger generations have in excess of 30 reactive sites per molecule.

1.3.4 Convergent Synthesis

From the first reported syntheses of dendrimers in the early 1980s until the early 1990s the only known means of synthesising dendrimers was via the divergent route. This changed in the 1990s with the publication of a paper by Hawker and Fréchet introducing the notion of convergent dendrimer growth[69,70]. While the divergent synthesis builds the molecule from the core with the addition of terminal groups last, the convergent synthesis begins with terminal groups and creates individual branches for attachment to the core in the final step. This method overcomes many of the restrictions and problems of the divergent synthesis, most importantly the need for quantitative yields. Large molecules are not formed until the final step, which makes purification simpler and more efficient. The branches can be purified at every step

ensuring that the dendrimer produced is structurally perfect. In addition, if the reaction attaching the branches to the core is lower yielding, the defects produced are large and consequently easier to remove. This makes many more reactions available for synthesis and that dendrimers with mixed branches (both composition and generation) can be created[71].
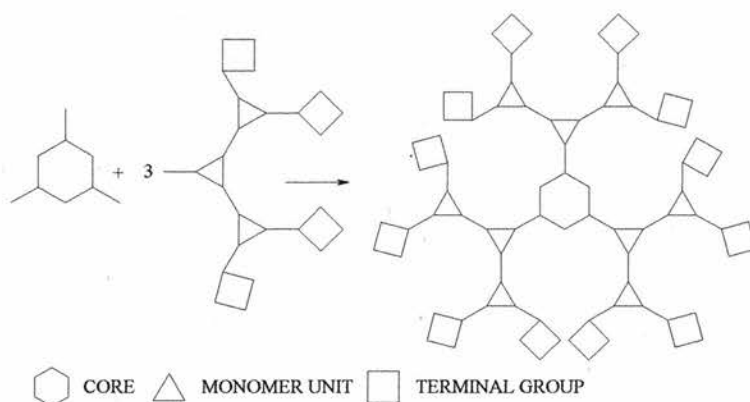
Figure 1.17: Schematic representation of convergent dendrimer synthesis resulting in a second-generation molecule.

The first convergent synthesis was of poly (aryl ether) dendrimers and involved the Williamson ether synthesis, reaction of benzyl bromides and 3,5-dihydroxybenzyl alcohol. The root of the dendrons are activated through the conversion of alcohol to bromide and then reacted further.

Figure 1.18: Synthesis of Fréchet type wedges, poly (benzyl ether).

Generally, 3,5-dihydroxybenzyl alcohol are the repeat units and benzyl groups the terminal units. Dendrons and dendrimers can be produced in this way up to the sixth generation, typically with cores like benzene triphenols. These dendrons are commonly referred to as 'Fréchet-type' dendrons or 'Fréchet Wedges' and have been used in their original or modified form in many syntheses.

Chapter 1. *Introduction, Aims and Objectives*

A vast number of convergent syntheses now exist, many based around aromatic type frameworks such as poly (arylalkyne), poly (phenylene) or poly (arylalkene) dendrimers.

Poly (aryl alkyne)

Poly (phenylene)
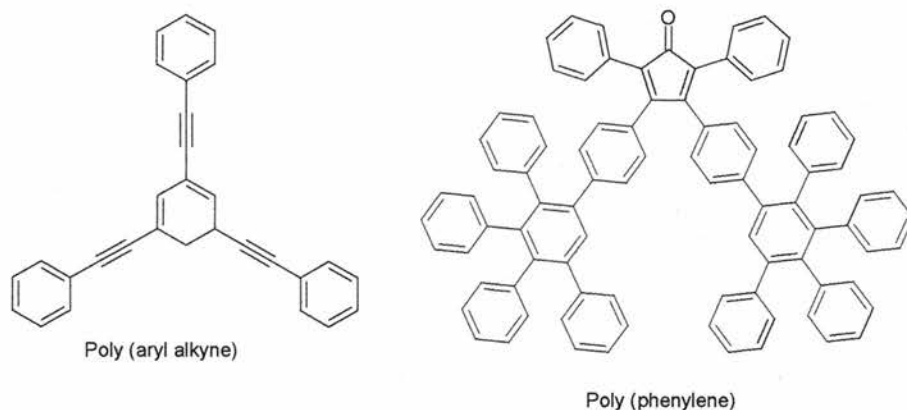
Figure 1.19: Rigid dendrimer frameworks[72]

Alkyl frameworks include poly (alkyl ester), poly (alkyl ether) and versions of divergent dendrimers such as poly (amido amine). One advantage of the convergent synthesis is that functional groups can be added to the dendrons by low yielding reactions and still give full coverage of the final dendrimer.

1.3.5 Characterisation of Dendrimers

The characterisation of dendrimers is complex due to their large size, structure and symmetry. Traditional means of characterisation have been applied with limited success and while it is relatively straightforward to assess the approximate size of dendrimers and composition, exact determination of molecular dimensions and purity is another matter. Defects in the structure arising from either side or incomplete reactions are difficult to see by normal characterisation methods. Solution Nuclear Magnetic Resonance spectroscopy has limited applications as signals from complete and incomplete reactions overlap obscuring information, especially for higher generations. This is especially true of the divergent method of

synthesis where there are many reactive sites. Dendrimers synthesised convergently

can be characterised by NMR up to the point where the branches are added to the

core. Some dendrimers, especially higher generations have been found to be

insoluble in common solvents further hindering characterisation.

Solid state NMR has been used with some success to gain more information about

dendrimers, but generally, solution or liquid state techniques are used. Size

exclusion chromatography is of limited use because dendrimers do not fit calibration

curves based on linear structures. There is a tendency to overestimate the molecular

mass of low generations and underestimate that of high generations. This means that

a correct molecular mass distribution cannot be obtained.

Matrix Assisted Laser Desorption Ionisation Time of Flight (MALDI-TOF) mass

spectrometry can generally be used to determine molecular masses and distributions

because fragmentation of the molecular ions does not occur, and the technique can

cope with large molecules. Electron Spin Ionisation (ESI) mass spectrometry has

also been used to identify impurities in some divergently synthesised dendrimers, but

mainly low generations.

1.3.6 Applications of Dendrimers

One of the great difficulties surrounding current dendrimer research is separating the

fantasy and fact concerning potential applications for functionalised dendrimers.

Indeed, the difficulties involved with dendrimer synthesis, the large number of steps,

amount of purification required, the complexity of the reactions used, especially in

the divergent synthesis, means that it is unlikely that many of these molecules will

survive the long journey from the laboratory bench to the industrial production plant.

The versatility of dendrimers is illustrated in many of the applications reported to

date, which include their use as MRI contrast agents. Other applications in the

biological field include dendrimers with suitable functionalities being used as

artificial cells or possibly even drug carriers[73]. Dendrimeric molecules can be

synthesised large enough to carry hundreds of drug molecules into the body attached

to its periphery whilst still being small enough to pass through a cell membrane. In a

similar way, the dendrimer may be used as a DNA transfer vector for targeted gene

therapy[74]. The novel materials field also gives rise to many potential applications.

Liquid crystal dendrimers[75-81] have been reported as well as a light emitting variety[82-85]. The controllable dimensions of dendrimers mean that they are ideal to calibrate

filters and sieves if a pure sample can be obtained. There are have been reports of

dendrimers being used as fluorescent sensors or selective molecular gates indicating

the wide range of used for these very versatile molecules. The environment may

benefit from these snowflake like molecules. Chelating groups present within

branches have been used to remove metal ions from solution, useful for cleaning up

contaminated water (especially mine workings) and their potential as catalysts may

one day lead to processes in greener solvents or at lower pressures or temperatures[86].

1.3.7 Dendrimers as Catalysts

The first dendrimer catalysts came in 1994 by van Koten *et al.* and subsequently

many different general types have been reported[87]. There are two main ways of

categorising dendrimer catalysts – by location of ligating/catalytic groups or by

effect (improved or reduced selectivity etc.) on reaction compared with small (non-

dendritic) equivalents.

The ligating groups can be located in several places within the dendrimer

architecture – on the periphery (as terminal units), within the branches (as monomer

units) or trapped within the structure (as guests, encapsulated or at the core). The presence of dendrimer arms around a core catalytic site may enhance selectivity, reduce rate (conversion) or inhibit reaction entirely depending on the nature of the branches, whereas the dendrimer structure might lend stability to colloidal metal particles trapped within its branches enhancing reaction.

The term 'dendritic effect' has been coined for influences apparently exerted by the dendrimer architecture on the function of the molecule. Hence, a positive dendritic effect might explain increased selectivity for a reaction. The effect is not limited to catalytic applications but is perhaps most widely documented due to the ease of measuring properties (physical quantities) in catalytic processes.

1.3.7.1 Peripheral Catalytic Groups

Attaching groups to the dendrimer periphery is one of the most direct routes to catalysts as dendrimers such as PAMAM, PPI, carbosilane etc can be used as scaffolds for ligating groups. Amine and silane terminated dendrimers lend themselves particularly well to this.

In 1994, van Koten reported carbosilane dendrimers (silicon atom core) functionalised with terdentate NCN type ligands[87]. Two variations have been reported with the same dendrimer with an organic spacer increasing the distance between the dendrimer and complex to eliminate any interactions between metal sites. The resulting nickel complexes were used as homogeneous catalysts for the Kharasch addition (Atom Transfer Radical Addition, ATRA) of carbon tetrachloride to methyl methacrylate. The activity was not found to be significantly lower for the dendrimer complex (calculated per nickel site compared to monomer nickel complexes) and a regioselective addition without side reactions was achieved. The

size of the molecules appeared to lend themselves to recovery by advanced filtration methods. Similar catalytic groups have been added to amino acid based dendrimers with no enhanced properties or decreased effects noted. While the dendrimers without spacers gave reduced activity with increasing generation, those with 1,4-butanediol spacers showed improved properties.
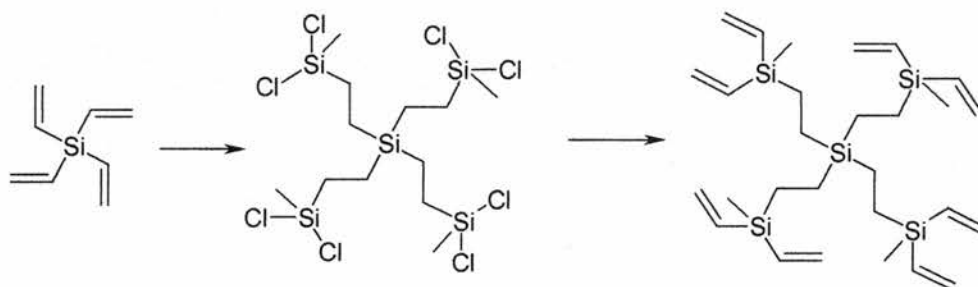
Figure 1.20: Synthesis of Carbosilane dendrimer from tetravinylsilane by hydrosilation and Grignard reaction.

The carbosilane framework (silicon core, tetravinyl or tetraallyl silane derived, figure 1.20) has been exploited for hydroformylation reactions by several researchers[88-90]. Carbosilane dendrimers with terminal Si-Cl groups are readily functionalised through Grignard or lithiation reactions. In this way van Koten reported 2-pyridylalcohol functionalised dendrimers[91], used as ligands for ruthenium based ring closing metathesis (RCM) polymerisation. The activity was found to be the same as small molecules, and investigations with nanofiltration membranes caused low conversion thought to be due to reaction of the dendrimer complexes with the membrane.

A more successful attempt at membrane nanofiltration with carbosilane dendrimers was demonstrated by van Koten and Vogt[92]. Palladium catalysed hydrovinylation was an ideal reaction for this, as constant removal of the desired product must be achieved in order to prevent isomerisation to internal olefins (seen at high conversions). Diphenylphosphine carboxylic acid ester groups were used as the ligating groups and while a low yield of 3-phenyl-1-butene was obtained, no

significant impurities were found and some retention of the dendrimer in the

nanofiltration system was achieved.
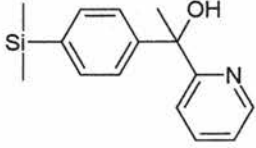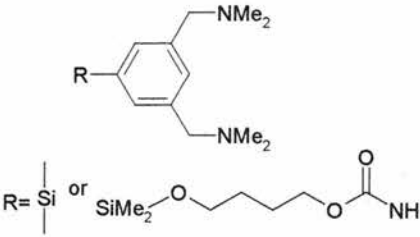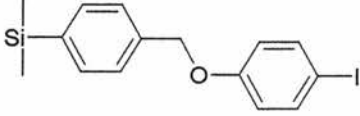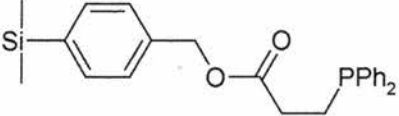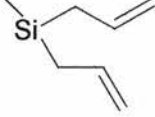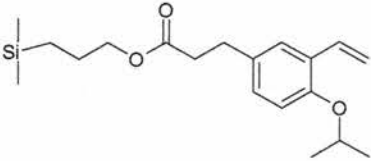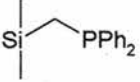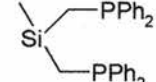
Terminal Group	Metal	Reaction	Ref.
	Ru	Ring Closing Metathesis	91
	Ni	ATRA Atom Transfer Radical Addition or Kharasch Addition of CCl_4 to methyl methacrylate	93
	Pd		92
	Pd	Hydrovinylation of Styrene, Membrane Reactor	92
	Ru	Ring Opening Metathesis Polymerisation	94,95
	Ru	Ring Opening Metathesis Polymerisation	96
	Rh	Hydroformylation	89
	Rh, Ir	Hydrogenation of 1-hexene	97,98

Table 1.5: Various terminal groups of carbosilane dendrimers with silicon cores used for catalysis (as shown in figure 1.20).

The research groups of Reek and Rossell have reported carbosilane dendrimers with

diphenylphosphine terminal groups used as ligands for rhodium catalysed

hydroformylation of 1-octene and rhodium or iridium catalysed hydrogenation of 1-hexene respectively. Reek *et al.* found a largely negative dendritic effect for diphenylphosphine terminated carbosilane dendrimers, with lower conversion for the dendrimers compared to small analogues[89,99,100]. Dendrimers with longer branches were found to give faster catalysis but the selectivity obtained did not differ from the small analogues.

Rossell *et al.* found iridium dendrimer complexes to be insoluble and gave irreproducible results for catalysis while rhodium complexes were efficient catalysts with reproducible results being obtained with fresh batches of the complex[97,98]. Neutral rhodium dendrimer complexes were found to be more active (by turn over frequency) than monomeric [RhCl(cod)PPh$_3$] and dimeric [RhCl(cod)]$_2$ complexes and the cationic rhodium dendrimer was less active than its corresponding monomer. A similar study by van Leeuwen *et al.*[88] into the allylic alkylation of sodium diethylmalonate with allyltrifluoroacetate in a continuous flow (membrane) reactor showed a decrease in yield compared to the same catalyst in batchwise reactions that showed quantitative substrate conversion and high activity. It was concluded that the catalyst had decomposed within the reactor.

Diphenylphosphine functionalised poly (propylene imine) dendrimers were reported by Reetz *et al.*[101]. The addition of two methyldiphenylphosphino groups to the primary amine groups on 1,4-diaminobutane cored molecules created ligands with the potential for terdentate binding (phosphorus-nitrogen-phosphorus, PNP). The activity of the dimethylpalladium dendrimer complex was higher than the monomer analogue for the Heck coupling of bromobenzene and styrene. The dendritic structure also appeared to inhibit decomposition to palladium metal, an example of a positive dendritic effect on the catalyst stability.

Kaneda used a similar system for palladium catalysed hydrogenation of olefins, showing efficient hydrogenation for conjugated olefins[102]. The dendrimers activity was again higher than the monomeric equivalent and the dendritic structure allowed its recovery when used heterogeneously. Interestingly, the activity of the dendrimer did not decrease on recycling.

Chiral dendrimers (1,4-diaminobutane cored poly(propylene imine)) with terminal chiral amino alcohols were reported by Meijer *et al.* and were used to generate chiral alkyl zinc catalytic sites for the reductive alkylation of benzaldehyde[103]. Increasing generation lead to decreasing enantioselectivity and conversion. The fifth generation showed no optical rotation and correspondingly no enantioselectivity for the reaction. This was believed to be due to interactions of the chiral groups caused by steric crowding at the periphery.

Phosphorus terminated dendrimers complexed to a variety of metals (Pd, Pt, Rh) have been reported by Majoral *et al.* and that Pd (II) and Ru (II) complexes were suitable homogeneous catalysts for organic reactions including Michael additions[104,105].

The chiral addition of diethylzinc to N-diphenylphosphinyl imines was catalysed by PAMAM dendrimers with chiral ephedrine terminal groups, giving only moderate enantioselectivities compared to high enantioselectivities for the non-dendritic equivalent[106]. A larger catalytic loading of the dendrimer was required to obtain these results. A more rigid dendrimer based on acetylene groups was found to give high enantiomeric excess. The less rigid PAMAM dendrimers may be allowing the ephedrine groups on each branch to interact, reducing the resulting enantiomeric excess [107].
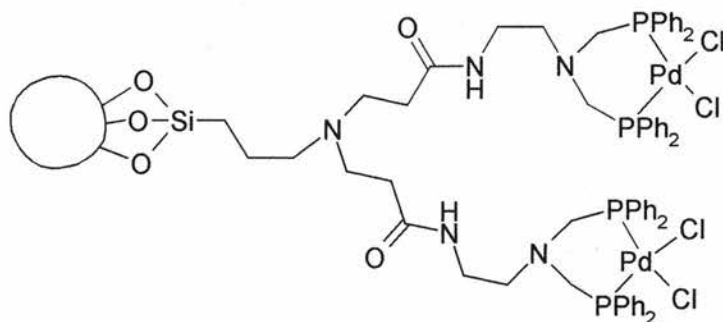
Figure 1.21: Heterogeneous PAMAM dendrimer system as reported by Alper *et al.*[108]. The circle represents a silica surface.

While dendrimers are largely thought of as homogeneous catalytic systems, there have been examples of heterogeneous systems. Alper and co-workers have explored dendritic wedges with terminal diphenylphosphine groups mounted on silica, creating heterogeneous systems used for rhodium catalysed hydroformylation. Both PAMAM and phenyl propionaldehyde branches were considered and gave good activities and selectivities for low generations. High generations showed lower activities thought to be due to steric congestion, a hypothesis proven by adding a spacer arm to the branches that showed higher activities[108-113, 114]. The silica bead support proved advantageous over polymer supports giving higher activities and speculate that co-operation between ligand groups is a factor in the high activities obtained. This heterogeneous system showed comparable activities with homogeneous systems.

1.3.7.2 Core Catalytic Groups

Placing ligating groups at the core of a dendrimer allows the dendritic branches to isolate the catalytic site or create a more sterically demanding environment to impart shape-, size- or enantio- selectivity. Many examples of terminal ligating groups have been reported but far fewer examples of core catalysis exist, perhaps due to more complex and less obvious synthetic routes to such molecules.

Suslick and Moore reported porphyrin cored dendrimers with polyphenylester

dendrons attached as ligands for manganese catalysed epoxidation of dienes[115,116].

The dendrimer complex showed increased selectivity for the conversion of external

alkenes with less hindered vinyl groups and an increased stability towards oxidation.
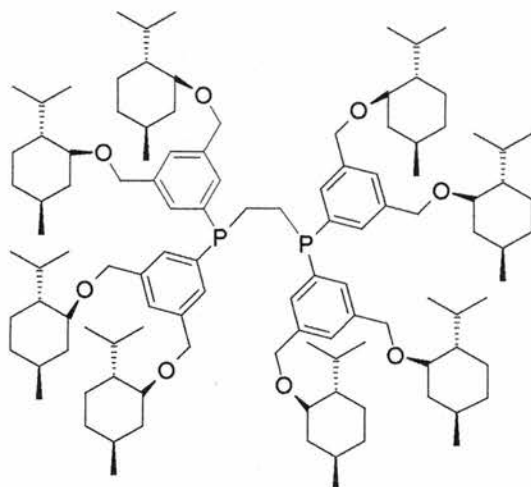
Figure 1.22: Adapted from Brunner *et al.*[117] Expanded phosphine ligand functionalised with (-)-
menthol.

Bis-Diphenylphosphinoethane provided the core for dendrimers reported by Brunner

et al.[117]. They coined the term *dendrizyme* as it was a large molecule with a single

active catalytic site similar to enzymes. The dendrimer was used as a ligand for the

transition metal catalysed enantioselective hydrogenation of acetamidocinnamic acid.

There was no great enantioselectivity observed in the products but some reduction of

hydrogenation of the substrate occurred and was thought to be due to defects in the

dendritic structure. A higher enantioselectivity was observed for the

cyclopropanation of styrene using a different dendritic ligand based on a 2,6-

pydridinediimine copper complex.

Copper catalysed Diels-Alder reactions were the subject of Chow's attention[118-120].

Three generations of dendritic bisoxazoline ligands were made and while G0 – 2

showed similar selectivities, G3 showed a large drop in activity thought to be due to

the greater steric congestion at the metal centre.

References for Chapter 1 begin on page 70

Oosterom *et al.* prepared carbosilane dendrimers with bis-diphenylphosphinoferrocene cores and studied the effects of generation on palladium catalysed allylic alkylation reactions[121,122]. Increasing generation again lead to decreasing activity and sterioselectivity also decreased over the model (non-dendrimeric) species.

The use of dendrimers as catalysts is an expanding area of research and the novel structures being created can impart unique properties to the reactions, be it higher activity, greater selectivity or enhanced catalyst stability. There have been few studies into this so-called *dendritic effect*, asking why some dendrimers make better catalysts than the small molecule analogues why dendrimers are poorer catalysts. It may simply be due to the number of catalytic sites available on the periphery co-operating constructively or because of the microenvironment created at the core of a molecule due to the dendritic branches. In any case, research into this area is likely to yield far more questions than answers.

1.4 Computer Modelling of Dendrimers

1.4.1 Introduction

The problem of accurately characterising dendrimers and determining some of their structural properties was discussed in section 1.3. There has been a great deal of interest in the location of the dendrimer's terminal groups – do they form a shell on the surface of the dendrimer, or do some of the terminal groups fold back into the interior of the molecule? The effect of generation on the location of terminal groups is of interest especially when there comes a point when no more monomer units can be added to a dendrimer without causing defects. This has implications for many applications of periphery functionalised dendrimers including catalysis, liquid crystals and some biological applications where perfect structures are required. It is likely that one reason for defects forming (except through side reactions) is that the reactive ends of branches have folded into the interior of the dendrimer making them unavailable to react further.

The size of dendritic macromolecules has limited the number of computational studies to date. Until recently, such calculations (on systems with over 500 atoms) have been limited to theoretical models resembling beads joined by sticks or lower generations of molecules. Quantum mechanics methods are not possible on such large molecules and so molecular mechanics/dynamics techniques have been widely used. Images generated from molecular mechanics/dynamics studies can give good insight into the size and shape of the molecule and so appear in many synthetic papers. For the purpose of this introduction to computational studies of dendrimers, these will be not be considered.

The first theoretical model of a dendrimer like molecule was proposed in 1983 by de Gennes[65]. This model predicted that the terminal groups of the dendrimers would be

located in concentric circles surrounding the core. As the number of generations increase so the number of terminal groups increase and at a certain size the dendrimer can grow no more due to the formation of a tightly packed outer shell of terminal units. The core of the molecule was predicted to be the least dense region and all monomers were assumed to be fully elongated. This became known as the de Gennes close packed state and did not allow for the possibility of backfolding of the terminal groups into the core to relieve unfavourable steric interactions on the periphery.
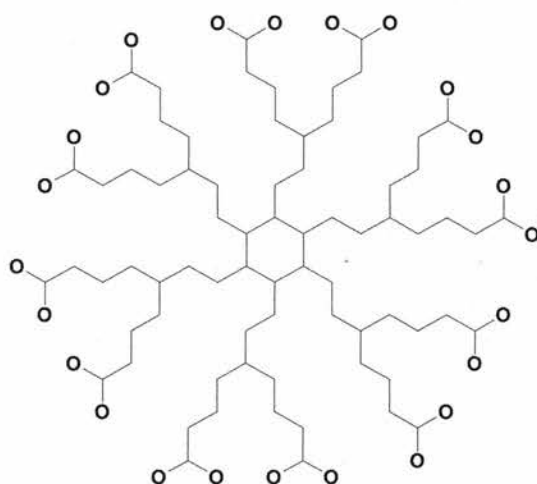
Figure 1.23: Schematic representation of dendrimer showing fully expanded branches and shell of terminal groups as predicted by de Gennes[65].

The idea of dendritic growth being limited by the size of the molecule has been confirmed by kinetic studies where it was found that above a certain generation, reaction kinetics fell and no more monomer units could be added without a great number of defects being created[123]. This is also called the starburst limiting generation, referring to one of the original names for dendrimers, starburst molecules.
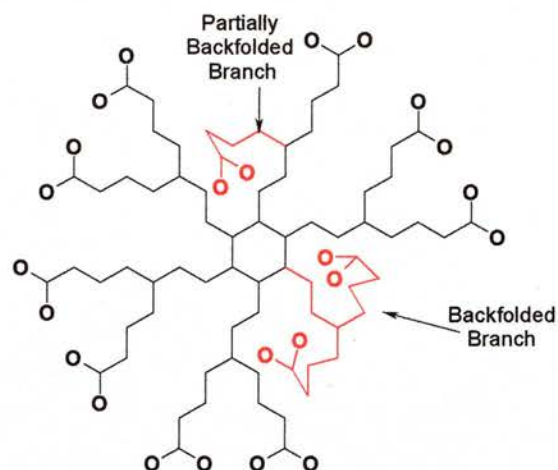
Figure 1.24: Schematic representation of a dendrimer showing backfolded branches eliminating steric congestion on molecules surface.

Other theoretical studies have explored the concept that branches may contract and fold back into the dendrimer, relieving some of the steric stress caused by the congestion but also removing some terminal groups from further reaction, leading to defects. There are some points on which the majority of modelling and experimental studies of dendrimers seem to agree. Firstly, the idea of the starburst or closepacking limit is widely acknowledged as the point at which it is no longer possible to synthesise perfect dendritic architectures. Whether it is due to back folding or close packing is still a matter for debate. Secondly, the shape of the dendrimer becomes increasingly spherical (globular) as it gets larger, regardless of core shape. The transition to a spherical shape is often reported as occurring between generations 3 and 5 of growth. Finally, the propensity of a branch to fold back into the interior of the dendrimer is largely dependent on the length and nature of the monomers of which the branch comprises, and the size of the terminal units.

Various molecular mechanics/dynamics programs have been used to model dendrimers and the emphasis for the studies lies largely with obtaining a suitably equilibrated structure for analysis. It is important that this represents the average structure of the molecule and is free from artefacts from the construction of the model.

As PAMAM dendrimers were the first examples of this polymer type, it is unsurprising that they have been widely studied by computational techniques. These studies have varied from simple assessments of the shape and distribution of terminal groups to studies on the effect of pH on amine terminated molecules.

Terao *et al.* studied the effect of varying pH on the conformation of a range of generations of PAMAM dendrimers and compared the results with small angle neutron scattering (SANS) studies made previously[124]. In order to study the effect of pH on the dendrimers, the following assumptions were made. In high pH, it was assumed that no amine groups of any kind were protonated while at neutral pH it was assumed that only primary (terminal) amines were protonated. At low pH all amines were assumed to be protonated, whether terminal or internal (secondary or tertiary). Monte Carlo simulations were used to generate structures for analysis and molecular dynamics was used to produce equilibrated structures and data for analysis. It was found that the radius of gyration depends strongly on the properties of solvents at low generations, while at high generations the greater steric demand of the molecule means that the solvent / pH dependence of the molecule is less. This was in agreement with several SANS studies.

Lee *et al.* carried out a similar study on PAMAM dendrimers with a 1,2-diaminoethane core at varying pH in aqueous media[125]. Initial calculations were carried out on second-generation dendrimers with explicit water molecules to obtain proper conditions and validate later simulations without explicit solvent. A 10 Å thick shell of water was incorporated around the dendrimers to ensure that hydrogen bonding would be accurately represented and under these conditions the second generation dendrimer was found to be globular at high pH with back folded

branches, moving to a more expanded structure at low pH. The simulation conditions best found to mimic the effect of water molecules was to include a distance dependent dielectric term without any cut-off. This was used for longer simulations of higher generation dendrimers that are very difficult to do with explicit solvent (more molecules, longer time required). The same assumptions with regard to effects of pH on the PAMAM dendrimer were made as Terao *et al.* but were made from pH titration data and low, neutral and high pH were studied[124]. The dendrimers were found to be globular and loosely compact at high pH and ordered, extended structures at low pH with an increasingly hollow interior with increasing generation. At neutral pH, back folding of the branches occurred, creating a density maximum between the core of the molecule and its maximum radius. This also increased with generation. Generations 4 and 5 were notable for high-density structures. The radius of gyration was also calculated and for neutral and low pH showed that dramatic increases in molecular volume occurred from generation 5 onwards.
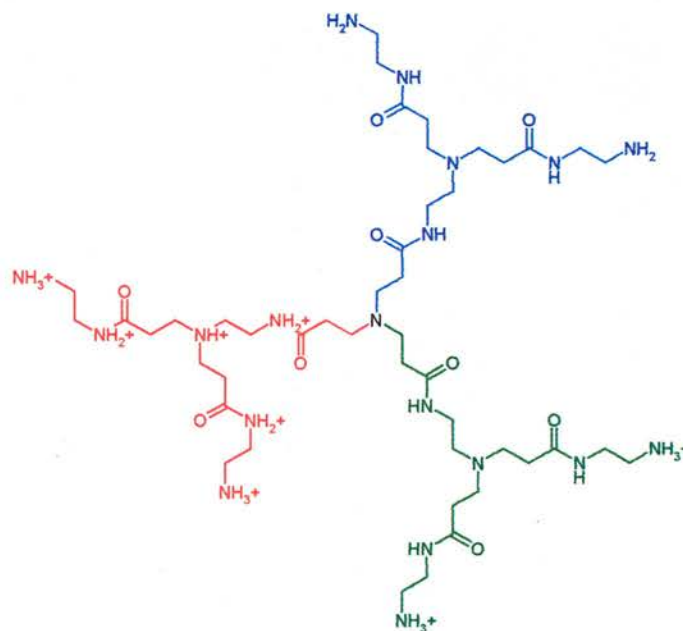
Figure 1.25: PAMAM dendrimer with three branches indicating different pH. Blue branch – high pH, no protonation of amines; Green branch – neutral pH, protonation of primary amines; Red branch - low pH, protonation of all amines[124].

Striegel *et al.* used a similar approach in to study PAMAM (again with a diaminoethane core), Poly (propyleneimine) dendrimers and polysaccharides using the CVFF force field[126]. A 10 Å thick shell of water was used in the simulation and the radii of gyration calculated. Comparison of this data to that obtained from size exclusion chromatography revealed similar values and identical trends for the three types of molecules studied.

Uppuluri *et al.* also studied PAMAM dendrimers from generation 0 – 6 with diaminoethane cores [127]. All structures were drawn, minimised and allowed to equilibrate at 300 K for 50 ps under the CVFF force field. The fourth generation dendrimer was found to have a dense impenetrable outer shell and it was thought that intermolecular penetration might occur at lower generations with hydrogen bonding occurring between internal amines for the first generation. In general, the structures were found to have dense outer shells and less dense cores above a certain generation. Above a certain size, around generations 3 - 5, the molecules were found to undergo a structural change characterised by a stepwise decrease in the primary aspect ratio indicating a change from plate-like to globular shapes.

In general, the terminal amines of PAMAM dendrimers are found to be distributed throughout the structure, with the limiting generation being found at G10 or G11. Maiti *et al.* suggested that the strain is sufficient beyond G10 to result in incomplete reaction[128]. For most studies, a change in shape of the dendrimers was noted, occurring between the third and fifth generations. Molecules larger than G5 were generally found to be spherical, those below G3 were found to reflect the shape of the core and G4 reflected the transition between those two shapes.

1.4.3 Other Dendrimers
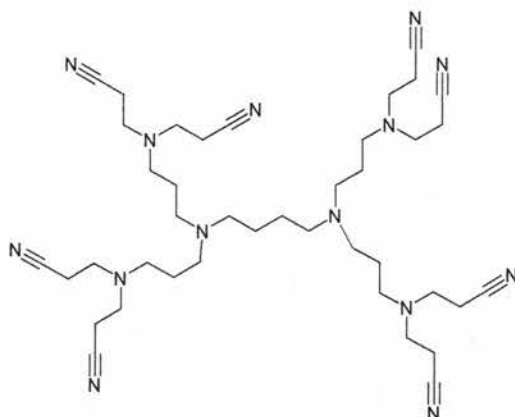
Figure 1.25: Second generation poly(propyleneimine) dendrimer with nitrile terminal groups. As modelled by Zacharopoulos[129] and Scherrenberg[130].

Comparisons of molecular modelling data to SANS and viscosimetry data were carried out by Scherrenberg *et al.* [130]. In general, molecular dynamics simulations were found to give good results that correlated well with data obtained from SANS and viscosimetry studies. Five generations of poly (propyleneimine) dendrimers with a 1,4-diaminobutane core and 4,8,16, 32 and 64 amine terminal groups respectively were studied. Both the amine and nitrile terminated dendrimers were studied by SANS and viscosimetry, but only the amine form was modelled. The CVFF force field was used and modified to represent the cases of good and poor solvents. CVFFC included both Coulombic and van der Waals interactions between non-bonded atoms and represented a poor solvent that enhanced intermolecular interactions. CVFFREP included only repulsive van der Waals interactions to represent a good solvent, shielding the molecule from intermolecular interactions. These solvent conditions cannot be directly correlated with standard dielectric constants (as measured physically for solvents) because altering the mathematical form of the force field produces a different effect for each type of molecule. Calculation of the radius of gyration for each of the molecules from SANS showed a linear relationship with generation and in general, amine terminated molecules had larger dimensions than nitrile terminated dendrimers. The polarity of the end groups

was thought to exert influence on the size resulting in a series of molecules with dimensions directly dependent on molecular mass, contradicting the conclusions of de Gennes[65]. Modelling the dendrimers in poor solvent gave more collapsed structures with a high degree of back folding of the branches. A good solvent resulted in more extended structures. In order to verify the validity of the simulations small angle scattering curves were generated from the structures and the radius of gyration calculated. These values were compared to the experimentally derived values and it was found that the simulations represented the extreme cases of a good and poor solvent with the experimental values lying between the extremes. This implies that the molecules in solution have a slightly compact structure with some back folding, not as much as observed with the poor solvent but more than in the good solvent. In general the dendrimers were found to be flexible molecules with relatively homogenous density distributions, again contradicting studies by de Gennes (predicted a dense shell and less dense interior)[65].

Poly (propyleneimine) dendrimers were also the subject of an in-depth study by Zacharopoulos *et al.*[129]. The properties of generations 2 - 5 in the melt were studied by molecular dynamics simulation at 400 K. Higher generations were found to be more spherical as the dendron overlap increases but a greater increase in dendron overlap was observed between generations 2 and 3 than 4 and 5. Generation 5 was found to have a greater instance of back folded branches. This was highlighted by the fact that the distribution of terminal groups, centred around the radius of gyration (Rg) for lower generations in a unimodal distribution, shifted to a trimodal distribution with the radius of gyration at the centre. It was predicted that very high generations would give a bimodal distribution with a corresponding depletion of terminal groups around Rg.

Careful studies of the relaxation properties of the dendrimers were also made. The relaxation time for the dendrimer was calculated using the autocorrelation function and used to measure the effect of molecular relaxation on the distribution of the terminal groups studied. In the case of the fifth generation, the terminal group distribution moved from a high-energy unimodal distribution to a lower energy trimodal distribution as the molecule relaxed.

The synthesis of a new family of polyamide dendrimers from 5-hydroxyisophthalic acid and diethanolamine prompted a computational study by Ashton *et al.*[131]. A stochastic approach with the AMBER force field was used and equilibrium structures were derived from a 300 K molecular dynamics run for six generations of the dendrimers. For low generations (generation 2) a high degree of conformational freedom was observed with increasing steric congestion becoming apparent by the fourth generation. This lead to a more globular structure with the terminal groups still mainly on the surface indicating that the steric congestion was not yet great enough to force much folding back of branches. Similar results were obtained for the sixth generation, which gave a globular structure with channels and voids in the interior and the majority of terminal groups on the surface. An assessment of the energetic properties of the sixth generation revealed that it could be feasible to synthesise it. In all cases the average radii of the dendrimers were calculated and compared to Gel Permeation Chromatography (GPC) results for solutions of the molecule. Good agreement was found in all cases, including the largest (G6).

An earlier publication by Ashton *et al.* involved the study of carbohydrate containing dendrimers[132]. These molecules were synthesised first by convergent means through the glycosylation of primary hydroxyl groups of tris(hydroxymethyl)methylamine. This created individual branches that could be

attached to a 1,3,5-trisubstituted benzene core creating dendrimers with nine and

eighteen saccharide groups.
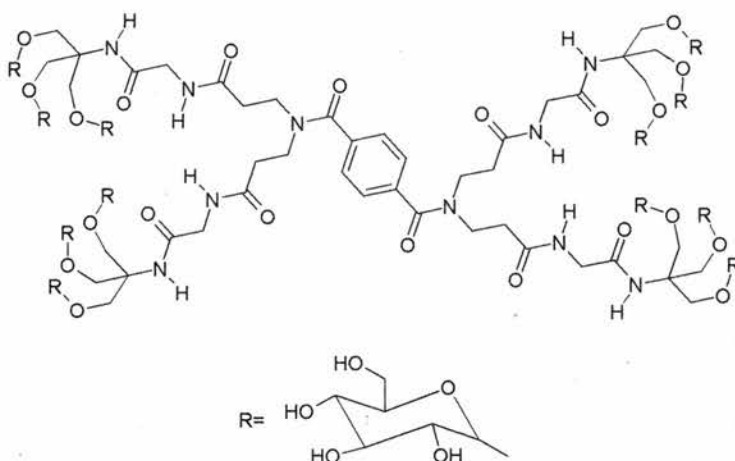
Figure 1.26: Carbohydrate terminated dendrimer with terephthaloyl core as reported by Ashton *et al.* [132]

Both the protected and unprotected molecules were studied. There was an increase

in the average molecular radius of about fifty percent on going from generation 1 to 2

but a small decrease in the expected distance of the terminal groups from the core of

about seven percent. This was measured between the quaternary carbon on the

benzene core and the monosaccharide terminal group. This was taken to imply that

there was further scope for enlargement of these dendrimers to a third and perhaps

fourth generation as there was no steric congestion of the surface or interior

observed. Deprotection of the dendrimers eased the steric compression of the

dendrimers, shown through a decrease in molecular radius. The molecular volume of

the deprotected versions was approximately half that of the protected version and in

general generation 2 had twice the volume of generation 1. The deprotected

dendrimers formed hydrogen bonded networks within the branches, most apparent in

generation 2, which might account for the observed decrease in molecular volume

(along with the loss of the large protecting groups). A visual inspection of the

equilibrated structures showed highly symmetrical molecules with G1 having an

open, spacious structure and G2 a more densely packed and annular configuration.

More rigid dendrimers were studied by Pricl *et al.*comparing three cores and

corresponding polyphenylene dendrimers[133].
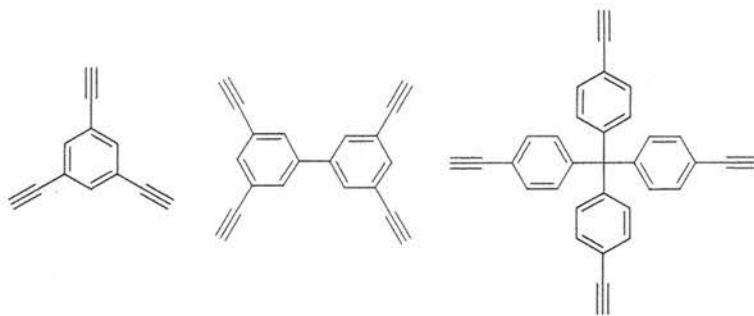
Figure 1.27: Tri- and Tetra- functionalised cores for polyphenylene dendrimers from Pricl *et al.*[133].

The structures were prepared for analysis through a simulated annealing protocol.

The dendrimers were generally found to be shape persistent with non-spherical

structures. The starburst limited generation was found to be the third generation..

During the simulations, the arms of the dendrimer can move but the overall shape

does not alter significantly. The core architecture is amplified by the dendrimer

structure for all three cores. The molecular surface was assessed using the Connolly

dot surfaces algorithm to calculate the solvent accessible surface. The surface area

increased predictably with generation and the largest of the three cores studied lead

to the greatest surface area. The surface area per terminal group was calculated

according to the formula:

$$Az = \frac{A}{Nz} \alpha \frac{R^2}{NcNb^g}$$

Figure 1.28: Az – Surface area per terminal group; A – surface area of molecule; Nz – Number of
terminal groups for generation z; R – Dendrimer radius; Nc – Core multiplicity; Nb – Branch juncture
multiplicity; g – Generation.

The surface area per terminal group increased going from generation 1 – 3 but the

rate of increase slowed owing to increasing steric congestion. This was taken to

imply that G3 was the starburst limit.

1.4.4 Encapsulation

Many potential applications of dendrimers arise from their ability to encapsulate species such as dye molecules or create microenvironments around parts of their structure. Examples that have been subject to molecular modelling studies include encapsulation of the root of a dendron[134], Bengal Rose type molecules[135] and protoporphyrinic cores on dendrimer for evaluation as myoglobin oxygen carriers[72]. Many applications for dendritic macromolecules involve their propensity for host-guest chemistry. Miklis *et al.* made a comparative study of encapsulation of Bengal Rose (BR) molecules with in poly (propyleneimine) dendrimers, with and without large tert-butyloxycarbonyl-L-phe terminal groups[135]. These terminal groups acted as caps on the molecular structure, containing the encapsulated groups. Fifth generation dendrimers without these capping groups allowed the BR molecules to leave their cavities within the dendrimer, moving to the surface and further into the bulk solvent whereas the terminal groups were bulky enough to create a more solid shell on the dendrimer inhibiting this diffusion.
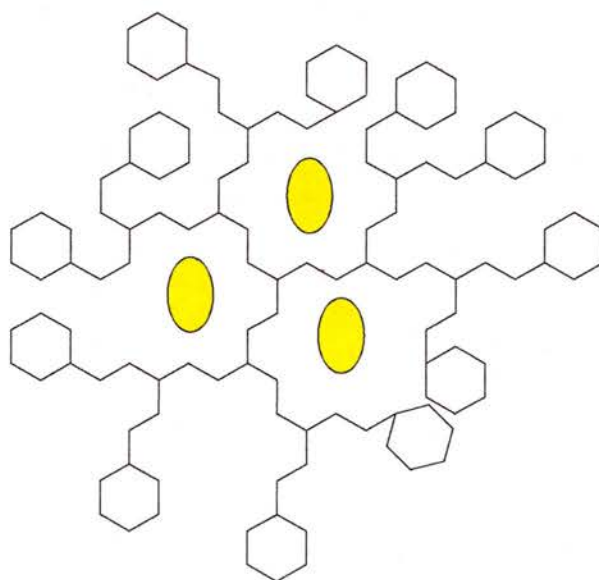
Figure 1.29: Schematic representation of three encapsulated molecules in second generation dendrimer, trapped by large terminal groups, adapted from Miklis *et al.* [135].

The molecules were modelled in explicit dichloromethane solvent molecules in order to mimic experiment as closely as possible and good agreement with actual chemical results was obtained. This is a good example of the benefits of a bulky shell of terminal groups.

Carbosilane dendrons were the subject of a molecular dynamics study by Gossage *et al.*[134]. 4-bromophenol was converted to first and higher generation dendrons by the addition of triallylsilane and larger derivatives. The gas phase structures were created for visual inspection and the terminal allyl groups were found to encapsulate the phenol (and protected phenol) core creating a distorted sphere shape.

Haemoglobin and Myoglobin mimics have long been a goal of medicinal chemistry. The problem lies in finding a discrete molecule large enough to bind oxygen to an iron centre in a stable manner whilst maintaining the reversibility of the reaction. Fermeglia *et al.* undertook a study into a dendrimer with a protoporphyrin core capable of binding to an iron (II)-dioxygen-hystidine residue[72]. At high generation (G5) this was found to behave similarly to myoglobin and bind oxygen reversibly. The core was surrounded by aryl ether branches forming dendrimers from G1 to G5.
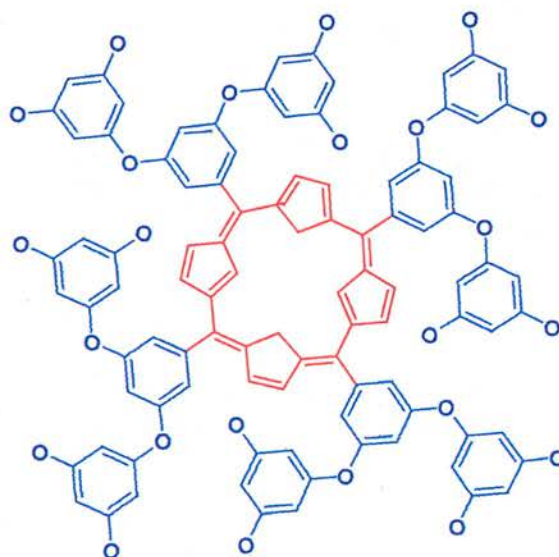
Figure 1.30: Aryl ether dendrimer with protoporphyrin core as studied by Pricl *et al.* [72]. Protoporphyrin core shown in red, dendritic branches in blue.

Two effects were obvious on increasing generation. Firstly, the molecules became more spherical, shown by the aspect ratios tending to one, and secondly, the core became more encapsulated as the branches surrounding it got larger. Generations 1 through 3 are asymmetric but generations 4 and 5 are nearly spherical. Importantly, the rigid shape of the protoporphyrin is not distorted as large branches are attached. Both the free dendrimer ligand and the Fe (II)-O_2-Hystidine complex were studied, and it was found that complexation to the iron caused the aspect ratios to increase. This implied that the molecule becomes less spherical due to the complex hindering closest packing of the dendrimer branches. The radius of gyration increased with increasing molecular mass in both cases. The surface area of the dendrimers and the dendrimer-complexes were calculated by the Connolly Algorithm and comparison of the van der Waals molecular surface for generation five and myoglobin revealed very similar configurations with similar fractal dimensions (approx. 3.2). The fractal dimension increases with increasing generation. The surface area per terminal group for the dendrimer increases for generation 1-3 and levels out for generations 4 and 5. The surface area per terminal group for the dendrimer-complex decreases from generation 1 – 5 due to the steric hindrance of the hystidine complex and increased hydrogen bonding between the complex and the dendrimer. On the whole, the presence of the complex does not alter significantly the behaviour of the parent molecule, most notably when the energetics are considered. The valence contribution to the total potential energy increases with generation while the non-bonded contribution decreases. This causes the potential energy to decrease for generations 1 – 3, increase sharply for generation 4 and begin decreasing again for generation 5. This means that the potential energy for generation five is lower than generation four due to the sharp decrease in the non-bonded contribution.

In contrast to porphyrin core dendrimers, Bhalgat evaluated PAMAM dendrimers with terminal porphyrin groups[136]. Generations 3 and 4 were studied with ammonium cores. The third generation was found to have an open, expanded structure where as the fourth was denser. This was in keeping with the findings of Naylor *et al.* who described G4 as an intermediate between asymmetrical G1-3 and the spherical G5[137]. All terminal groups lay on the exterior but the large size of the porphyrins covered a large proportion of the dendrimer surface, potentially limiting access to the surface for other porphyrins or smaller molecules.

1.4.5 Dendritic structure and Chirality

While the majority of dendrimers are not chiral, several examples have been reported of dendrimers functionalised with chiral amino acids. Cavallo *et al.* studied poly (propylene) dendrimers functionalised with L-phenylalanine[138]. The amino acids were protected and generations 1 – 5 with 4, 8, 16, 32 and 64 terminal groups were investigated. In general, the shape of the molecules was found to be generation dependent with higher generations more spherical, indicated by aspect ratios tending to 1. The amino acids were not confined to the surface despite their bulk (and the bulk of the protecting groups).
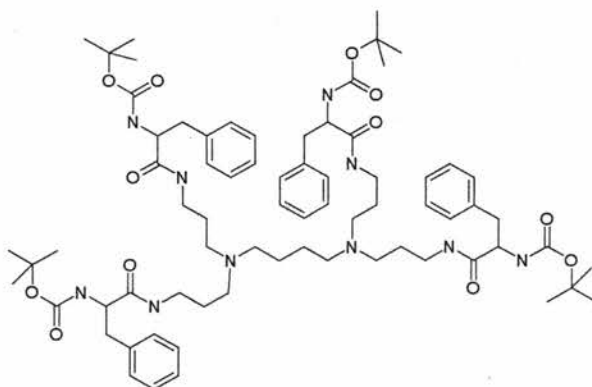
Figure 1.31: First generation poly (propylene imine) dendrimer modified with N-tBoc-L-Phenylalanine terminal groups[138].

The dendrimers were also found to have increasingly less dense interiors at higher generations with a lower percentage of interresidue hydrogen bonds occurring at the highest generations. The dendrimers possessed a flexible core and rigid chiral shell. Generation 6 with 128 protected amino acids could not be fully functionalised due to steric influences and it was found that the optical activity of the dendrimer solutions decreased with increasing generation. Importantly this was not due to common influences such as racemization, concentration, temperature or solvent effects.

The radius of gyration increased linearly with generation, as did the distance of the alpha carbon on the amino acids from the centre of mass. The distribution of the distances of Cα from the centre of mass was sharp for low generations indicating that the amino acids were all on the surface and broad for high generations indicating backfolding of the amino acids. There was less flexibility in high generations leading to closer packing of the branches and the general density profiles went from smooth (G1) to broad and bumpy (G5). The overlap of individual dendrons decreased with increasing generation, sharply for G1 – 3 and less so for G3 – 5. The solvent accessible area was smaller per atom for the higher generation with greater excluded volumes being present. The decrease in optical activity was thus ascribed to the increasing conformational disorder in the higher generations, including back folding of branches, change in density distribution and steric crowding effects.

Fréchet type poly (benzyl phenyl ether) dendrimers (PBPE) were studied by Ortiz *et al.* to gain insight in to the topology of the molecules for better understanding of experimental investigations into their photophysical properties[139]. It was demonstrated that the closeness of the terminal groups to the core of the molecule had a significant effect on energy transfer rates throughout the molecule through short donor-acceptor distances.
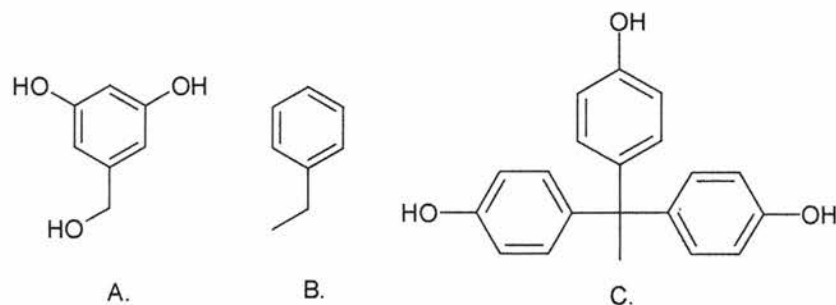
Figure 1.32: A: 3,5-dihydroxybenzylalchol, repeat unit; B: benzyl terminal unit and C: 1,1,1-tris(4'-hydroxyphenyl)-ethane[139].

The core of the molecule was 1,1,1-tris(4'-hydroxyphenyl)-ethane with 3,5-dihydroxybenzyl alcohol repeat units and benzyl groups for terminal groups and four generations were studied. Structures were drawn, minimised and equilibrated at 273 K before data was collected for analysis. The average radius of gyration was found to increase with generation, increasing linearly with the increasing number of terminal groups. This was taken to imply that the dendrimers were globular, with dense cores, backed up by visual inspection of structures from the simulation. The results also correlated well with a previous study by Naidoo *et al.* but gave only qualitative agreement[140]. This discrepancy was thought to be because the simulations were carried out with no solvent and in vacuo while the experiments were performed in THF, interactions with solvent leading to structures that are more open. The impact of various branches on the core was measured through calculation of the root-mean-square displacement of the core atoms showing that the displacement falls as the size of the branches increases. It was proposed that the steric effects of longer branches may make movement of the core more difficult, or that the structure is more stiff and so individual parts are not as free to move in high generations when compared to lower generations. The location of the terminal groups was probed by looking at the atomic density profile of the molecules. Evidence for backfolding was found in the fourth generation, in the form of a greater atomic density where the other generations had less density. In general, the

molecules were found to have dense interiors contradicting findings by de Gennes

and Hervet[65].

1.4.6 Summary

The wide range of molecules studied by molecular modelling techniques throw up a

number of apparent contradictions. The most debated is whether de Gennes was

right, and dendrimers have a very dense outer shell of terminal groups, or whether

other theories involving back folding are correct. A recent review by Ballauff *et al.*

sheds some light on this problem by summarising the theoretical models to date[141].

Authors	Density Profile	Terminal Group Distribution
De Gennes and Hervet	Dense shell	Localized
Boris and Rubinstein	Dense core	Spread out
Timoshenko, Kuznetsov and Connelly	Dense core	Spread out
Zook and Pickett	Dense core	Spread out

Table 1.6: Adapted from Ballauff *et al.* showing contrasting theories on the location of terminal groups and the density of dendrimers[141].

In general, the majority of theoretical studies, both molecular modelling and other

techniques favour the idea that the terminal groups in a dendrimer are located

through out the molecule, perhaps folding back into the structure to relieve the steric

stress at the surface. The idea of a dense shell of terminal groups has proved useful,

with Miklis *et al.* using a shell of large terminal groups to encapsulate molecules

within the dendrimer[135].

1.5 Modular Materials

POSS organic-inorganic hybrid materials are generally small molecules, large random polymeric systems or large macromolecular systems with some order such as dendrimers. Small POSS crystals are ordered but that is less apparent in large polymeric networks. It is extremely desirable to synthesise a large POSS network structure with long range order, structures that would mimic many zeolite type frameworks with chains, sheets or 3-dimensional cage structures. Such materials could be thought of as being made from POSS building blocks, often referred to as "*Lego Chemistry*" although the execution of the concept is far more complex than the name suggests. The idea of synthesising suitable building blocks and trying to link them together produces materials often referred to as metal-organic frameworks (MOF) or co-ordination polymers (although the latter tends to be based more in supramolecular chemistry and self-assembly rather than mesoporous materials techniques).
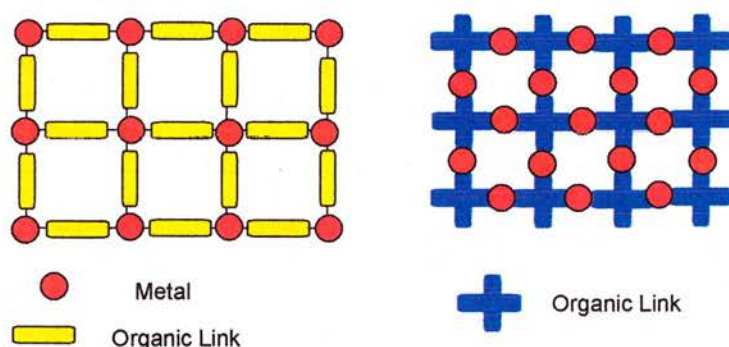
Figure 1.33: Schematic representation of metal organic framework showing metal centres linked by organic groups in a regular way using the metal as either a 'node' or a linear link.

These materials comprise a metal atom (can be thought of as a node) and organic molecules (linkers) with suitable functional groups for co-ordination. The way in which the linkers and nodes are assembled defines the structures. Suitable functional groups on the organic linkers include amines, phosphines but mostly carboxylic acids

creating metal carboxylate structures. The reaction conditions are generally mild –
solvothermal synthesis at room temperature or above[142]. Sun *et al.* reported silver
carboxylate polymers based on di-, tri- and tetrasubstituted benzenes shown in figure
1.34[143].
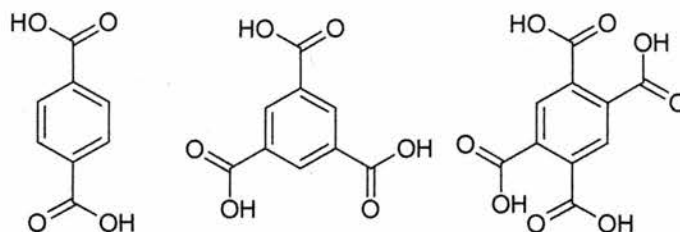
Figure 1.34: Building blocks used by Sun *et al.* for silver carboxylate polymers[143].

Open framework metal carboxylates have been reviewed by Rao *et al.* and
demonstrate the variety of structures synthesised and metals used, as well as other
functionality that can be incorporated[144]. The modular nature of these materials was
well demonstrated by Yaghi *et al.* who showed that varying the lengths between
carboxylate groups on the organic linkers controlled the size of the pores or could be
used to introduce additional functionality[145]. A class of metal organic frameworks
with the role of the metal and organic molecules inverted was reviewed by
Papaefstathiou *et al.* (figure 1.33) [146]. Such inverted-MOFs have organic nodes and
transition metal ions as linear bridges and utilise principles from supramolecular
chemistry for further functionalisation.

More bulky groups such as tris(diphenylphosphanyl)benzene have been used to
produce 2D-networks by reaction with silver salts[147,148], and examples of gold co-
ordination polymers have been reported[149].

The idea of designed materials with controllable pore sizes and functionality is
essential for many potential applications for these materials such as catalysis[150]. It
has been demonstrated that incorporating pre-existing ligands into larger assemblies
can positively influence the catalytic processes, gas storage or non-linear optical
applications[151]. While all the examples above use small organic molecules formed

into frameworks or polymers, POSS molecules offer a chance at MOF synthesis

using preformed cages. This would greatly increase the chances of producing

framework structures with D4R cages and similar structures to zeolites but with

functionality and through reaction conditions associated with co-ordination

polymers.

1.6 Aims and Objectives

There are two main aims of this project:

1. Gain a better understanding of POSS based dendrimers, particularly catalysts, by molecular modelling techniques

2. Synthesis of new dendritic architectures with POSS cores as supports for homogeneous catalysts by the convergent route.

The aims can be broken down individually into a series of objectives.

Aim 1:

a. Develop a molecular modelling protocol for POSS dendrimers using the Materials Studio Program to produce structures for analysis. This should include assessing the effects of temperature and solvent on the structures.

b. Develop methods of analysing molecular modelling data to gain information about the shape, size and distribution of the terminal groups of the dendrimers

c. Carry out molecular modelling studies of three POSS based alcohol dendrimers using Materials Studio

d. Carry out molecular modelling studies of a series of POSS based diphenylphosphine dendrimers used as catalysts using Materials Studio

e. Develop suitable parameters and protocol for the MM+ force field in the Hyperchem program to enable bite angle and flexibility calculations to be carried out on the POSS based diphenylphosphine dendrimers

f. Develop a suitable protocol for the MM+ force field in the Hyperchem program to enable a rhodium complex to be modelled and the effect of the complex on POSS based diphenylphosphine dendrimers to be assessed.

Aim 2:

a. Devise feasible routes towards the convergent synthesis of dendrimers with the POSS core, with the potential to be functionalised on the periphery with ligating groups for catalysis.

b. Synthesise suitable dendritic branches for attachment to the POSS core for convergent dendrimer synthesis.

c. Synthesise suitably modified POSS molecules for convergent dendrimer synthesis.

d. Synthesise multifunctional POSS cubes with potential to be functionalised in different ways to create molecules with ligating groups and modifying groups (e.g. fluourous ponytails, water-soluble groups etc.).

e. Attach dendritic branches to the POSS core and fully characterise the products by solution NMR, Mass Spectrometry (MALDI-TOF) and other methods.

f. Synthesise POSS dendrimers by a totally convergent approach, forming the POSS core in the final reaction step through condensation of appropriately functionalised trichloro- or triethoxy- silanes.

g. Modify the POSS dendrimers with ligating groups suitable for supporting transition metal complexes for homogeneous catalysts.

All of the goals set for aim 1 were achieved successfully during this project as were goals a, b and c for aim 2. 2d, 2e and 2f were partially achieved but due to this, 2g was not attempted.

1.7 References

1. A. K. Cheetham, G. Ferey and T. Loiseau, *Angew. Chem., Int. Ed. Engl.*, 1999, **38**, 3269.

2. C. S. Cundy and P. A. Cox, *Chem. Rev*, 2003, **103**, 663.

3. R. H. Baney, M. Itoh, A. Sakakibara and T. Suzuki, *Chem. Rev*, 1995, **95**, 1409.

4. P. A. Agaskar and W. G. Klemperer, *Inorg. Chim. Acta*, 1995, **229**, 355.

5. Armitage D. A., Edward Arnold Ltd, London, 1972, p. 218.

6. H. Burgy, G. Calzaferri, D. Herren and A. Zhdanov, *Chimia*, 1991, **45**, 3.

7. N. Auner, B. Ziemer, B. Herrschaft, W. Ziche, P. John and J. Weis, *Eur. J. Inorg. Chem.*, 1999, 1087.

8. D. Hoebbel, C. Weber, H. Schmidt and R. P. Kruger, *J. Sol-Gel Sci. Techn.*, 2002, **24**, 121.

9. C. Bolln, A. Tsuchida, H. Frey and R. Mulhaupt, *Chem. Mater.*, 1997, **9**, 1475.

10. P. A. Agaskar, *Inorg. Chem.*, 1991, **30**, 2707.

11. C. Bonhomme, P. Toledano, J. Maquet, J. Livage and L. Bonhommecoury, *J. Chem. Soc., Dalton Trans.*, 1997, 1617.

12. S. Lucke and K. Stoppek-Langner, *Appl. Surf. Sci.*, 1999, **145**, 713.

13. S. Lucke, K. Stoppek-Langner, J. Kuchinke and B. Krebs, *J. Organomet. Chem.*, 1999, **584**, 11.

14. F. J. Feher and K. D. Wyndham, *Chem. Commun.*, 1998, 323.

15. J. W. Choi, R. Tamaki, S. G. Kim and R. M. Laine, *Chem. Mater.*, 2003, **15**, 3365.

16. R. M. Laine, J. W. Choi and I. Lee, *Advanced Materials*, 2001, **13**, 800-+.

17. R. Tamaki, Y. Tanaka, M. Z. Asuncion, J. W. Choi and R. M. Laine, *J. Am. Chem. Soc.*, 2001, **123**, 12416.

References for Chapter 1 begin on page 70

18. A. Barry, *J. Am. Chem. Soc.*, 1955, 77, 4248.

19. F. J. Feher, K. D. Wyndham, D. Soulivong and F. Nguyen, *J. Chem. Soc., Dalton Trans.*, 1999, 1491.

20. A. R. Bassindale, I. A. Mackinnon, M. G. Maesano and P. G. Taylor, *Chem. Commun.*, 2003, 1382.

21. I. Richter, C. Burschka and R. Tacke, *J. Organomet. Chem.*, 2002, **646**, 200.

22. D. Scott, *J. Am. Chem. Soc.*, 1946, **68**, 356.

23. R. Muller , *J. Prackt. Chem.*, 1959, **9**, 71.

24. C. Frye and W. Collins, *J. Am. Chem. Soc.*, 1970, **92**, 5586.

25. M. D. Nyman, S. B. Desu and C. H. Peng, *Chem. Mater.*, 1993, **5**, 1636.

26. M. G. Voronkov and V. I. Lavrentyev, *Top. Curr. Chem.*, 1982, **102**, 199.

27. K. R. Gopidas, J. K. Whitesell and M. A. Fox, *Nano Letters*, 2003, **3**, 1757.

28. F. J. Feher, K. D. Wyndham, M. A. Scialdone and Y. Hamuro, *Chem. Commun.*, 1998, 1469.

29. H. Kobayashi, *Makromol. Chem.*, 1993, **194**, 2569.

30. J. Speier, *J. Am. Chem. Soc.*, 1957, **79**, 974.

31. B. Karstedt, *United States of America* 3,775,452, 1973.

32. U. Dittmar, B. J. Hendan, U. Florke and H. C. Marsmann, *J. Organomet. Chem.*, 1995, **489**, 185.

33. B. Hong, T. P. S. Thoms, H. J. Murfee and M. J. Lebrun, *Inorg. Chem.*, 1997, **36**, 6146.

34. H. J. Murfee, T. P. S. Thoms, J. Greaves and B. Hong, *Inorg. Chem.*, 2000, **39**, 5209.

35. F. J. Feher, D. Soulivong, A. G. Eklund and K. D. Wyndham, *Chem. Commun.*, 1997, 1185.

36. F. J. Feher, F. Nguyen, D. Soulivong and J. W. Ziller, *Chem. Commun.*, 1999, 1705.

37. F. J. Feher and S. H. Phillips, *J. Organomet. Chem.*, 1996, **521**, 401.

38. F. J. Feher, D. Soulivong and A. G. Eklund, *Chem. Commun.*, 1998, 399.

39. F. J. Feher, R. Terroba and J. W. Ziller, *Chem. Commun.*, 1999, 2309.

40. F. J. Feher, R. Terroba and J. W. Ziller, *Chem. Commun.*, 1999, 2153.

41. R. W. J. M. Hanssen, R. A. Van Santen and H. C. L. Abbenhuis, *Eur. J. Inorg. Chem.*, 2004, 675.

42. H. Dorn, E. Vejzovic, A. J. Lough and I. Manners, *Can J Chem*, 2002, **80**, 1650.

43. T. Kudo and M. S. Gordon, *J. Phys. Chem. A.*, 2001, **105**, 11276.

44. F. J. Feher and R. L. Blanski, *J. Chem. Soc., Chem. Commun.*, 1990, 1614.

45. F. J. Feher and R. L. Blanski, *Makromol. Chem., Macromol. Symp.*, 1993, **66**, 95.

46. F. J. Feher, D. A. Newman and J. F. Walzer, *J. Am. Chem. Soc.*, 1989, **111**, 1741.

47. R. Murugavel, V. Chandrasekhar and H. W. Roesky, *Acc. Chem. Res.*, 1996, **29**, 183.

48. R. Duchateau, *Chem. Rev*, 2002, **102**, 3525.

49. G. Gerritsen, R. Duchateau, R. A. Van Santen and G. P. A. Yap, *Organometallics*, 2003, **22**, 100.

50. R. Andres, E. De Jesus, F. J. De La Mata, J. C. Flores and R. Gomez, *Eur. J. Inorg. Chem.*, 2002, 2281.

51. J. R. Severn, R. Duchateau, R. A. Van Santen, D. D. Ellis, A. L. Spek and G. P. A. Yap, *J. Chem. Soc., Dalton Trans.*, 2003, 2293.

52. B. Devreese, P. Smet, F. Verpoort, L. Verdonck and J. Van Beeumen, *Rapid Commun. Mass Spectrom.*, 1998, **12**, 1204.

53. T. Maschmeyer, M. C. Klunduk, C. M. Martin, D. S. Shephard, J. M. Thomas and B. F. G. Johnson, *Chem. Commun.*, 1997, 1847.

54. I. Hasegawa and S. Sakka, *ACS Symp. Ser.*, 1989, **398**, 140.

55. I. Hasegawa, S. Sakka, Y. Sugahara, K. Kuroda and C. Kato, *J. Chem. Soc., Chem. Commun.*, 1989, 208.

56. D. Hoebbel, I. Pitsch, D. Heidemann, H. Jancke and W. Hiller, *Zeitschrift Für Anorganische Und Allgemeine Chemie*, 1990, **583**, 133.

57. I. Pitsch, D. Hoebbel, H. Jancke and W. Hiller, *Zeitschrift Fur Anorganische Und Allgemeine Chemie*, 1991, **596**, 63.

58. M. Wiebcke and D. Hoebbel, *J. Chem. Soc., Dalton Trans.*, 1992, 2451.

59. M. Backer, A. R. Grimmer, N. Auner, P. John and J. Weis, *Solid State Nucl Mag*, 1997, **9**, 241.

60. R. Darton, University of St Andrews, 2004.

61. D. Azinovic, J. Cai, C. Eggs, H. Konig, H. C. Marsmann and S. Veprek, *J. Lumin.*, 2002, **97**, 40.

62. S. H. Phillips, T. S. Haddad and S. J. Tomczak, *Curr Opin Solid St M*, 2004, **8**, 21.

63. D. A. Tomalia, *Sci Am*, 1995, **272**, 62.

64. D. A. Tomalia, *Advanced Materials*, 1994, **6**, 529.

65. P. G. Degennes and H. Hervet, *J. Phys. Lett-Paris*, 1983, **44**, L351-L360.

66. R. Moors and F. Vogtle, *Chem. Ber-Recl.*, 1993, **126**, 2133.

67. G. R. Newkome, Z. Q. Yao, G. R. Baker and V. K. Gupta, *J. Org. Chem.*, 1985, **50**, 2003.

68. G. R. Newkome, Z. Q. Yao, G. R. Baker, V. K. Gupta, P. S. Russo and M. J. Saunders, *J. Am. Chem. Soc.*, 1986, **108**, 849.

69. J. M. J. Frechet, C. J. Hawker and K. L. Wooley, *J. Macromol. Sci., Chem.*, 1994, **A31**, 1627.

70. K. L. Wooley, C. J. Hawker and J. M. J. Frechet, *J. Chem. Soc. Perkin Trans. 1*, 1991, 1059.

71. S. Grayson and J. Frechet, *Chem. Rev*, 2001, **101**, 3819.

72. M. Fermeglia, M. Ferrone and S. Pricl, *Bioorgan. Med. Chem.*, 2002, **10**, 2471.

73. Y. M. Chung and H. K. Rhee, *Cr. Chim.*, 2003, **6**, 695.

74. C. Hawker and J. M. J. Frechet, *J. Chem. Soc., Chem. Commun.*, 1990, 1010.

75. V. Percec, C. H. Ahn, T. K. Bera, G. Ungar and D. J. P. Yeardley, *Chem. Eur. J.*, 1999, **5**, 1070.

76. I. M. Saez and J. W. Goodby, *Liq. Cryst.*, 1999, **26**, 1101.

77. I. M. Saez, J. W. Goodby and R. M. Richardson, *Chem. Eur. J.*, 2001, **7**, 2758.

78. P. Busson, J. Ortegren, H. Ihre, U. W. Gedde, A. Hult, G. Andersson, A. Eriksson and M. Lindgren, *Macromolecules*, 2002, **35**, 1663.

79. I. M. Saez and J. W. Goodby, *J. Mater. Chem.*, 2001, **11**, 2845.

80. M. V. Bhatt and S. S. Elmorey, *Synthesis-Stuttgart*, 1982, 1048.

81. M. Melnik, M. Kabesova, M. Koman, L. Macaskova and C. E. Holloway, *J. Coord. Chem.*, 2000, **50**, 177.

82. J. P. J. Markham, S. C. Lo, S. W. Magennis, P. L. Burn and I. D. W. Samuel, *Appl. Phys. Lett.*, 2002, **80**, 2645.

83. S. Setayesh, A. C. Grimsdale, T. Weil, V. Enkelmann, K. Mullen, F. Meghdadi, E. J. W. List and G. Leising, *J. Am. Chem. Soc.*, 2001, **123**, 946.

84. M. Dongge, J. M. Lupton, R. Beavington, P. L. Burn and I. D. W. Samuel, *J. Phys. D: Appl. Phys.*, 2002, **35**, 520.

85. Y. M. Chung and H. K. Rhee, *J Mol Catal A-Chem*, 2003, **206**, 291.

86. M. S. Diallo, L. Balogh, A. Shafagati, J. H. Johnson, W. A. Goddard and D. A. Tomalia, *Environ. Sci. Technol.*, 1999, **33**, 820.

87. J. W. J. Knapen, A. W. Vandermade, J. C. Dewilde, P. W. N. M. Van Leeuwen, P. Wijkens, D. M. Grove and G. Vankoten, *Nature*, 1994, **372**, 659.

88. D. De Groot, E. B. Eggeling, J. C. De Wilde, H. Kooijman, R. J. Van Haaren, A. W. Van Der Made, A. L. Spek, D. Vogt, J. N. H. Reek, P. C. J. Kamer and P. W. N. M. Van Leeuwen, *Chem. Commun.*, 1999, 1623.

89. D. De Groot, P. G. Emmerink, C. Coucke, J. N. H. Reek, P. C. J. Kamer and P. W. N. M. van Leeuwen, *Inorg Chem Commun*, 2000, **3**, 711.

90. M. Benito, O. Rossell, M. Seco and G. Segales, *Inorg. Chim. Acta*, 1999, **291**, 247.

91. G. Van Koten and J. T. B. H. Jastrzebski, *J Mol Catal A-Chem*, 1999, **146**, 317.

92. N. J. Hovestad, E. B. Eggeling, H. J. Heidbuchel, J. T. B. H. Jastrzebski, U. Kragl, W. Keim, D. Vogt and G. Van Koten, *Angew. Chem., Int. Ed. Engl.*, 1999, **38**, 1655.

93. A. W. Kleij, R. A. Gossage, R. J. M. K. Gebbink, N. Brinkmann, E. J. Reijerse, U. Kragl, M. Lutz, A. L. Spek and G. Van Koten, *J. Am. Chem. Soc.*, 2000, **122**, 12112.

94. H. Beerens, F. Verpoort and L. Verdonck, *J Mol Catal A-Chem*, 2000, **159**, 197.

95. H. Beerens, F. Verpoort and L. Verdonck, *J Mol Catal A-Chem*, 2000, **151**, 279.

96. S. B. Garber, J. S. Kingsbury, B. L. Gray and A. H. Hoveyda, *J. Am. Chem. Soc.*, 2000, **122**, 8168.

97. I. Angurell, G. Muller, M. Rocamora, O. Rossell and M. Seco, *J. Chem. Soc., Dalton Trans.*, 2003, 1194.

98. O. Rossell, M. Seco and I. Angurell, *Cr. Chim.*, 2003, **6**, 803.

99. D. De Groot, B. F. M. De Waal, J. N. H. Reek, A. P. H. J. Schenning, P. C. J. Kramer, E. W. Meijer and P. W. N. M. Van Leeuwen, *J. Am. Chem. Soc.*, 2001, **123**, 8453.

100. D. De Groot, J. N. H. Reek, P. C. J. Kamer and P. W. N. M. Van Leeuwen, *European Journal of Organic Chemistry* , 2002, 1085.

101. M. T. Reetz, G. Lohmer and R. Schwickardi, *Angew. Chem., Int. Ed. Engl.*, 1997, **36**, 1526.

102. T. Mizugaki, M. Ooe, K. Ebitani and K. Kaneda, *J Mol Catal A-Chem*, 1999, **145**, 329.

103. J. A. Kremers and E. W. Meijer, *React Funct Polym*, 1995, **26**, 137.

104. M. Bardaji, M. Kustos, A. M. Caminade, J. P. Majoral and B. Chaudret, *Organometallics*, 1997, **16**, 403.

105. V. Maraval, R. Laurent, A. M. Caminade and J. P. Majoral, *Organometallics*, 2000, **19** , 4025.

106. T. Suzuki, Y. Hirokawa, K. Ohtake, T. Shibata and K. Soai, *Tetrahedron: Asymmetr*, 1997, **8**, 4033.

107. I. Sato, T. Shibata, K. Ohtake, R. Kodaka, Y. Hirokawa, N. Shirai and K. Soai, *Tetrahedron Lett.*, 2000, **41**, 3123.

108. H. Alper, *Abstr. Pap. Am. Chem. S*, 2001, **221**, 4-INOR.

109. H. Alper, P. Arya, S. C. Bourque, G. R. Jefferson and L. E. Manzer, *Can J Chem*, 2000, **78**, 920.

110. S. Antebi, P. Arya, L. E. Manzer and H. Alper, *J. Org. Chem.*, 2002, **67**, 6623.

111. S. M. Lu and H. Alper, *J. Am. Chem. Soc.*, 2003, **125**, 13126.

112. J. P. K. Reynhardt and H. Alper, *J. Org. Chem.*, 2003, **68**, 8353.

113. P. P. Zweni and H. Alper, *Advanced Synthesis & Catalysis*, 2004, **346**, 849.

114. R. O. R. Costa, W. L. Vasconcelos, R. Tamaki and R. M. Laine, *Macromolecules*, 2001, **34**, 5398.

115. P. Bhyrappa, J. K. Young, J. S. Moore and K. S. Suslick, *J. Am. Chem. Soc.*, 1996, **118**, 5708.

116. P. Bhyrappa, J. K. Young, J. S. Moore and K. S. Suslick, *J Mol Catal A-Chem*, 1996, **113**, 109.

117. H. Brunner, *J. Organomet. Chem.*, 1995, **500**, 39.

118. H. F. Chow and C. C. Mak, *J. Org. Chem.*, 1997, **62**, 5116.

119. H. F. Chow and C. C. Mak, *J. Chem. Soc. Perkin Trans. 1*, 1997, 91.

120. C. C. Mak and H. F. Chow, *Macromolecules*, 1997, **30**, 1228.

121. G. E. Oosterom, S. Steffens, J. N. H. Reek, P. C. J. Kamer and P. W. N. M. Van Leeuwen, *Top. Catal.*, 2002, **19**, 61.

122. G. E. Oosterom, R. J. Van Haaren, J. N. H. Reek, P. C. J. Kamer and P. W. N. M. Van Leeuwen, *Chem. Commun.*, 1999, 1119.

123. R. Lescanec and M. Muthukumar, *Macromolecules*, **23**, 2280.

124. T. Terao and T. Nakayama, *Macromolecules*, 2004, **37**, 4686.

125. I. Lee, B. D. Athey, A. W. Wetzel, W. Meixner and J. R. Baker, *Macromolecules*, 2002, **35**, 4510.

126. N. G. Vasilenko, E. A. Rebrov, A. M. Muzafarov, B. Esswein, B. Striegel and M. Moller, *Macromolecular Chemistry and Physics*, 1998, **199**, 889.

127. S. Uppuluri, S. E. Keinath, D. A. Tomalia and P. R. Dvornic, *Macromolecules*, 1998, **31**, 4498.

128. P. K. Maiti, T. Cagin, G. F. Wang and W. A. Goddard, *Macromolecules*, 2004, **37**, 6236.

129. N. Zacharopoulos and L. G. Economou, *Macromolecules*, 2002, **35**, 1814.

130. R. Scherrenberg, B. Coussens, P. Van Vliet, G. Edouard, J. Brackman, E. De Brabander and K. Mortensen, *Macromolecules*, 1998, **31**, 456.

131. P. R. Ashton, D. W. Anderson, C. L. Brown, A. N. Shipway, J. F. Stoddart and M. S. Tolley, *Chem. Eur. J.*, 1998, **4**, 781.

132. P. R. Ashton, S. E. Boyd, C. L. Brown, N. Jayaraman and J. F. Stoddart, *Angew. Chem., Int. Ed. Engl.*, 1997, **36**, 732.

133. S. Pricl, M. Fermeglia, M. Ferrone and A. Asquini, *Carbon*, 2003, **41**, 2269.

134. R. A. Gossage, E. Munoz-Martinez, H. Frey, A. Burgath, M. Lutz, A. L. Spek and G. Van Koten, *Chem. Eur. J.*, 1999, **5**, 2191.

135. P. Miklis, T. Cagin and W. A. Goddard, *J. Am. Chem. Soc.*, 1997, **119**, 7458.

136. M. K. Bhalgat and J. C. Roberts, *Eur. Polym. J.*, 2000, **36**, 647.

137. A. M. Naylor, W. A. Goddard, G. E. Kiefer and D. A. Tomalia, *J. Am. Chem. Soc.*, 1989, **111**, 2339.

138. L. Cavallo and F. Fraternali, *Chem. Eur. J.*, 1998, **4**, 927.

139. W. Ortiz, A. E. Roitberg and J. L. Krause, *J Phys Chem B*, 2004, **108**, 8218.

140. K. J. Naidoo, S. J. Hughes and J. R. Moss, *Macromolecules*, 1999, **32**, 331.

141. M. Ballauff and C. N. Likos, *Angew. Chem., Int. Ed. Engl.*, 2004, **43**, 2998.

142. B. Moulton and M. J. Zaworotko, *Curr. Opin. Solid. St. M.*, 2002, **6**, 117.

143. D. Sun, R. Cao, W. Bi, J. Weng, M. Hong and Y. Liang, *Inorg. Chim. Acta*, 2004, **357**, 991.

144. C. N. R. Rao, S. Natarajan and R. Vaidhyanathan, *Angew. Chem., Int. Ed. Engl.*, 2004, **43**, 1466.

145. H. Li, M. Eddaoudi, M. O'keeffe and O. M. Yaghi, *Nature*, 1999, **402**, 276.

146. G. S. Papaefstathiou and L. R. Macgillivray, *Coord. Chem. Rev.*, 2003, **246**, 169.

147. X. L. Xu, M. Nieuwenhuyzen and S. L. James, *Angew. Chem., Int. Ed. Engl.*, 2002, **41**, 764-+.

148. M. C. Brandys and R. J. Puddephatt, *J. Am. Chem. Soc.*, 2002, **124**, 3946.

149. R. J. Puddephatt, *Coord. Chem. Rev.*, 2001, **216**, 313.

150. G. A. Morris, S. T. Nguyen and J. T. Hupp, *J Mol Catal A-Chem*, 2001, **174**, 15.

151. Z. F. Chen, R. G. Xiong, B. F. Abrahams, X. Z. You and C. M. Che, *J. Chem. Soc., Dalton Trans.*, 2001, 2453.

Chapter 2. Methodology

2.1 Molecular Modelling

2.1.1 Introduction

Molecular modelling is the study of single molecules and systems of molecules by theoretical means and includes molecular mechanics, dynamics, and quantum mechanics. Molecular mechanics can be assumed to be an *a priori* method, that is, prior knowledge of the types of compounds modelled is required to construct the force field. Quantum mechanics is an *ab initio* method for examining molecules as it requires no prior knowledge and is often used to create accurate force field parameters. Molecular mechanics considers the motion of nuclei and does not deal with electrons explicitly; while quantum mechanics methods deal with electrons and the potential energy function is a sum of the nuclear and electronic energy.

In molecular mechanics, the molecules are treated as a set of masses joined by springs and as such, Hooke's law and other simple analytical functions can be used to approximate their behaviour. Atoms are represented by atom types dictated by the atom's environment (valency, bonded neighbours, bond hybridisation etc.) and together with parameters specific for each atom type, form the force field. Molecular mechanics can be used to produce equilibrium structures, conformational transition states, and can calculate energies (strain or heat of formation) and vibrational frequencies when correctly used. Molecular mechanics uses energy minimisation techniques to find minimum energy configurations of the molecule under scrutiny, the energy being calculated from the sum of the contributions due to bond stretches, angle bends and so forth, relative to equilibrium values.

Chapter 2. *Methodology*

Molecular dynamics relates to the study of molecules over time and uses models

constructed and ruled by molecular mechanics techniques in collaboration with

Newton's equations of motion to advance the system over time. Molecular dynamics

techniques are used to find minimum energy configurations of molecules through

heating and cooling protocols and to examine equilibrium structures over time.

2.1.2 Molecular Mechanics

A molecule can be thought of as a collection of atoms distributed on a potential

energy surface. Finding the potential energy possessed by this collection of atoms is

one of the main requirements of molecular mechanic calculations. The molecular

mechanics force field is an expression for the energy of a system in terms of simple

processes. This includes the deviation of bond lengths or angles from equilibrium

values, torsional terms dealing with rotation about bonds, and terms to describe

interactions between parts of the system that are not bonded directly together. While

the exact terms vary from one force field to another, generally the same format is

used in all cases.

$$U_{total} = \sum U_r + \sum U_\theta + \sum U_\varphi + \sum U_{NB}$$

Generic form of a force field where U_{total} - total potential energy, U_r - contribution from bond stretch
terms, U_θ - contribution from angle bends, U_φ - contribution from torsions and U_{NB} - contribution
from non-bonded interactions.

Depending on the program, other terms may be added to these including improper

torsions, out-of-plane bends and cross-terms to improve the accuracy. Cross-terms

represent the interaction between bond stretches and angle bends on adjacent bonds

and angles. These are especially important in force fields used to predict vibrational

spectra of molecules. The precise mathematical form of each component also varies

between force fields. The more terms present in a force field, the more accurate the

energy calculation; but increasing accuracy always comes with a corresponding

increase in computational cost. A summary of the basic terms found in force fields is

below with particular reference to the two force fields used in this project – MM+

(molecular mechanics +) and CVFF (Consistent Valence Force Field)

Bond Stretch
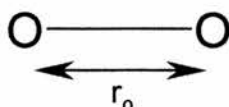
Hooke's Law Function:

$$U_r = \frac{k}{2}(r - r_0)^2$$

U_r - potential energy of bond, k - stretching constant of the bond,
r – bond length, r_0 – equilibrium bond lengths.

Morse Function:

$$U_r = D_e\{1 - \exp[-a(r - r_0)]\}^2$$

$$a = \omega\sqrt{\frac{\mu}{2D_e}} \qquad \omega = \sqrt{\frac{k}{\mu}}$$

D_e – the depth of the potential energy minimum, a – constants, r – bond length, r_0 – equilibrium bond
length, ω – frequency of bond vibration, μ – reduced mass, k – stretching constant of the bond.

Hooke's Law or the harmonic oscillator gives a reasonable approximation of bond

lengths close to their equilibrium value, but at larger deformations (> 0.1 Å from

ideal) the harmonic oscillator is a poor approximation. Other functions such as the

cubic equation and the Morse function can offer better approximations but these can

increase the number of parameters required in the latter case and the computational

complexity in both cases.

$$U_r = 143.88 \sum_{bonds} \frac{1}{2} k_r (r - r_0)^2 [1 + CS(r - r_0)]$$

CS is an arbitrary value, set by default to –2.0 within the program. 143.88 is a conversion factor between kcal mol^{-1} and ergs, the internal units of energy used by MM+

MM+ uses a cubic expression for the stretch term where the cubic stretch term is a fixed value, CS, times the quadratic stretch term. In this form, the equation becomes repulsive when r - r_0 > 2/3 CS. This is overcome bysetting CS to zero eliminating the cubic term and leaving only the quadratic part of the function. To enable this to be done smoothly, a switching function is applied which allows the cubic term to be turned on and off as necessary.

$$U_r = k_1(r - r_0)^2 + k_2(r - r_0)^3 + k_3(r - r_0)^4$$

k_1, k_2 and k_3 - force constants

CVFF on the other hand uses an expression with quadratic, cubic and quartic terms that requires three force constants to be added to the parameter file.

Angle Bend
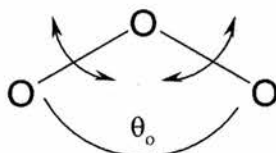
$$U_\theta = \frac{k}{2}(\theta - \theta_0)^2$$

U_θ – potential energy, k – force constant, θ- angle, θ_0 – equilibrium angle

Simple harmonic functions are used for angle bends but many force fields include higher order terms to improve the accuracy of the force field. Again, a compromise must be reached between accuracy and high computational complexity. This is the form used by CVFF. MM+ uses a more complicated form.

$$U_\theta = 0.043828 \sum_{angles} \frac{k}{2}(\theta - \theta_0)^2 [1 + SF(\theta - \theta_0)^4]$$

SF – scale factor

MM+ includes a quadratic angle bend term and a sextic angle bend term. The sextic term is a scale factor times the quadratic term and SF is set by default to 7.0×10^{-8}. The constant 0.043828 converts bending constants from millidyne-Å rad^{-2} to kcal $mol^{-1}deg^{-2}$. Special values are included in the MM+ force field for bending force contants in 3 and 4 membered rings.

Torsions
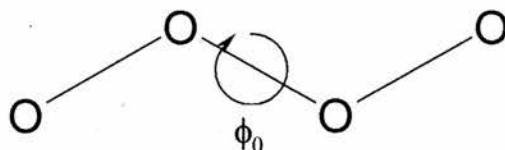
$$U\varphi = \sum_{n=0}^{N} \frac{V_n}{2} [1 + \cos n\varphi]$$

n – multiplicity (number of minimum points in function as bond rotated through 360 °),
U_φ – energy, Vn – Barrier height (indication of barriers to rotation), φ – torsion angle.

For molecules in which rotation about single bonds is common, torsions must be included in the force field. Both MM+ and CVFF use torsion terms like that above. MM+ uses the expanded form for n = 1, 2, 3 and, consequently, the force field contains three values for V_n.

Non-bonded interactions

$$U_{NB} = \sum_{i=1}^{N} \sum_{j=i+1}^{N} (4\varepsilon_{ij}[(\frac{\sigma_{ij}}{r_{ij}})^{12} - (\frac{\sigma_{ij}}{r_{ij}})^6] + \frac{q_i q_j}{4\pi\varepsilon_0 r_{ij}})$$

U_{NB} – potential energy, ε_{ij} – well depth parameter, σ_{ij} – collision diameter, r_{ij} – distance between atoms i and j, q_i – partial charge on atom i, q_j – partial charge on atom j, ε_0 - dielectric constant *in vacuo*.

The non-bonded terms are modelled using a Lennard-Jones potential function for the van der Waals interactions and a Coulomb function for the electrostatic interactions.

Chapter 2. *Methodology*

Evaluating the non-bonded energy is the most computationally expensive part of a molecular mechanics calculation. Often, cut-off distances are used to limit the number of non-bonded interactions taken into consideration by limiting the maximum distance two atoms can be apart and still interact with one another. Non-bonded cut-offs are often used with potential switching functions to eliminate non-physical behaviours caused by these cut-offs. These functions allow non-bonded potential energy to be turned off smoothly and systematically, removing artefacts. CVFF uses a similar form for the non-bonded and van der Waals interactions as that detailed above.

$$U_{vdW} = \sum_{ij \in vdW} \varepsilon_{ij} (2.9 \times 10^5 \exp(-12.5\rho_{ij}) - 2.25\rho_{ij}^{-6})$$

$$\text{where } \rho_{ij} = \frac{R_{ij}}{r_{ij}^*} \text{ and } r_{ij}^* = r_i^* + r_j^*$$

U_{vdW} – van der Waals energy, ε_{ij} – hardness parameter,
R_{ij} – distance between atoms i and j, r_{ij}^* - van der Waals radius,
various constants are conversion factors for units

MM+ does not use a Lennard-Jones potential for the van der Waals interactions. A combination of an exponetial repulsion and $1/R^6$ attractive interaction are used. For each atom type, the van der Waals radius r_i^* and a hardness parameter ε_i are required. The hardness parameter determines how easy it is to push two atoms close together.

Improper Torsions and Out of Plane Interactions
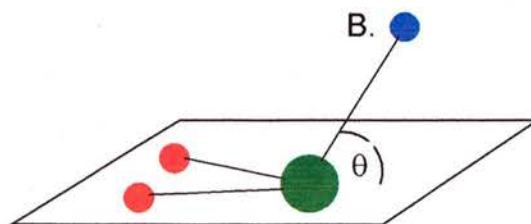
Representation of out-of-plane behaviour by atom B.
$\theta = 0°$ for a coplanar arrangement of all atoms.

$$U_{oop} = \frac{k}{2}\theta^2$$

U_{oop} – potential energy, k – force constant, θ – angle between bond and plane

For molecules that posses a well defined plane of atoms, (e.g. benzene, cycloalkanes etc.) it is necessary to add special terms to the force field. Out-of-plane interactions can be treated by a number of approaches. Improper torsions, where the four atoms described by a torsion angle are not bonded directly together, can be used to dictate better geometry in a ring. Alternatively, an out-of-plane bend might be used to calculate the angle between a bond from a central atom and the plane defined by the central atom and the other two atoms. If this angle is 0 °, the atoms are coplanar. Out of plane interactions are dealt with by modifying the angle bending calculations to use inplane angles and standard force constants in MM+. The out of plane agles are also calculated using special out of plane bending constants. In CVFF the following form is used:

$$U_{oop} = k_1(\theta - \theta_0)^2 + k_2(\theta - \theta_0)^3 + k_3(\theta - \theta_0)^4$$

This means that upto three force constants might be included in the parameters.

Bond stretch and angle bend cross term
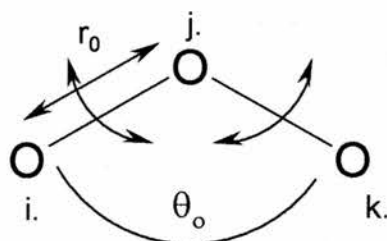
$$U_{SB} = \sum_{angles} k(\theta - \theta_0)_{ikj}[(r - r_0)_{ik} + (r - r_0)_{jk}]$$

U_{SB} - potental energy, k – force constant, θ – angle ijk,
θ_0 – equilibrium angle ijk, r – bond length, r_0 – equilibrium bond length

Many force fields contain cross terms to define the coupling between bond stretching and angle bending. For three atoms i, j and k, where j is central, the cross term

between the ij and kj bond stretches and ijk angle bend is as above. In some force fields (e.g. MM+) the stretch bend force constants are fixed and determined by the atom types.

$$U_{SB} = k(r - r_0)(\theta - \theta_0)$$

$$U_{BBT} = k \cos \varphi (\theta - \theta_o)(\theta' - \theta_0')$$

Some cross terms for CVFF: U_{BBT} – energy, angle-angle-torsion interaction.

CVFF includes cross terms to account for bond-bond, bond-angle, angle-angle and angle-angle-torsion interactions (above) whereas MM+ includes a bond-angle cross term. No bond-angle interactions are defined for XH_2 groups.

$$U_{SB} = 2.51118 \sum_{angles} k(\theta - \theta_0)_{ikj}[(r - r_0)_{ik} + (r - r_0)_{kj}]$$

For three atoms, ijk, where k is the central atom. Stretch bend terms for MM+

Potential Energy Surfaces

Points on the potential energy surface are generated by solving the force field equation for many configurations of the nuclei. The potential energy surface has 3N+1 dimensions where 3N dimensions specify the positions of N atoms and the additional dimension gives the molecules potential energy. Each point on the potential energy surface corresponds to a configuration of the molecule and minima on this surface correspond to stable conformations. The main goal of a molecular mechanics calculation is to locate these minima and identify the molecular configuration that exists at its lowest point. A potential energy surface may have many minima and by calculating the potential energy of the corresponding structures, information about their relative stability can be gained. Additionally, the potential energy surface will have saddle points that correspond to transition states. The

complexity of the potential energy surface means that a single stable conformation may not adequately represent the properties of a molecule, and a number of thermally accessible structures should be investigated. For all but the smallest molecules, determining the global minimum might be impossible.

The potential energy calculated by this equation is relative to a hypothetical zero energy geometry in which all bonds, angles and torsions are at their equilibrium values and the van der Waals interactions calculated for infinite separation. Negative energies are still possible for this representation if the van der Waals attractive forces are large enough. It is highly unlikely that this zero energy geometry can be obtained and so most molecules are strained to some extent.

Choice of Force Field for Modelling Dendrimers

Both Materials Studio[1] and Hyperchem[2] offer a choice of force fields and selecting the ideal one was not random or left to default settings. Materials studio offered the Consistent Valence Force Field (CVFF), Polymer Consistent Force Field (PCFF) or COMPASS (Condensed-phase Optimised Molecular Potentials for Atomistic Simulation Studies). Previous molecular modelling studies had compared PCFF and CVFF, stating that CVFF lead to more compact structures and PCFF was better[3]. Initial experiments with these two force fields showed that PCFF was prone to poor minimisation. The structures, after heating and cooling, could not be minimised to a low enough gradient. When the length and complexity of the materials studio simulations were taken into consideration, the more reliable CVFF was used but also no significant compression of structures was observed. In Hyperchem the choice was far greater with both all atom force fields and united force fields available. United force fields were eliminated because one of the properties under scrutiny was

the size of the molecules and it was unclear how accurate united atoms could be for

this task. The all atom force field MM+ had the greatest variety of parameters

making it more versatile. Several previous modelling studies on ligands, dendrimers

and metal complexes have been done with the MM family of the force fields.

2.1.3 Parameterisation

Most force fields are designed for specific classes of organic molecules and the parameters are generally obtained from crystal data and *ab initio* calculation on small examples of the class. For example, *ab initio* calculations of small chain alkanes (C_1 – C_5) could be used to create a parameter set applicable to the entire homologous series of alkanes. Good sets of parameters are transferable within the same class of molecules, but can also be applicable to other classes of molecules with the same functional groups. Class one force fields are parameterised for specific systems, mainly from experimental data, while class two force fields contain more parameters derived from *ab initio* calculations and, as such, are more generally applicable. Atom types in force fields are assigned to atoms in structures based on hybridisation, formal charge and neighbouring atoms to which they are bonded. This allows the distinction to be made between a methyl group, a methylene group, or a methine group, as well as aromatic C-H bonds. For example:

(i)   (ii)
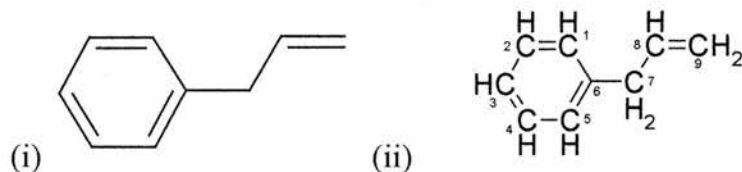
Figure 2.1: Two representations of allylbenzene showing the structure (i) and the number of carbon atom types (ii)

Allyl benzene contains three, four or five carbon atom types depending on the force field. Carbons 1-5, 6, 7, 8 and 9 all have unique environments and could be given different parameters accordingly.

Parameters are the set of equilibrium values such as r_0, θ_0 etc. that are used to define how atom types behave. The equilibrium bond length will be different for C-H in each of the five cases above, as will the bond angles and torsions.

Force fields are generally specific to certain classes of compounds but some have been developed with more general modelling capabilities in mind. UFF (Universal Force Field) was designed to model the entire periodic table using parameters calculated from atomic parameters. The parameters depend on the hybridisation state of the atom in combination with a set of simple rules[4].

2.1.3.1 CVFF

CVFF is mainly parameterised from experimental detail, but includes some *ab initio* results. It is not suitable for unusual systems due to the limited number of parameters included. It was originally parameterised for 20 common amino acids and hydrocarbons. CVFF uses a Morse potential to describe bond stretches and contains cross terms for bond stretch, angle bend, bond stretch-angle bend and torsion-angle bend interactions. The non-bonded interactions can be modified to make dielectric constants distance dependant.

2.1.3.2 MM+

MM+ is a combination of several force fields (MM1, MM2, MMP2 and MMX) and MM3. It has a large selection of parameters and includes a system to assign parameters and atom types to unknown species.

MM+ has a three tier system for assigning parameters. Initially, the atoms in the system are assessed against a list of atom types and criteria. Those that do not fit any of the specified types may then be assigned as wild cards and finally, a default scheme is available to define the behaviour of unknown atom types. The default scheme takes into consideration the hybridisation of the atoms, the types of bonding present, and the standard covalent radii for elements in the periodic table to create a set of suitable parameters.

There are five kinds of hybridisation that might be assigned: null, sp, sp^2, $sp^{2.5}$ and sp^3. Aromatic systems are treated as $sp^{2.5}$ hybrids. For simplicity, no d orbital hybridisation states are considered by the force field and for transition metals the number of valence electrons are those in the ns and np orbitals. The default hybridisation is then defined by the number of s and p valence electrons and the number of neighbouring atoms, between 0 and 4. MM+ does not take into account transition metal complexes that might have greater than four neighbours. It is because of this that problems may arrise when modelling molecules containing transition metals with greater than four ligands. In such a case, specific parameters must be added to the force field to deal with the more complex systems.

The equilibrium bond distance r_0 is taken to be the sum of the covalent radii of the atoms except in certain cases where specific bonds are defined. The default bond stretching force constants are defined in table 2.2.

Bond	Force Constant
Single	700 kcal mol^{-1}Å
Double or aromatic	1400 kcal mol^{-1} Å
Triple	2100 kcal mol^{-1} Å

Table 2.2: Default bond lengths for three general classes of bonds.

For angle bends, the force constant is simply set to 100 kcal mol^{-1} rad^{-2}, and stretch-bend terms are not included. At sp^2 centres the out-of-plane interaction angles are taken from the first parameters found for the central atom. Torsions have three potential interactions with 1, 2 or 3 fold contributions.

2.1.3.3 Constraints vs Restraints

In Hyperchem, there are two ways of defining the geometry of a structure. The first is called a constraint and is used during the model building process to fix the geometry, for example to define the distance between two atoms, the angle between three or a torsion between four. Constraints apply only for the model build facility and allow a good starting structure to be created for a calculation. Restraints are the second and are used to fix the position of an atom, the length of a bond, the size of an angle or a torsion at a specific value and with a specific force constant.

It is important to note that restraints do not replace interactions, they add to them. Two main types of restraints can be used, hard and soft. Hard restraints involve a large force constant to force the geometry specified by the restraint to remain fixed. This means that the energy of the system will increase, if the atoms, which are restrained, move from the set values. Soft restraints involve force constants that are similar to those found in the parameter files and are a more gentle way to imply desired geometries. As the restraints add to the computed interactions this will result in a preferred geometry for the structure where restraints have been applied, but other geometries will be accessible without the dramatic increase in energy of hard

restraints. Unlike constraints, restraints are active throughout the whole calculation until removed by the user.

Materials studio also includes the facility to add restraints to the molecule but offers only the chance to 'freeze' certain atoms and sections of molecules in space. This means that they cannot move at all throughout the calculation and can anchor unfrozen parts of the molecule. There is no way to add soft restraints such as those found in Hyperchem.

2.1.4 Molecular Dynamics

2.1.4.1 Geometry Optimisations

Geometry optimisation is the process through which a minimum of energy can be determined for a conformation of a molecule. The basic process involves taking the Cartesian co-ordinates of a structure and searching for new co-ordinates with lower potential energy resulting in a set of co-ordinates with minimum potential energy. Potential energy barriers cannot be crossed by the minimisation process so care must be taken to assess whether the minimum found is a local or global minimum. This is mainly used to generate a structure for a single point energy calculation or to create a starting structure for a molecular dynamics simulation. There are various algorithms available for these and are discussed in detail below.

Materials studio uses a combination of three types of minimisation algorithms whereas Hyperchem allows the user to select one from a number of individual algorithms.

The first is the steepest descent, which might be considered the crudest method of minimisation. It is a first order method and calculates the first derivative of the potential energy with respect to the Cartesian co-ordinates. This method is particularly useful for the initial minimisation of structures just drawn.

The Conjugate Gradient method is also a first order method and uses both the current gradient and the previous search to drive the minimisation. This results in faster convergence because the history is used to determine decreasing gradient. Two versions of the conjugate gradient method are Polak-Ribiere and Fletcher-Reeves. Polak-Ribiere is thought of as being the more refined version and is the default setting on Hyperchem.

Chapter 2. *Methodology*

The third method is the block-diagonal method, specifically the Newton-Rhapson block diagonal method. It is a second order optimiser and calculates the first and second derivative of the potential energy with respect to the Cartesian co-ordinates. This allows information about both the slope and curvature of the potential energy surface to be determined. The full Newton-Rhapson method is very computationally expensive and unsuitable for systems with a large number of atoms, or when far from the minima. The block-diagonal Newton-Rhapson method is less computationally expensive, but still inappropriate for systems with many atoms. The smart minimiser facility in Materials Studio uses all Steepest Descent, Fletcher-Reeves and Newton Rhapson in series for small molecules, and only the first two methods for larger molecules (>250 atoms).

2.1.4.2 *Molecular Dynamics Simulations*

Molecular dynamics simulations sample phase space (region defined by atomic positions and velocities) by integrating numerically Newton's equations of motion. This method can cross potential barriers unlike geometry optimisation, account for thermal motion, and ultimately give information about possible conformations, thermodynamic properties, and dynamic behaviour.

Molecular dynamics simply calculates the future positions and velocities of the atoms based on current positions and velocities. Initially, the simulation determines the forces on each atom as a function of time equal to the negative gradient of the potential energy.

$$F_i = -\frac{\partial V}{\partial r_i} \qquad a_i = \frac{F_i}{m_i}$$

F – force, V – potential energy; r_i – radius, a_i – acceleration, m_i – mass of atom

The acceleration a_i is calculated and the change in velocities v_i is equal to the integral

of the acceleration over time.

$$K = \frac{1}{2} \sum_{i=1} m_i v_i^2$$

K - Kinetic energy, v_i velocity of atom

The change in position is the integral of velocity over time and these quantities can

be used to calculate the energy.

2.1.4.3 Integration Algorithms

Every molecular dynamics program has an integration algorithm used to integrate

Newton's equations of motion resulting in a trajectory that demonstrates how the

positions of the atoms in the system change over time. There are many methods and

algorithms for this and the method used by Hyperchem, the LeapFrog Algorithm is

described below. The algorithm updates the positions of the atoms and the velocities

for the next time step according various equations.

At time t, the atomic positions are $r_i(t)$, acceleration $a_i(t)$, and the velocities $v_i(t)$:

$$v_i(t) = \frac{d}{dt} r_i(t)$$

$$v_i(t + \tfrac{1}{2}\Delta t) = v_1(t - \tfrac{1}{2}\Delta t) - \Delta t a_i(t)$$

In the first time step Δt, the velocities advance from time $t = 0$ to $t + \frac{1}{2} \Delta t$, leaping

over the positions at time t. The current velocities are calculated:

$$v_i(t) = \tfrac{1}{2}[v_i(t + \tfrac{1}{2}\Delta t) + v_i(t - \tfrac{1}{2}\Delta t)].$$

The acceleration is then calculated and the cycle restarted.

Hyperchem stores the current positions $r_i(t)$ and midstep velocities $v_i(t - 1/2\Delta t)$.

This means that the total energy at time t is calculated approximately due to the

calculation of midstep velocities.

2.1.4.4 Other Molecular Dynamics Techniques

Monte Carlo Simulations

Monte Carlo simulations sample phase space by generating random configurations

from a Boltzmann distribution at specific temperature. A sequence of successive

configurations from a Monte Carlo simulation constitutes a trajectory in phase space

and enables a minimum to be determined. Both temperature and solvent effects can

be incorporated into this model. A Monte Carlo simulation samples random

configurations from a Boltzmann weighted distribution at a specific temperature.

Langevin Dynamics

Langevin dynamics simulate molecules in solution where the molecule undergoes

collisions and experiences friction as it moves through the solvent. The dynamic

behaviour of molecular systems as liquids can be assessed and because of the

implicit solvent molecules, it is far faster than methods utilising explicit solvent

molecules. The effects of solvents are primarily modelled through random forces

applied to the molecule that simulates collisions then frictional forces are added to

model energy losses associated with these collisions. The simulations are carried out

at temperatures above absolute zero. This allows study of the time dependent

properties of solvated systems, which is particularly useful for large molecules in

solution. It is possible and necessary to decouple the time scales of molecular motion and focus on just the slow modes associated with conformational changes. Langevin dynamics are used to simulate the motion of molecules subject to random collisions and frictional forces and can be used to model solvated systems without explicitly including solvent molecules. The simulation includes a friction coefficient and a larger friction coefficient means motions over short time periods are less important, so a larger timestep can be used.

2.2 Modelling Protocols

The protocols for Materials Studio and Hyperchem differ due to different features in the programs. For instance, Hyperchem allows the structures to be cooled from high to low temperature automatically whereas Materials Studio requires that this be done manually in steps. For both programs the general features were the same, the molecules were drawn, minimised, heated, cooled, minimised and equilibrated. The equilibration step took place at a series of different temperatures when necessary to assess the effects of temperature on the structure of the dendrimers.

All modelling experiments were run on PCs running one of Windows NT, 2000 (Professional) or XP (Professional) with a minimum of an 800 MHz processor and 512 Mb of Memory. Data Analysis, when not done directly by the program was carried out in Microsoft Excel. Typical simulation times were 24 hours for Materials Studio and 48 hours for Hyperchem.

2.2.1 Materials Studio

The Materials Studio[1] package was used to model dendritic alcohols (Chapter 3) and dendritic diphenylphosphine ligands (Chapter 4). The models were constructed using the build module contained within the package from a selection of individually constructed subunits – the POSS core and branches. The diphenylphosphine dendrimers were then subjected to intense visual inspection to ensure that the phenyl rings were not interlocked or highly deformed. The various settings and modelling protocol is detailed in table 2.3.

Program Feature	Setting
Force Field:	Consistent Valence Force Field (CVFF)
Thermostat:	Andersen
Minimiser:	Steepest Descent/Conjugate Gradient
Dielectric Constant, ε:	1 (as standard but variable)
Maximum Energy Derivative:	< RMS 0.001 kcal mol^{-1} Å^{-1}
Time step:	1 fs
Ensemble:	Constant Number, Temperature, Volume (NVT)
Heating Step:	100 ps, 1000 K
Annealing Step:	950 K – 50 K in 50 K steps, 5 ps per step
Equilibrating Step:	100 ps at required temperature (273 K standard)
Production Step:	500 ps at required temperature (273 K standard)

Table 2.3: Materials Studio settings, including simulation protocols.

The initial structure was minimised to a maximum energy derivative of less than

RMS 0.1 kcal mol^{-1} Å^{-1} using the smart minimiser module of Materials Studio. This

used the methods of Steepest Descent and Conjugate Gradient in sequence to obtain

a minimum of energy more rapidly. The dendrimers were too large for the third

method (Newton-Rhapson). The structures were then heated to 1000 K for 100 ps to

facilitate full expansion of the branches and overcome any deformed configurations

created in molecules construction. Various temperatures were investigated for the

heating step. 500 K was found to be too low to overcome some energy barriers and

did not allow the branches to expand fully. 1500 K was found to offer no significant

advantage over 1000 K and meant a longer cooling stage was needed. The molecule

was cooled in 50 K steps, running for 5 ps at each temperature down to 50 K. The

slow cooling process is essential to avoid 'freezing' the molecule in a distorted

configuration and while smaller temperature steps (e.g. 25 K or 10 K) might be more

effective at this, they are far more computationally expensive. The structure at 50 K

was minimised to maximum energy derivative of less than RMS 0.001 kcal mol^{-1} Å^{-1}

using the smart minimiser module before being equilibrated at the desired

temperature for 100 ps. During the heating, annealing and equilibrating steps only

the final frame of the trajectories was saved, but during the production step every

1000th configuration was saved creating a file of 500 individual conformations for

analysis.

Simulations were generally run with an inbuilt dielectric constant of 1 but for the

diphenylphosphine dendrimers solvent dependent work, it was varied. The dielectric

constant values inbuilt in Materials Studio do not correspond to experimental values.

Hence $\varepsilon = 1$ represents an apolar solvent and $\varepsilon = 8$ represents a highly polar solvent.

The dendritic alcohols were modelled in the general case of a good or poor solvent

simply by changing the mathematical form of the force field to modify the

intermolecular forces. The CVFF force field was used and modified to represent the

cases of good and poor solvents. CVFFpoor included both Coulombic and van der

Waals interactions between non-bonded atoms and represented a poor solvent while

CVFFgood included only repulsive van der Waals interactions to represent a good

solvent[5].

2.2.2 Hyperchem

In Hyperchem, simulations can be set up to run heating and cooling protocols

automatically and saves only the final frame of the run as default. The

diphenylphosphine dendrimers were modelled with Hyperchem to allow the bite

angle to be calculated using Casey's method and also to model the dendrimer with a

dummy complex attached[6]. Materials Studio could not be used for this due to the

difficulties of parameterising the CVFF force field but fortunately, MM+ was

comparatively easy to modify where necessary. Models were constructed by

exporting a minimised structure from Materials studio and adding additional atoms

where required. The drawing function in Hyperchem is not suitable for drawing

large three-dimensional macromolecules and so equilibrated structures were exported

from Materials Studio and altered where necessary. The protocols for calculating the

bite angle of the dendrimers and the dummy complex differ because restraints had to

be used to model the complex attached to the dendrimer in the correct geometry.

Program Feature	Setting
Force Field:	MM+
Minimiser:	Polak-Ribiere
Dielectric Constant, ε:	*In vacuo*
Maximum Energy Derivative:	< RMS 0.001 kcal mol^{-1} Å^{-1}
Time step:	1 fs
Heating Step:	10 ps at 1000K
Annealing Step:	60 ps from 1000 – 0 K
Equilibration and Production	70 ps at required temperature

Table 2.4: Molecular Modelling protocol for Bite Angle calculations.

The protocol for the bite angle calculations was similar to the Materials Studio

protocol in all aspects bar one. Materials Studio carries out calculations relatively

rapidly (600 ps at 300 K on an average dendrimer would take 12 hours on an 800

MHz processor) and saves the calculation as it goes. Hyperchem carries out

calculations at a far slower rate and if the calculation is interrupted, all work is lost.

Program Feature	Setting
Force Field:	MM+
Minimiser:	Polak-Ribiere
Dielectric Constant, ε:	*In vacuo*
Maximum Energy Derivative:	< RMS 0.001 kcal mol^{-1} Å^{-1}
Time step:	1 fs
Heating Step:	10 ps heating from 0 – 1500K, 10 ps at 1500 K
Annealing Step 1:	50 ps from 1500 – 300 K
Annealing Step 2:	10 ps at 300 K, 60 ps from 300 – 0 K
Equilibration and Production	70 ps at required temperature

Table 2.5: Molecular Modelling Protocol for Dendrimer-Complex Calculations.

Simulations in Hyperchem are, therefore, a factor of 10 shorter than Materials Studio

and automatic features such as heating and cooling were employed to the fullest.

Parameters were added to the MM+ force field to enable rhodium to be recognised as

the atom type rh and to fix the Rh-P bond length at 2.315 Å. The parameters for related bond lengths, angle bends and torsions were also modified but this is discussed in more detail in Chapter 5.

The protocol for modelling the dendrimer complex differed from the bite angle work with the addition of an additional cooling step and higher temperature for heating. The difference between the two protocols was to take into account the use of restraints when modelling the dendrimer complex. The dendrimer complex's geometry was fixed in place by use of restraints that set the force constants for angle bends and bond stretches to very high values meaning that the complex was essentially fixed to a specific geometry. A good starting geometry was essential for this system because any significant distortion resulted in very high energies and gradients when heating that usually resulted in the simulation becoming unstable. The model was then heated to 1500 K to avoid shocking and then run at 1500 K for a short period. The higher temperature was chosen to allow the molecule to move more freely despite the restraints imposed by the complex. The initial restraints were 'hard' restraints with very high force constants to withstand the high temperature but were reduced to 'soft' restraints before the second annealing step to allow the branches to move around the complex more. The restraints that included phosphorus atoms were reduced to even lower values to enable the PRhP angle to be calculated. A short equilibration period at 300 K was incorporated to allow the model to adjust to the new restraints. The molecule was minimised at 0 K and then equilibrated at 300 K for 70 ps with soft restraints. The exact nature of the restraints involved is described in detail in Chapter 5.

2.3 Analysis of Modelling Data

The modelling protocols produced a production trajectory of results to be analysed. This was typically 500 frames in length for Materials Studio work (the first 100 frames of a 600 frame trajectory were excluded as an equilibration period) and 7002 frames in length for most Hyperchem work. Hyperchem data were saved as a text file of values such as lengths, angles and other measurable quantities. Materials Studio contains many inbuilt modules for property analysis and these were used where appropriate.

2.3.1 Radial Density Distribution Function, $g_{\alpha\beta}(r)$

Radial Density Distribution Functions (also known as Pair Correlation Functions) were used to calculate the distribution of various atom types (Oxygen or Phosphorus) through out the dendrimer as a function of both distance and time.

$$g_{\alpha\beta}(r) = \frac{V}{N} \left\langle \frac{n(r)}{4\pi r^2 \delta r} \right\rangle$$

The number of pairs $n(r)$ are r_i and $r_i + \delta r$ apart, V is the simulation volume and N is the number of molecules in the system. The probability of finding a particle α at distance r away from particle β and is normalised to 1 at large r. The radial distribution function is calculated by dividing the interval with $r = 0$ and the cut off radius into segments size δr and counting the number of atomic pairs (α,β) with distances falling in a given range. The results are averaged over different time steps. The calculation gives the density of atom centres in a shell 0.01 Å thick at radial distance r from a given point in space. Each atom in turn is used as this point and the distances to each other atom selected is calculated and summed over time.
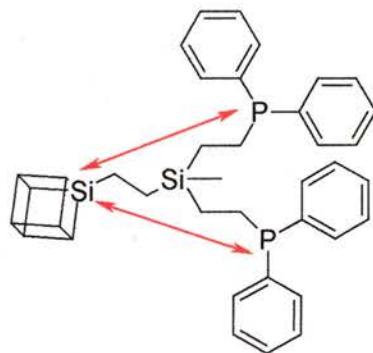
Figure 2.2: Diagram showing how core-phosphorus distances were calculated, using the silicon on the core to compensate for no atom being present at the centre of mass.

It is difficult to measure g(r) from the centre of mass of a POSS based dendrimer, as there is no atom at the centre of mass (generally the centre of the cubic core). This function has been used to calculate the distance between terminal groups on each branch, on all branches or between terminal groups and the silicon on the POSS core to which the branches are attached.

2.3.2 Measurement of Distances and Angles

The distance between sets of atoms was calculated using distance measurement functions, which returned a graph of the variation of the distance or angle with time and also the average angle and standard deviation. This was done automatically with Materials Studio or manually in Hyperchem from data files generated. When calculating the distance between two terminal groups, the standard deviation from the average was taken as giving some measure of the flexibility of the branch, i.e. how much it could move. For calculating angles, the standard deviation was taken to be a measure of the flexibility in the angle. More importantly, the range between the highest and lowest values for the angle was taken to give a measure of its flexibility.

2.3.3 Size and Shape Properties – Inertia, Aspect Ratios and Asphericity

Moments of Inertia are calculated automatically in Hyperchem when a single point calculation is carried out and so were calculated for the final frame of the production trajectory. Hyperchem does not permit selection of specific frames for analysis and so an average value was not possible. Similarly, moments of inertia were calculated from the atomic co-ordinates of various frames from Materials Studio.

The moments of inertia were calculated thus: for any given atom of mass m at position (a,b,c) and distance r from the centre of mass (A,B,C), the moment of inertia, I_a, relative to one axis, a, is defined:

$$R_{bc} = \sqrt{(b-B)^2 + (c-C)^2}$$

For one atom relative to axis a, where m is the mass of the atom:

$$I_a = mR_{bc}^2$$

For all atoms relative to axis a:

$$I_a = \sum m \sum (R_{bc})^2$$

Where M is the total mass of the molecule:

$$\sum m = M$$

Therefore:

$$I_a = M \sum (R_{bc})^2$$

I_b and I_c are calculated similarly.

The principal axis is taken to be in the z direction and the largest moment of inertia is assigned I_z so that $I_z > I_y > I_x$. Aspect ratios can be calculated from the moments of inertia and the principal ratio is considered I_z/I_x and the other I_z/I_y. For a perfect

sphere $I_x = I_y = I_z$ and all aspect ratios equal one. The greater the deviation from 1, the less spherical the molecule is.

The asphericity (δ) was also calculated as a measure of how spherical the dendrimer was[7].

$$\delta = 1 - 3\left(\frac{<I_2>}{<I_1^2>} \right)$$

where $I_1 = I_x + I_y + I_z$ and $I_2 = I_x I_y + I_y I_z + I_x I_z$

For a perfect sphere, all the aspect ratios are equal to one and so the asphericity equals zero.

The radius of gyration, R_g, gives an approximation to its size and is calculated:

$$R_g = \sqrt{\frac{I_r}{M}}$$

where M is the total mass of the molecule and Ir is calculated from the co-ordinates of each atom (a,b,c) and the co-ordinates of the centre of mass (A,B,C):

$$I_r = \sqrt{((a-A)^2 + (b-B)^2 + (c-C)^2)}$$

The molecular radius of the dendrimer is related to the radius of gyration by the relationship:

$$R = \frac{R_g}{\sqrt{\frac{3}{5}}}$$

This assumes that the dendrimers are indeed spheres with uniform surfaces[8].

2.3.4 Surface Area and Molecular Volume

The surface area per terminal group was calculated according to the formula[9]:

$$Az = \frac{A}{Nz} \alpha \frac{R^2}{NcNb^g}$$

where Az – Surface area per terminal group; A – surface area of molecule; Nz – Number of terminal groups for generation z; R – Dendrimer radius; Nc – Core multiplicity; Nb – Branch juncture multiplicity; g – Generation.

This was used to calculate the surface area of the dendrimer to assess the size of the molecules and to give some idea of the surface congestion. At higher generations it is expected that the surface area per terminal groups should decrease to the point of forcing terminal groups from the surface at the de Gennes close packed limit[10]. It takes into account the size of the dendrimer (which is affected by the size of the core), the number of branch points and the number of terminal groups.

The molecular volume was calculated from the molecular radius to give some idea of the quantity of space occupied by the dendrimer, by using simple maths:

$$\text{Volume} = 4/3 \, \pi \, R^3$$

where R is the molecular radius, assuming that the dendrimers are spheres.

The volume per terminal group was calculated by taking the distances of the terminal groups from the silicon on the core to which the branches are attached. When these values are taken as an average over all branches, the distances are measured effectively from the centre of the core. This means that the volume per terminal group is calculated from the full number of frames, not just random structures as in the case of the surface area.

The distances furthest and closest to the core are used and the volume per terminal group is calculated:

$$\text{Volume per T} = [4/3\,\pi\,(Rmax)^3 - 4/3\,\pi\,(Rmin)^3]/N$$

where N is the number of terminal groups and Rmax and Rmin the maximum and minimum distances of terminal groups from the core.

This gives a good assessment of the steric congestion at the periphery of the dendrimer, similar to that gained by the surface area per terminal group. The volume calculation is perhaps more useful for large terminal groups such as diphenylphosphine, which occupy a larger portion of space than, for instance, alcohol groups. Examination of the Rmax and Rmin can reveal any back folding of the terminal groups.

2.4 Miscellaneous Techniques

2.4.1 NMR

Solution State NMR was used as a general characterisation technique and was run on a Bruker Avance 300 spectrometer operating at 300 MHz for ^{1}H, 75 MHz for ^{13}C and 121 MHz for ^{31}P. All NMR samples were run at room temperature with TMS as a primary standard.

2.4.2 Single Crystal X-Ray Diffraction

Some of the crystals produced in the course of this work were too small for a conventional laboratory X-ray diffractometer and, therefore, experiments were performed at the high-flux single-crystal diffraction station 9.8 at the CCLRC Daresbury Laboratory Synchrotron Radiation Source, Cheshire, UK. The data were collected at low temperature (150 K) using a Bruker AXS SMART CCD area-detector diffractometer with X-rays of wavelength between 0.68 and 0.70 Å. The wavelength of the X-rays was selected by a horizontally focussing silicon (111) monochromator and focussed vertically using a cylindrically bent palladium-coated zerodur mirror. The data sets covered more than a hemisphere of reciprocal space with several series of exposures, each series with a different crystal orientation and each exposure taken over 0.2° rotation. Corrections were made for the decay of the synchrotron beam intensity as part of the standard inter-frame scaling procedures. The refinements of the data were carried out using a least-squares method using the programs SHELX-97 and WINGX.

2.4.3 CHN

Elemental Analysis was carried out using a Carlo Erba CHNS analyser for carbon hydrogen nitrogen sulphur determination.

2.4.4 DSC

Differential Scanning Calorimetry was carried out on a Perkin Elmer DSC7 instrument.

2.5 References

1. Accelyrs, Materials Studio, 2001.

2. Hypercube Inc., HyperChem(TM) Professional 5.1, 1115 NW 4th Street, Gainesville, Florida 32601, USA.

3. C. B. Gorman and J. C. Smith, *Polymer*, 2000, **41**, 675.

4. A. K. Rappe, C. J. Casewit, K. S. Colwell, W. A. Goddard and W. M. Skiff, *J. Am. Chem. Soc.*, 1992, **114**, 10024.

5. R. Scherrenberg, B. Coussens, P. Van Vliet, G. Edouard, J. Brackman, E. De Brabander and K. Mortensen, *Macromolecules*, 1998, **31**, 456.

6. C. P. Casey and G. T. Whiteker, *Isr. J. Chem.*, 1990, **30**, 299.

7. J. Rudnick and G. Gaspari, *J. Phys. A: Math. Gen.*, 1986, **19**, L191-L193.

8. P. K. Maiti, T. Cagin, G. F. Wang and W. A. Goddard, *Macromolecules*, 2004, **37**, 6236.

9. S. Pricl, M. Fermeglia, M. Ferrone and A. Asquini, *Carbon*, 2003, **41**, 2269.

10. P. G. Degennes and H. Hervet, *J. Phys. Lett-Paris*, 1983, **44**, L351-L360.

Chapter 3. Molecular Modelling of Dendritic Alcohols

3.1 Introduction

Dendrimers with alcohol terminal groups are common synthetic targets due to the many chemical reactions that can be performed on that group. The POSS core was used to synthesise second generation dendrimers with 24, 48 and 72 terminal alcohol groups respectively creating a very high number of terminal groups within a low generation dendrimer[1].
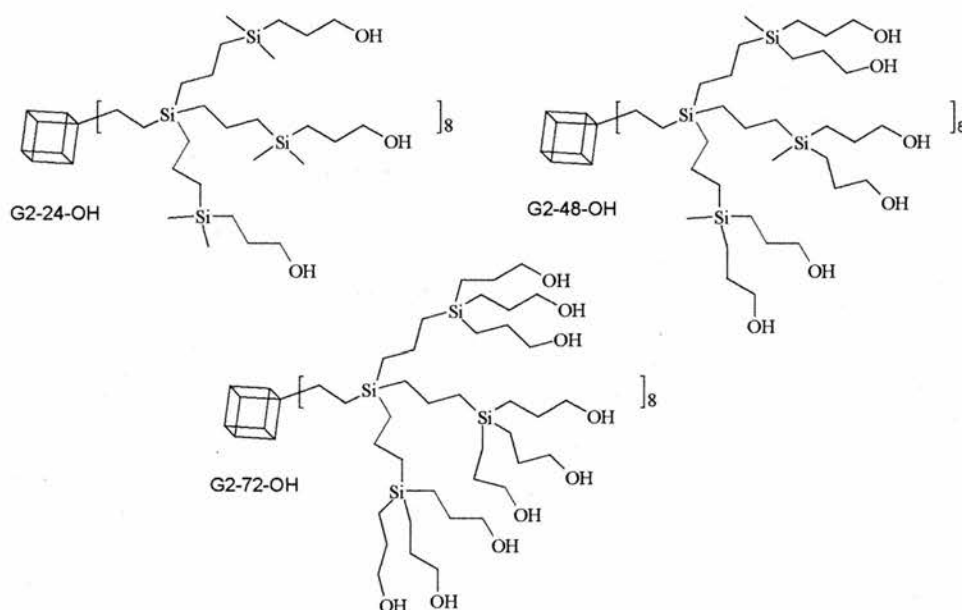
Figure 3.1: Three dendrimers modelled in this chapter with 24, 48 and 72 terminal groups respectively. Only one branch is shown for clarity.[1]

The number of reactive sites on the core allowed for this large number of terminal groups without the synthetic problems that high generation dendrimers have, due to steric crowding within the molecule. For example, a PAMAM dendrimer with ammonia core would be in its fourth generation before 24 terminal groups were produced yet here the second generation can produce up to 72 terminal groups. Additionally, the hydroxyl group is a small end group. Larger terminal groups such

as diphenylphosphine have been shown to create a sterically crowded periphery resulting in incomplete reaction[2-4].

The dendrimers were synthesised from a vinyl POSS core by repetitive hydrosilation and allylation reactions. This produced dendrimers with 24, 48 and 72 terminal allyl groups, similar to first generation equivalents published previously[5]. It is an interesting property of these carbosilane dendrimers that means that the multiplicity of each branch point can be varied. The final reaction sequence of hydroboration and oxidation produced hydroxyl-terminated dendrimers, and was found to have given the primary alcohol product almost exclusively. The physical properties of the molecules are detailed in table 3.1.

Molecule	C	H	O	Si	End Groups	Mass (amu)
G2-24-OH	208	488	36	40	24	4689.56
G2-48-OH	256	584	60	40	48	5746.8
G2-72-OH	304	679	84	40	72	6803.1

Table 3.1: Physical properties of the three molecules modelled.

These dendrimers were characterised by conventional means including multinuclear solution NMR and microanalysis, but while this proved the existence and purity of the product, no information could be gained about the structure of the dendrimers. Molecular modelling studies offered a chance to examine the size, shape of the molecules, and configuration, paying particular attention to the location of the terminal groups.

The dendrimers were modelled according to the protocol described in chapter 2 using the method of Scherrenberg *et al.* to modify the CVFF forcefield to act as a good or poor solvent[6].

3.2 Results and Discussion

3.2.1 Shape and Size of Dendrimers

The size and shape of the three dendrimers was of particular interest due to the size of the POSS core and its multiplicity. The POSS core is nearly spherical and it was proposed that this might influence the shape of the dendrimers making them more spherical. In previous work on dendrimers with low multiplicity cores, spherical molecules are only found at high generations. The hypothesis was that even low generation POSS dendrimers would be spherical.

Firstly the radius of gyration was calculated (table 3.2, figure 3.2) and showed a linear relationship with increasing number of terminal groups. This was as expected for a series of molecules where the outer shell is becoming more populated without any corresponding change in length of branch. Other modelling studies[7] have shown that radius of gyration is known to increase linearly with generation and this shows that the increase is linear within a generation.

Molecule	Solvent	T Groups	Rg (Å)	R (Å)
G2-24-OH	poor	24	9.65	12.45
G2-24-OH	good	24	9.70	12.52
G2-48-OH	poor	48	10.33	13.33
G2-48-OH	good	48	10.03	12.95
G2-72-OH	poor	72	10.80	13.94
G2-72-OH	good	72	10.88	14.04

Table 3.2: Calculated Radius of Gyration (Rg) and Molecular Radius (R) for three dendrimers in both solvent conditions.

Figure 3.2 also shows the calculated molecular radius for the dendrimers, calculated by the method shown in chapter 2, assuming the molecules to be perfectly spherical. In all cases, the molecular radius is approximately 3 Å greater than Rg. The molecules are of approximately the same radius in both good and poor solvent,

implying that solvent quality as calculated has a limited effect on the size of the

dendrimer.
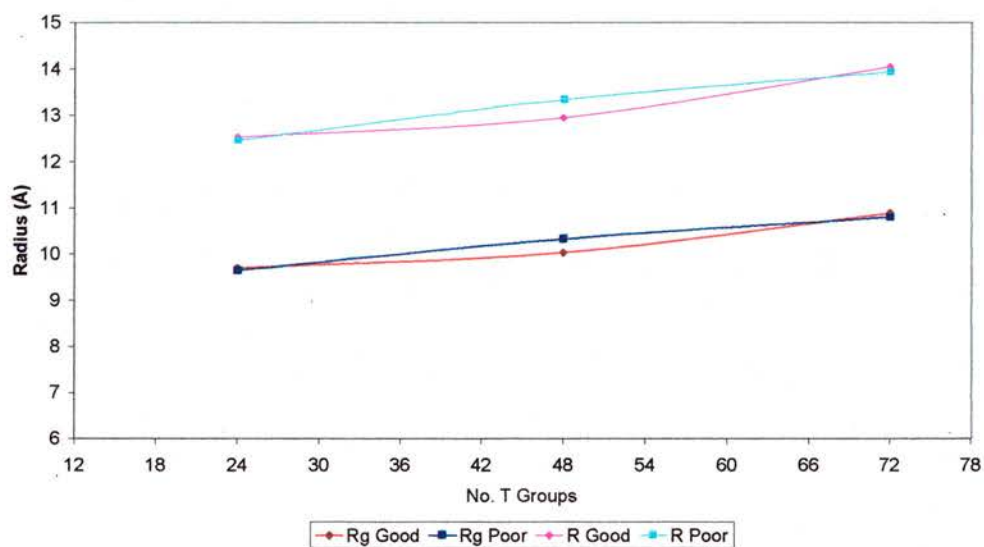
Figure 3.2: Radius of Gyration (Rg), Å, and Molecular Radius (R) Å, for the three dendrimers in both good and poor solvents plotted against number of terminal groups.

The molecular radius of the dendrimers was calculated under the assumption that the

molecules were approximately spherical, but how good an assumption was this? A

good measure of sphericity is the aspect ratio where the ratio of moments of inertia

equal 1 for a perfect sphere. Figure 3.3 shows the aspect ratios of the dendrimers as

functions of number of terminal groups in both solvent conditions. In general, G2-

24-OH was found to be the most spherical but no real correlation could be made

beyond this.

Overall, the aspect ratios are very close to one implying that the dendrimers are close

to spherical. This is interesting when compared to findings by Gorman and Smith[8-

10], Cavallo and Fraternali[7] who report aspect ratios greater than two for fourth and

fifth generation dendrimers with smaller cores of lower multiplicity. This is perhaps

the best evidence yet that the POSS core exerts a strong influence on the shape of the

dendrimer.
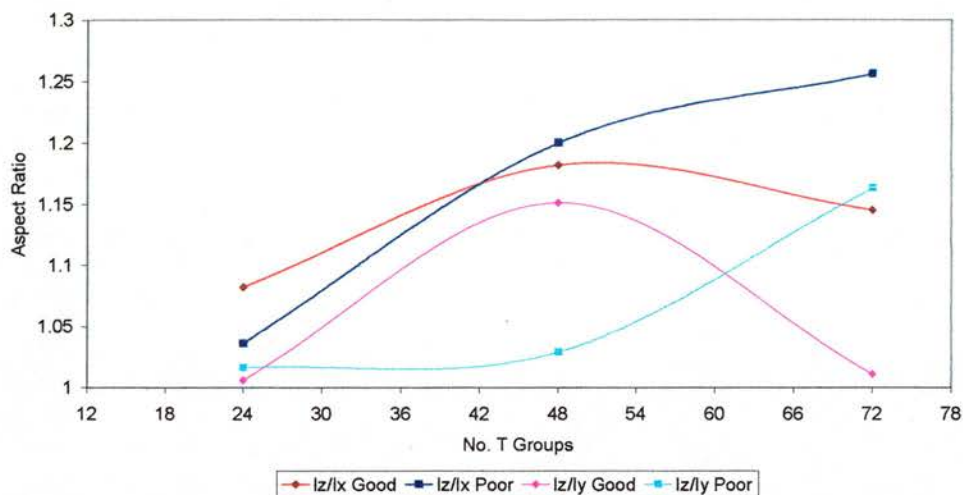
Figure 3.3: Aspect Ratios calculated for each dendrimer and solvent condition as a function of number of terminal groups.

A measure of asphericity can also be made to assess the shape of the dendrimers, shown in figure 3.4. This takes into consideration all moments of inertia, not just the ratio of two.
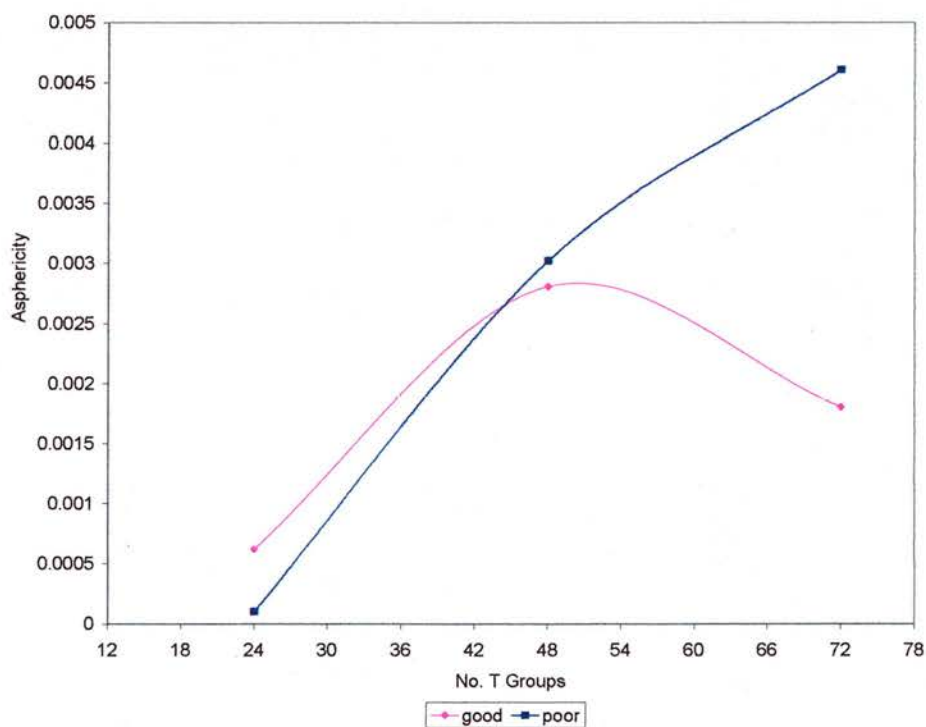
Figure 3.4: Asphericity (δ) plotted against number of terminal groups.

G2-24-OH is again found to be the most spherical ($\delta \sim 0$) but this time a large difference is noted between the good and poor solvent cases for G2-72-OH. This is perhaps due to the increased molecular interactions causing the dendrimer in the poor

solvent to adopt a distorted sphere shape. The values for delta are still very close to that of a perfect sphere and this deviation might also be due to variation caused by experimental error.
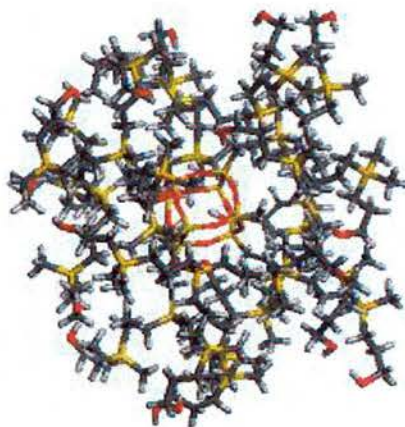
Figure 3.5: G2-24-OH, Carbon: grey; Hydrogen: white; Oxygen: red; Silicon: yellow
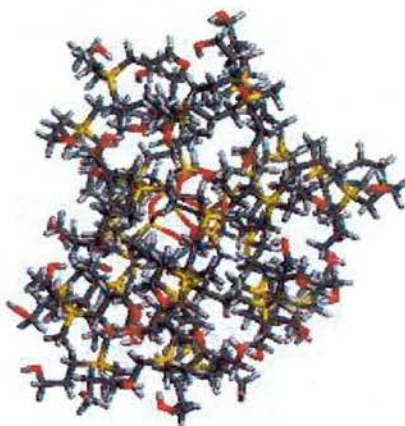
Figure 3.6: G2-48-OH, Carbon: grey; Hydrogen: white; Oxygen: red; Silicon: yellow
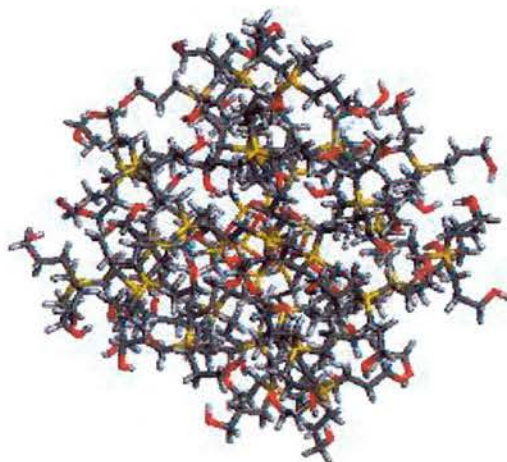
Figure 3.7: G2-72-OH, Carbon: grey; Hydrogen: white; Oxygen: red; Silicon: yellow

Figures 3.5 – 3.7 show snapshots of the three dendrimers to elucidate their globular nature. G2-72-OH appears to amplify the core architecture to the greatest extent, appearing almost cubic. The core is visible in both G2-24-OH and G2-48-OH but there is little information about the molecule's dynamic structure that can be determined from visual inspection of a 2 dimensional image taken from one of five hundred frames.

3.2.2 Location of Terminal Groups
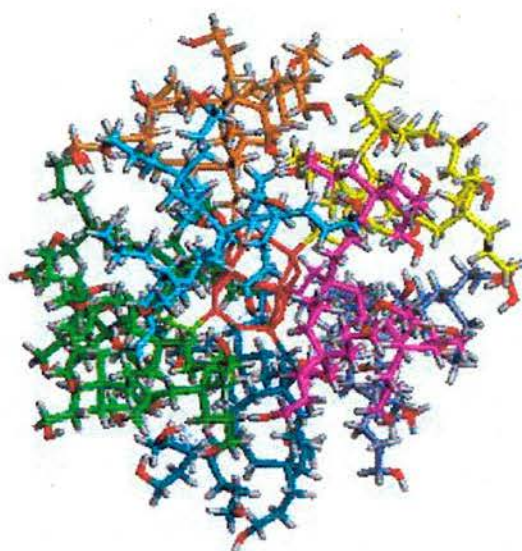
Figure 3.8: G2-72-OH, each branch has been coloured individually to highlight its conformation, terminal groups and the POSS core are red.

Figure 3.8 shows a representation of G2-72-OH in which each branch has been coloured a different colour to illustrate the mixing of the branches. The branches do not intertwine as might be expected and adopt an expanded configuration. It is not possible to assess accurately from one image the distribution of the terminal groups but it can be done from the 500 frames of the production trajectory.

There are three main distance distributions of interest within these dendrimer structures. Firstly, the distance between the core and the terminal groups will show any backfolding. Secondly, the average distance between alcohol groups on individual branches will show the flexibility inherent within the branches, and

finally, the average distance between alcohol groups considering the whole molecule will give a sense of the overall distribution. These three sets of distances would be important if for example, the terminal groups were chelating species and the ease of bidentate co-ordination to a metal complex was to be studied. It is important to know whether terminal groups on the same branch were closer than those on adjacent branches as this could influence the various binding modes to be studied. Alternatively, if further reaction was desired, back-folded branches may be incapable of participating in any reaction.
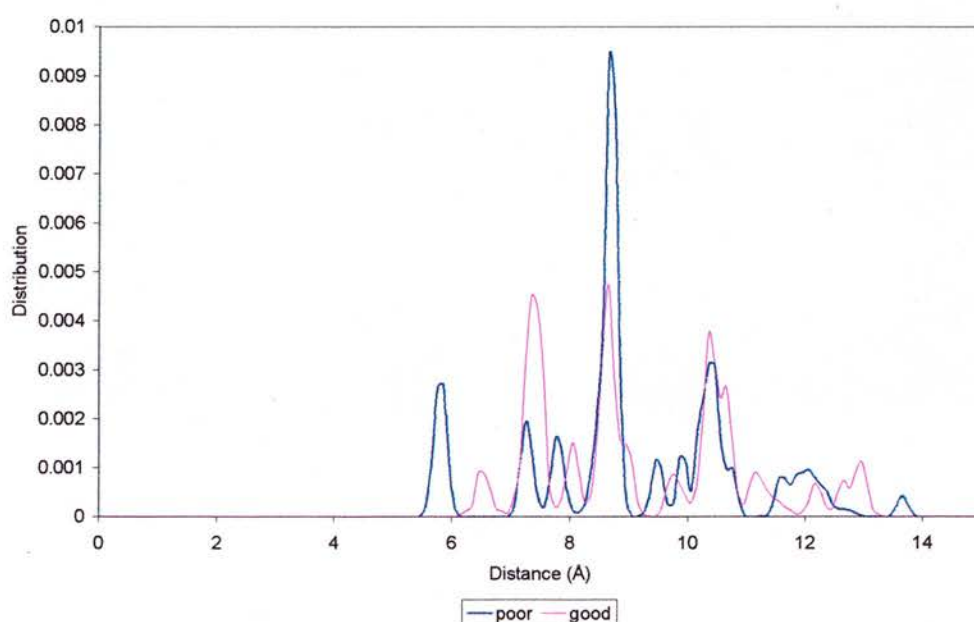
Figure 3.9: G2-24-OH, Distribution of distances between the core silicon atom and the oxygen atoms in the terminal groups of the branch attached to the silicon atom.
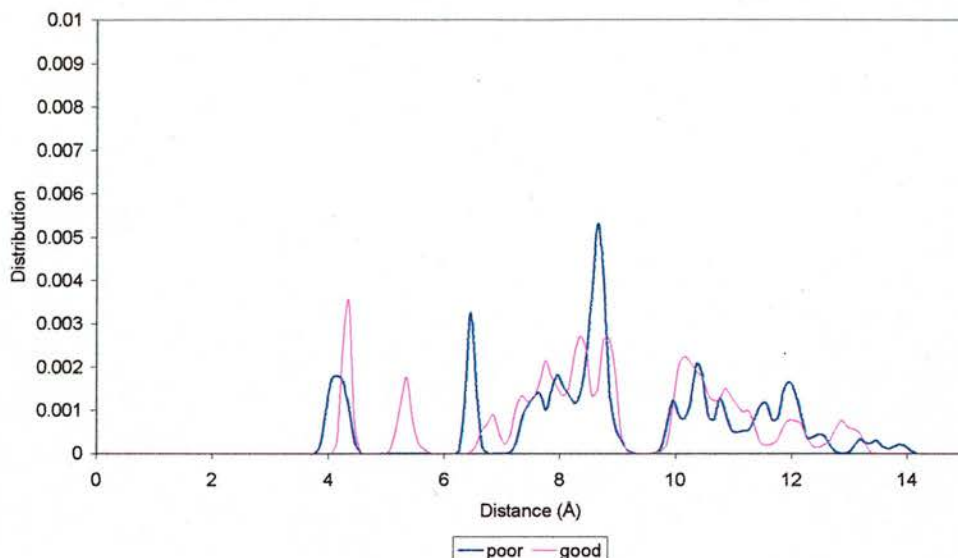
Figure 3.10: G2-48-OH, Distribution of distances between the core silicon atom and the oxygen atoms in the terminal groups of the branch attached to the silicon atom.
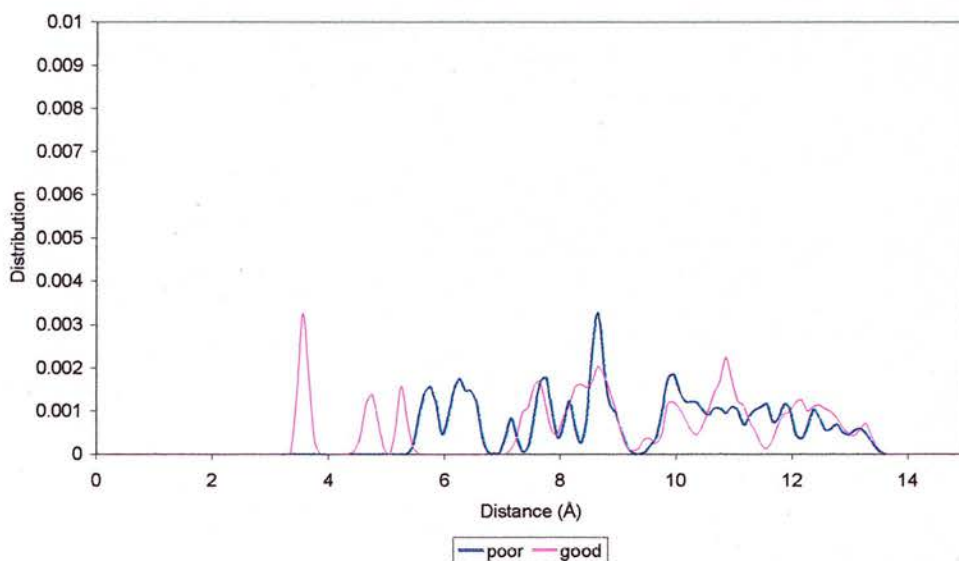
Figure 3.11: G2-72-OH, Distribution of distances between the core silicon atom and the oxygen atoms in the terminal groups of the branch attached to the silicon atom.

Figures 3.9 – 3.11 show the distribution of distances from the terminal oxygen atoms on a branch to the silicon, to which the branch is attached on the core, averaged over 500 ps at 273 K. It can be seen that both solvent and increasing number of terminal groups has an effect on this distribution. The alcohol groups are forced closer to the core as their number increases although none are found within 2.5 Å of the core. This is most likely due to the length and composition of the branches. Longer branches with greater distances between branch points and terminal groups may be

capable of a greater degree of back folding. Zacharopoulos and Economou reported that the distribution of terminal groups in poly (propylene imine) dendrimers changed from unimodal at low generation to trimodal for the fifth generation[11]. They also predicted that for high generations the region around the radius of gyration would become depleted of terminal groups creating a bimodal distribution. Close inspection of figures 3.9 – 3.11 reveals a largely trimodal distribution of end groups for G2-24-OH (figure 3.9) with a large peak around 8.5 Å, just before the calculated radius of gyration (9.65 and 9.70 Å). The distributions for G2-48-OH and G2-72-OH are more bimodal in nature with a distinct minimum in each graph near the radius of gyration. This kind of distribution, predicted for high generations is seen here within a series of generation 2 POSS dendrimers showing that the core gives these molecules structural characteristics of higher generations. The bimodal distribution implies that the terminal groups are forming two shells, one above and one below the calculated radius of gyration, thereby relieving the strain and congestion that extra terminal groups create at the surface.

T Groups	Solvent	Inner limit (Å)	Outer limit (Å)	Thickness of shell (Å)	Volume of shell (Å^3)	Volume/terminal group (Å^3)
24	Poor	5.45	13.95	8.50	10693.25	445.55
24	Good	6.15	13.35	7.20	8991.92	374.66
48	Poor	3.75	14.25	10.50	11899.96	247.92
48	Good	4.15	13.45	9.30	9892.52	206.09
72	Poor	5.35	13.85	8.50	10487.10	145.65
72	Good	3.35	13.65	10.30	10495.88	145.78

Table 3.3: Calculated properties of dendrimers.

The core-terminal group distances can be used to calculate the average volume available to each terminal group on the dendrimer. The volume of the shell occupied by the terminal groups decreases with increasing generations as might be expected for this series of dendrimers. As the density of the terminal groups increases, the branches become less mobile and less able to alter their configuration. The

penetration of terminal groups into the interior increases with number of terminal

groups most noticeably for the good solvent.
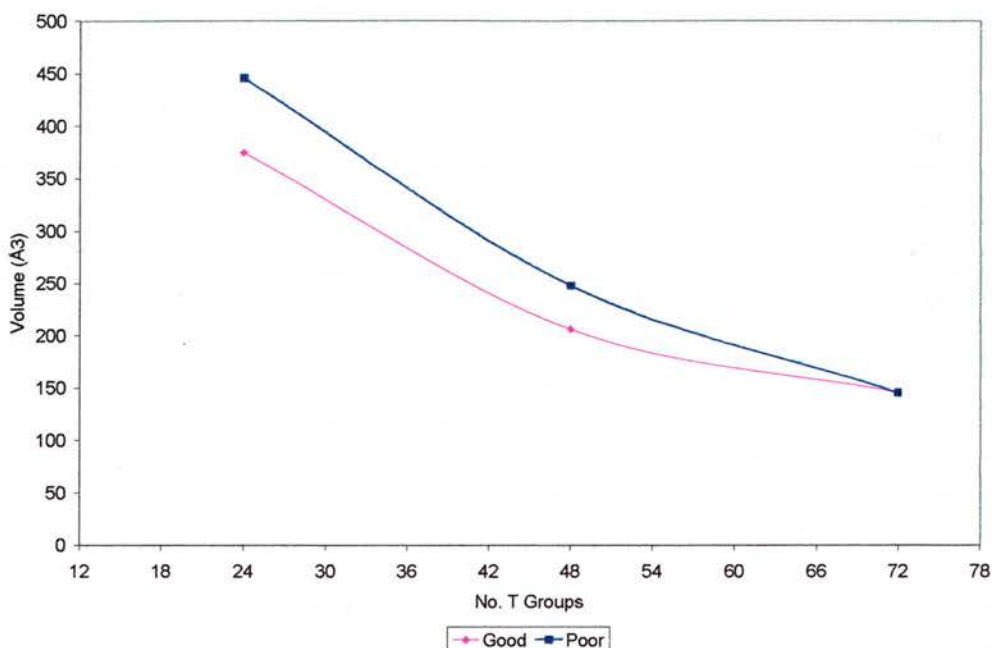
Figure 3.12: Volume per terminal group

The effect of changing the quality of the solvent shows that the region of the

dendrimer occupied by the terminal groups is larger for poor solvent than for good.

This is most apparent for G2-24-OH and G2-48-OH, implying the dendrimers are

more compact in the good solvent. This creates a decrease in volume when

comparing the poor solvent to the good solvent. This implies that the terminal

groups invade the interior of the dendrimer more in poor solvent conditions without

resulting in a smaller molecule, as the outermost radius, at which terminal groups are

found, is in fact larger. The calculated radius gives the outer limits of the terminal

groups and, the difference maybe due to deviation from a perfect sphere. More

volume/terminal group is available in poor solvent conditions because the terminal

groups are distributed through a larger shell.

The molecular volume available to each terminal group is calculated by assuming the

dendrimers are perfect spheres. It is possible to compare the limits of the shell in

which the terminal groups are found with the calculated molecular radius also

calculated assuming a perfect sphere (table 3.4).

T Groups	Solvent	Inner limit (Å)	Outer limit (Å)	R (Å)
24	poor	5.45	13.95	12.45
24	good	6.15	13.35	12.52
48	poor	3.75	14.25	13.33
48	good	4.15	13.45	12.95
72	poor	5.35	13.85	13.94
72	good	3.35	13.65	14.04

Table 3.4: Limits of volume shell in which terminal groups are located with the calculated molecular radius, R, for comparison.

There is good agreement in the trends shown between the two data sets. The

calculated molecular radius was calculated from one frame of the production

trajectory whereas the outer limit for the terminal groups was taken from a

distribution over 500 ps (500 frames).

Figures 3.13 – 3.15 show the effect of adding more terminal groups on the distances

between terminal oxygen atoms throughout the molecule.
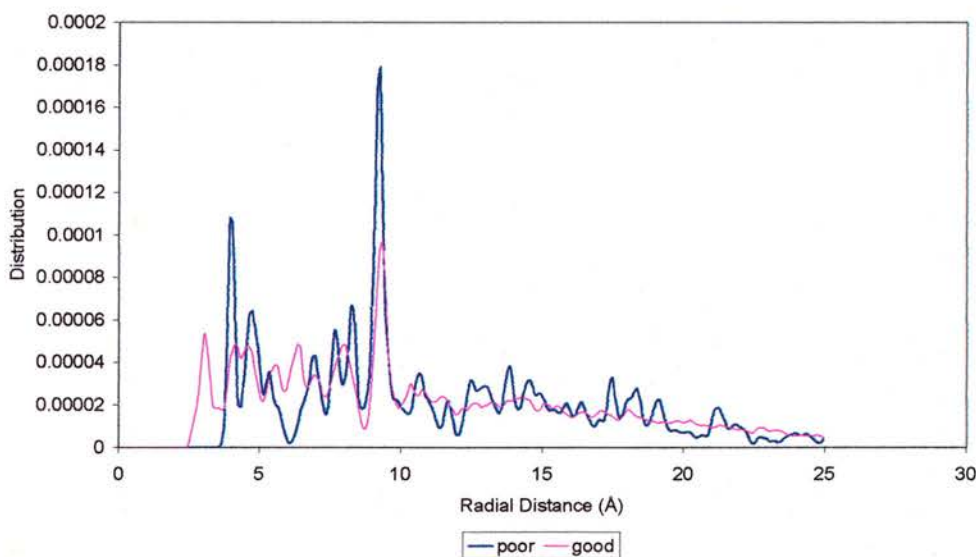
Figure 3.13: G2-24-OH, distance distribution of all terminal oxygen atoms
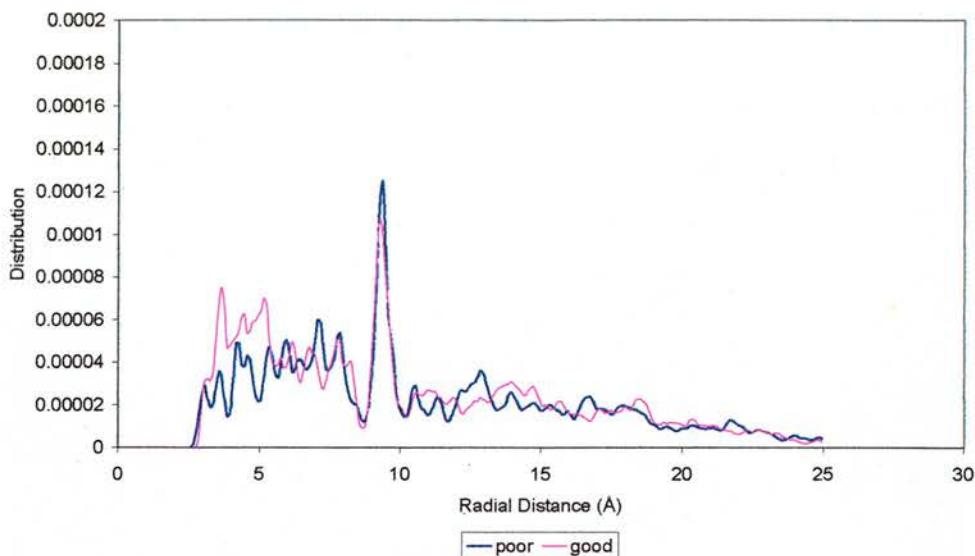
Figure 3.14: G2-48-OH, distance distribution of all terminal oxygen atoms
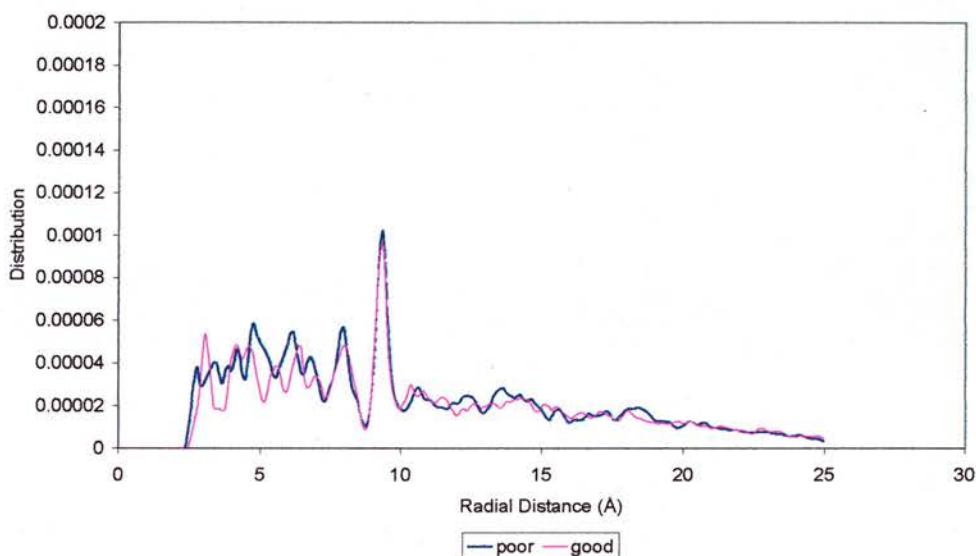
Figure 3.15: G2-72-OH, distance distribution of all terminal oxygen atoms.

These figures (3.13 – 3.15) show the same general features for all molecules and solvents. There is a large peak at approximately 10 Å, an optimum distance between terminal alcohol groups, a distribution in the region between 3 and 8 Å, and a third area above 10 Å. This shows the distances between more remote alcohol groups that tails off. The cutoff for distance measurement was 25 Å, explaining the abrupt end to the graph.

The large peak could be due to intrabranch effects such as the distance between the terminal alcohol groups dictated by the length of the carbon and silicon spacer. On

the other hand, it could be the ideal closest distance for terminal groups between

branches, the first region in the graphs being due mainly to intrabranch distances.

The different solvent has apparently little effect on this distribution.

If the large peak at approx. 10 Å is due to an optimum distance within individual

branches then this should be obvious in the intrabranch distributions (figures 3.16 –

3.18).
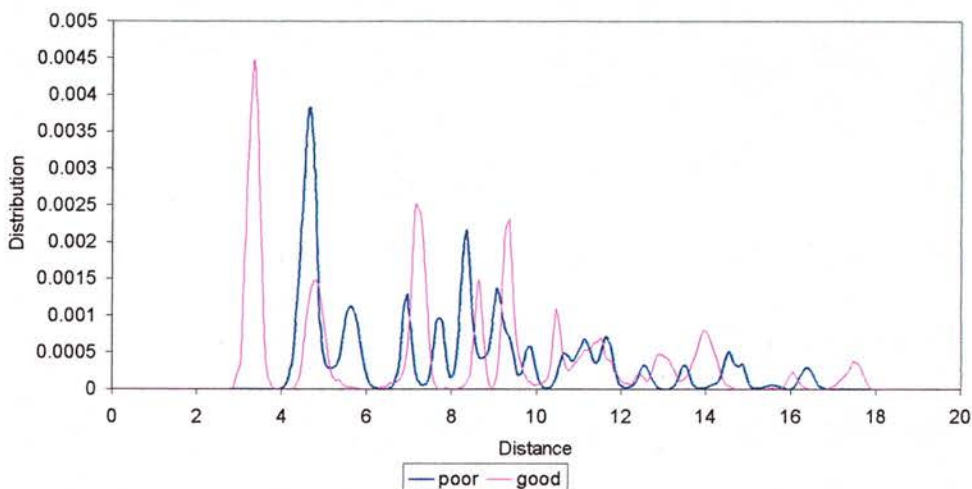
Figure 3.16: G2-24-OH, distance distribution of terminal oxygen atoms within each branch.
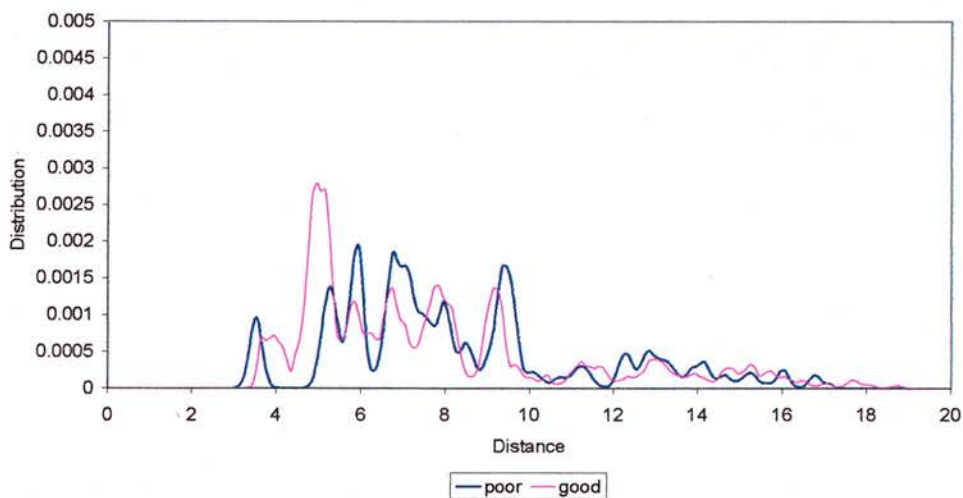
Figure 3.17: G2-48-OH, distance distribution of terminal oxygen atoms within each branch.
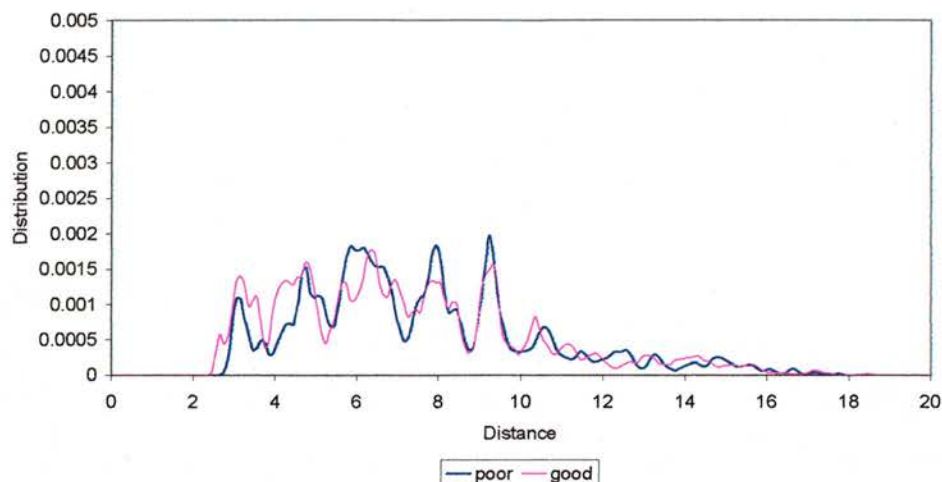
Figure 3.18: G2-72-OH, distance distribution of terminal oxygen atoms within each branch.

There is a change in distribution apparent for all molecules after 10 Å, and peaks

before 10 Å, similar to those in figures 3.13 – 3.15. The average distances between

alcohol groups within the same branch is in the region 3 – 10 Å, a range of distances

easily accessible because of the length of spacers between the groups. This is more

obvious for G2-72-OH than for the smaller molecules. There are more terminal

groups closer together for G2-72-OH, and the distribution is smoother than that of

the other dendrimers. G2-24 and 48-OH show distributions that are more irregular

with sharp peaks from 3.5 – 10 Å. The effects of solvent are more noticeable in

these small molecules with more terminal groups being closer together for the good

solvent. The effect of solvent is negligible for G2-72-OH indicating that the greater

density of terminal groups exerts a greater influence on the structure than the solvent.

This is also indicated by other data such as the molecular volume available per

terminal group (figure 3.13) which shows a difference for G2-24 and 48-OH but not

G2-72-OH. There is a peak at or near 10 Å for all three molecules, regardless of

solvent conditions that could be responsible for the prominent peaks in figures 3.13 –

3.15.

The distributions take roughly the same shape showing that increasing the density of

the terminal groups does not force them much closer together unlike the effect of

solvent. In the good solvent, terminal alcohol groups are closer together for the molecules with 24 and 48 groups.

Overall, the good solvent promotes greater mobility of the terminal groups where it is sterically feasible to do so. This is shown by the terminal groups being both closer together and further apart in the case of G2-24-OH, but also in G2-48-OH the terminal groups are closer to one another in the good solvent case.

G2-72-OH is an example of a dendrimer exhibiting many of the characteristics of higher generations such as a bimodal distribution of terminal groups and less mobility of those terminal groups. G2-24-OH has the least dense structure and this makes it easier for the alcohol groups to penetrate the inner regions of the dendrimer. This might be explained by the fact that the branches are smaller and so do not require such a large internal void to occupy should they curl in.

3.3 Conclusions

The method of Scherrenberg[6] provides a reasonable approximation to the effects of good and poor solvent on the three dendrimers studied. While a simulation with explicit solvent molecules might allow for more precise measurement of these effects, the size of the dendrimers means that this is not feasible with current computing capabilities. A method that allows for more variation in the implicit solvent would allow more information to be gained on the solution behaviour of these molecules, rather than considering two extremes.

The effects of different solvents are more apparent for fewer terminal groups. This is not easy to explain but may be that the solvent effects are more important when there are fewer intramolecular interactions. When the number of terminal groups increases the solvent effects become less significant and eventually exert little effect on the structure.

No mixing of the branches is observed, probably due to the branches being too short and despite the molecular volume per terminal group decreasing upon increasing numbers of terminal groups, the alcohols are not forced closer together. The terminal groups are found in a shell approximately 7 - 10 Å thick and no significant back folding is observed. This is a consequence of the high multiplicity and large dimensions of the core, the length of the monomer units and insufficient steric congestion to force the terminal groups closer together.

No terminal groups approach within 2.5 Å of the core due to the size of the branches and limited flexibility of the arms.

3.4 References

1. X. J. Zhang, K. J. Haxton, L. Ropartz, D. J. Cole-Hamilton and R. E. Morris, *J. Chem. Soc., Dalton Trans.*, 2001, 3261.

2. L. Ropartz, K. J. Haxton, D. F. Foster, R. E. Morris, A. M. Z. Slawin and D. J. Cole-Hamilton, *J. Chem. Soc., Dalton Trans.*, 2002, 4323.

3. L. Ropartz, R. E. Morris, D. F. Foster and D. J. Cole-Hamilton, *Chem. Commun.*, 2001, 361.

4. L. Ropartz, R. E. Morris, G. P. Schwarz, D. F. Foster and D. J. Cole-Hamilton, *Inorg Chem Commun*, 2000, **3**, 714.

5. P. I. Coupar, P. A. Jaffres and R. E. Morris, *J. Chem. Soc., Dalton Trans.*, 1999, 2183.

6. R. Scherrenberg, B. Coussens, P. Van Vliet, G. Edouard, J. Brackman, E. De Brabander and K. Mortensen, *Macromolecules*, 1998, **31**, 456.

7. L. Cavallo and F. Fraternali, *Chem. Eur. J.*, 1998, **4**, 927.

8. C. B. Gorman and J. C. Smith, *Polymer*, 2000, **41**, 675.

9. C. B. Gorman and J. C. Smith, *Acc. Chem. Res.*, 2001, **34**, 60.

10. Z. W. Yang, Q. X. Kang, H. C. Ma, C. L. Li and Z. Q. Lei, *J Mol Catal A-Chem*, 2004, **213**, 169.

11. N. Zacharopoulos and L. G. Economou, *Macromolecules*, 2002, **35**, 1814.

Chapter 4. Molecular Modelling of Dendritic Ligands

4.1 Introduction

A series of diphenylphosphine terminated dendrimers were synthesised by Ropartz *et al.*[1] with the POSS core and used as ligands for rhodium catalysed hydroformylation reactions. These dendrimers were derived from vinyl POSS cores functionalised mainly by hydrosilation and reaction of Grignard reagents with chlorosilanes as shown in figure 4.1.
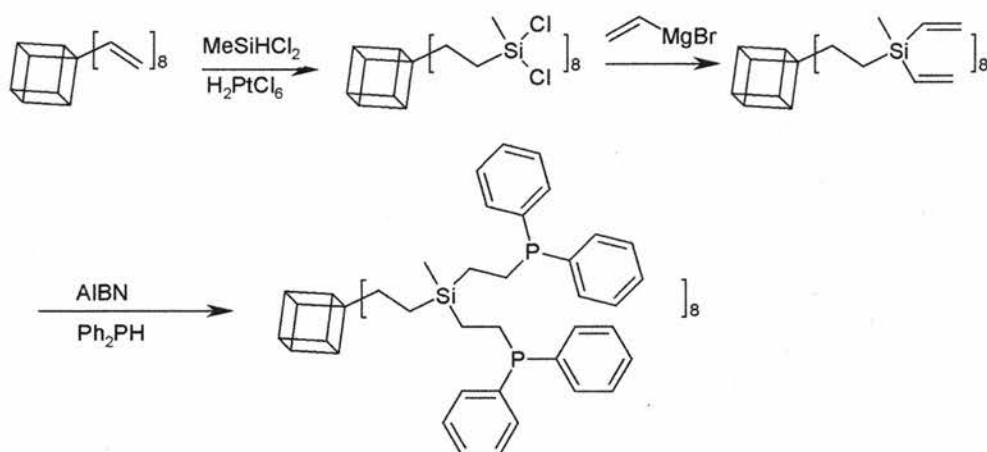
Figure 4.1: Synthesis of G1-ethylPPh$_2$, adapted from Ropartz *et al.*[1].

For example, hydrosilation of dichloromethylsilane to vinyl POSS creates G1- 16Cl which can be reacted with vinylmagnesium bromide to produce G1-16vinyl and then functionalised through a radical reaction with diphenylphosphine to produce G1-16ethylPPh$_2$ (figure 4.1). In some cases LiCH$_2$PPh$_2$-TMEDA or Ph$_2$PCH$_2$OH was added directly to the silicon-chlorine terminated dendrimers. The structure of the dendrimers was varied generation, composition of branches and size of branches following results by de Groot *et al.*[2] and preliminary results on some of these dendrimers[3-5]. The dendrimers synthesised are listed in table 4.1 along with details of molecular modelling studies.

Dendrimer	Yield (%)	Conversion (%)	Modelling (b)
G1-16ethylPPh$_2$	95	>99 %	Both
G2-propyl-48ethylPPh$_2$	77	84	Not Modelled
G2-propyl-32ethylPPh$_2$	(c)	(c)	Materials Studio
G1-24ethylPPh$_2$	95	60	Materials Studio
G1-16propylPPh$_2$	96	56	Both
G1-16ethylPAr$_2$ (a)	92	75	Not Modelled
G1-24methylPPh$_2$	93	60	Not Modelled
G1-16methylPPh$_2$	60-70	>95	Hyperchem
G1-16methoxyPPh$_2$	76	>86	Materials Studio
G1-16ethoxyPPh$_2$	85	>92	Materials Studio

Table 4.1: Nine dendrimers synthesised for catalytic testing, adapted from Ropartz *et al.*[1] *(a):* Ar = 3,5-C$_6$H$_5$(CF$_3$)$_2$; *(b):* Both – studied with both Materials Studio and Hyperchem (chapter 5), Materials Studio or Hyperchem – studied with either one program or the other, Not Modelled – not studied. Yield refers to the isolated chemical yield, conversion refers to the success of the reaction adding PPh$_2$ to the periphery; (c): not synthesised, modelled instead of G2-propyl48ethylPPh$_2$.

The reactions to functionalise the exterior of the dendrimer gave a range of results with some dendrimers being fully functionalised (G1-16ethylPPh$_2$, also determined by MALDI-TOF and NMR) and others only partially. G1-24ethyl- and methyl-PPh$_2$ were found to have the lowest conversion, most likely due to increased steric crowding. G1-24methylPPh$_2$ was found to be most affected by this having both low yield and conversion and along with the ethyl analogue was not used as a ligand. G1-16ethylPAr$_2$ was also obtained in lower conversion. Trifluoromethyl groups were added in an attempt to improve the selectivity of the hydroformylation reaction through their electron withdrawing effect. Due to difficulties dealing with the more extensive hydrogen bonding in this system, it was not modelled. G2-propyl48ethylPPh$_2$ was too large to model effectively and so a slightly smaller version, G2-propyl32ethylPPh$_2$ was studied instead.

The catalysis results obtained are summarised in table 4.2. The dendrimers were complexed to rhodium under an atmosphere of syngas and used to catalyse the hydroformylation of oct-1-ene. This reaction, like many catalytic processes can

create a range of products, most notably the desired linear product nonan-1-al and the most common by-product in some processes, the branched molecule 2-methyloctan-1-al. The selectivity of the catalysts for these two products are quoted as a linear:branched (l:b) ratio. The higher it is, the more selective the catalyst is.

Ligand	T/h	Rate/$10^{-3}s^{-1}$	Isomerisation (%)	Nonan-1-al (%)	l:b ratio
G1-16methylPPh$_2$	0.3	6.2	12.1	68.5	3.9
G1-16ethylPPh$_2$	2	1.2	6.6	86.0	13.9
G1-16propylPPh$_2$	2	1.5	5.1	78.0	5.0
G1-16methoxyPPh$_2$	2	0.7	9.0	76.2	5.7
G1-16ethoxyPPh$_2$	2	2.0	8.3	78.1	6.4
G1-16ethylAr$_2$	2	1.1	20.0	73.0	15.0
G2-propyl-48ethylPPh$_2$	3	0.6	7.5	83.8	11.5

Table 4.2: Results of hydroformylation of oct-1-ene. Reaction Conditions: [Rh(acac)(CO)$_2$] (2.0 x 10^{-5} mol), toluene (4 cm^3), oct-1-ene (3.8 x 10^{-3} mol), P:Rh = 6:1, 120 °C , 10 bar, conversion all >99.9 %, % isomerisation refers to formation of internal alkenes. Adapted from Ropartz *et al.*[1].

The above data is for a series of dendrimers related by the same core and terminal groups with a variety of internal structures. The effect of the length and composition of the spacer between terminal group and branch point is clear from the catalytic data, and one dendrimer, G1-16ethylPPh$_2$ gives far better selectivity (l:b = 13.9) than the others studied in this chapter. A related family of dendrimers with different phosphorus groups (dialkylphosphines) were synthesised and used as ligands for hydrocarbonylation reactions but showed no improved selectivity over small molecular analogues[6].
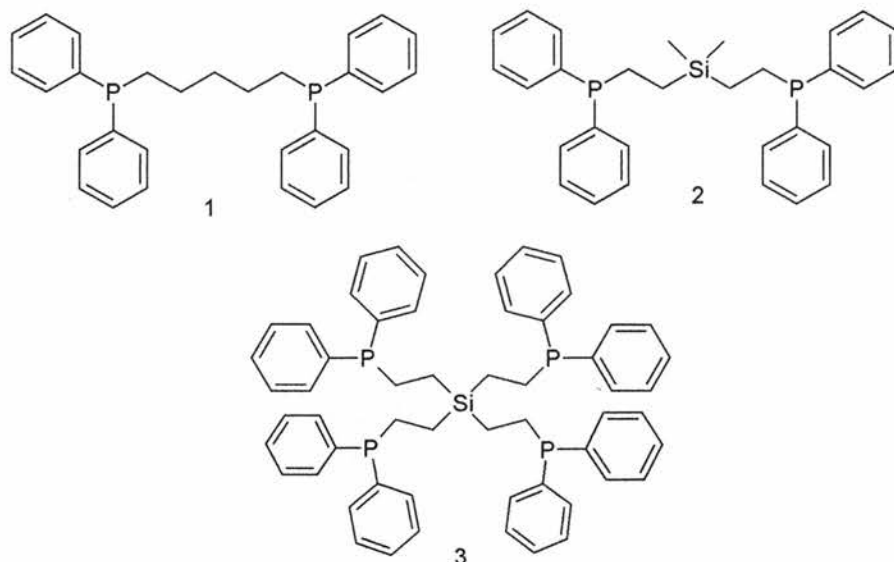
Figure 4.2: Three small molecules synthesised as non-dendritic branch analogues of G1-16ethylPPh$_2$. Molecule 1: 1,5-bis(diphenylphosphino)pentane; molecule 2: bis(diphenylphosphinoethyl)dimethylsilane; molecule 3: tetrakis(diphenylphosphino)silane.

Three small molecule analogues of the branches were synthesised to help determine the influence of the dendritic structure on the catalytic results. The results obtained for catalytic experiments are detailed in table 4.3.

Ligand	T/h	Rate / $10^{-3}s^{-1}$	Oct-2-ene (%)	3- + 4-Octene (%)	Nonan-1-al (%)	L:b ratio
1	2	3.6	10.6	0.83	70.1	3.4
2	2	3.0	5.8	0.90	72.7	3.8
3	2	2.1	6.2	0.40	77.4	5.2

Table 4.3: Results of hydroformylation of oct-1-ene. Reaction Conditions: [Rh(acac)(CO)$_2$] (2.0 x 10^{-5} mol), toluene (4 cm^3), oct-1-ene (3.8 x 10^{-3} mol), P:Rh = 6:1, 120 °C , 10 bar, conversion all >99.9 %. Adapted from Ropartz *et al.*[1].

Comparison of the results from the catalytic experiments indicate that the dendritic structure exerts a positive effect on the selectivity for the linear product.

The main goals of this work were to study the size and shape of the various dendrimers, particularly as dendrimers are viable candidates for recycling from homogeneous catalysis mixtures by filtration techniques. In keeping with the ligating properties of the molecules, the location of the terminal groups was examined to determine whether these groups were readily available for complexation

on the surface of the molecule or folded back inward and shielded from reaction.

The effects of solvent were studied for G1-16ethylPPh$_2$ because previous studies

have shown that the quality of the solvent can affect the location of the terminal

groups. The catalytic reactions were carried out at 120 °C and the effects of

temperature were investigated to measure the effects on the dendrimer structure. It is

not possible to measure the natural bite angle[7] for these dendrimers using Materials

Studio[8] but further discussion of this is made in chapter 5.
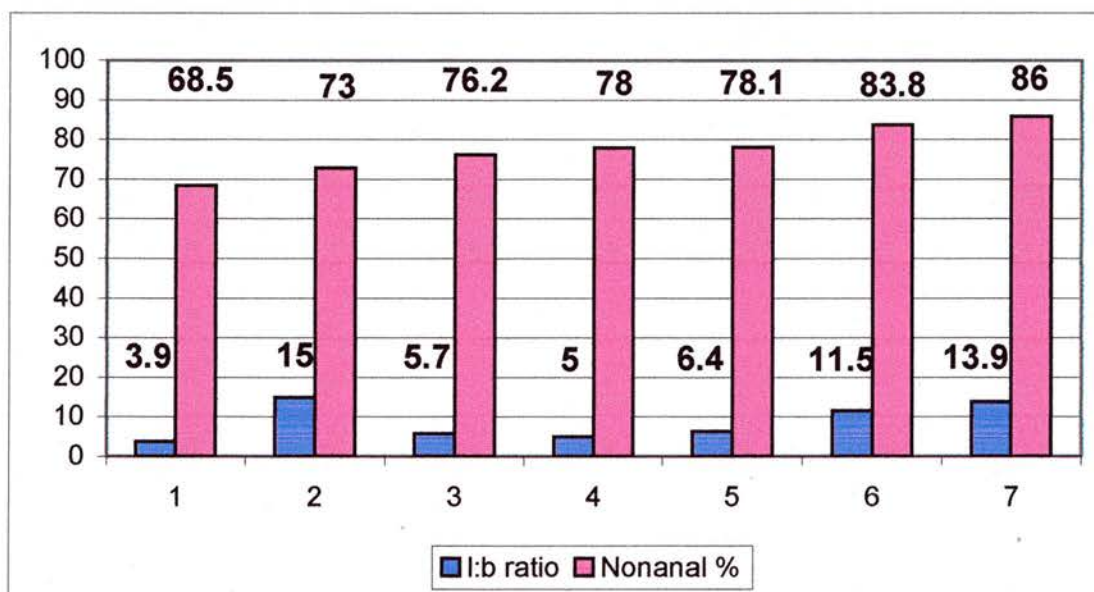
Figure 4.3: Selectivity to nonan-1-al and l: b ratio using different POSS dendritic ligands, *1* = G1-16methylPPh$_2$, *2* = G1-16ethylPAr$_2$, *3* = G1-16methoxyPPh$_2$, *4* = G1-16propylPPh$_2$, *5* = G1-16ethoxyPPh$_2$, *6* = G2-propyl-48ethylPPh$_2$, *7* = G1-16ethylPPh$_2$ (Dendrimer B), adapted from Ropartz *et al.* [1]

It is known that diphosphine ligands with flexible backbones (e.g. 1,5-bis-

diphenylphosphinopentane or the hexane equivalent) give low l: b. Due to the nature

of these ligands, they are less likely to form bidentate complexes and more likely to

form dimers. Bidentate binding of diphosphine ligands is thought to favour good

selectivity and this is best achieved with ligands with constrained backbones such as

xantphos or BISBI (figure 4.35). The results from the three small molecules (figure

4.2) can be compared to G1-16ethylPPh$_2$ to assess the effect of the dendrimer

structure on the selectivity. If the dendrimer structure is causing the ligand part to be

more constrained, evidence of this should be found in modelling the uncomplexed ligands. Simply by comparing the distances between the PPh_2 groups, the amount of constraint exerted on the ligand can be assessed and insight gained into the catalytic results. The three small molecules in figure 4.2 were also studied to investigate how their PPh_2 distances compare with the dendrimer.

For simplicity, this work is split into several parts. Firstly a study of four first generation dendrimers whose structures vary slightly are compared, followed by a series of molecules linked by generation, then two more in-depth studies on the effects of temperature and solvent on G1-16ethylPPh$_2$. The final analysis is a comparison of the results from both modelling and the catalytic experiments, looking for trends between the varying selectivity of the dendrimers and the location of the terminal groups.

4.2 Results and Discussion

4.2.1 First Generation Series
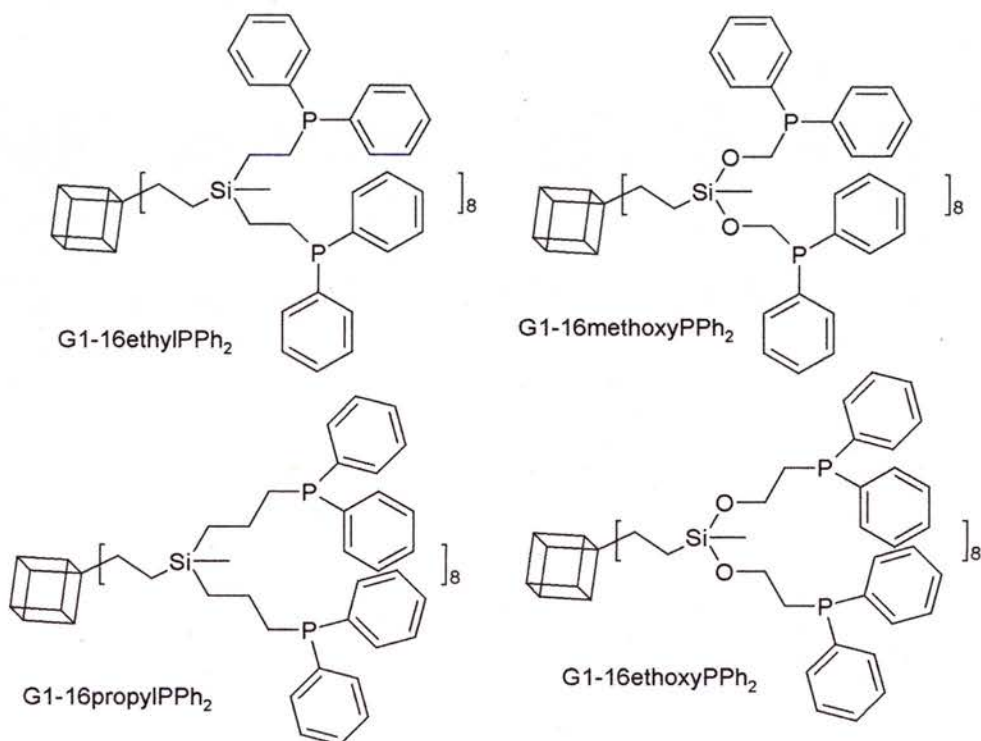
Figure 4.4: Four dendrimers under consideration in section whose structures vary by addition or substitution of CH_2 or O to the branches.

These four dendrimers (figure 4.4) were modelled according to the standard protocol using Materials Studio[8] outlined in chapter 2, and analysed similarly.

Molecule	C	H	O	P	Si	End Groups	Molecular Mass (amu)
G1-16ethylPPh$_2$	248	280	12	16	16	16	4397.9
G1-16methoxyPPh$_2$	232	248	28	16	16	16	4429.45
G1-16propylPPh$_2$	264	312	12	16	16	16	4622.33
G1-16ethoxyPPh$_2$	248	280	28	16	16	16	4653.88

Table 4.4: Physical properties of diphenylphosphine dendrimers.

Table 4.4 outlines the basic composition of the four molecules. The main aim of this work is to see how the addition or substitution of CH_2 or O influences the location of the terminal groups.

4.2.1.1 Size and Shape of Molecules

The general shape of the molecule was considered first and table 4.5 details some calculated values for the dendrimers. The moments of inertia with respect to each axis were calculated from the atomic co-ordinates and it was found that the addition of oxygen caused a decrease in moment as shown in figure 4.5.

Molecule	Mass (amu)	Ix	Iy	Iz	Ir	Iz/Ix	Iz/Iy
G1-16ethylPPh$_2$	4397.90	247149.69	259204.04	291917.24	399135.49	1.18	1.13
G1-16methoxyPPh$_2$	4429.45	237682.40	242759.42	252657.04	366549.42	1.06	1.04
G1-16propylPPh$_2$	4622.33	253829.38	293284.66	307525.29	427319.66	1.21	1.05
G1-16ethoxyPPh$_2$	4653.88	250915.81	262480.87	279080.75	396238.71	1.11	1.06

Table 4.5: Calculated properties of dendrimers, Ix, Iy, Iz are the moments of inertia about axes x, y and z respectively. Iz/Ix is the principle aspect ratio, Ir the total moment of inertia.

The aspect ratios indicate that the addition of oxygen makes the molecules more spherical whilst the addition of CH$_2$ makes the molecule slightly less spherical and the moments of inertia larger.
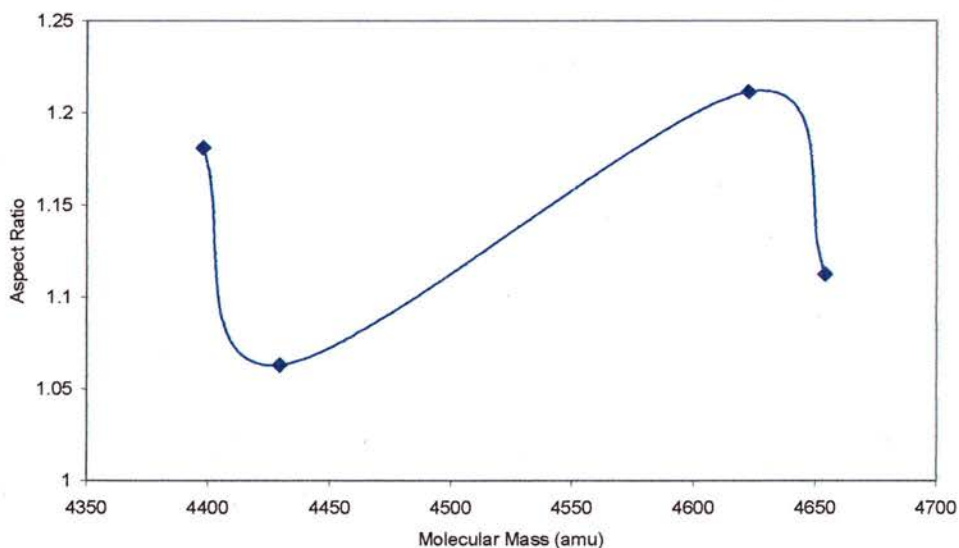
Figure 4.5: Aspect Ratio vs Molecular Mass. Line as a guide to the eye only.

The aspect ratio of a perfect sphere is 1 (Iz = Iy = Ix) and all the dendrimers have aspect ratios in the range 1.04 – 1.18 making them highly spherical. This is unusual for first generation dendrimers but provides evidence that the near-spherical

architecture of the core is being amplified by the branches. In previous studies, near-spherical dendrimers are only found from the fifth generation onwards[9].
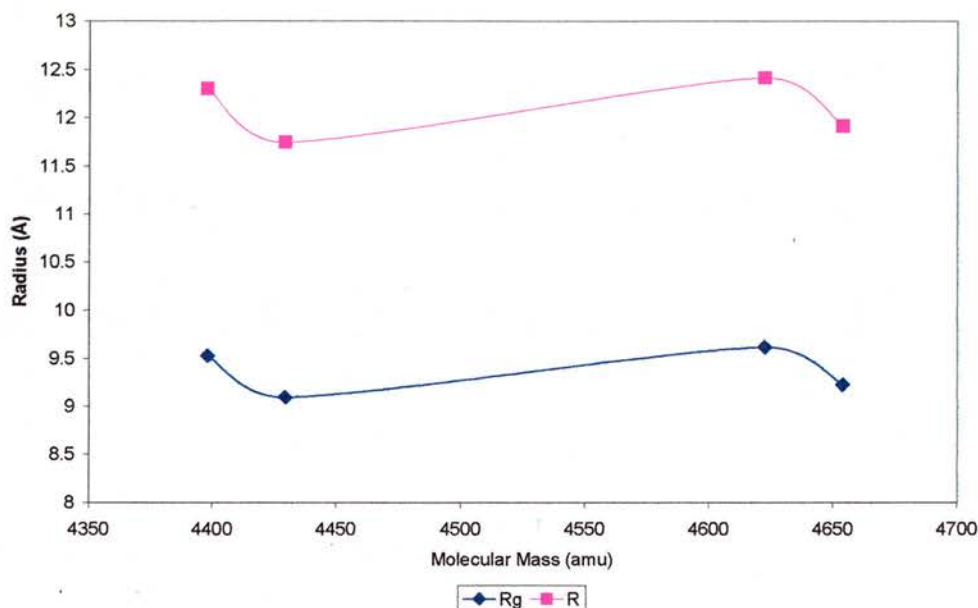
Figure 4.6: Radii of Gyration (Rg) and Molecular Radius (R) versus molecular mass.

The radii of gyration show similar trends to the aspect ratio. The molecules are generally slightly smaller when CH_2 is replaced by oxygen and the addition of oxygen results in a smaller radius regardless of the increase in mass or branch length. The molecular radius predictably follows the same trends and is used to calculate the surface area of the molecule assuming it to be perfectly spherical.

Molecule	Mass (amu)	Rg (Å)	R (Å)	Surface Area ($Å^2$)	S per T ($Å^2$)	δ
G1-16ethylPPh$_2$	4397.90	9.53	12.30	1900.79	118.80	0.001342
G1-16methoxyPPh$_2$	4429.45	9.10	11.74	1733.17	108.32	0.000063
G1-16propylPPh$_2$	4622.33	9.61	12.41	1936.20	121.01	0.003847
G1-16ethoxyPPh$_2$	4653.88	9.23	11.91	1783.20	111.45	0.000781

Table 4.6: Comparison of the Radius of Gyration (Rg) and Molecular Radius (R), the surface area of the dendrimer assuming a perfect sphere, radius R, and surface area per terminal group and asphericity (δ).

The surface area per terminal group indicates how much space is available at the periphery of the dendrimer for each terminal group and again follows the same trend. The asphericity shows the same trends as the principal aspect ratio (Iz/Ix) with the

addition of oxygen creating a more spherical molecule. For a perfect sphere, $\delta = 0$ as all moments of inertia are equal. Asphericity, δ, is a better measure of sphericity as it takes all three moments of inertia into account, not just two like the principle aspect ratio (Iz/Ix).

4.2.1.2 Location of Terminal Groups

The location of the terminal groups in these four dendrimers was studied in three ways. The distance between phosphorus atoms on each individual branch, the distance between all phosphorus atoms and the distance between the phosphorus on a branch and the silicon on the core to which the branch is attached. These were calculated by the method detailed in chapter 2.

Table 4.7 shows the average distance between phosphorus atoms and the standard deviation in the measurement. The distance between the pair of phosphorus atoms on each branch decreases upon substitution of a CH_2 group with oxygen, this effect being most pronounced between the propyl and ethoxy branches.

Molecule	Distance (Å)	Standard Deviation
G1-16ethylPPh$_2$	6.37	0.91
G1-16methoxyPPh$_2$	6.31	0.93
G1-16propylPPh$_2$	8.87	1.25
G1-16ethoxyPPh$_2$	7.19	1.20

Table 4.7: Average intra-branch phosphorus distances.

Increasing the length of the branch has a greater effect on the distance between the phosphorus groups than substitution of CH_2 with oxygen. The standard deviations can give some indication about how much variation there is in the distances, a high standard deviation in the average distance would indicate that there is a greater range of lengths from which the average is calculated. This indicates in turn that the

branch is more flexible and that the terminal groups find it easier to move. As might be expected, the longer branches of G1-16propyl- and ethoxy-PPh$_2$ have larger standard deviations, indicating more flexibility. This trend can also be clearly seen in figure 4.7, which gives the distances between all terminal groups in the molecule over all frames.
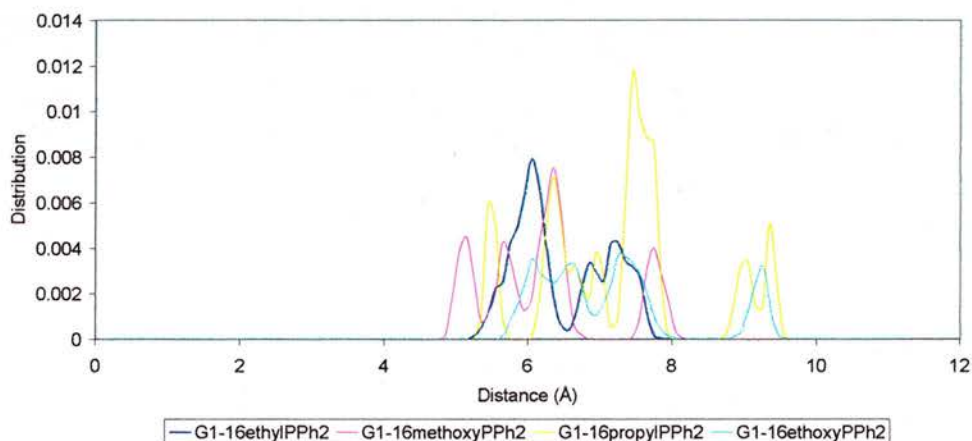
Figure 4.7: The distribution of phosphorus distances within the four dendrimers, between branches. The distribution shows large peaks around 6 Å for G1-16ethyl and methoxy-PPh$_2$ corresponding to their average distances and peaks at 8 Å and 7 Å for G1-16propylPPh$_2$ and G1-16ethoxyPPh$_2$ respectively. G1-16ethylPPh$_2$ shows the most compact distribution while the more flexible branches, G1-16ethoxy- and propyl-PPh$_2$ show more expanded distributions of distances indicating a wider range of conformations are energetically accessible.
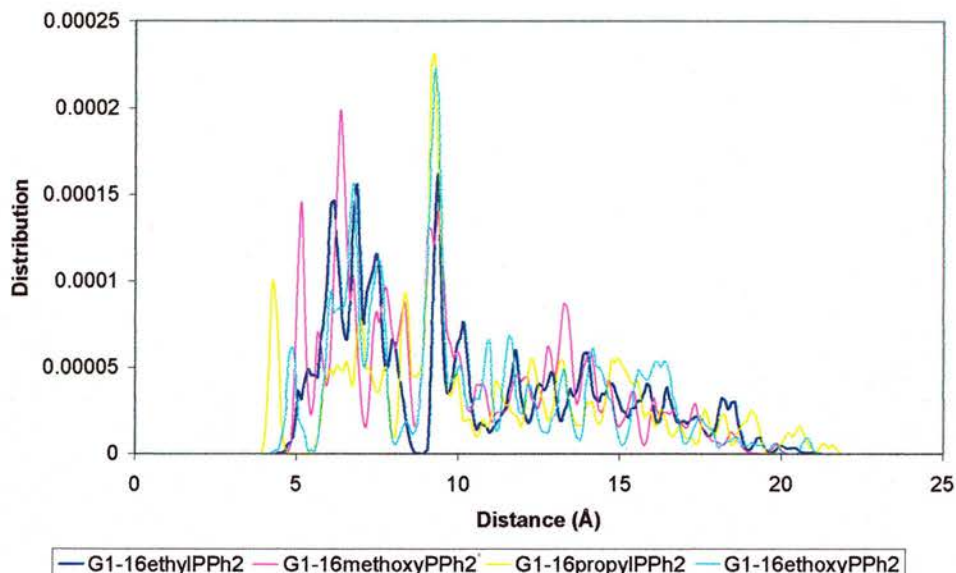
Figure 4.8: P-P distance distribution over all terminal groups and frames.

The distance distributions for all PPh_2 show three main regions. Firstly, the large area under the distribution graph between approx. 5 – 9 Å indicates that these distances are most common in the molecule both from inter- and intra-branch contributions. Around 10 Å is a large peak that is relatively sharp, indicating a significant number of atoms are this distance apart. As no peaks occur around 10 Å in the intra-branch graph (figure 4.7), it can be concluded that this is not due to P atoms on the same branch. It may be due to terminal groups on branches attached to silicon on adjacent edges of the core. Above 10 Å is the third region and is relatively low density, which tails off around 23 Å. This is most likely due to very remote terminal groups such as those attached to the core on silicon atoms across the face and body diagonals of the core. This is the opposite effect to that found for the alcohol dendrimers (chapter 3) where it is likely that similar peaks noted around 10 Å are due to alcohol groups within the same branch. This is possibly a combined effect of the longer arms and smaller terminal groups possessed by the alcohol dendrimers.
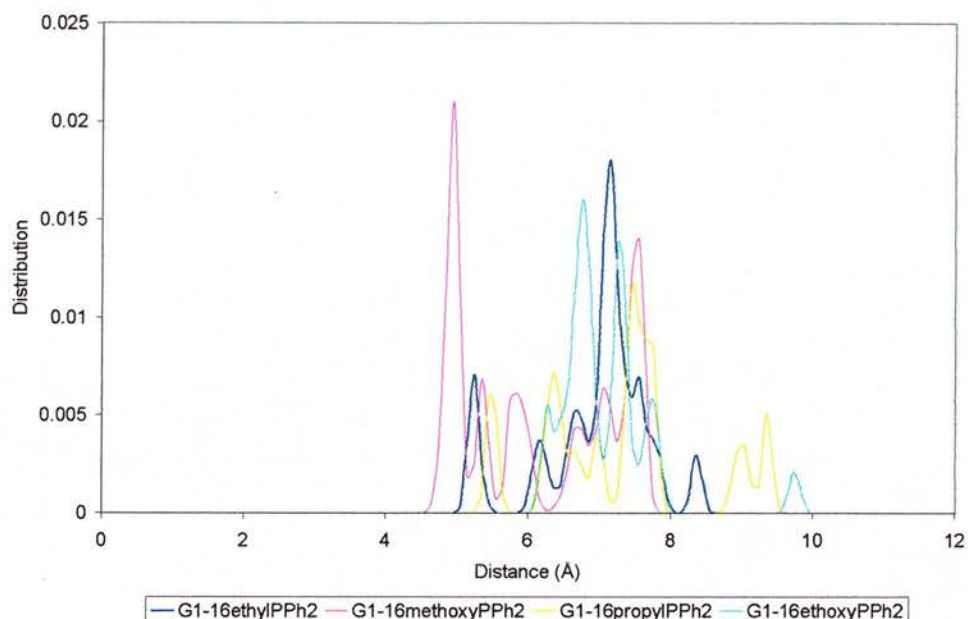
Figure 4.9: Distance of terminal groups from core of molecule as a distribution over time and all branches.

Diphenylphosphine units are very bulky and in such low generation would not be expected to back-fold into the core regions. Measuring the Si-P distances for each branch shows that no P atoms are found within 4 Å of their core silicon (figure 4.9). The most inflexible arms (G1-16methoxyPPh$_2$) have the smallest core – terminal group distance, while the most flexible (G1-16propylPPh$_2$) have the most expanded distribution.

4.2.2 Effects of Generation

Most studies of dendrimers involve synthesis and subsequent analysis of several generations of dendrimers. Variation in the composition of branches are not normally investigated, usually due to the limited reactions used for big dendrimer synthesis (e.g. PAMAM[9]). In order to compare these POSS dendrimers with other studies, comparison of three generations has been made.
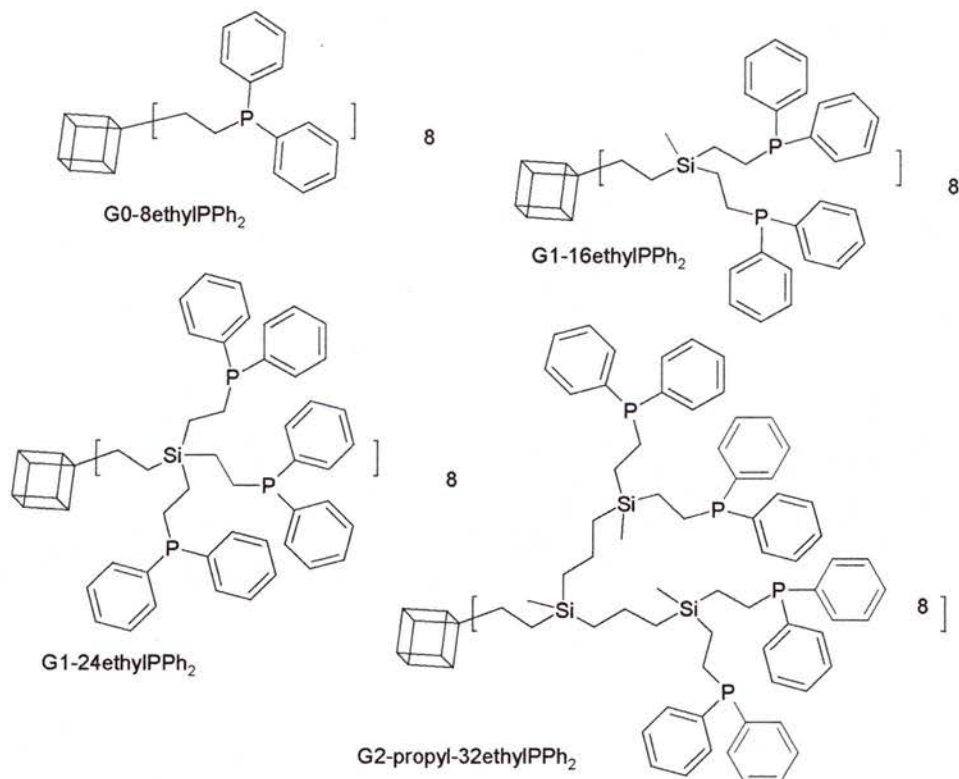
Figure 4.10: Series of dendrimers from G0 to G2.

G0-8ethylPPh$_2$ was synthesised by Hong *et al.* and used as a core for Fréchet type

dendrimers[10,11]. While it has not been used as a ligand for hydroformylation, it

would form monophosphine complexes or dimers. It has been included as it gives

some useful data on the size and shape properties of these molecules.

Generation	C	H	O	P	Si	T-Groups	Mass (amu)
G0-8ethylPPh$_2$	112	112	12	8	8	8	2122.6
G1-16ethylPPh$_2$	248	280	12	16	16	16	4397.9
G1-24ethylPPh$_2$	352	368	12	24	16	24	5983.4
G2-propyl32ethylPPh$_2$	520	616	12	32	32	32	8948.5
G2-propyl48ethylPPh$_2$	784	920	12	48	40	48	10824

Table 4.8: Physical properties of three generations of diphenylphosphine dendrimers.

G1-24ethylPPh$_2$ was studied to attempt to explain why incomplete functionalisation

of the periphery occurred. Data from experiments suggest that this molecule is very

crowded and so offers an important opportunity for comparison with the other

molecules. The catalytic data was obtained for G2-propyl48ethylPPh$_2$ but this

molecule was too large to model efficiently and a smaller molecule was studied instead, G2-propyl32ethylPPh$_2$.

4.2.2.1 Size and Shape of Molecules

The calculated physical properties of G0 – G2 show that the molecules are globular due to the core architecture being amplified by the branches, even in G0-8ethylPPh$_2$ (table 4.9).

Generation	Ix	Iy	Iz	I$_r$	Iz/Ix	Iz/Iy
G0-8ethylPPh$_2$	65349	66386.4	75647.9	103691.8	1.158	1.14
G1-16ethylPPh$_2$	234667.5	263379.3	287245.1	392646	1.18	1.13
G1-24ethylPPh$_2$	369057.6	394449.4	400979.6	582243.3	1.096	1.017
G2-propyl32ethylPPh$_2$	818635.3	864686.4	919679.3	1301501	1.123	1.064

Table 4.9: Calculated properties for 3 generations, moments of inertia Ix, Iy and Iz relative to each axis; Ir – the total moment of inertia and the two aspect ratios Iz/Ix and Iz/Iy.

The principal aspect ratio (Iz/Ix) reveals that G1-24ethylPPh$_2$ is the most spherical but in all cases the aspect ratios are never above 1.18. Interestingly, G1-16ethylPPh$_2$ is the least spherical (relatively) of the four molecules but these calculations represent only one frame.
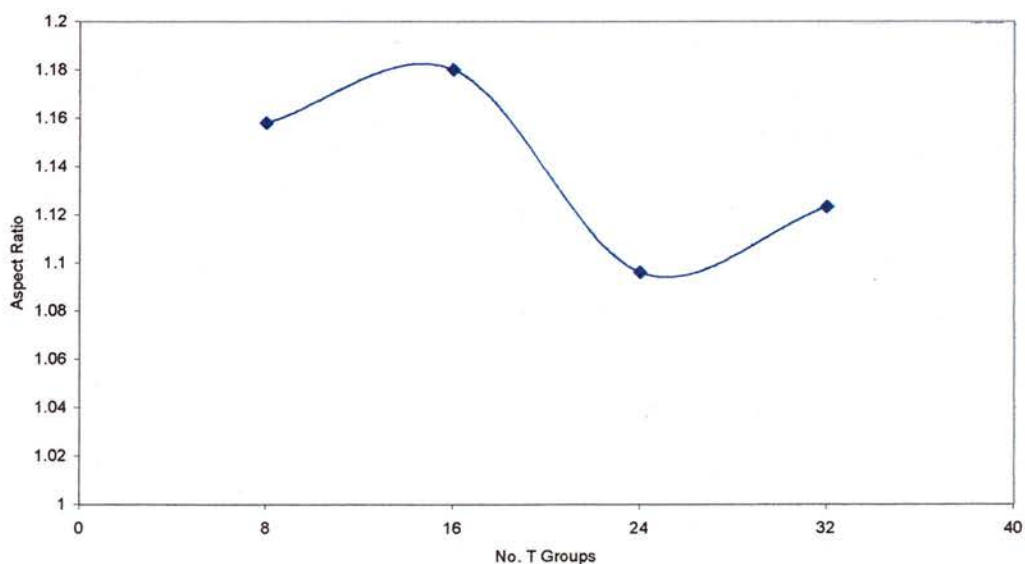
Figure 4.11: Principle aspect ratio (Iz/Ix) vs. number of terminal groups. Line as guide to the eye only.

The radii of gyration increase with mass except for G1-24ethylPPh$_2$ which shows a relatively small increase (4 %) compared to the increase in mass (36 %), shown in figure 4.12. This provides the first evidence for a close packed outer shell – the terminal groups are held rigidly in the outer sphere resulting in a more compact structure. Alternatively, the length of the branch has a greater influence over the Rg than the increase in mass.
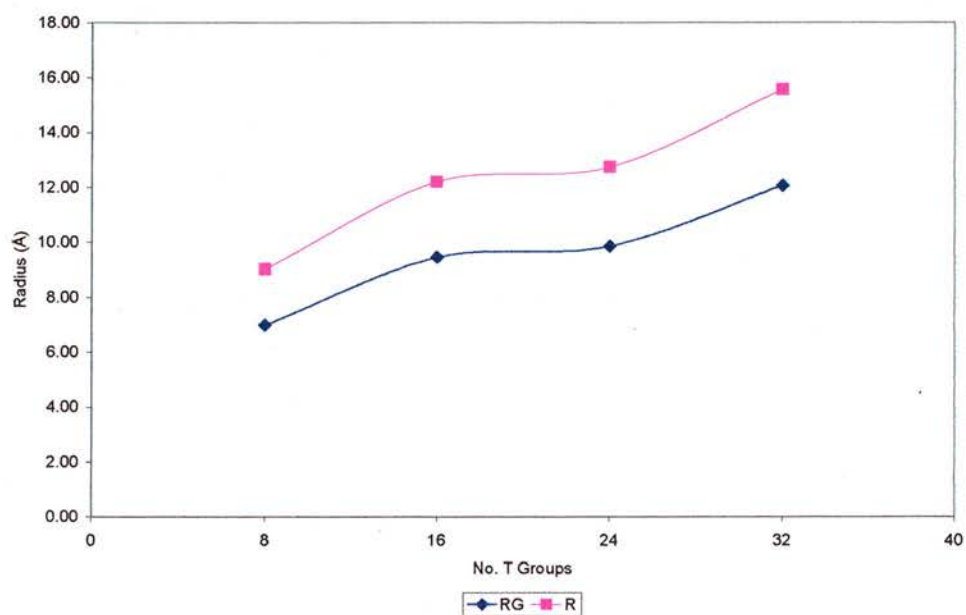
Figure 4.12: Calculated radius of gyration (Rg) and molecular radius (R).

The molecular radius follows the same trends as Rg and from this, the surface area of the molecule was calculated. The surface areas increase with generation and molecular mass and the surface area per terminal group decreases with generation except G1-24ethylPPh$_2$ (table 4.10).

Generation	Rg (Å)	R (Å)	Surface Area (Å^2)	SA per T (Å^2)	δ
G0-8ethylPPh$_2$	6.99	9.02	1023.03	127.88	0.002243
G1-16ethylPPh$_2$	9.53	12.30	1900.79	118.80	0.001342
G1-24ethylPPh$_2$	9.87	12.74	2038.23	84.93	0.000629
G2-propyl32ethylPPh$_2$	12.06	15.57	3046.16	95.19	0.001133

Table 4.10: Calculated size and surface area properties of four dendrimers. δ – asphericity, SA per T – surface area per terminal group.

G1-24ethylPPh$_2$ shows the lowest surface area per terminal group indicating that the PPh$_2$ groups are closer together. This indicates a more crowded exterior that may explain the synthetic difficulties.
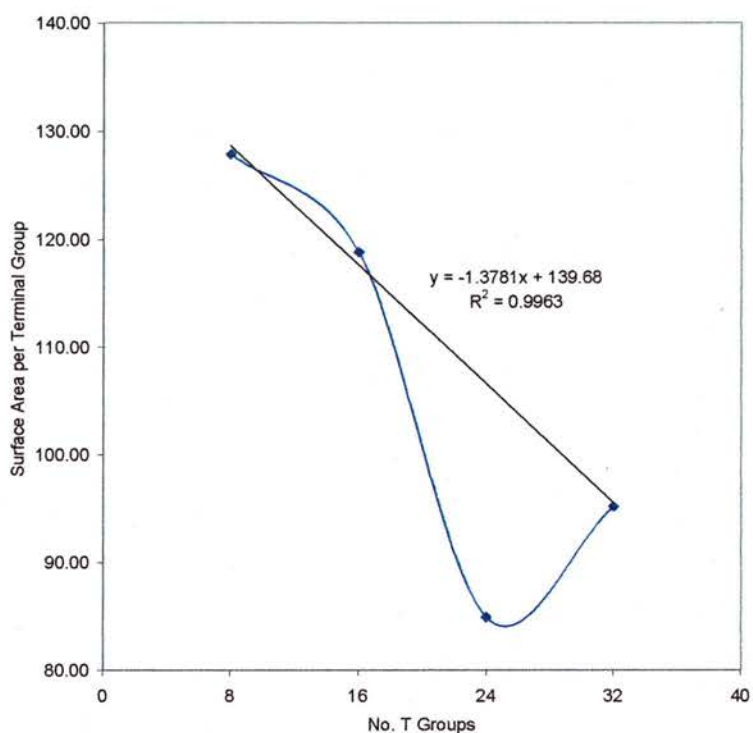
Figure 4.13: Surface area per terminal group (Å^2), thick line indicates linear relationship of terminal group with generation.

Measuring the asphericity (δ) reveals similar trends to the principle moment of inertia but on the whole the deviation from a sphere ($\delta = 0$) is very small. The surface area per terminal group decreases linearly with generation for molecules of the same composition (figure 4.13).

Visual inspection of the structures as modelled indicates very globular shapes (figure 4.14) in which little crossing over of individual branches occurs. The dendrimers were coloured branch by branch to assess the extent to which the branches mix on the surface.
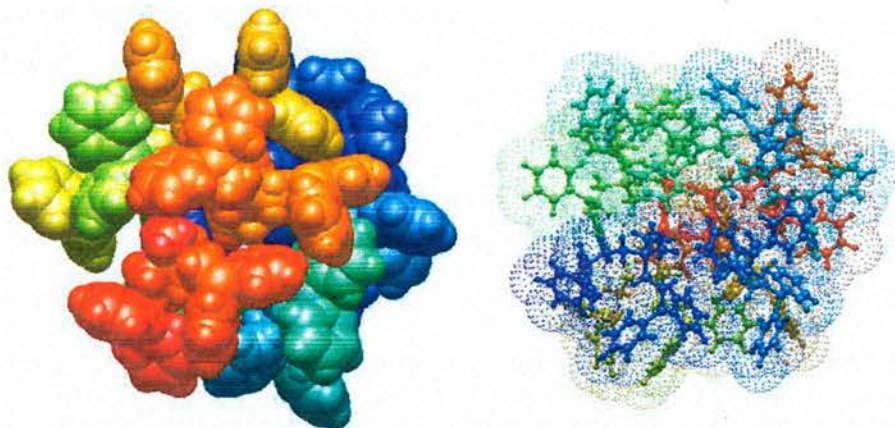
Figure 4.14: CPK and van der Waals surface representations of G1-16ethylPPh$_2$. Each branch is coloured individually to indicate the extent to which the branches mix on the surface of the molecule.
The branches mainly exist as discrete units, potentially because they are not long enough or flexible enough to intermix.

4.2.2.2 Location of Terminal Groups

The distance between terminal groups and the distance between the molecular core and terminal groups gives insight into the ligating properties of these dendrimers. The radial density distribution function for all phosphorus atoms measures the distance between all phosphorus in the molecule and shows some interesting trends (figures 4.15 – 4.18).
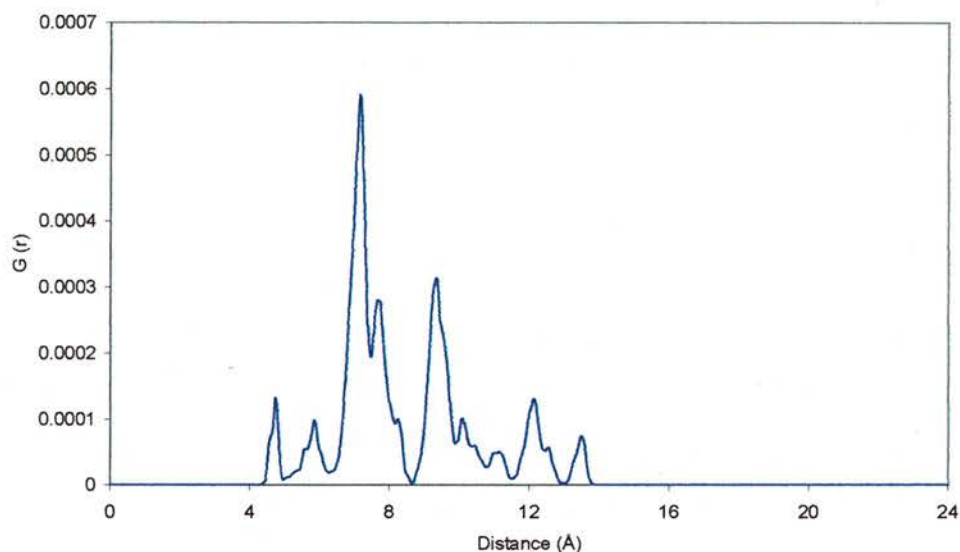
Figure 4.15: G0-8ethylPPh$_2$, Radial density distribution function, G(r) for all P atoms.

Firstly, it must be noted that these graphs have different scales on the y-axis so care must be taken comparing peak sizes. In all cases, no phosphorus atoms come within 4 Å of each other and the largest distance between groups is directly related to the size of the branches.
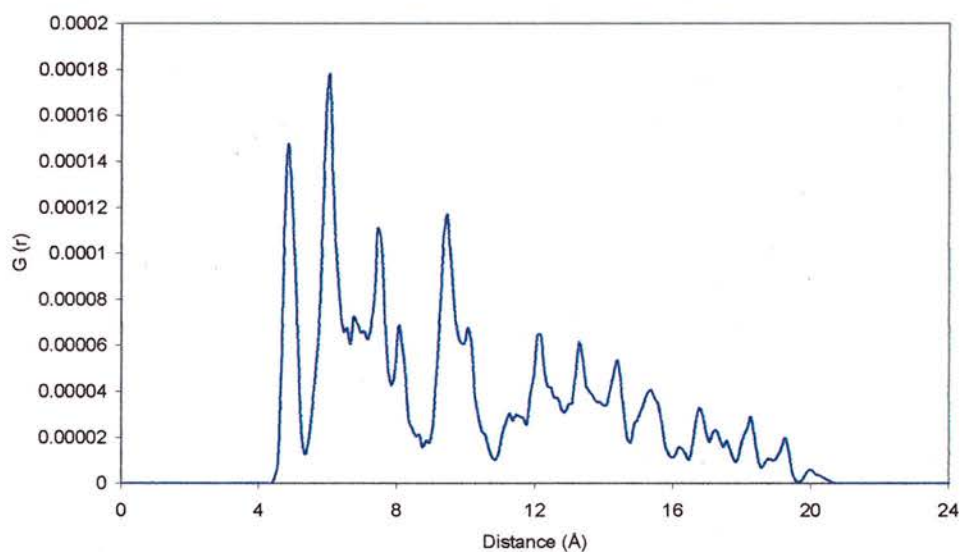
Figure 4.16: G1-16ethylPPh$_2$, Radial density distribution function, G(r) for all P atoms.
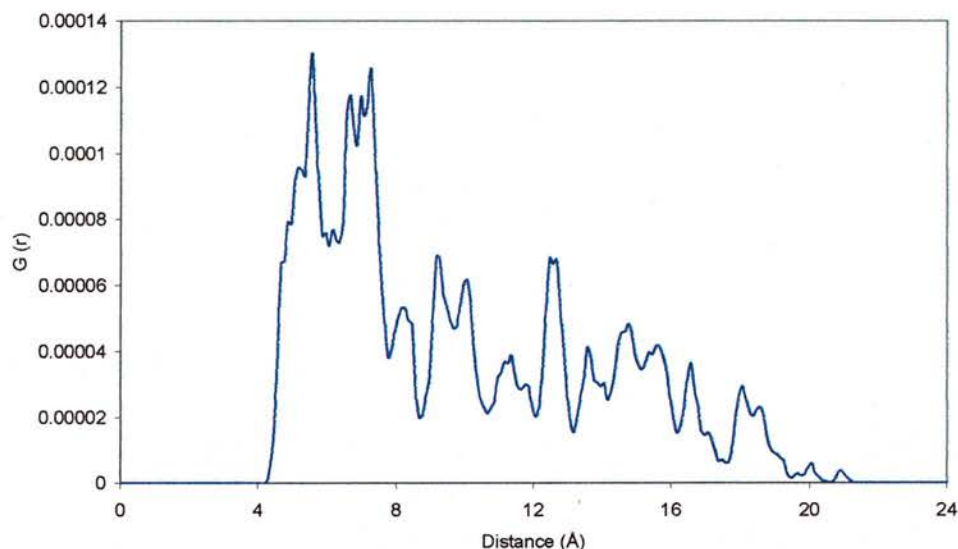
Figure 4.17: G1-24ethylPPh$_2$, Radial density distribution function, G(r) for all P atoms.

Figure 4.17 shows a far larger distribution between 4 and 8 Å corresponding to the greater number of terminal groups on each branch for G1-24ethylPPh$_2$ compared to G1-16ethylPPh$_2$ (figure 4.16) but the furthest distance between groups remains the same. This indicates that the furthest distance between groups is not influenced by the density of the terminal groups but rather by the size of the core and length of the branches. These three areas are not as noticeable in the smaller molecules and are a feature of higher generation POSS dendrimers.
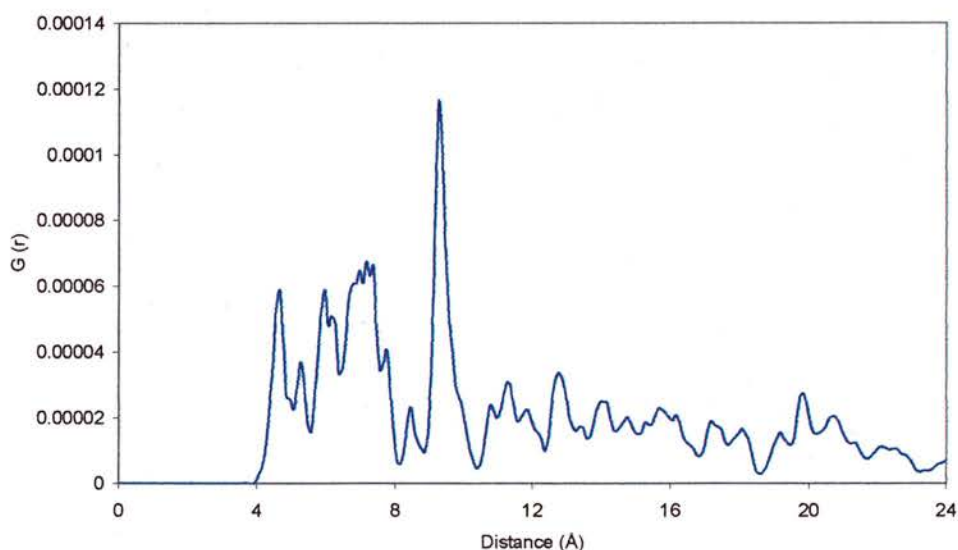
Figure 4.18: G2-32ethylPPh$_2$, Radial density distribution function, G(r) for all P atoms.

G2-32ethylPPh$_2$ shows a similar distribution to those examined in chapter 3 and the dendritic alcohols G2-32ethylPPh$_2$ has similar structural features to the alcohols. The distribution is broken up into three main regions. From 4 – 8 Å is most likely to correspond to intrabanch distances. A large peak at approximately 10 Å is most likely due to interbranch distances with branches attached to silicons on adjacent edges. The distribution from 11 Å to the calculation cutoff of 24 Å could be due to interbranch distances of more remote branches. This is confirmed by figures 4.19 – 4.21 which show no peaks or small peaks at 10 Å for intrabranch P-P distances. The distribution of distances within each branch reveals more information about the orientation of these molecules. This is not calculated for G0-8ethylPPh$_2$ because there is only one PPh$_2$ group per arm.
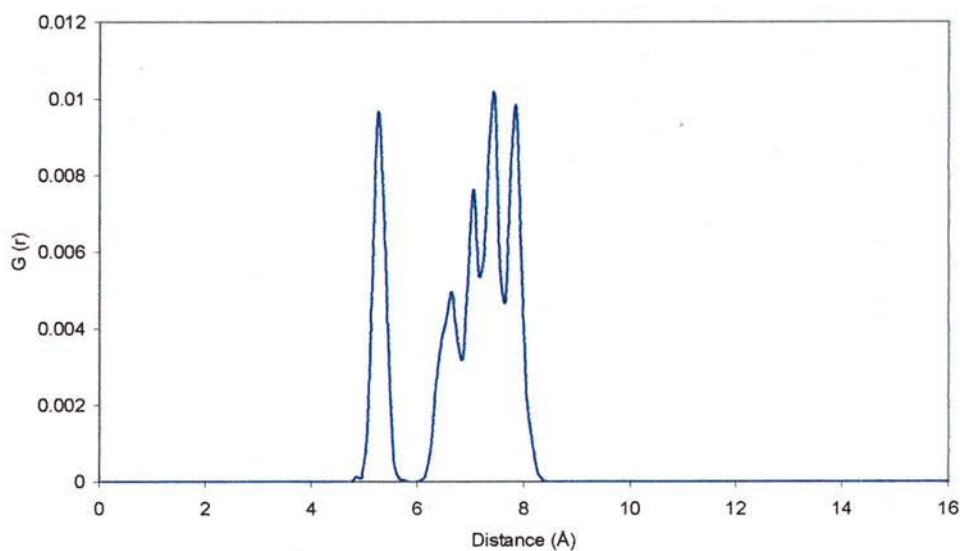
Figure 4.19: G1-16ethylPPh$_2$, Radial distribution function for P atoms on each branch, averaged over all branches.
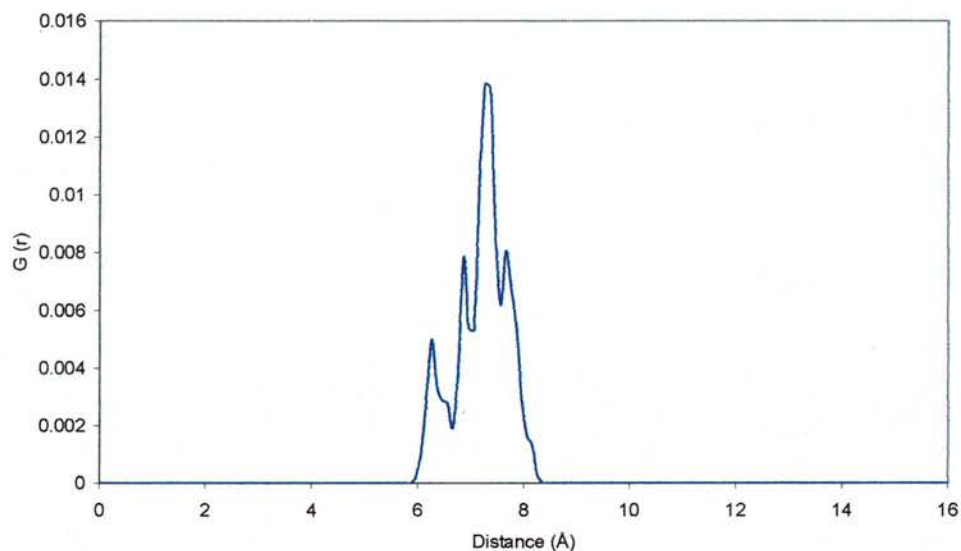
Figure 4.20: G1-24ethylPPh$_2$, radial distribution function for P atoms on each branch, averaged over all branches.

Interestingly, figures 4.19 and 4.20 do not show large distributions between 4 and 8 Å implying that the assumption that the closest P-P distances must come from the same branch (figures 4.16 and 4.17) is incorrect. It is actually the case that P atoms on adjacent branches can be closer together than those on the same branch. This implies that the branches adopt an expanded configuration on the surface of the molecule, which was shown in figure 4.14 graphically.
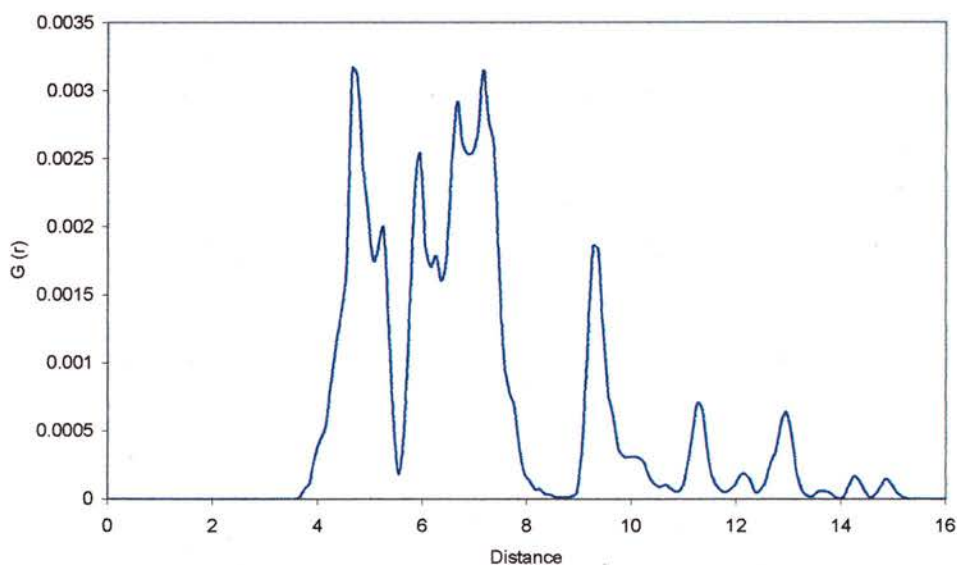
Figure 4.21: G2-32ethylPPh$_2$, Radial distribution function for P atoms on each branch, averaged over all branches.

Figure 4.21 shows a larger distribution between 4 and 8 Å implying that some of the features noted in figure 4.18 are due to internal branch distances, not interbranch distances. This means that for second generation POSS dendrimers the greater density of terminal groups may be forcing the branches to adopt more compact configurations and perhaps interacting with each other less.

If the branches are forced to adopt a more compact configuration, does this process go as far as forcing the terminal groups to move closer to the POSS core? The diphenylphosphino group is quite large and bulky and it is unlikely that it will fold back to any significant degree into the interior of the dendrimer. Figures 4.22 – 4.25 show the radial density distributions of the P atoms from silicon atoms on the POSS core. For the smallest molecule under consideration (G0-8ethylPPh$_2$), the P atoms never get closer than approx. 3 Å to the core silicon. This might be due to the inflexibility of such small branches.
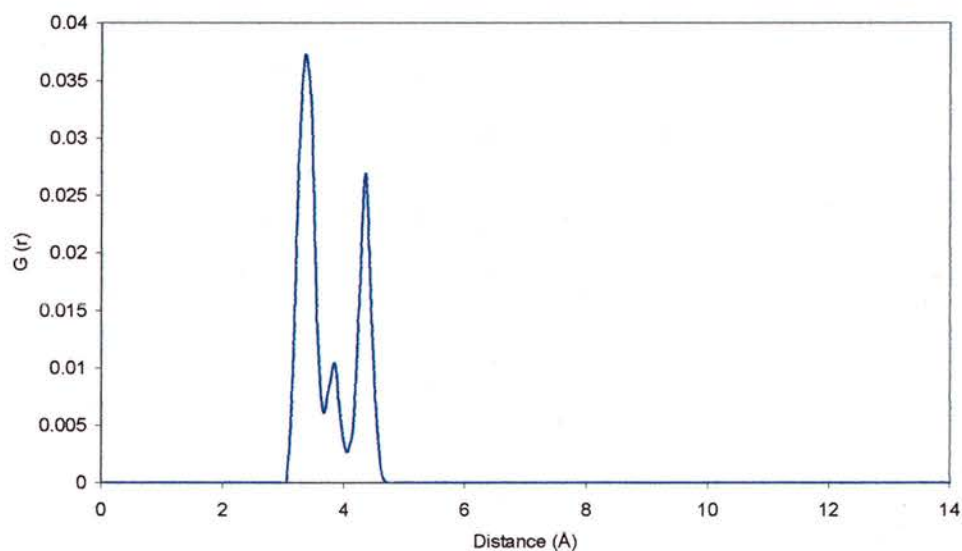
Figure 4.22: G0-8ethylPPh$_2$, radial distribution function calculated between terminal P atoms and the silicon on the POSS core to which the branch is attached. This is averaged over all branches.

For the first generation dendrimers, the Si-P distances are in the region of 4 – 8 Å which is most likely governed by the length of the branches. This is a trend also shown by G2-32ethylPPh$_2$ with its distances between 7 and 11 Å.
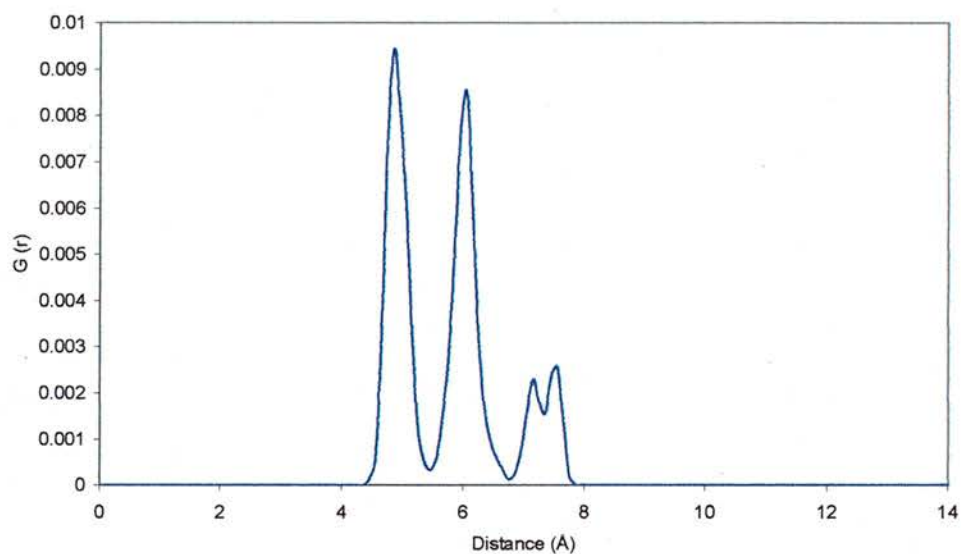
Figure 4.23: G1-16ethylPPh$_2$, radial distribution function calculated between terminal P atoms and the silicon on the POSS core to which the branch is attached. This is averaged over all branches.
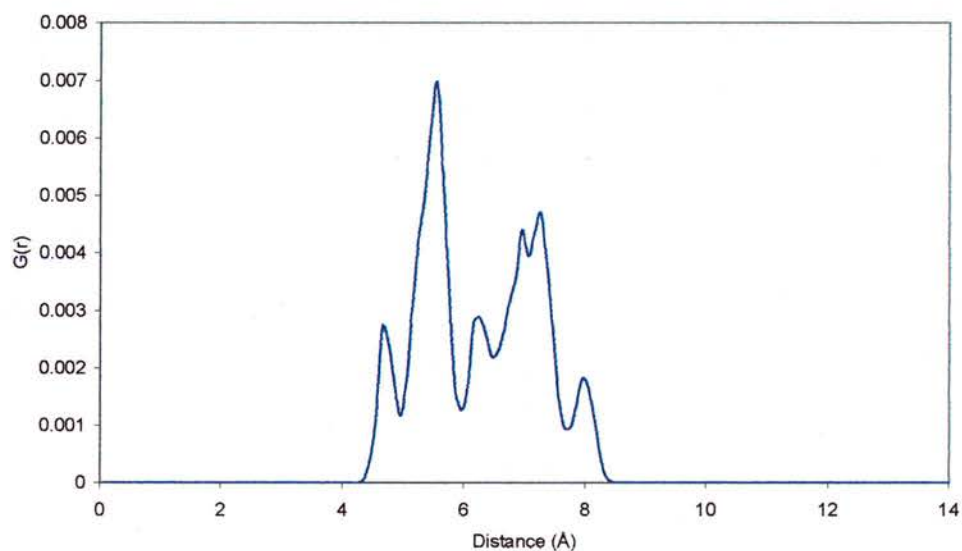
Figure 4.24: G1-24ethylPPh$_2$, radial distribution function calculated between terminal P atoms and the silicon on the POSS core to which the branch is attached. This is averaged over all branches.
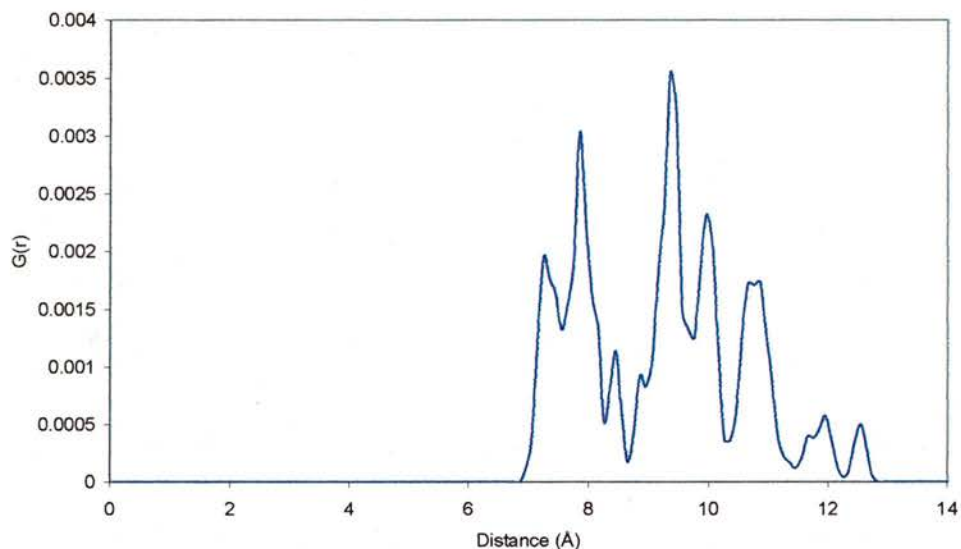
Figure 4.25: G2-32ethylPPh$_2$, radial distribution function calculated between terminal P atoms and the silicon on the POSS core to which the branch is attached. This is averaged over all branches.

In general, no evidence of PPh$_2$ groups penetrating the interior of the dendrimer can be found in these graphs. The branches must be long enough and with low enough density of terminal groups to inhibit back folding. This does not explain the experimental findings regarding G1-24ethylPPh$_2$ where the reaction with PPh$_2$ showed poor conversion. While the density of the terminal groups is not sufficient to cause the back-folding of a large bulky diphenylphosphine group, a process that would create considerable steric issues within the molecule, it may yet be great enough to inhibit reaction at the surface. One possibility might be that the molecule G1-24vinyl may, during reaction with Ph$_2$PH, gain a shell of PPh$_2$ groups that block further access to unreacted vinyl groups. It might also be that the Ph$_2$PH groups cannot get into the correct orientation to react successfully with a terminal vinyl group once 50 % of the vinyl groups have reacted.

Dendrimer	Inner shell limit (Å)	Outer shell limit (Å)	Outer Sphere Volume (Å^3)	Inner Sphere Volume (Å^3)	Shell Volume (Å^3)	Per T Group (Å^3)
G0-8 PPh$_2$	3.05	4.65	421.16	118.85	302.31	37.79
G1-16 PPh$_2$	4.45	7.85	2026.27	369.12	1657.15	103.57
G1-24 PPh$_2$	4.35	8.45	2527.31	344.79	2182.52	90.94
G2-32 PPh$_2$	6.95	12.95	9096.99	1406.19	7690.81	240.34

Table 4.11: Calculation of molecular volume occupied by terminal groups from P-Si radial distribution graphs assuming each dendrimer is a perfect sphere.

Some measure of steric crowding can be made if the volume of space in the molecule available to each terminal group is calculated. This assumes that the molecules are perfectly spherical and that the terminal groups are located in a shell concentric with the core.
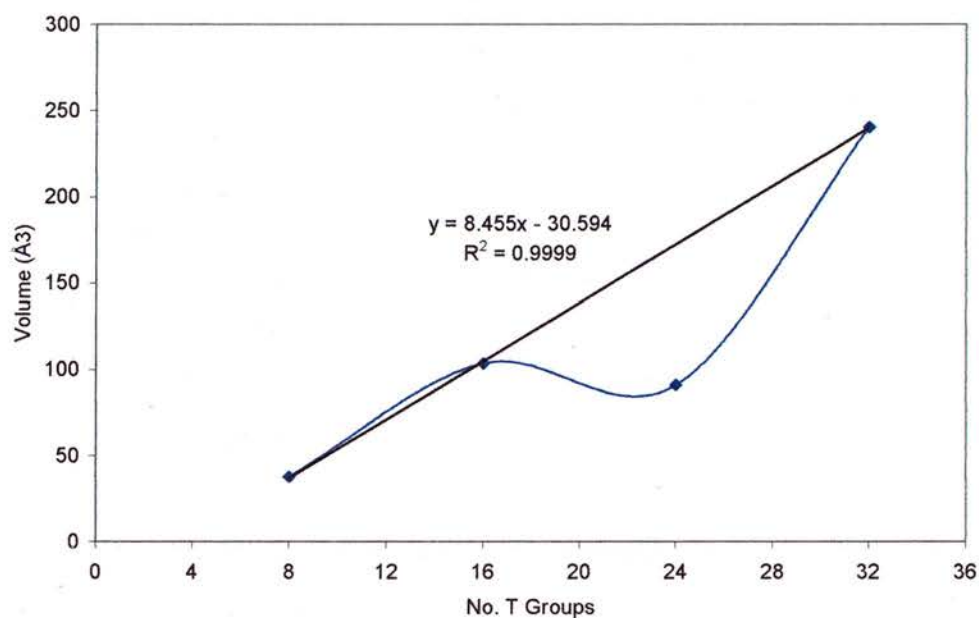
Figure 4.26: Portion of molecular volume available per terminal group for each dendrimer. Black line to indicate the linear relationship of volume with number of terminal groups for G0 – G2. Blue line as guide to eye only.

Table 4.11 shows the calculation of shell volume and the results per terminal group are summarised in figure 4.26. There is a clear linear relationship between the size of the dendrimer (generation) and the volume available per terminal group. G1-24ethylPPh$_2$ has significantly less space available to its greater number of terminal groups. It could be predicted from this that if a dendrimer could be constructed to

have a volume of 150 Å^3, it would be possible to fit 24 diphenylphosphine terminal groups on its periphery. This might be done by using the allyl-POSS as a core, giving slightly more volume, or using allylmagnesiumbromide creating slightly longer branches.

4.2.3 Effects of Solvent

G1-16ethylPPh$_2$ was modelled with four different dielectric constants from $\varepsilon = 1$ to $\varepsilon = 8$. The values of the dielectric constants within the Discover program in Materials Studio[8] do not directly correlate to values used for physical chemistry. A dielectric constant, $\varepsilon = 1$ was used to represent the case of a non-polar solvent, a dielectric constant, $\varepsilon = 8$ for a highly polar solvent and values of 2 and 4 to represent moderate polarity.

Dielectric Constant (ε)	Molecular Mass (amu)	Iz/Ix	Iz/Iy
1	4397.90	1.18	1.12
2	4397.90	1.10	1.05
4	4397.90	1.12	1.06
8	4397.90	1.23	1.10

Table 4.12: Calculated properties of G1-16ethylPPh$_2$.

The aspect ratios (figure 4.27, table 4.12) show that in solvents of low and high polarity the molecules are less spherical and that there is a solvent of moderate polarity in which the dendrimer is most spherical.
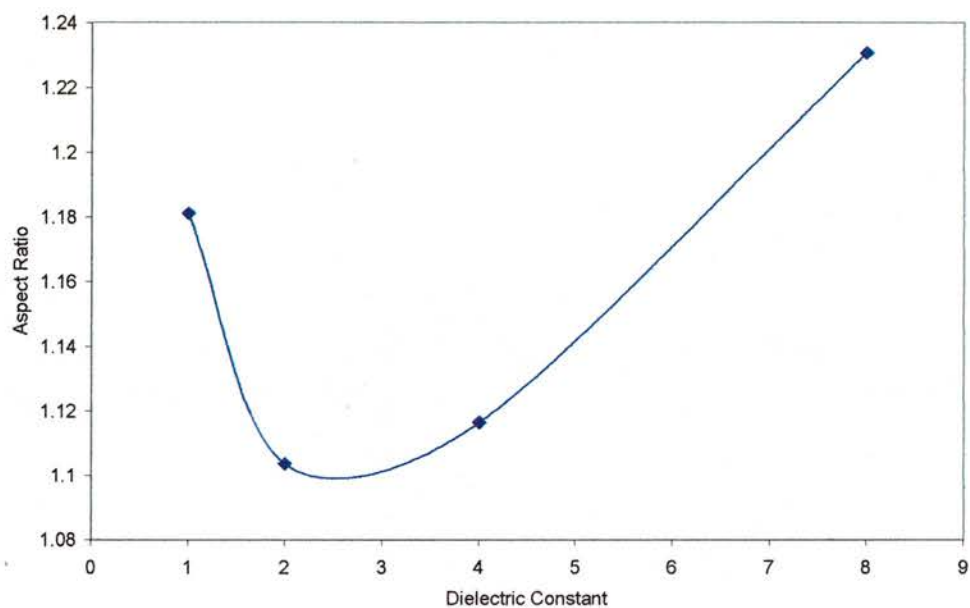
Figure 4.27: Iz/Ix, principal aspect ratio vs. dielectric constant

This is best illustrated in figure 4.27 showing the dendrimer to be most spherical for

a dielectric, $\varepsilon \sim 2$ - 3. The radius of gyration (figure 4.28) shows a different trend to

the aspect ratio. As the dielectric constant increases, Rg decreases implying that the

dendrimer becomes more compact in highly polar solvents. The molecular radius, R,

naturally follows the same trend illustrated in figure 4.28.

ε	Rg (Å)	R (Å)	Surface Area(Å^2)	SA per T (Å^2)
1	9.53	12.30	1900.79	118.80
2	9.16	11.83	1757.52	109.85
4	9.01	11.64	1701.81	106.36
8	8.97	11.58	1684.02	105.25

Table 4.13: Calculated physical properties, R – molecular radius, SA per T – Surface Area per
Terminal Group.

In both cases the decline in radius is most apparent going from $\varepsilon = 1$ to 2 and starts to

level off towards $\varepsilon = 8$. This is also shown by the surface area and surface area per

terminal group. The decrease in area is most noticeable for $\varepsilon = 1$ to 2.
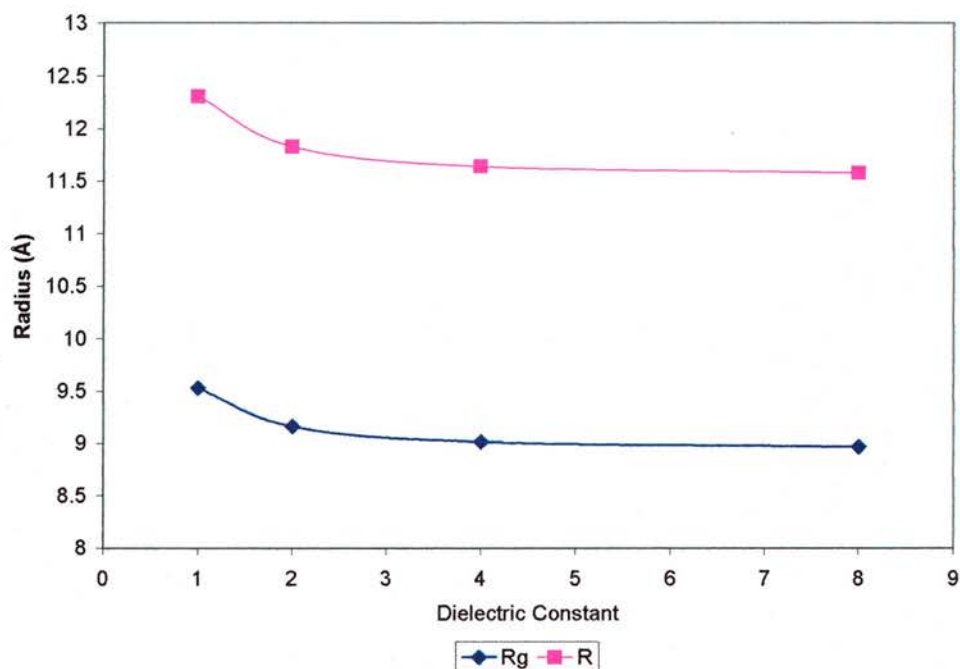
Figure 4.28: Radius of Gyration R_g and Molecular Radius, R.

Increasing solvent polarity affects the physical size of the dendrimer, but what effect

does it have on the location of the terminal groups?
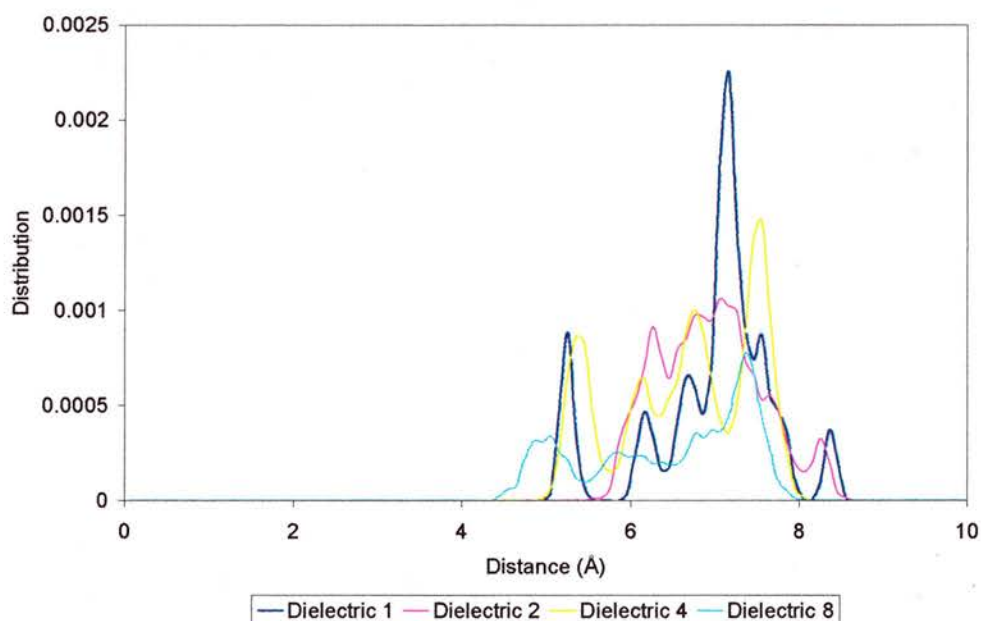
Figure 4.29: Distance of phosphorus atoms in a branch from the silicon on the core to which the branch is attached, averaged over all branches.

Figure 4.29 shows the core-terminal group distance for each dielectric constant. The

distributions become more even with increasing polarity, perhaps implying that as

the molecules are becoming more compact, the terminal groups are becoming more evenly spread throughout the molecule.

The terminal groups can now be found as close to the core as 5 Å ($\varepsilon = 8$) indicating that some contraction of the branches occur as the molecular radius decreases.
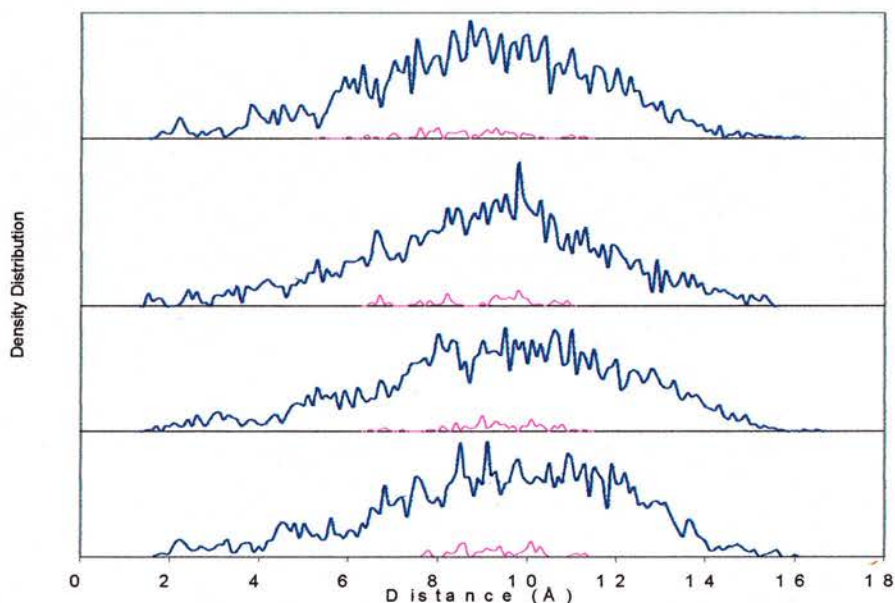
Figure 4.30: Density distribution of all atoms in G1-16ethylPPh$_2$. Dielectric goes from $\varepsilon = 1$ at bottom to $\varepsilon = 8$ at top. The blue line represents the distribution of all atoms; the pink represents the distribution of the phosphorus atoms.

This is further enforced by figure 4.30 showing that as the dielectric constant increases the phosphorus atoms become more evenly distributed throughout the molecule. The phosphorus atoms are located in the region of highest atom density, due to being surrounded by phenyl rings.

4.2.4 Effects of Temperature

The structure of G1-16ethylPPh$_2$ was analysed after equilibration at a range of different temperatures to investigate the effects of temperature on the dendrimer. G1-16ethylPPh$_2$ was drawn, heated, annealed and minimised to give the starting structure that was then equilibrated at the range of temperatures shown below. This

meant that the only variable was the temperature of equilibration and production allowing for better comparison.

Temp (K)	Iz/Ix	Iz/Iy	Rg (Å)	R (Å)	Surface Area (Å^2)	SA per T (Å^2)	δ
50	1.18368	1.12119	9.53258	12.31	1903.18	118.95	0.002536
273	1.18114	1.12621	9.52659	12.30	1900.79	118.80	0.002526
350	1.17565	1.12621	9.42631	12.17	1860.98	116.31	0.002418
500	1.11782	1.08342	9.38184	12.11	1843.46	115.22	0.001124

Table 4.14: Calculated properties of G1-16ethylPPh$_2$, equilibrated and then analysed at different temperatures. SA per T – Surface Area per Terminal Group, δ - asphericity.

Table 4.14 gives general shape properties of the molecule and shows that the varying temperature does not create great distortions in the molecular shape. The molecules become slightly more spherical at 350 K and above (figure 4.31), although this is a small increase by comparison with the effect of solvent dielectric.
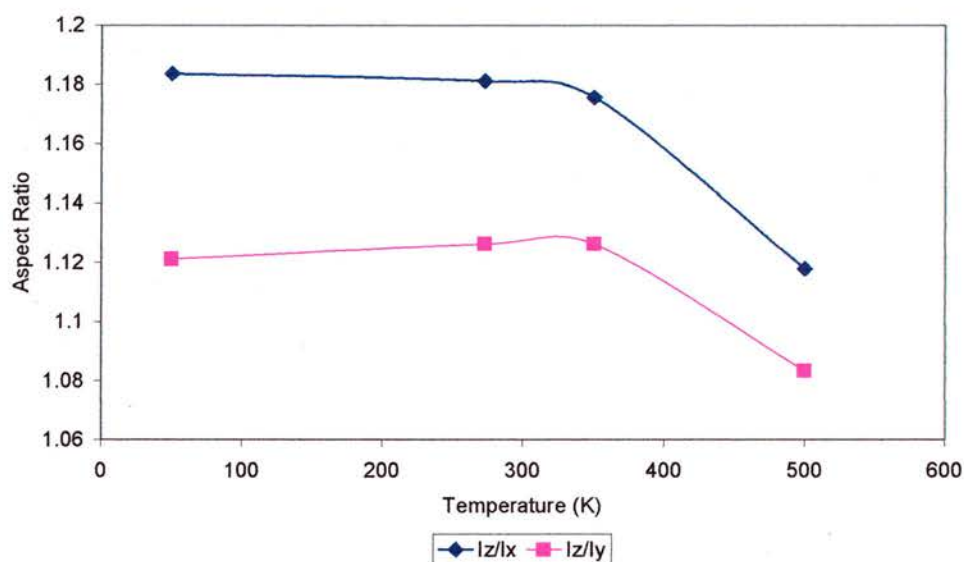
Figure 4.31: Aspect ratio vs.Temperature for G1-16ethylPPh$_2$

Interestingly the molecules appear to become slightly smaller with increasing temperature, which is perhaps counterintuitive until the distance between the terminal groups on each branch is considered (figure 4.33, table 4.15). It can be seen that the distance between phosphorus atoms initially decreases with temperature and then sharply increases. This may mean that the increase in temperature allows the branches to be more expanded, creating an effective decrease in molecular size.
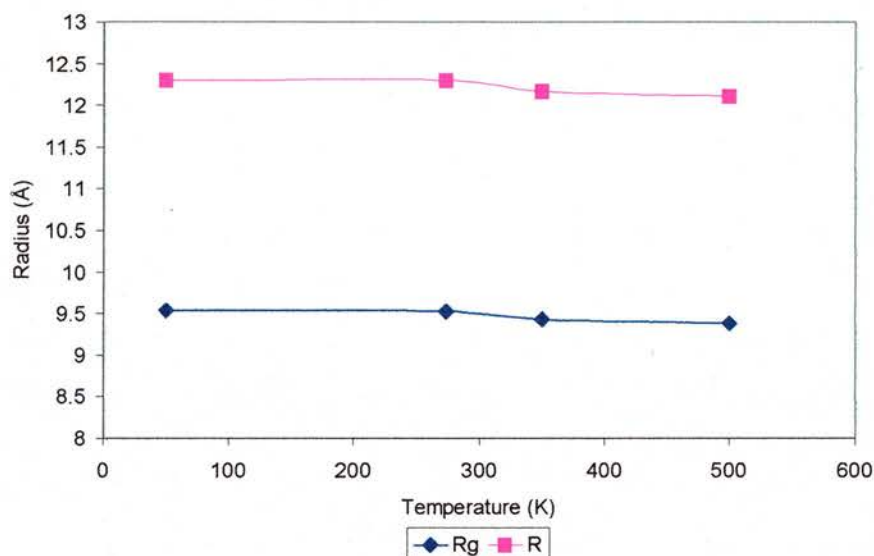
Figure 4.32: Radius of Gyration (R_g) and Molecular Radius (R) of G1-16ethylPPh$_2$ at various temperatures.

The decrease in molecular radius is slight with temperature.

Figure 4.33 and table 4.15 summarises the average distances between phosphorus atoms on individual branches over the entire production trajectory. The standard deviations are given and can be taken as a measure of branch flexibility. More flexible branches will result in greater variation of the P-P distances and so larger standard deviations about the average. It can be seen from table 4.15 and figure 4.33 that the standard deviation increases with temperature. This means that at low temperature the branches are not as flexible as at high temperature, which is as expected given the relative amounts of energy within the systems.

Temperature (K)	Distance (Å)	St. Dev.
50	6.65	0.05
273	6.60	0.17
350	6.57	0.23
500	6.75	0.32

Table 4.15: The average intra-branch phosphorus distances given with the standard deviation (St. Dev.) at four temperatures.

The average P-P distance does not follow the same trend as the standard deviations, instead it decreases between 50 and 350 K and increases sharply at 500K. This may

be due to the additional energy in the system at 500K allowing an energy barrier for

a torsion to be breached allowing the branches to move further apart.
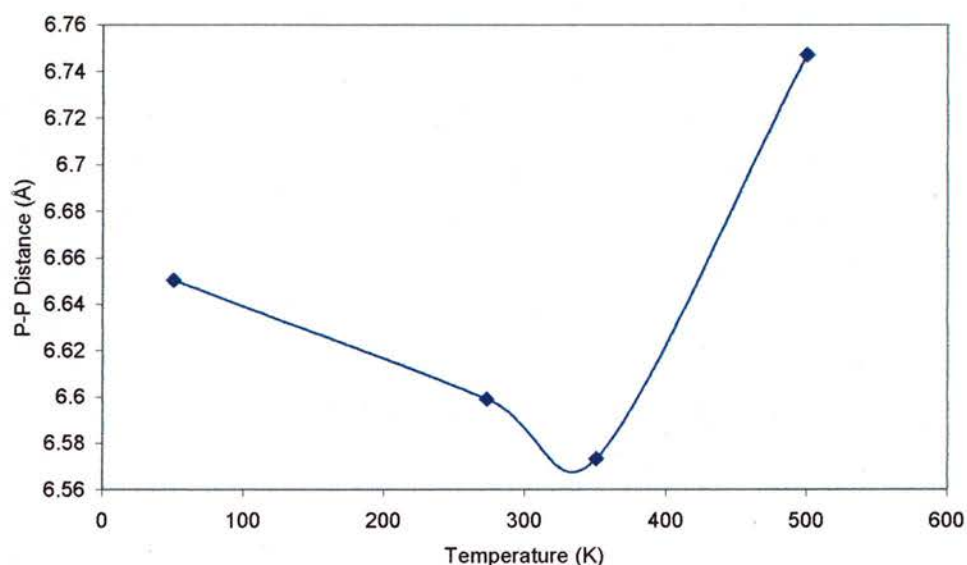
Figure 4.33: Intra-branch average phosphorus distances calculated at various temperatures, line as guide to eye only.

The decrease in P-P distance may also be down to energy. The branches do not

move much at 50 K (indicated by low standard deviations) and perhaps there is

insufficient energy for the branches to move closer together due to strain created by

the phenyl rings. At 273 and 350 K there is more energy in the molecule, maybe

enough to allow the branches more freedom to move, both closer and further apart.

4.2.5 Catalytic Data

The dendrimers were used as ligands for the rhodium catalysed hydroformylation of

oct-1-ene. Of particular interest when considering dendrimer catalysts is the

dendritic effect – does the dendritic structure influence the selectivity on the rate of

catalysis? The previous modelling sections report various properties of the

dendrimers and of G1-16ethylPPh$_2$ under many conditions. Here the results are

compared to the results of catalytic experiments and to the small molecule analogues

of the G1-16ethylPPh$_2$ dendritic arm.

Ligand	l:b ratio	Nonan-1-al (%)	P-P Distance
G1-16methylPPh$_2$	3.9	68.5	*1
G1-16ethylPPh$_2$	13.9	86.0	5.25 – 7.85
G1-16propylPPh$_2$	5.0	78.0	5.15 – 9.55
G1-16methoxyPPh$_2$	5.7	76.2	4.85 – 8.15
G1-16ethoxyPPh$_2$	6.4	78.1	5.65 – 9.55
G1-16ethylAr$_2$	15.0	73.0	*1
G2-propyl-48ethylPPh$_2$	11.5	83.8	*1
Molecule 1	3.4	70.1	4.65 – 7.55
Molecule 2	3.8	72.7	4.75 – 6.05
Molecule 3	5.2	77.4	4.65 – 7.85
BISBI [*2]	80.5[*3]	89.6[*3]	5.05 – 5.75
XANTPHOS [*2]	53.5[*3]	97.7[*3]	4.35 – 4.95

Table 4.16: Results of hydroformylation of oct-1-ene. Reaction Conditions: [Rh (acac)(CO)$_2$] (2.0 x 10^{-5} mol), toluene (4 cm^3), oct-1-ene (3.8 x 10^{-3} mol), P:Rh = 6:1, 120 °C , 10 bar, conversion all >99.9 %. * *1*: Molecule was not modelled. * *2*: Not tested as ligand under same reaction condition, data from [12]. Reaction Conditions: [Rh (acac)(CO)$_2$] (3.0 cm^3 of 5mM solution in toluene), substrate/Rh = 674, ligand/Rh = 2.2, 80 °C , 10 bar.[13]

The table above summarises the results shown in figures 4.36 and 4.37, showing both

catalytic data obtained and the P-P distance distributions calculated. G1-16ethylPPh$_2$

is the best ligand structurally (not considering G1-16ethylAr$_2$ due to its CF$_3$ groups

and their electronic effects) giving the highest l:b ratio. It was proposed that the

distance between ligating groups might be similar to that of BISBI or XANTPHOS

(figure 4.35). This uses uncomplexed ligating group distance as a measure of the

constrained nature of the ligand backbone. It is well known that ligands with more

constrained backbones are more selective.
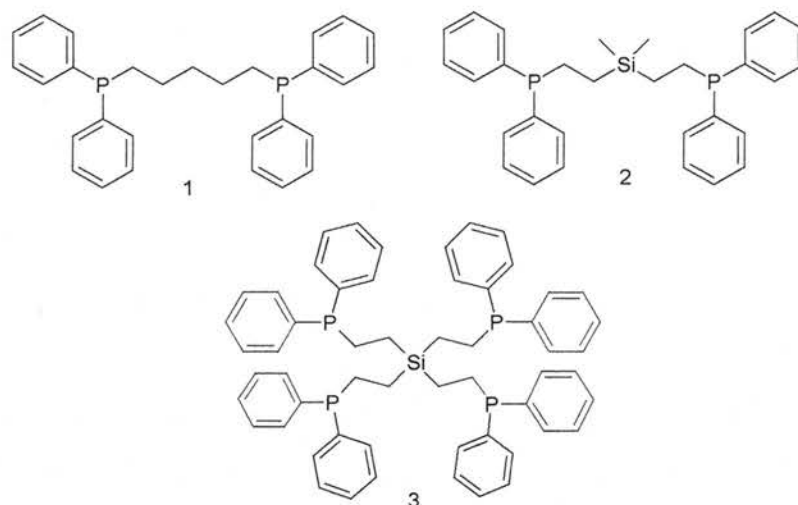
Figure 4.34: Three small molecules synthesised as non-dendritic branch analogues of G1-16ethylPPh$_2$. Molecule 1: 1,5-bis(diphenylphosphino)pentane; molecule 2: bis(diphenylphosphinoethyl)dimethylsilane; molecule 3: tetrakis(2-diphenylphosphinoethyl)silane.

Comparison of figures 4.34 and 4.35 reveal the small molecule analogues of G1-16ethylPPh$_2$ to have far more flexible structures than BISBI or Xantphos so if the hypothesis above is true, the dendritic structure as a whole would have to be constraining the flexibility of the branches.

Xantphos　　　　BISBI
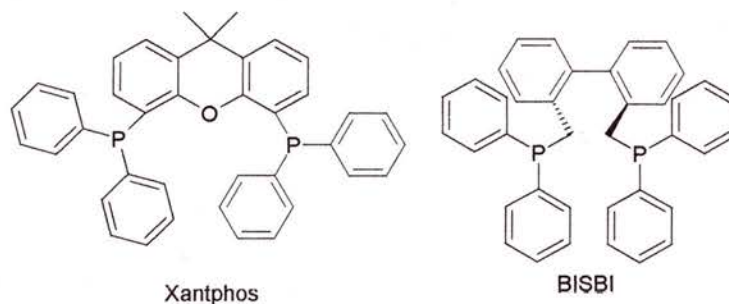
Figure 4.35: Two ligands commonly used in rhodium catalysed hydroformylation reactions.

The distribution of P-P distances are shown in figures 4.36 and 4.37. It can be seen that G1-16ethylPPh$_2$ has a similar P-P distance to BISBI and model compound 1.
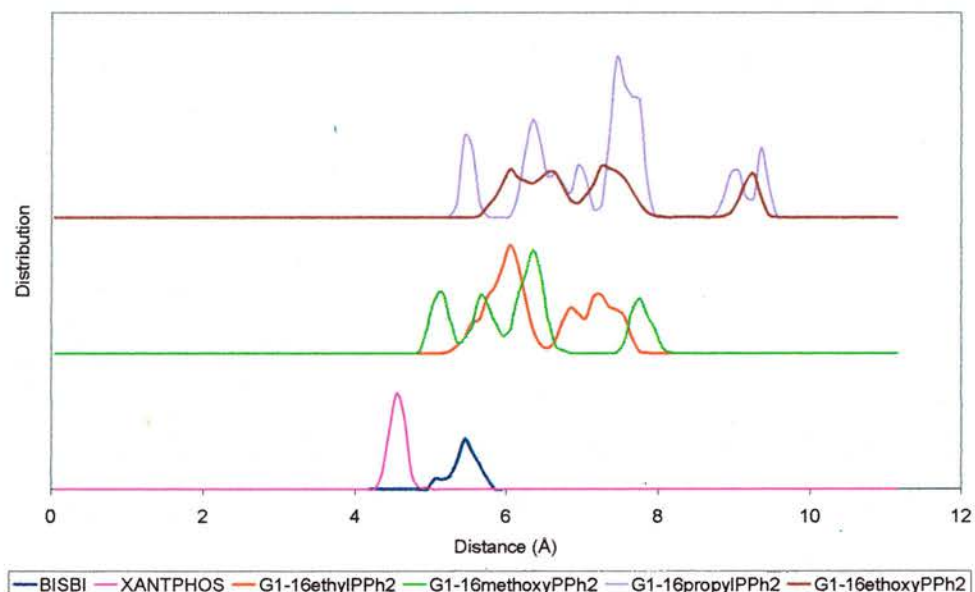
Figure 4.36: P-P distance distribution for BISBI, XANTPHOS and four dendrimers modelled. Graph has been staggered for clarity.

G1-16methoxyPPh$_2$ has a wider distribution but with a greater proportion of it at lower distances and G1-16propyl and G1-16ethoxyPPh$_2$ have broader distributions with the average P-P distances lying in the region of 7 – 8 Å.
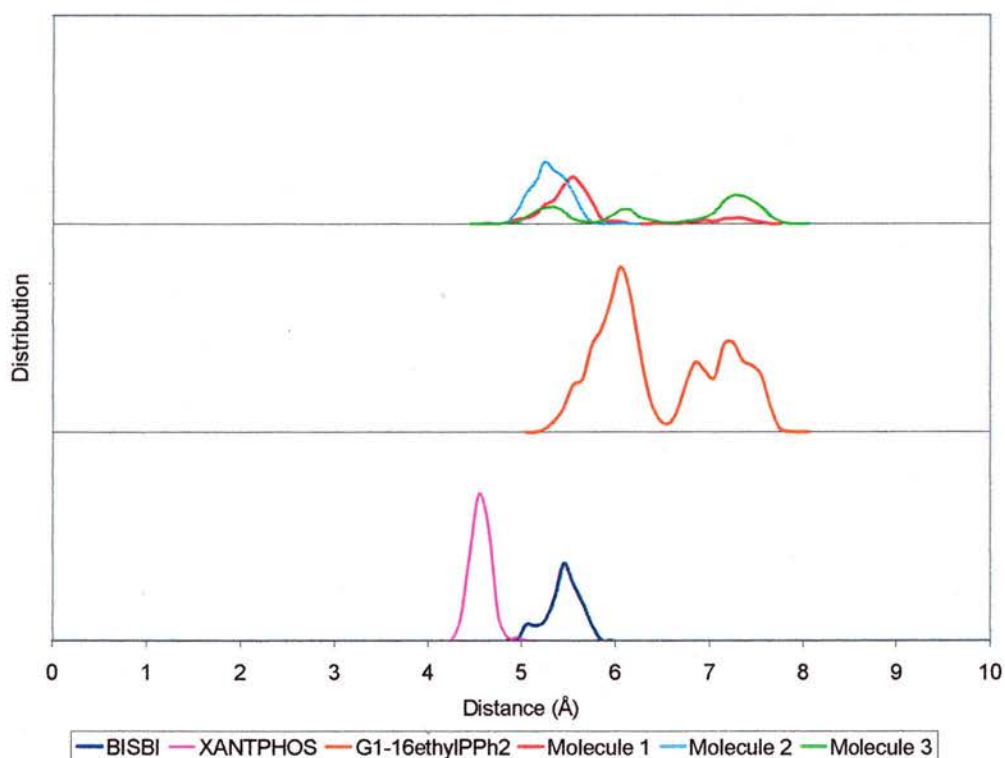
Figure 4.37: P-P distance distribution for model compounds 1 – 3 compared to BISBI, Xantphos and G1-16ethylPPh$_2$. The graph has been staggered for clarity.

The fact that BISBI and G1-16ethylPPh$_2$ have similar uncomplexed P-P distances is insufficient to explain the selectivities obtained although both form eight membered rings upon co-ordination and a deeper explanation must be sought. As the terminal groups on the dendrimer are quite flexible (especially at reaction temperature and pressure), moving to the correct distance for complexation should not create undue steric strain within the dendritic branches. This allows the atoms the freedom to move and rotate as necessary to adopt an ideal conformation for complexation to rhodium, which may have a positive effect on the selectivity. Additionally, with so many diphenylphosphines being present on the surface of the dendrimer should a rhodium become uncomplexed at any point there are plenty of phosphines nearby to bond to it, possibly further influencing the selectivities obtained.

4.3 Conclusions

The effects of branch composition, generation, solvent and temperature have been studied in an attempt to understand the selectivities obtained for the series of dendritic ligands during catalysis. Several interesting results have arisen, including the tendency of the dendrimer to grow smaller when heated, explicable only when considering that more energy permits the branches to expand sideways and not necessarily outwards. This is substantiated by the increase in intrabranch terminal group distances at high (500 K) temperature.

The addition of oxygen to a branch made the molecule far more spherical and smaller, regardless of the corresponding increase in branch length or mass. The surface area per terminal group also decreases upon oxygen addition.

Increasing generation causes an increase in molecular radius and radius of gyration resulting in a decrease in the available surface area per terminal group. Within the first generation, G1-24ethylPPh$_2$ had significantly less space available to its terminal groups, both by measuring area and volume. This explains the difficulty in synthesising G1-24ethylPPh$_2$ and allows a prediction that if a dendrimer with a molecular volume (as calculated) of 150 Å^3 could be synthesised, 24 diphenylphosphine units should fit around its exterior.

For G1-16ethylPPh$_2$ there exists an ideal solvent in which the dendrimer would be most spherical. The change in sphericity of the dendrimer in various solvents shows no relationship with the change in their size, which decreases in increasing solvent polarity. At high solvent polarity, the terminal groups penetrate the interior of the dendrimer and become more evenly distributed. The use of intrabranch phosphorus distances to explain the catalytic selectivities is indicative more of the effect of the dendrimer on the branch than the dendritic structure on the catalytic data. While G1-16ethylPPh$_2$ has a certain distribution of P-P distances, the model compounds have a

wider distribution indicating greater flexibility. Comparison to BISBI reveals that of each of the four dendrimers and three model compounds, G1-16ethylPPh$_2$ and G1-16methoxyPPh$_2$ have the largest distributions of PP distances in common with BISBI.

This is not conclusive and to truly assess the dendrimers steric properties a study in to the steric effect of the ligand on a metal complex, such as bite angle, would have to be carried out. This would also open up a wealth of data for comparison as bite angles for diphosphine complexes have been widely studied.

4.4 References

1. L. Ropartz, K. J. Haxton, D. F. Foster, R. E. Morris, A. M. Z. Slawin and D. J. Cole-Hamilton, *J. Chem. Soc., Dalton Trans.*, 2002, 4323.

2. D. De Groot, P. G. Emmerink, C. Coucke, J. N. H. Reek, P. C. J. Kamer and P. W. N. M. van Leeuwen, *Inorg Chem Commun*, 2000, **3**, 711.

3. L. Ropartz, R. E. Morris, D. F. Foster and D. J. Cole-Hamilton, *Chem. Commun.*, 2001, 361.

4. L. Ropartz, R. E. Morris, D. F. Foster and D. J. Cole-Hamilton, *J Mol Catal A-Chem*, 2002, **182**, 99.

5. L. Ropartz, R. E. Morris, G. P. Schwarz, D. F. Foster and D. J. Cole-Hamilton, *Inorg Chem Commun*, 2000, **3**, 714.

6. L. Ropartz, D. F. Foster, R. E. Morris, A. M. Z. Slawin and D. J. Cole-Hamilton, *J. Chem. Soc., Dalton Trans.*, 2002, 1997.

7. C. P. Casey and G. T. Whiteker, *Isr. J. Chem.*, 1990, **30**, 299.

8. Accelyrs, Materials Studio, 2001.

9. P. K. Maiti, T. Cagin, G. F. Wang and W. A. Goddard, *Macromolecules*, 2004, **37**, 6236.

10. B. Hong, T. P. S. Thoms, H. J. Murfee and M. J. Lebrun, *Inorg. Chem.*, 1997, **36**, 6146.

11. H. J. Murfee, T. P. S. Thoms, J. Greaves and B. Hong, *Inorg. Chem.*, 2000, **39**, 5209.

12. M. Kranenburg, Y. E. M. Vanderburgt, P. C. J. Kamer, P. W. N. M. Van Leeuwen, K. Goubitz and J. Fraanje, *Organometallics*, 1995, **14**, 3081.

13. W. A. Herrmann, C. W. Kohlpaintner, E. Herdtweck and P. Kiprof, *Inorg. Chem.*, 1991, **30**, 4271.

Chapter 5. Bite Angle Calculations on Dendritic Ligands

5.1 Introduction

The diphenylphosphine dendrimers modelled in Chapter 4 were used as catalysts but the molecular modelling study using Materials Studio assessed the molecules as free ligands. This gave very little insight into the catalytic results obtained. To gain more insight into these results, an attempt was made to measure the bite angle of three of the dendritic ligands. The computational chemistry program Hyperchem had to be used for this because parameters had to be added into the force field to enable this work to be done. The consistent valence force field of Materials Studio was not suited to easy modification.

There have been many means of assessing the properties of a ligand in an attempt to explain its catalytic properties and they largely depend on the nature of the ligand. Tolman's cone angle[1] and Casey's bite angle[2] are two such methods[3]. There are many studies into the effect of the bite angle on the selectivity of catalytic processes with diphosphine ligands creating a great deal of data for comparison.

5.1.1 Steric Properties of Ligands

The effect that ligands have on metal complexes can be split into two main effects. Firstly, electronic properties caused by the electronic character of the ligand-metal bond (i.e. the overlap of orbitals and amount of net charge transfer between the ligand and the metal) and secondly, steric effects that are a measure of the ligands size and spatial requirements in the co-ordination environment. While electronic effects are out with the remit of any molecular modelling study, attempts to quantify

the steric effects of ligands are plentiful. Homogeneous catalysis is an area in which structure-activity relationships between ligands are widely explored and a number of methods have been developed to do that. Essentially, they all involve measurement of a physical quantity and comparison to stereo- or regio-selectivity or activity in the catalytic process.

Tolman's Cone Angle was one of the first attempts to quantitatively measure the amount of space a ligand occupied (figure 5.1)[1].
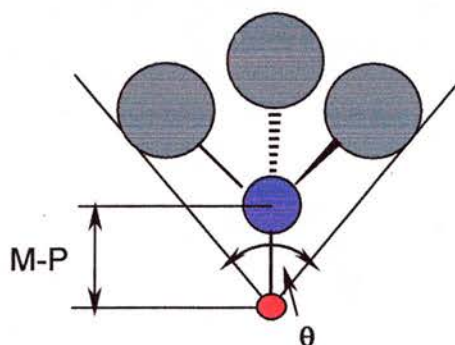
Figure 5.1: Schematic representation of Tolman's Cone Angle (θ). Phosphorus: purple, organic substituents: grey, metal: red. *"The apex angle of a cylindrical cone with origin 2.28 Å (M-P) from the centre of the phosphorus atom, whose sides just touch the van der Waals surfaces of the outermost atoms of the organic substituents"* [1].

 If various conformations of the three R groups are possible, they are folded back to give the smallest possible cone angle whilst retaining a three-fold axis of symmetry. The advantages of the cone angle method are its simplicity and it is generally applicable to all kinds of phosphorus ligands. Space filling models are inflexible however, and assume a tetrahedral geometry about the ligating atom. Additionally, the smallest possible cone angle may be a poor approximation for systems with variable substituents and the sum of the half angles in this case may not accurately reflect the ligand properties.

There have been some variations of the cone angle concept. Imyanitov came up with a mathematical procedure for determining the cone angle of any ligand ABn where A and B are atoms with A co-ordinated to the metal[4]. In order to calculate the angle in

this way the covalent radii of A, B and the metal, M, must be known along with the molecular geometry and the van der Waals radius of B. The M-P distance used by this method is 2.23 Å and so the cone angles are systematically 5 ° higher than Tolman's method (M-P distance of 2.28 Å).

If the Tolman's cone angle is a two-dimensional measurement of a ligand steric requirements and measured in a plane, the three-dimensional equivalent is the solid angle[5]. The solid angle is essentially the shadow cast by an atom or group of atoms when placed relative to an apex atom (metal) or 'light source'. The solid angle shadow is viewed as being cast on the inside of a sphere where the metal is the centre of the sphere and again applies mainly to monodentate phosphine ligands.

It has been reported that the chelate ring size can have a significant effect on the catalytic activity, for instance, with a diphosphine ligand and transition metal. Several methods have been developed to characterise the nature of that effect, considering mainly steric influences. The Pocket Angle was developed by Koide *et al.* to explain the selectivity of palladium catalysed polyketone synthesis[6]. In this reaction, it was found that a propyl-bridged bis-diphenylphosphine (dppp) had maximum activity and it was suggested that this ligand was capable of stabilising both square planar and trigonal bipyramidal geometries. Maximum activity was generally observed for phosphines in which the bite angle allowed complexation in either geometry. There is an optimum size for the active site at the metal and catalysis was found to be dependent on the size of the interior cone angle in the plane of the ligands around the metal. A small pocket angle may inhibit further chelation at the metal because of the steric repulsion between the PR groups and the carbonyl. The pocket angle gives some measure of the ease of chelation at the metal centre and a related method is the Accessible Molecular Surface Model[7] (AMS). The AMS is used to investigate the influence of structural changes in the ligand on the co-

ordination geometry of the corresponding complex. The fragment [(P$_2$) Rh] is used

for a chelating diphosphine and cannot be considered rigid during catalysis as it is

influenced by steric and electronic interactions with other ligands. The bite angle is

not taken into consideration with this method which is known to have a strong

influence on the reactivity of metal chelate complexes. The AMS for some common

ligands is detailed in table 5.1 and compared to results from single crystal XRD,

^{103}Rh NMR and molecular modelling.

Ligand	P-Rh XRD	PRhP XRD	PRhP NMR	PRhP Model	P-Rh Model	AMS
Dppe	2.191 Å	84.34°	86.9 °	83.26 °	2.171 Å	7.578 Å^2
Dppp	2.194 Å	90.77 °	90.9 °	88.79 °	2.182 Å	5.704 Å^2
Dppb	2.206 Å	93.08 °	93.4 °	91.13 °	2.195 Å	4.654 Å^2

Table 5.1: P-Rh and P-Rh-P data from ref [7] .XRD and NMR data from analysis of [(P$_2$) Rh (hfacac)] a square planar Rh complex (hfacac - hexafluoroacetylacetonate). XDR data from single crystals of complex, NMR data based on correlation of ^{103}Rh shifts with bite angle, AMS is accessible molecular surface. Dppe – bis-diphenylphosphinoethane; Dppp – bis-diphenylphosphinopropane; Dppb – bis-diphenylphosphinobutane.

The above methods all involve the calculation of physical characteristics of the

ligand such as bond distances, geometric parameters or surface areas. Brown *et al.*

devised a method based around the energy of the molecule, the Ligand Repulsive

Energy[8]. This takes into account the multitude of conformational configurations

when flexible groups are attached to the co-ordinating atoms, and acknowledges that

the reaction context (spectator or participating ligand) affects which aspects of a

ligand's steric characteristics are important. In general, it is the rate determining step

that affects which aspect of a ligand's steric requirements are important in a reaction.

In the case of spectator ligands, the bulk of the molecule may influence the approach

of reagents to the co-ordinating metal. On the other hand, it could be that the

repulsive interactions between the ligands at the metal centre represent the greater

influence of the steric properties of the ligand. The Ligand Repulsive Energy E$_R$ is a

measure of the steric requirement for the co-ordinated ligand and is used to evaluate

the steric repulsive interactions between a ligand and the rest of the complex. This can be represented as an equation:

$$E_R = r_e \left[\frac{-dE_{vdW}(repulsive)}{dr_{M-L}} \right]$$

$E_{vdW(repulsive)}$ van der Waals repulsive energy between the ligand and the rest of the molecule, r_e is the equilibrium ligand-metal distance.

The method for determining E_R involves using molecular mechanics to find the global minimum of energy. The computed energy is generally found to vary linearly with respect to P-Rh within ± 0.08 Å. The above equation is then used with the gradient from this linear relationship to calculate E_R.

A method so dependent on molecular modelling has some obvious limitations – it is being used to measure energy in a metal complex, a system for which accurate parameters are few. The calculated values of E_R are sensitive to the force field form and as such, results obtained from different force fields and parameter sets should not be directly compared quantitatively, although trends may be similar. It is the gas phase structure that is considered, and so no solvent effects are taken into consideration. It is also important to pick the lowest energy conformer possible for this calculation, as variations will occur for similar structures of differing energy. The advantage over cone angle is that E_R is calculated for each ligand in a conformation appropriate to complexation. Cone angles are usually calculated from a folded back conformation, and use CPK models that do not account for lone pairs. E_R can be calculated for all kinds of ligands and metal centres including asymmetric ligands.

5.1.2 Bite Angle[2]
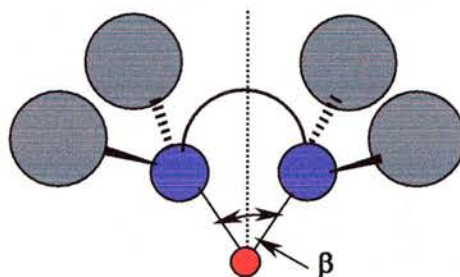
Figure 5.3: P-M-P Bite Angle β. Purple – phosphorus, Grey – non-bridging organic substituents, Red – metal atom, M.

For a diphosphine ligand the cone angle at each phosphorus atom is defined as the angle between one M-P bond and the vector bisecting the P-M-P bite angle plus steric contributions of the non-bridging substituents on P. This means that the cone angle in chelating diphosphines is partially dependent on the bite angle, P-M-P. It is possible for ligands with the same bite angle to have different cone angles, caused mainly by steric crowding from non-bonding parts of the ligand or other ligands present.

The natural bite angle, β_n, is the preferred chelation angle of a diphosphine ligand determined only by the ligand backbone, and not by electronic properties of the metal such as valence angles or by other ligands at the metal centre[2]. This makes β_n independent of any electronic preference for chelation angle the metal centre may possess.

Natural bite angles are calculated using molecular modelling techniques where a dummy atom is used to represent the metal centre and the P-M-P angle bend force constant is set to 0 kcalmol^{-1}rad^{-2}. As the metal-phosphine bond length can vary with the type of complex, a M-P bond length of 2.30 Å is used to standardise the results. β_n is then calculated for the global minimum energy representation of the ligand. The structures obtained during the minimisation process are often compared to crystal structures of the ligand complex to evaluate the accuracy of the orientation of

the ligand groups. The bite angle can also be measured from a crystal structure, but then includes the metal's electronic and other ligand's steric influences. This is not the same as the natural bite angle, dependant only on the ligand backbone. It is widely accepted that a minimum energy structure would not represent the case of a ligand at high temperature or pressure and so a measure of the flexibility of the ligand backbone is made. This is carried out by varying the P-M-P angle by 5 ° increments, setting the P-M-P angle bend force constant to a very large value to inhibit the angle changing, and calculating the strain energy. The strain energy due to the fixed bite angle is subtracted from the total strain energy of the molecule and plotted against angle. This use of molecular mechanics means that β_n is dependent on the parameters and force field used and making quantitative comparisons between methods impossible. The trends seen between ligands can be compared however and this is useful in determining the accuracy of bite angle calculations. The natural bite angle is one method of measuring the effect of the ligand backbone on the metal centre and, in the case of dendrimers, simpler to calculate than either the pocket angle or the cone angle.

5.1.3 Metal Complexes

Hydroformylation is one of the most important applications of transition metal homogeneous catalysis, particularly rhodium catalysed processes. The chemical industry requires the most efficient processes creating desirable products through the least expensive route, consequently much research has gone into the development of catalytic systems that show good selectivity for particular reactants, reactions or products. A wide range of new ligands have been developed with different

properties, both sterically and electronically that have led to improved selectivities (regio- and stereo-) and activity.

Ligands with phosphorus based groups have been shown to give the highest selectivity or activity for hydroformylation and there have been many investigations into such systems through actual means such as kinetic studies, analytical techniques and also through theoretical techniques. Calculation of the bite angle measures the effect of adding just one atom into the ligand, the metal centre, and assesses only the response of the phosphine groups to that metal group. This chapter deals with calculating the bite angle for a series of dendritic ligands. An investigation into the effects of adding a rhodium complex [Rh (CO) $_2$H] to the dendrimer, both on the ligating branch and the rest of the structure was carried out. It is hypothesised that the dendrimer complex would have to sit on the surface of the molecule to participate fully in the hydroformylation process, and that the bulk of the remainder of the molecule can in some way influence the selectivity, particularly in G1-16ethylPPh$_2$. There have been several studies to date using quantum mechanics methods or combined Quantum Mechanics/Molecular Mechanics methods to investigate the process of hydroformylation with bis-diphenylphosphine ligands and the influence of the ligand on the reaction products[9,10]. This number is far outweighed by the number of studies assessing purely steric influences of the ligands. The electronic properties of ligands are outwith the scope of molecular modelling studies such as those described later in this chapter, but the results from previous studies will be used to effect a qualitative description of the effect of the dendritic structure on the selectivity of the hydroformylation reaction.

Electronic effects in metal complexes include the basicity of the ligand and its σ-donor/ π-acceptor capabilities, whereas the steric effects refer only to the size and orientation of the ligand. It is believed that there are two steric effects in

diphosphine ligands, the influence of the ligand through non-bonded interactions and the influence of the ligand through its bite angle. The bite angle affects both the bulkiness of the ligand and the metal hybridisation (and hence contributes to electronic effects).

Van der Veen *et al.* investigated a series of thixantphos ligands and showed that the l:b ratio was independent of the diphosphine's mode of chelation (ee-ea equilibrium)[11,12].
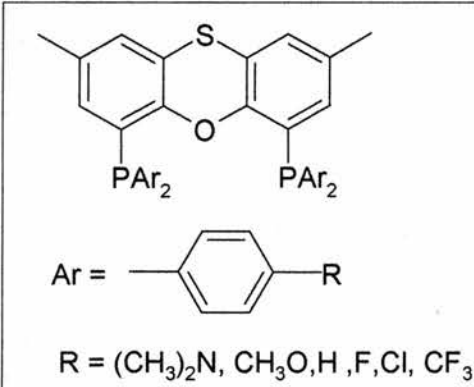
R	β_n (flexibility) / °	L:b ratio
N(CH$_3$)$_2$	109.1 (92 – 124)	44.6
OCH$_3$	106.9 (91 – 123)	36.9
CH$_3$	106.7 (91 – 125)	44.4
H	106.4 (91 – 127)	50.0
F	106.6 (92 – 128)	51.5
Cl	107.8 (91 – 126)	67.5
CF$_3$	109.3 (92 – 128)	86.5

Table 5.2: Series of ligands based on thixantphos synthesised by van der Veen *et al*[11] with varying basicity at the phosphine caused by the substituent on the diarylphosphine. Natural bite angle (β_n) calculated for the ligands, l:b ratios calculated for the hydroformylation of oct-1-ene at 80 °C , 20 bar, CO/H$_2$ = 1,

It was found that the overall trend in selectivity for the hydroformylation of oct-1-ene could not be explained by the changing basicity of the phosphine. The selectivity for the linear aldehyde correlated better to the natural bite angle as calculated by Casey and Whiteker[2,3].
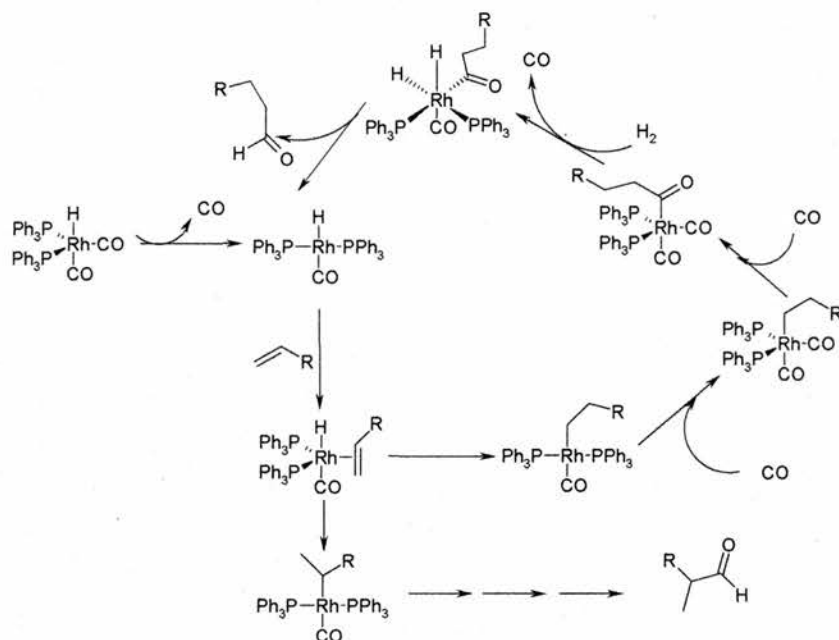
Figure 5.3: Catalytic cycle for hydroformylation, adapted from van der Veen *et al.* [11].

Figure 5.3 shows the catalytic cycle for the hydroformylation of a generic alkene, including the initial dissociation of the phosphine complex into a four co-ordinate precursor.

Figure 5.4: Diequatorial (ee) to equatorial-apical (ea) binding modes of bis-diphenylphosphine complex.

The equilibrium between ee and ea is dependent on the phosphine in as much as decreasing phosphine basicity will shift the equilibrium shown in figure 5.4 towards ee mode. Van der Veen *et al.* observed an increase in l:b ratio and activity for the hydroformylation of oct-1-ene as the basicity of the phosphine ligand decreased[11]. The selectivity for the linear aldehyde in the hydroformylation of oct-1-ene remained the same at approximately 92% indicating that the electronic properties of the ligands and co-ordination mode do not influence the regioselectivity. This may imply that CO dissociation from the ea or the ee forms of the complex leads to the same four-co-ordinate intermediate. The regioselectivity is determined by two consecutive

steps of alkene co-ordination and hydride migration, specifically by the alkene attack on the four co-ordinated intermediate.

Figure 5.5 outlines a possible mechanism for regioselectivity by way of alkene attack on the four co-ordinate intermediate. The size of the bite angle will influence how the alkene approaches the metal centre by creating more steric hindrance at wider angles. If this possible mechanism is considered for the dendritic ligands, there are more than just bite angle effects at work.
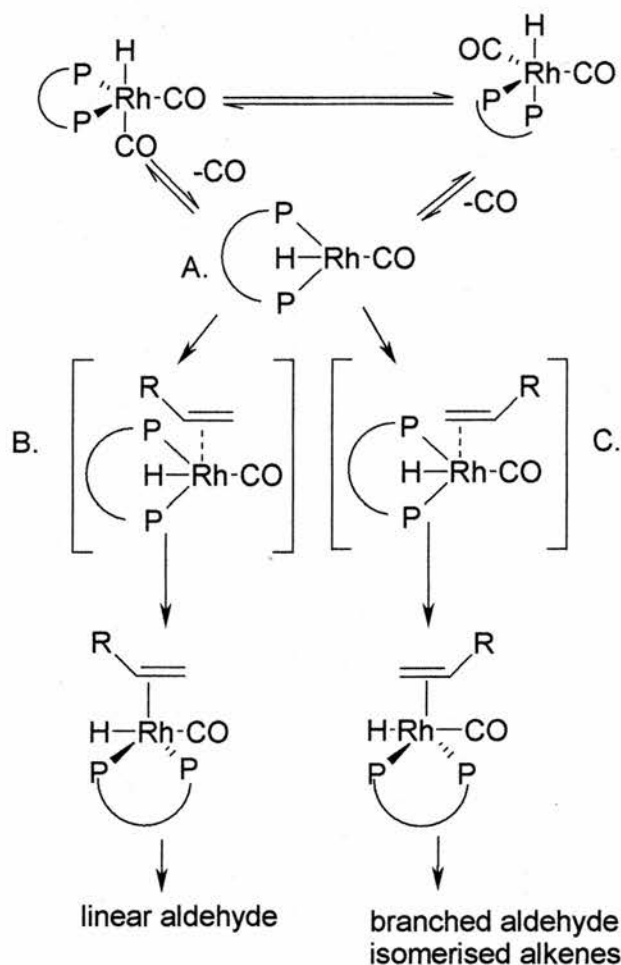
Figure 5.5: Possible origin of regioselectivity through alkene attack on a four co-ordinate intermediate as proposed by van der Veen *et al.*[11] A. – reactive four-co-ordinate (square planar) intermediate created from the loss of CO from either the ee or ea complex; B. – square-pyramidal transition state thought to favour a linear product; C. – square-pyramidal transition state thought to favour a branched product. Curved line linking phosphines represents ligand backbone and diphenyl groups have been omitted for clarity.

Firstly, the bite angle of the dendritic ligand will have an important effect on the steric constraints in the co-ordination sphere but the bulk of the dendritic ligand and

the orientation of the complex will also have an effect. The orientation of the metal complex on and within the surface of the dendrimer will directly influence the degree to which the dendrimer exerts steric influence on the metal complex. Increasing the steric bulk around the rhodium centre as the bite angle widens leads to more selective formation of the sterically less demanding linear alkyl rhodium species. In addition, the ability of the ligand (flexibility) to encompass the whole range of bite angles associated with different rhodium species in the hydroformylation cycle may be more important than the absolute value of the natural bite angle.

5.2 Results and Discussion

5.2.1 Parameterisation of Force Field
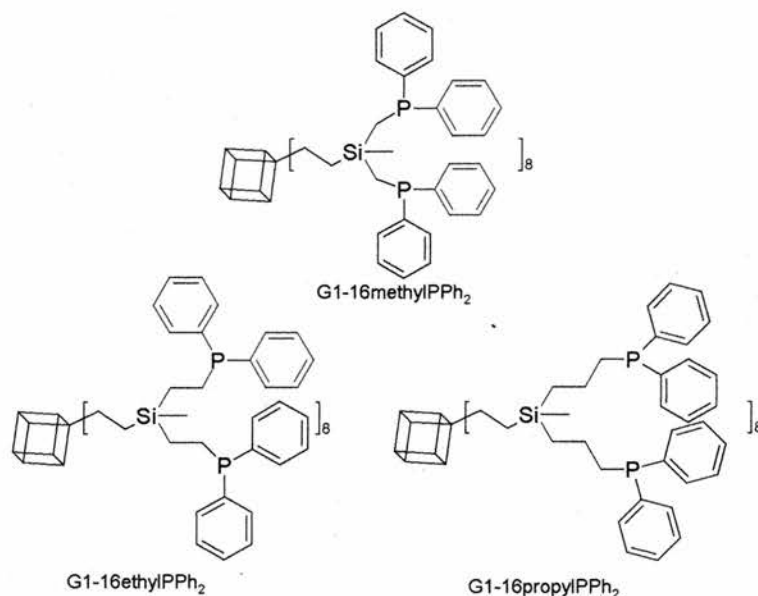
Figure 5.6: Three dendrimers studied in this chapter.

The first stage of this work was the addition of parameters to the MM+ force field to

enable the bite angle to be calculated. Parameters are generally obtained from X-ray

crystallography structures or quantum mechanics studies, and require equilibrium

values and force constants for bonds, angles, and torsions. To calculate the bite

angle, one atom type (the metal) must be added to the force field. A series of

corrections and modifications must be made to other parameters for those atoms that

interact directly with the metal centre. This work was done in stages to ensure that

only those parameters that were necessary were added to the force field to avoid

creating a large number of variables each requiring testing and modifying. To

simplify matters further, three dendrimers were picked for this work with closely

related structures (figure 5.7).
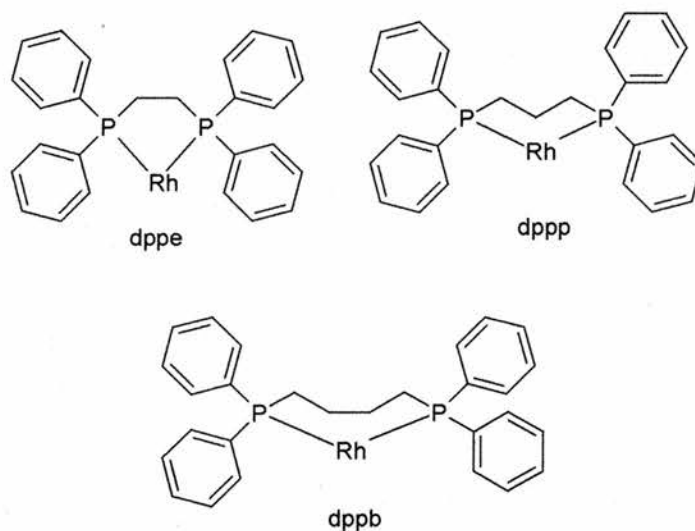
Figure 5.7: Three small ligands used for parameter development. Dppe – Bis-diphenylphosphinoethane, Dppp – Bis-diphenylphosphinopropane, Dppb – Bis-diphenylphosphinobutane. Only the rhodium atom of the complex is shown for clarity.

The parameters were developed using a trial and error approach with a series of small molecules (figure 5.7) for which both the X-ray crystal structure had been reported in literature as well as previous bite angle calculation values. Angermund *et al.* reported crystal structures for square planar rhodium complexes of the three small ligands shown in figure 5.7 complexed to hexafluoroacetylacetonate (hfacac)[7]. A set of crystal structures with trigonal bipyramidal co-ordination at rhodium would be preferred for comparison with modelling data. It is not ideal to compare the structures of these square planar rhodium complexes to the modelling data. The advantages of using this data is that the other ligands used for the X-ray study are identical (hfacac), and that the PRhP angles were extensively investigated by Angermund and co-workers by NMR and molecular modelling. These three ligands give linear: branched ratios typically in the region of 2 for the hydroformylation of oct-1-ene and other alkenes.

A successful set of parameters was defined as those that could reproduce the same trends in this series of ligands and were within $\pm 4\,^\circ$ of the values calculated by X-ray diffraction.

5.2.1.1 First Approximation

The first attempt to model rhodium diphosphine complexes with the Hyperchem

Program was made using the MM+ force field with no modifications. This was

because it automatically assigns the atom type ** to elements for which no atom type

exists (such as rhodium), and creates values for bond stretches, bond angles, torsions

and non-bonded interactions that are not found in the parameters based on a series of

rules.

Element	Atom Type	Notes
Carbon	C_4	Aliphatic carbon, sp3
Carbon	Ca	Aromatic carbon
Hydrogen	H	Hydrogen atom singly bonded
Phosphorus	P	General phosphorus atom
Generic	**	Unassigned atom

Table 5.3: Atom types present within MM+ force field

In this way, the series of small ligands were modelled with an atom bonded to both

phosphines and the bite angle calculated.

Ligand	Calculated Bite Angle	PRhP XRD
Dppe	144.35 °	84.34°
Dppp	148.95 °	90.77 °
Dppb	156.01 °	93.08 °

Table 5.4: Calculated Bite Angles and XRD values from[7]

It can be seen that while the bite angle calculations reproduce the trend in values, the

magnitude is at least 60 ° too large (table 5.4).

5.2.1.2 Second Approximation

Basic force field parameters were added to the MM+ force field, based on Casey 's

work. An atom type rh for Rhodium (mass: 102.906 amu, atom type 73.) was added

as well as a selection of bond stretches and angle bends.

Parameter	Details	Equilibrium Value	Force Constant
Bond Stretch	rh-p	2.315 Å	201
Angle Bend	rh-p-ca	109.2 °	0.7
Angle Bend	rh-p-c4	109.2 °	0.7
Angle Bend	p-rh-p	*	0

Table 5.5: Parameters added to MM+ for the second approximation. * - no equilibrium value entered.

In keeping with the method of Casey, the force constant for the P-Rh-P bend was set to zero and no equilibrium value was entered. Values were entered for Rh-P-C bends and the P-Rh bond length was set to a standard value of 2.315 Å with a very high force constant to ensure it did not deviate.
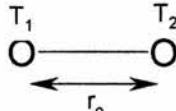
Ligand	Calculated Bite Angle	PRhP XRD
Dppe	77.51	84.34°
Dppp	86.21	90.77 °
Dppb	104.16	93.08 °

Figure 5.6: Calculated Bite Angles and XRD values from[7]

The calculated values for the bite angle were closer to those from XRD (between 6 and 9 Å out) and again showed the same trends. The parameters present for the phosphorus atoms were for either 3 or 5 co-ordinate species and so it was felt that the trends observed could be improved through the addition of parameters specific to an R_3P-Rh phosphine.
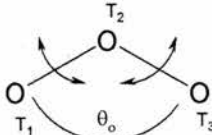
5.2.1.3 Third Approximation

For the third approximation, another atom type was added to the force field, this time for tetrahedral phosphorus (pa, atom type no. 74). The parameters for this were derived from Casey *et al.*[2] and Gleich *et al.*[13] and also from modifying pre-existing parameters for phosphorus-carbon bonds to include the new phosphorus atom type. While this meant that a large number of parameters were created, most of them did not have 'new' values. Bonds and angles including rhodium were created (similar to the second approximation) from various sources[2,13].

$$V_{stretch} = \sum_{bond} K_r (r - r_0)^2$$

T₁	T₂	Kᵣ	r₀ (Å)	L1	DIPOLE
rh	**pa**	**201**	**2.315**	**0**	**0**
c3	*pa*	*2.91*	*1.828*	*0*	*1.04*
c4	*pa*	*2.91*	*1.856*	*0*	*0.83*
ca	*pa*	*2.91*	*1.828*	*0*	*1.04*

Table 5.7: Bond parameters added to MM+. Entries in italics refer to parameters that were modified by changing the atom type from p to pa, entries in bold were added. Note the very high force constant for the pa-rh bond is designed to restrain that bond length.

$$V_{bend} = K_\theta \sum_{angle} (\theta - \theta_0)^2$$

T₁	T₂	T₃	K_θ (°)	Θ₀
pa	**rh**	**pa**	**0**	**0**
rh	**pa**	**c4**	**0.4**	**109.2**
rh	**pa**	**ca**	**0.7**	**117**
c4	c4	pa	0.48	109.5
c4	pa	c4	0.576	96
c4	pa	ca	0.7	109.5
ca	*ca*	*pa*	*0.38*	*120*
h	c4	pa	0.36	109.5

Table 5.8: Angle parameters added to MM+. Entries in italics refer to parameters that were modified by changing the atom type from p to pa, entries in bold were added and entries in standard script were modified both by changing the atom type from p to pa and by altering the equilibrium value to reflect the tetrahedral phosphorus.

$$V_{dihedral} = \sum_{dihedrals} \frac{V_n}{2} [1 + \cos(n\phi - \phi_0)]$$

n – periodicity of Fourier term, ϕ_0 – Phase Angle,

ϕ – Dihedral Angle
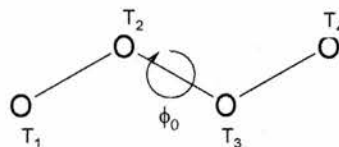
T_1	T_2	T_3	T_4	V_1	V_2	V_3
c4	pa	rh	pa	0.2	0	0
rh	pa	c4	c4	0.2	0	0
rh	pa	c4	c4	0.2	0	0
rh	pa	ca	ca	0.2	0	0
rh	pa	ca	ca	0.2	0	0
ca	*ca*	*ca*	*pa*	*0*	*16.25*	*0*
ca	*ca*	*pa*	*c4*	*0*	*0*	*0.4*
ca	*ca*	*pa*	*ca*	*0*	*0*	*0.33*
ca	*pa*	*rh*	*pa*	*0.2*	*0*	*0*
h	*c4*	*c4*	*pa*	*0*	*0*	*0.33*
h	*c4*	*pa*	*ca*	*0.05*	*0*	*0.2*
h	*c4*	*pa*	*h*	*0*	*0*	*0.428*
h	*ca*	*ca*	*pa*	*0*	*16.25*	*0*

Table 5.9: Torsion parameters added to MM+. Entries in italics refer to parameters that were modified by changing the atom type from p to pa, entries in bold were added and entries in standard script were modified both by changing the atom type from p to pa and by altering the equilibrium value to reflect the tetrahedral phosphorus.

Ligand	Calculated Bite Angle	PRhP XRD	PRhP Model
Dppe	81.1964 °	84.34 °	83.26 °
Dppp	88.9423 °	90.77 °	88.79 °
Dppb	96.4888 °	93.08 °	91.13 °

Table 5.10: Bite Angle as calculated for the third approximation and XRD data from[7].

5.2.1.4 Restraints

In order to gain additional insight into the dendrimer-metal complex, modelling simulations of the dendrimer with a rhodium complex attached at one branch were attempted.
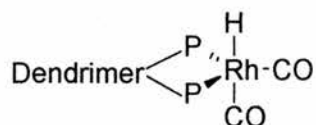
Figure 5.8: Rhodium complex attached to G1-16ethylPPh$_2$ by diequatorial binding. The phenyl rings have been omitted for clarity.

Adding parameters to an empirical force field for transition metal complexes is extremely difficult especially when required to define specific positions of binding such as axial or equatorial. This is best appreciated when considering the two carbonyls in the complex (figure 5.8). The axial carbonyl would require very different parameters in terms of angles with such as HRhC = 180 ° and PRhC = 90 °, compared to the equatorial carbonyl HRhC = 90 ° and PRhC = undefined. It would not be possible to add values for PRhC for an equatorial co-ordinated carbonyl because defining those two angles with high force constants to enforce trigonal bipyramidal geometry at the metal centre would define the third angle, PRhP. The problem is mainly to do with getting the computer program to recognise two identical atoms in two subtly different environments. No way could be found to solve this by adding parameters to the force field.

Bond	R$_0$ (Å)	K$_b$ Hard	K$_b$ Soft
Rh-H	1.65	7	5
Rh-Ca	1.90	7	5
Rh-Ce	1.90	7	5
Ca-Oa	1.18	7	5
Ce-Oe	1.18	7	5

Table 5.11: Bond length restraints used for simulation of metal complex.

Hyperchem offers the use of restraints to set lengths, angles and torsions to fixed values to keep part of a molecule in a specific orientation and this offered the best route for modelling a rhodium-dendrimer complex. Hard restraints were used in the first instance, creating extremely rigid geometry around the metal centre to allow the molecule to be heated to a high enough temperature to overcome any energy barriers induced by these restraints.

References for Chapter5 begin on page 215

Angle	R_0 (°)	K_0 Hard	K_0 Soft
P_1RhCa	90	125	5
P_2RhCa	90	125	5
HRhCa	180	125	25
HRhCe	90	125	25
RhCaOa	180	125	25
RhCeOe	180	125	25
$HRhP_1$	90	125	5
$HRhP_2$	90	125	5

Table 5.12: Angle bend restraints used for simulation of metal complex.

The hard restraints are detailed in tables 5.11 and 5.12 and include high force

constants. The dendrimer complexes were heated to 1500 K then cooled to 300 K.

At this point, the restraints were reduced to allow more freedom of motion. Angles

that included the phosphorus atoms were reduced to very low values to enable

calculation of the bite angle and the others were reduced to moderately low values.

The dendrimer complex was cooled to 0 K and equilibrated at the 300 K after a short

period of energy minimisation.

5.2.2 Calculation of Bite Angle

The bite angle of small ligands such as bis-diphenylphosphinoethane is usually

calculated using an energy-minimised structure[2]. The flexibility in the ligand is

calculated by fixing the bite angle at various values and calculating the strain energy

created within the molecule. Deviations from the natural bite angle of around ± 3

kJmol[-1] are deemed accessible for the complex. This works very well for small

systems where low energy configurations are easily found and small deviations in the

bite angle alone lead to changes in energy. For large molecules such as dendrimers,

it is unlikely that a global minimum energy structure will ever be found and so most

properties are calculated from trajectories giving an average view of the structure.

The flexibility of the bite angle in a dendrimer could not be calculated as described above because without fixing the remainder of the molecule, it would be impossible to determine what was responsible for a reduction or increase of strain energy. With so many other atoms within the system, a series of changes in them could counteract any associated change in strain energy.

Dendrimer	Bite Angle (°)	Flexibility (°)
Dppe	86.3	70.0 – 98.0
Dppp	94.5	79.5 – 116.8
Dppb	107.1	85.0 – 135.8
Bis-diphenylphosphinopentane	134.6	99.5 – 157.3
Tetrakis-diphenylphosphinoethylsilane	123.5	91.0 – 167.0
Bis-diphenylphosphinoethyldimethylsilane	134.8	104.0 – 166.5
G1-16methylPPh$_2$	105.8	83.0 – 125.0
G1-16ethylPPh$_2$	128.8	92.8 – 157.0
G1-16propylPPh$_2$	139.9	102.3 – 171.0

Table 5.13: Average bite angle and flexibility of test compounds, model compounds and dendrimers. The bite angle is calculated at 300 K, with an average of 21000 frames of data.

The bite angle is calculated for these dendrimers and associated molecules by dynamics, making it temperature dependent. The flexibility of the ligand is then viewed as the range of bite angles accessible at a given temperature. The bite angles quoted in table 5.13 are the average of three molecular dynamics runs generating three production trajectories for analysis each consisting of 7002 frames. The data is represented graphically in figures 5.9 – 5.11.

The three small ligands used to create the force field parameters show the same trends as those values derived from XRD or previous studies. They also show the same trends as the values calculated during parameter testing when minimisation was used to generate structures. These compounds typically give l: b ratios in the region of 2 – 3 for hydroformylation reactions. The bite angle calculated from a minimum energy structure is within approximately 3 ° of that obtained by X-ray diffraction. The bite angle obtained from dynamics at 300 K is between 2 and 14 ° higher than

the XRD structure (table 5.13). This is to be expected, as at 300 K there is more energy in the system available for overcoming energy barriers, which leads to an increase in the number of energetically accessible conformations. In general, the addition of a CH_2 group increases the average bite angle by approximately 8 – 13 ° and raises the flexibility range accordingly. The increase in size of ring formed on co-ordination also broadens the flexibility range.
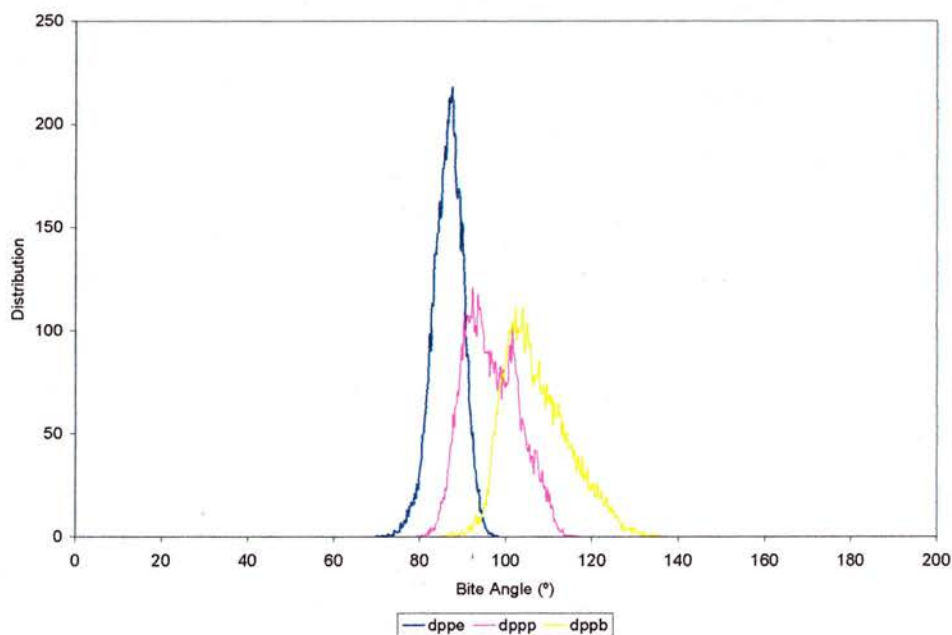
Figure 5.9: Small Ligands, *bis-diphenylphosphino-* dppe – *ethane*, dppp – *propane*, dppb- *butane*. The compounds synthesised to mimic the branches of G1-16ethylPPh$_2$ show much wider flexibility ranges, reflecting the larger size of the ring formed (figure 5.10). The average bite angles calculated reflect composition of the ligand backbone, where the most constrained ligand, Tetra- (diphenylphosphinoethyl)-silane has the smallest average bite angle but the largest flexibility. This simply means that while the ligand can adopt quite narrow and broad conformations, the preferred configuration is much smaller than the other compounds that also form a 8 membered ring with rhodium. The distributions of bis-diphenylphosphinopentane and bis-diphenylphosphinoethyldimethylsilane appear to be skewed to the right, creating a higher average bite angle.
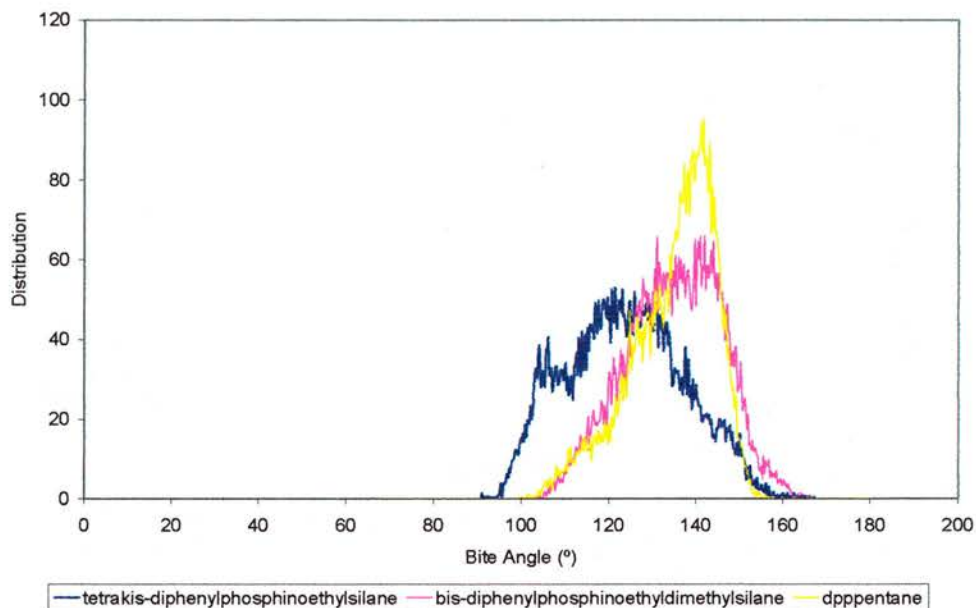
Figure 5.10: Model compounds bis-diphenylphosphinopentane, tetrakis-diphenylphosphinoethylsilane and bisdiphenylphosphinoethyl dimethylsilane.

The three dendrimers show a similar trend to the small molecules (dpp ethane etc) in that the addition of a CH_2 group to the arm of the ligand results in an increase in average bite angle and flexibility. G1-16methylPPh$_2$ has a narrow distribution indicating that there is not great room for movement within the branches. G1-16propylPPh$_2$ has a wider distribution but also one that is more biased towards the middle range of its values. This implies that while there is greater flexibility within this ring (forming a 10 membered ring), something inhibits it from its maximum and minimum values. G1-16ethylPPh$_2$ has an equally wide distribution but one that is more even implying that the ring formed has fewer constraints on its configuration.

Figure 5.11: Bite Angle Distribution for all three dendrimers over 70 ps at 300 K averaged over three simulations.

If these results are now compared to the catalytic data obtained by Ropartz *et al.* The average bite angle may go some of the way to explaining the selectivities recorded[14].

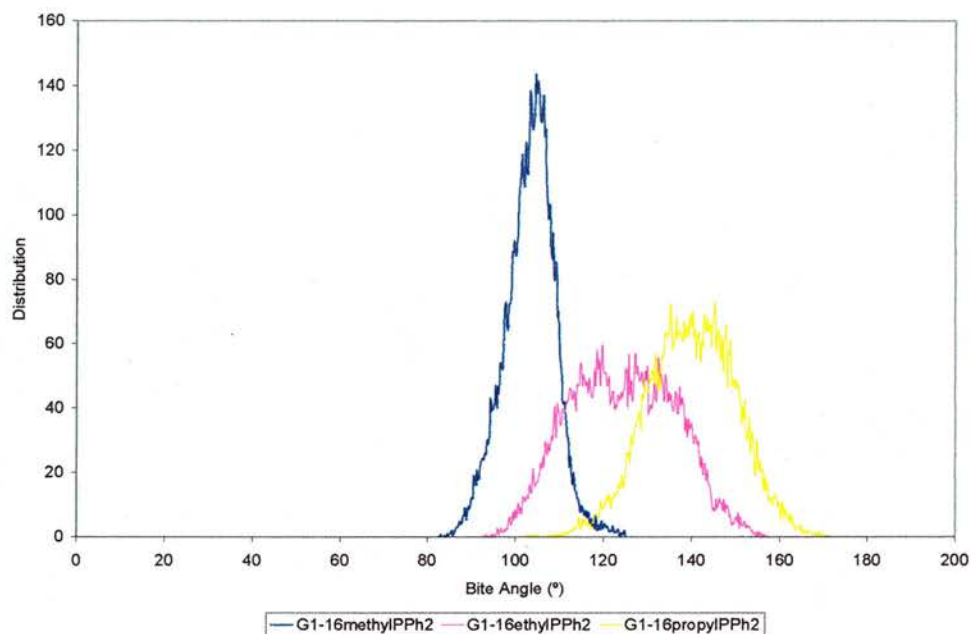| Ligand	l:b ratio	Nonan-1-al (%)	Average Bite Angle (°)	Flexibility (°)
G1-16methylPPh$_2$	3.9	68.5	105.8	83.0 – 125.0
G1-16ethylPPh$_2$	13.9	86.0	128.8	92.8 – 157.0
G1-16propylPPh$_2$	5.0	78.0	139.9	102.3 – 171.0
Bis-diphenylphosphinopentane	3.4	70.1	134.6	99.5 – 157.3
Bis-diphenylphosphinoethyldimethylsilane	3.8	72.7	134.8	104.0 – 166.5
Tetrakis-diphenylphosphinoethylsilane	5.2	77.4	123.5	91.0 – 167.0

Table 5.14: Hydroformylation of oct-1-ene catalysed by Rh complexes of ligands[14].

Ligands with a bite angle in the region of 120 ° are thought to prefer equatorial-equatorial binding modes which in turn is thought to show enhanced regioselectivity for the linear product. The trends shown by the dendrimer ligands clearly support this theory. The dendrimer with an average bite angle closest to 120 ° is the most selective ligand. The trends shown by the smaller molecules also support this to a lesser degree due to the tendency of small molecules to dimerise. It is possible that the size of the dendrimer ligands prevents such processes and results in greater selectivity.

It should be noted that the average bite angles (at 300 K) of the test ligands were between 2 and 10 ° higher than the natural bite angle (from minimum energy structure). This implies that the dendrimers will probably show the same trend. In order to test this theory, the average bite angle of each dendrimer was calculated at different temperatures.

G1-16propylPPh$_2$ was equilibrated at 100 and 50 K in addition to 300 K and the increase in temperature leads to an increase in the flexibility range. The average bite angle also increases with temperature.

Temperature (K)	Average Bite Angle (°)	Flexibility (°)
300	139.9	102.3 – 171.0
100	138.7	121.5 – 159.5
50	133.4	120.3 – 142.5

Table 5.15: Average bite angle and flexibility of G1-16propylPPh$_2$. Calculated at 300 K with an average of 21000 frames of data.

The bite angle calculated at 50 K gives a very sharp peak in figure 5.12 due to the low energy in the system inhibiting movement from the minimum energy structure obtained.
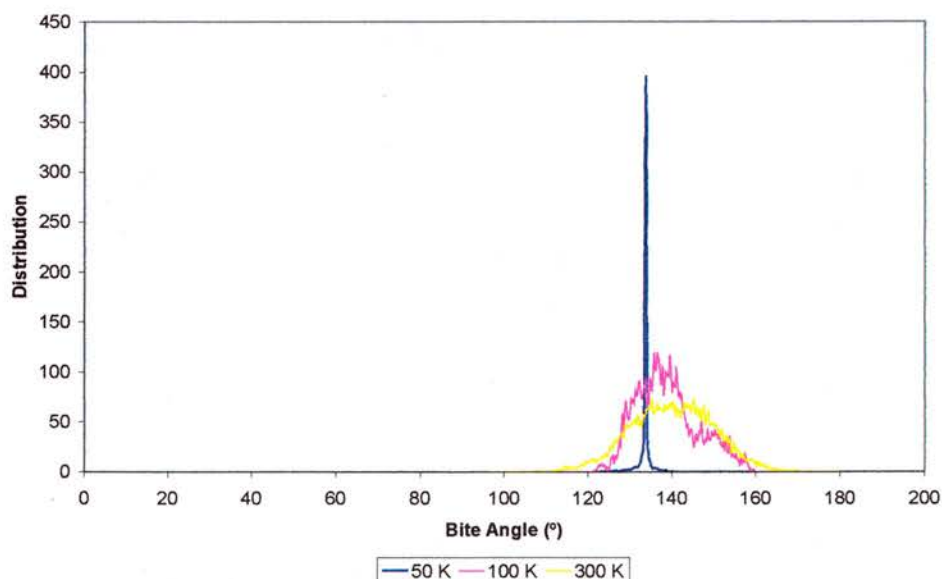

Figure 5.12: G1-16propylPPh$_2$ bite angle distribution at 50 and 300 K, Distribution for 50 K has been reduced by a factor of 20 for easier comparison.

G1-16methlPPh$_2$ shows almost the opposite trend with the bite angle decreasing with increasing temperature but the flexibility range becoming broader all the same. While this might appear counterintuitive at first, it is important to remember that at 50 K there is very little energy in the system making some energy barriers impossible to cross. The additional energy at 300 K means that the ligand has more energy to change configuration.

Temperature	Average Bite Angle (°)	Flexibility (°)
300	105.8	83.0 – 125.0
50	113.0	102.0 – 125.0

Table 5.16: Average bite angle and flexibility of G1-16methylPPh$_2$ at various temperatures.

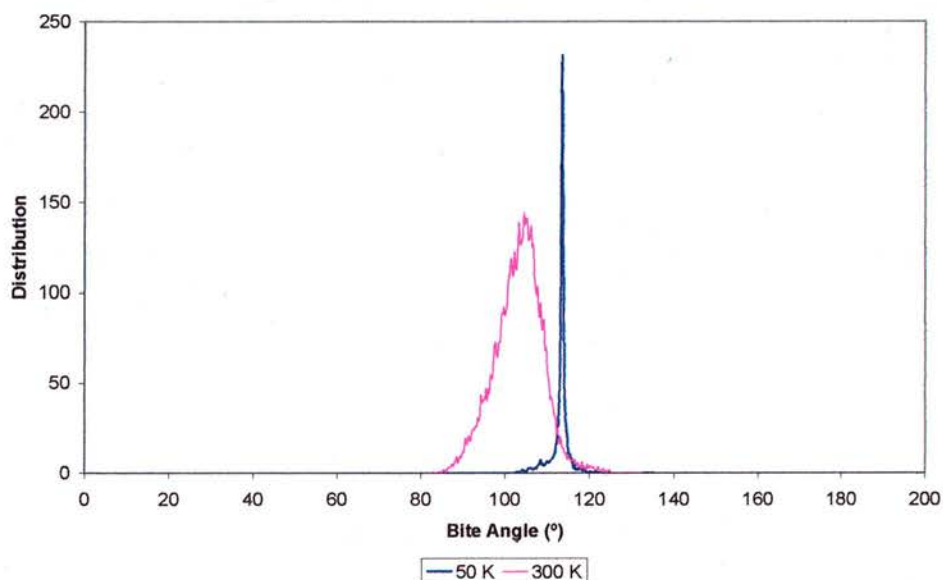**Figure 5.13:** G1-16methylPPh$_2$ bite angle distribution at 50 and 300 K, Distribution for 50 K has been reduced by a factor of 10 for easier comparison.

G1-16ethylPPh$_2$ was modelled at a far wider range of temperatures and in general, the flexibility ranges increased with temperature. The average bite angle varied between 125 and 136 ° implying no clear correlation between temperature and angle (table 5.17).

Temperature (K)	Average Bite Angle (°)	Flexibility (°)
500	124.4	93.5 – 167.0
400	127.8	96.5 – 173.8
300	128.8	92.8 – 157.0
200	136.1	108.8 – 161.3
100	126.1	106.3 – 152.5
50	125.2	107.3 – 159.8

Table 5.17: Average bite angle and flexibility of G1-16ethylPPh$_2$ at various temperatures.

Figure 5.14 illustrates how the distributions move from very sharp peaks at low temperatures to broad peaks at the highest temperatures. The value that occurs most frequently in the distribution is not necessarily the average bite angle. Instead, it may represent a configuration in which the ligand was trapped for a longer period while the rest of the branch or dendrimer moved.
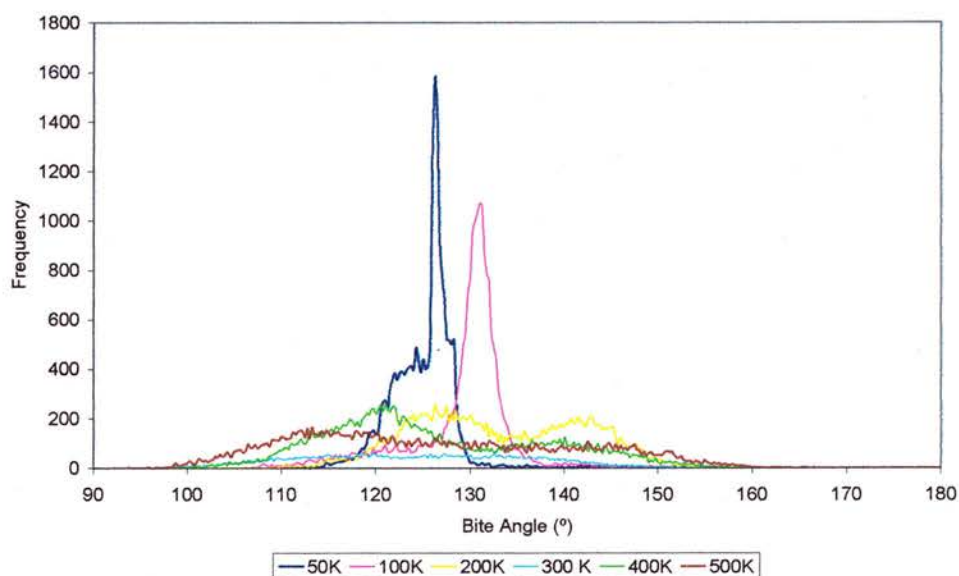
Figure 5.14: G1-16ethylPPh$_2$ bite angle distribution at various temperatures

There is one problem with the notion of bite angles and dendrimers and it is only apparent when the simulations are inspected closely. Figures 5.15 shows a snapshot of one frame from the dendrimer bite angle production trajectory. The branch forming the complex appears to be orientated in a manner that directs the rhodium into the interior of the dendrimer.

197
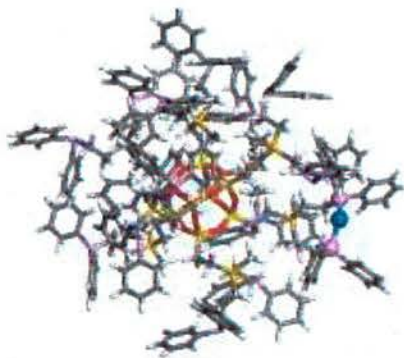
Figure 5.15: View of G1-16ethylPPh$_2$ showing PRhP unit as balls pointing inward. Rhodium – green, oxygen – red, carbon –grey, hydrogen – white, phosphorus – purple, silicon – yellow.

The phosphorus rhodium ring is in a conformation that means the rhodium, where any catalytic reaction would take place, is masked from the solvent and other reactive species by phenyl rings on adjacent branches. In small ligands, this does not occur because the ligand backbone is smaller and less flexible. The rhodium is quite a small unit and is able to fit into such a pocket in the dendrimer; a metal complex would be far less likely to do so.

The inclusion of a metal complex into the dendrimer would cause this branch to re-orientate itself in relation to the rest of the molecule, most likely so that it was sitting on the surface of the dendrimer. As this may affect the bite angle, the bite angles have been calculated using a small metal complex instead of just a rhodium atom.

5.2.3 Calculation of PRhP Angle using metal complex

The PRhP angle was calculated from simulations of a dendrimer-rhodium complex using restraints as described above (section 5.2.1.4). The trends in the PRhP angle and flexibility are very similar to the bite angle calculations as illustrated in figure 5.16.
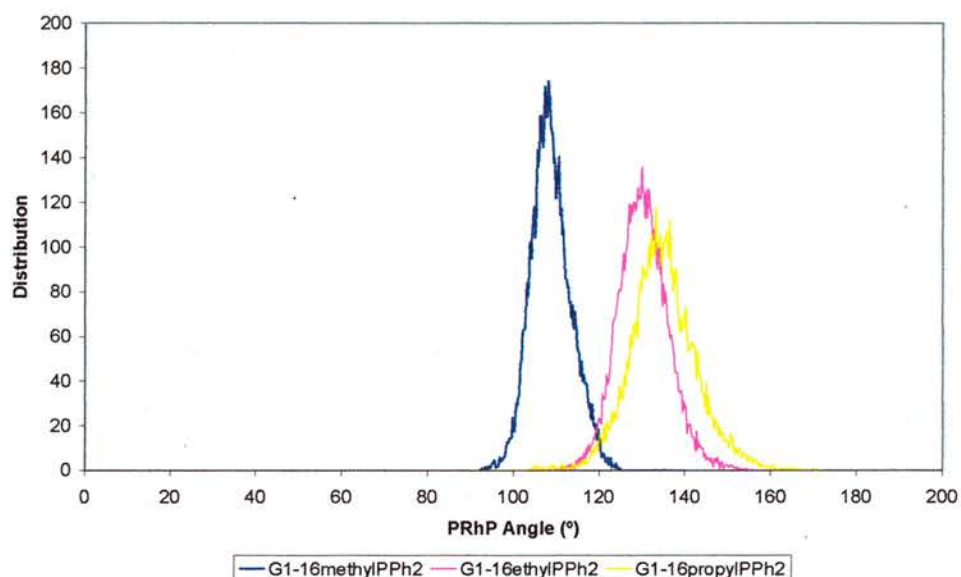
Figure 5.16: PRhP angle calculated for three dendrimers at 300 K averaged over 21000 frames. The flexibility of G1-16methylPPh$_2$ is narrower with the complex attached and the average PRhP angle is now 10 ° higher than the average bite angle. G1-16ethylPPh$_2$ has an increase in PRhP angle of 2 ° and G1-16propylPPh$_2$ has a decrease in angle of 5 °. The flexibility of G1-16propylPPh$_2$ has not changed but the flexibility of G1-16ethylPPh$_2$ has become more narrow and decreased by 20 ° (table 5.18). There are no obvious trends in these changes, but with the most flexible dendrimer changing least, the branch conformation must have a role to play. In the case of G1-16methylPPh$_2$ the branches are very short so attaching a large metal complex to the end of one branch can only serve to further reduce the flexibility in the branch. The difference between the bite angle and PRhP complex flexibility is most likely due to the complex forcing the branch into certain conformations so that the other ligands on the rhodium are not crowded by the rest of the dendrimer.

Ligand	Average Bite Angle (°)	Flexibility (°)	Complex PRhP Angle (°)	Flexibility (°)
G1-16methylPPh$_2$	105.8	83.0 – 125.0	115.2	92.3 – 125.0
G1-16ethylPPh$_2$	128.8	92.8 – 157.0	130.2	110.3 – 155.8
G1-16propylPPh$_2$	139.9	102.3 – 171.0	134.8	103.8 – 170.8
Tetrakis-diphenylphosphinoethylsilane	123.5	91.0 – 167.0	133.3	112.8 – 154.8
Bis-diphenylphosphinoethyldimethylsilane	134.8	104.0 – 166.5	134.26	128.3 – 140.3
Bis-diphenylphosphinopentane	134.6	99.5 – 157.3	136.1	111.5 – 165.3

Table 5.18: Table showing comparison of average bite angle (with just rhodium) and complex bite angle (with rhodium complex) and corresponding flexibilities at 300 K.

A similar explanation can be found for G1-16ethylPPh$_2$. The PRhP angle does not change by much but the flexibility range changes a great deal. In both cases, it is the smallest angle that changes, the largest accessible angle remains the same, perhaps indicating that this is governed by the lengths of the branches rather than the nature of the complex.

The model compound tetra-diphenylphosphinoethyl-silane (Tppsie) shows an increase in PRhP angle of 10 ° and a decrease in flexibility of at least 20 ° over the range. Bis-diphenylphosphinopentane on the other hand shows little increase in PRhP angle and approximately 9 ° over the flexibility range. Bis-Diphenylphosphinoethyldimethylsilane (Dppsie) shows both of these features – no change in average bite angle and a reduction in flexibility range by 20 °. This indicates that smaller ligands are less affected by the complex being attached. Bis-diphenylphosphinopentane is a ligand with a straight backbone whereas the other model compounds have a central silicon atom and a branch of some description. The presence of this silicon and its other substituents acts like a mini dendrimer – it forces certain conformations of the ring to be more desirable than others. This results in a greater change in values for the complex compared to the bite angle calculation.
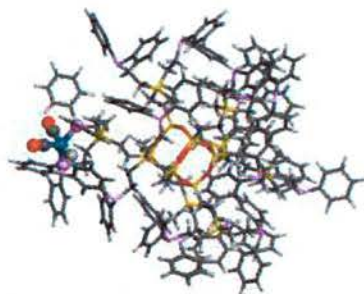
Figure 5.18: G1-16ethylPPh$_2$ with rhodium complex viewed down the H-R-CO (axial) axis of the molecule. The complex is shown as ball and stick and the bulk of the dendrimer as sticks. Rhodium – green, oxygen – red, carbon –grey, hydrogen – white, phosphorus – purple, silicon – yellow.

Visual inspection of the models now reveals that the rhodium complexes are located on the surface of the dendrimer, with the equatorial co-ordinated carbonyl group pointing outwards (figure 5.18). The addition of the rhodium complex has clearly had an effect on the dendrimer as a whole. To gain further understanding of how complexation alters the dendrimer configuration, more studies of the structure were undertaken similar to those described in chapter 4.

5.2.4 Analysis of Dendrimers

The shape of the dendrimers was calculated from one frame of the production trajectory. The moments of inertia I_x, I_y and I_z are calculated automatically by Hyperchem from the co-ordinates of the atoms and the co-ordinates of the centre of mass of the molecule. The average values from three frames from three runs are quoted below and the trends are quite difficult to interpret from such a small set of data. G1-16methylPPh$_2$ and G1-16propylPPh$_2$ show a decrease in sphericity as the size of the complex attached is increased.

Molecule	Iz/Ix	Iz/Iy	δ
G1-16methylPPh$_2$	1.37	1.22	0.0088
G1-16methylPPh$_2$ Bite	1.60	1.37	0.0202
G1-16methylPPh$_2$ Complex	1.62	1.15	0.0207
G1-16ethylPPh$_2$	1.63	1.63	0.0302
G1-16ethylPPh$_2$ Bite	1.59	1.21	0.0217
G1-16ethylPPh$_2$ Complex	1.33	1.20	0.0333
G1-16propylPPh$_2$	1.75	1.26	0.0245
G1-16propylPPh$_2$ Bite	1.94	1.32	0.0348
G1-16propylPPh$_2$ Complex	2.07	1.26	0.0424

Table 5.19: Aspect Ratios and Asphericity (δ) for the three dendrimers as free ligands, complexed for a bite angle calculation and complexed with a small rhodium complex.

G1-16methylPPh$_2$ appears to be the most spherical, with the lowest aspect ratios and asphericity, while G1-16propylPPh$_2$ show the greatest deviation from a perfect sphere. G1-16propylPPh$_2$ has one moment of inertia roughly half that of the other two. This implies a saucer like shape (table 5.20).

Molecule	Ix	Iy	Iz
G1-16methylPPh$_2$	31771.94	35728.34	43560.77
G1-16methylPPh$_2$ Bite	32953.80	39639.29	52219.19
G1-16methylPPh$_2$ Complex	32593.80	38637.39	50738.00
G1-16ethylPPh$_2$	34520.14	34520.14	56324.15
G1-16ethylPPh$_2$ Bite	37138.28	40615.72	46468.26
G1-16ethylPPh$_2$ Complex	38059.13	41161.04	49208.62
G1-16propylPPh$_2$	38156.46	53115.8	66727.58
G1-16propylPPh$_2$ Bite	33424.59	56919.98	66962.89
G1-16propylPPh$_2$ Complex	37963.71	75262.3	95032.59

Table 5.20: Moments of Inertia for the dendrimers as calculated directly by Hyperchem and averaged.

The phosphorus-phosphorus distances were calculated branch by branch for the free

dendrimer ligands. This was to ensure that the data was comparable, with the same

force field and parameters. Figure 5.19 shows the distribution of P-P distances in

G1-16propylPPh$_2$ at 300 K. The bulk of the distribution lies between 6 and 10 Å

with several large peaks corresponding to preferred distances. For example, the large

peak for P5 at approximately 9.5 Å indicates an expanded branch, while the large

peak for P2 at approximately 6 Å indicated a compact branch. G1-16propylPPh$_2$ has
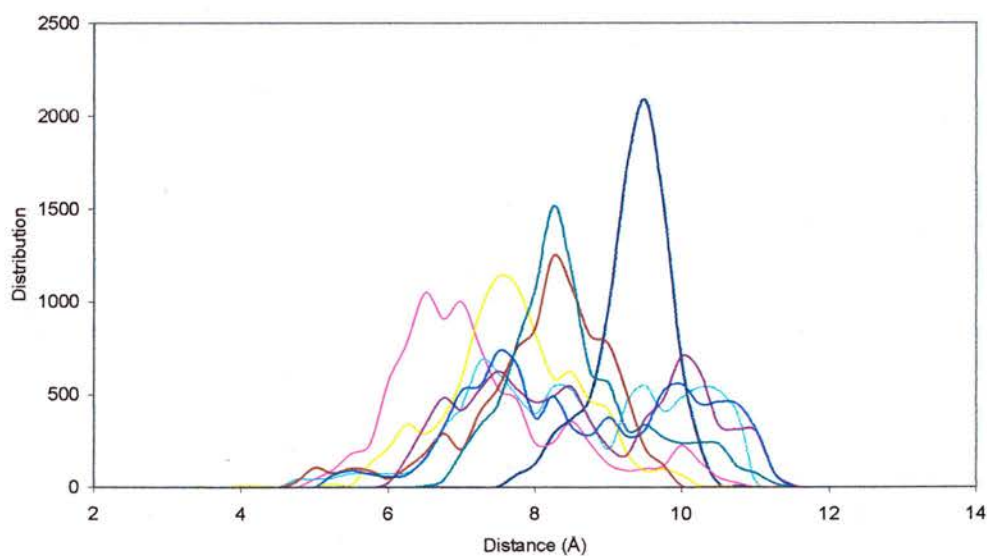
the most flexible branches.

Figure 5.19: Graph showing distribution of P-P distances in uncomplexed G1-16propylPPh$_2$ at 300 K. In this graph and those that follow each coloured line represents a different branch on the dendrimer.

The bite angle calculation caused an immediate and expected change in the distribution of P-P distances caused by complexation to rhodium. The large peak at 4 Å in figure 24 is for the two phosphorus atoms bonded to rhodium and is essentially fixed in place by the rigid unit created (from the high force constant used for P-Rh bonds for the bite angle parameters). The only variation in this PP distance comes from the P-Rh-P angle varying and so the reasonably sharp peak emphasises that despite a large change in bite angle, only small changes in PP distances are registered. This may mean that the flexing of the bite angle has limited impact on the rest of the dendrimer structure.

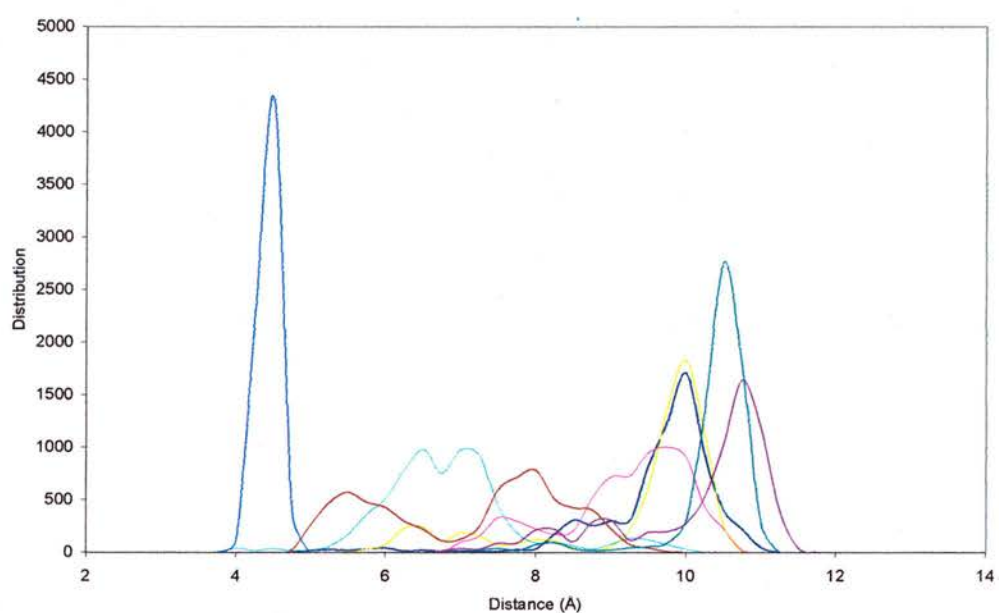**Figure 5.20:** Graph showing distribution of P-P distances in G1-16propylPPh$_2$ bite angle at 300K. The other branches show a similar distribution to the free ligand with a large range of distances. There is slightly more bias towards longer lengths here, and this may be because the restriction of one branch by the rhodium causes the other branches to expand and fill the newly created space.
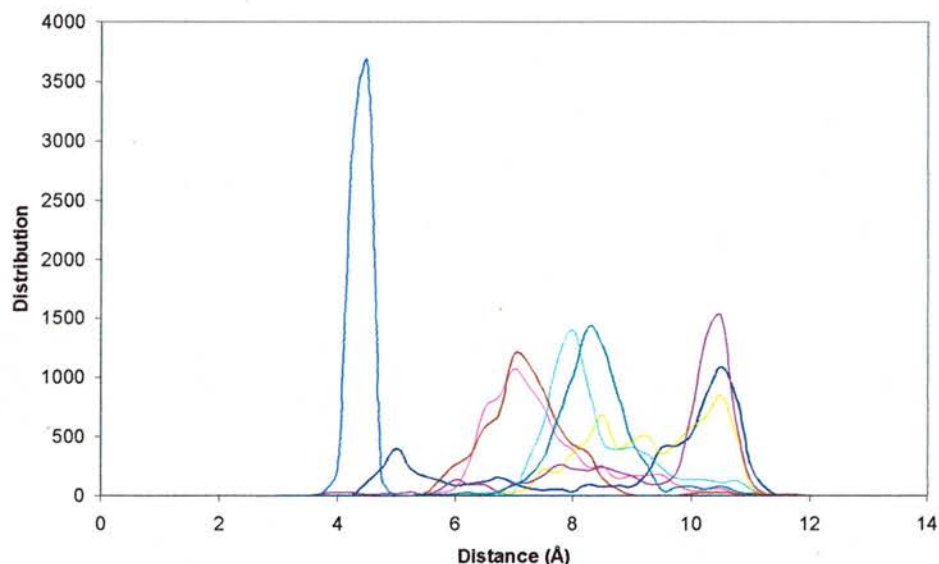
Figure 5.21: Graph showing distribution of P-P distances in G1-16propylPPh$_2$ complex at 300K.

This is more noticable in figure 5.21 for the metal complex as the distribution of

distances in the other branches becomes even broader.

The distribution of distances in the free dendrimer G1-16ethylPPh$_2$ are confined to

between 4 and 10 Å, implying that each branch is expanded to the same degree.
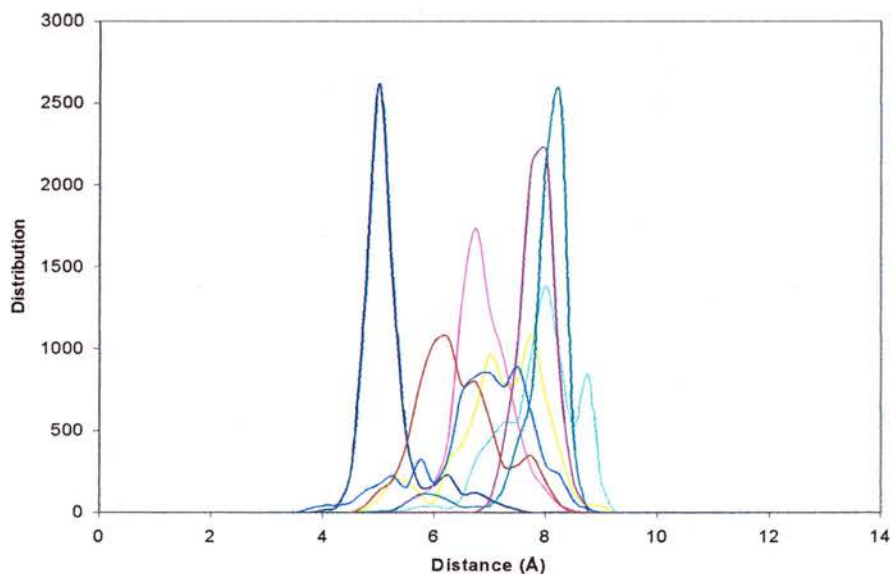
Figure 5.22: Graph showing distribution of P-P distances in G1-16ethylPPh$_2$ dendrimer at 300K

The following series of graphs show how the distribution of P-P distances in the bite

angle dendrimer G1-16ethylPPh$_2$ alter with temperature.
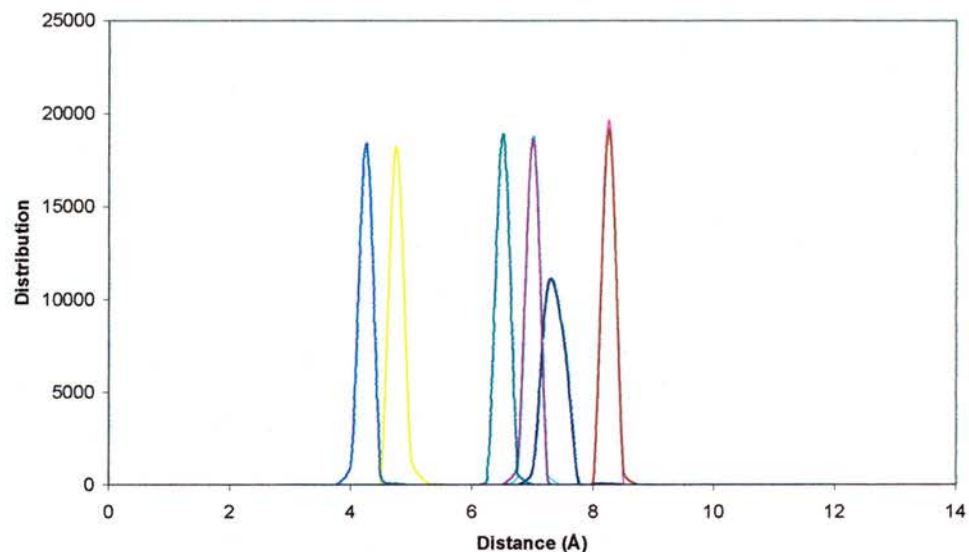
Figure 5.23: Phosphorus-phosphorus distances in G1-16ethylPPh$_2$ bite angle at 50 K.

At low temperatures, the peaks for each branch are sharp, indicating little movement

of the branches. By 200 K there is more energy available and the peaks become

broader as there is more motion in the molecule.

Figure 5.24: Phosphorus-phosphorus distances in G1-16ethylPPh$_2$ bite angle at 100 K

Figure 5.25: Phosphorus-phosphorus distances in G1-16ethylPPh$_2$ bite angle at 200 K.
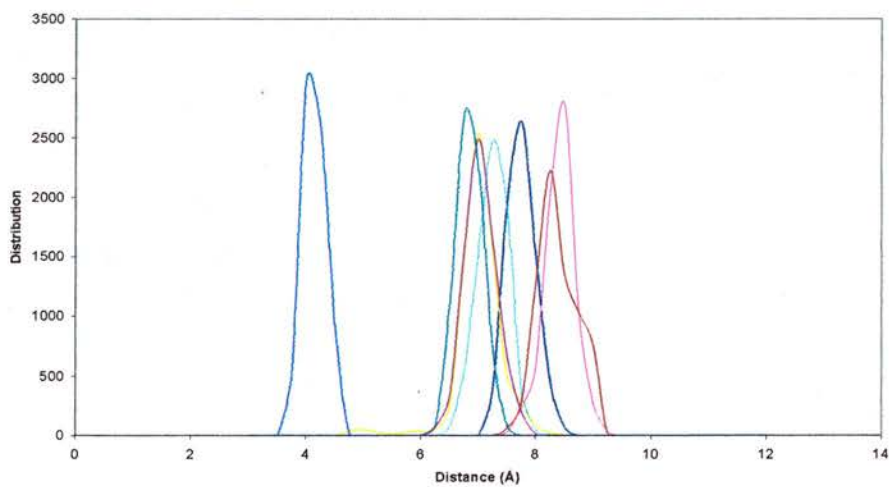
Figure 5.26: Phosphorus-phosphorus distances in G1-16ethylPPh$_2$ bite angle at 300 K.
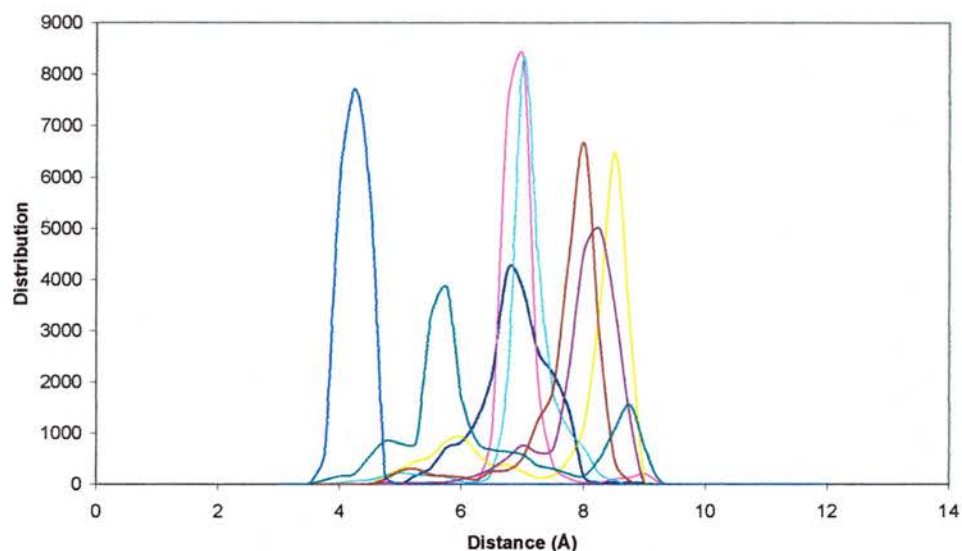
Figure 5.27: Phosphorus-phosphorus distances in G1-16ethylPPh$_2$ bite angle at 400 K
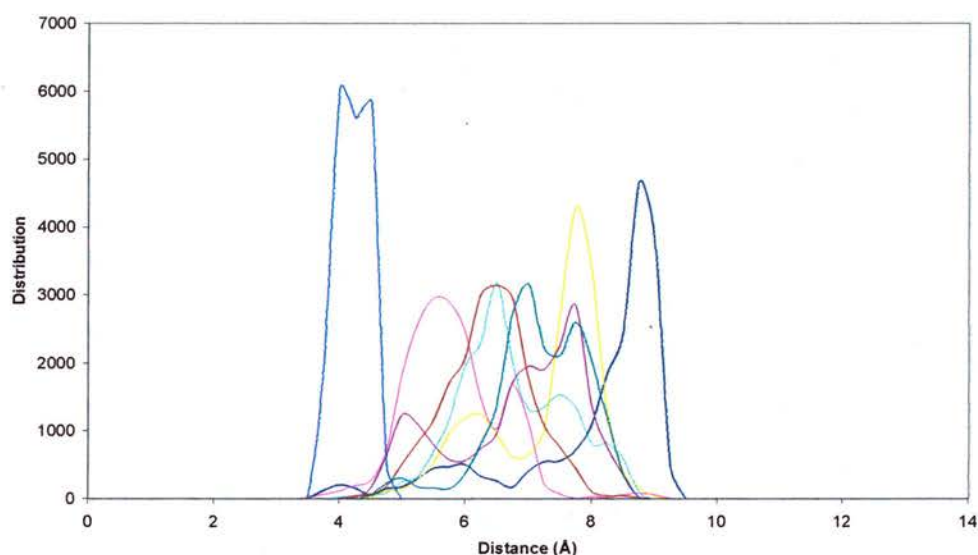
Figure 5.28: Phosphorus-phosphorus distances in G1-16ethylPPh$_2$ bite angle at 500 K

At 300, 400 and 500 K the distributions are broader still indicating that there is even greater mobility in the branches, the greatest shown at 500 K. This is similar to the distribution shown for the free ligand. Greater mobility does mean that the phosphorus atoms are both closer together and further apart although never more than 10 Å, a distance dictated by the length of the branches. G1-16ethylPPh$_2$ complex shows that at 300K the branches have a greater range of values than for the bite angle dendrimer at 300 K.
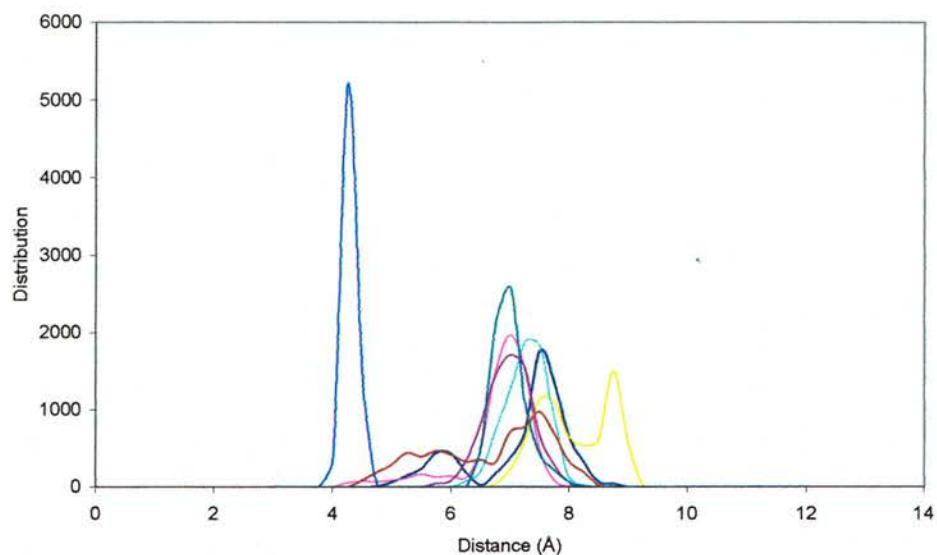
Figure 5.29: Phosphorus-phosphorus distances in G1-16ethylPPh$_2$ complex at 300 K.

The peak corresponding to the PRhP branch is similar but the distribution of the other branches has changed. The branches are more mobile, perhaps due to a greater amount of space created by the branch and complex moving to the surface of the dendrimer.
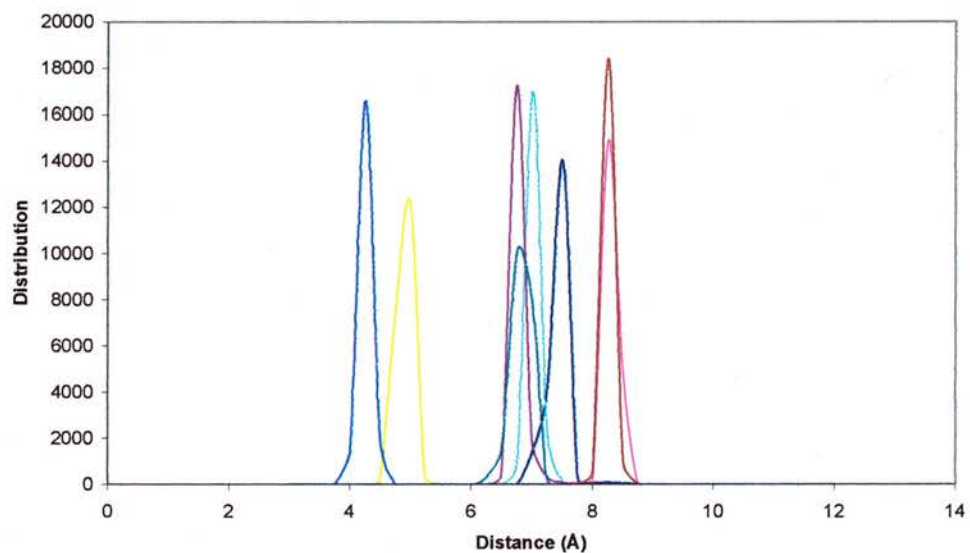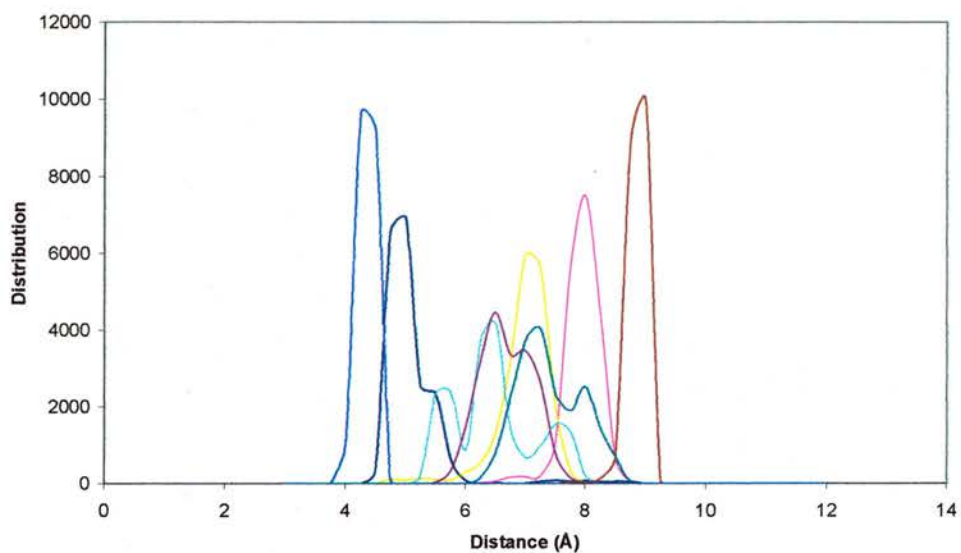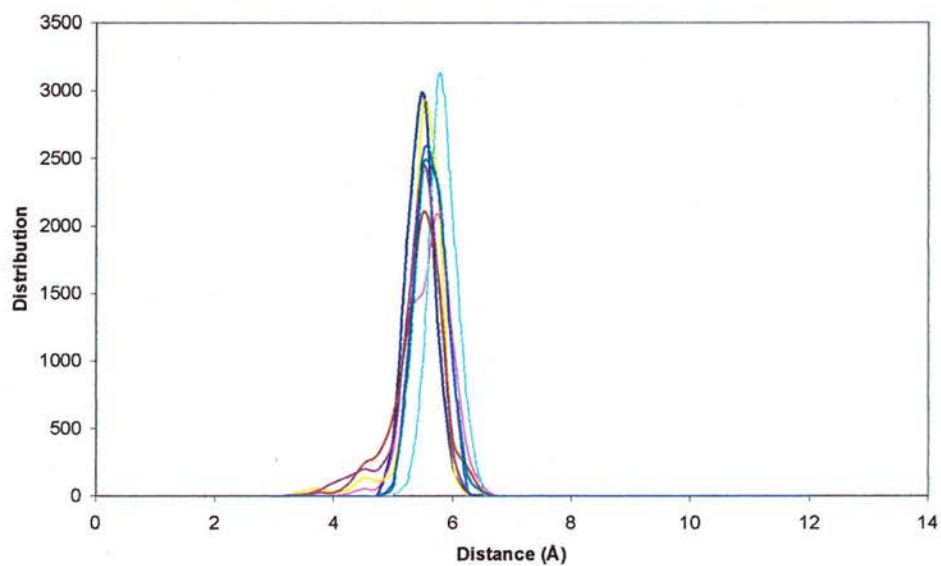

Figure 5.30: Phosphorus-phosphorus distances in G1-16methylPPh$_2$ at 300 K.
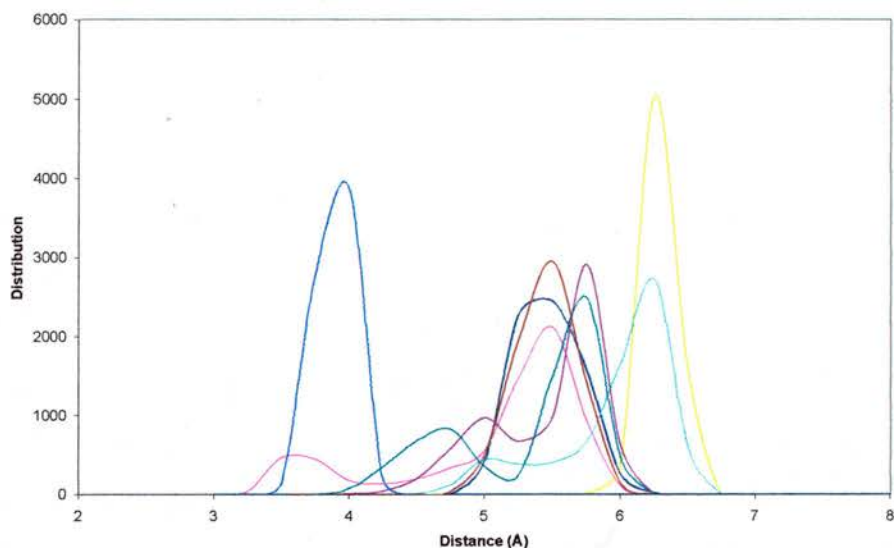
Figure 5.31: Phosphorus-phosphorus distances in G1-16methylPPh$_2$ bite angle at 300 K.

For G1-16methylPPh$_2$, the distributions for the P-P distances for the complex and the

bite angle are very similar. The complex would seem to create less mobility in the

branches indicated by the sharper peaks in figure 5.32.
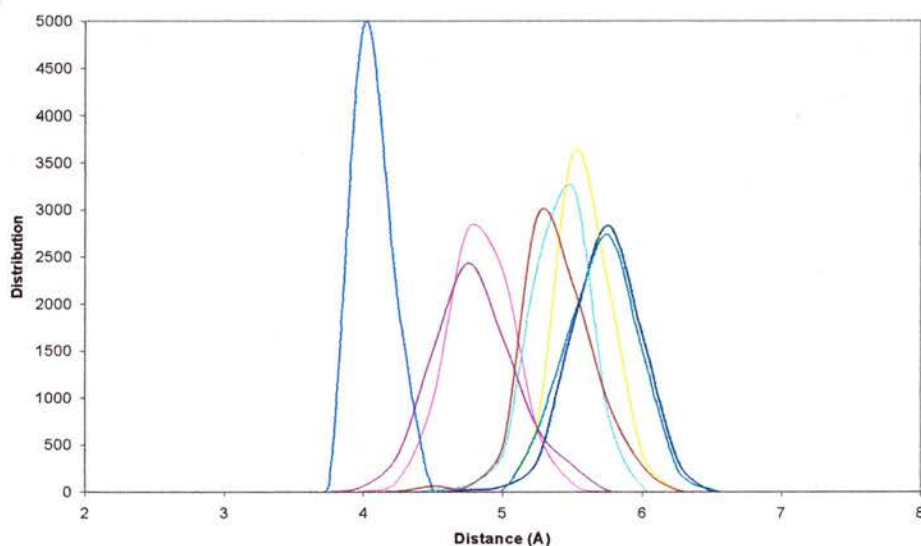
Figure 5.32: Phosphorus-phosphorus distances in the G1-16methylPPh$_2$ complex at 300 K.

Of equal interest, are the P-Rh distances, how close do the other branches come to

the rhodium atom?
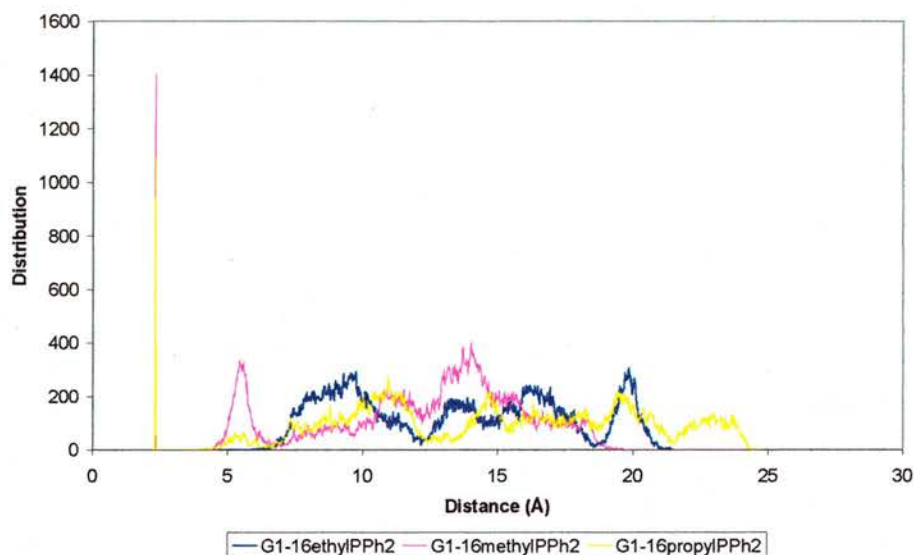
Figure 5.33: P-Rh distances calculated for each dendrimer bite angle, large peak between 0 and 5 Å corresponds to P-Rh that are bound together and has been scaled down by a factor of ten

This is important for catalysis because it gives some indication of whether any of the other diphenylphosphine groups on adjacent branches come close enough to the complex to interfere with the metal centre. Both G1-16methylPPh$_2$ and G1-16propylPPh$_2$ (bite angle) have peaks at around 5 Å, indicating that there is a phosphorus atom as close to the metal centre as 5 Å. This is not seen when contemplating the complex of the three dendrimers, indicating that the complex is in a less sterically hindered environment.
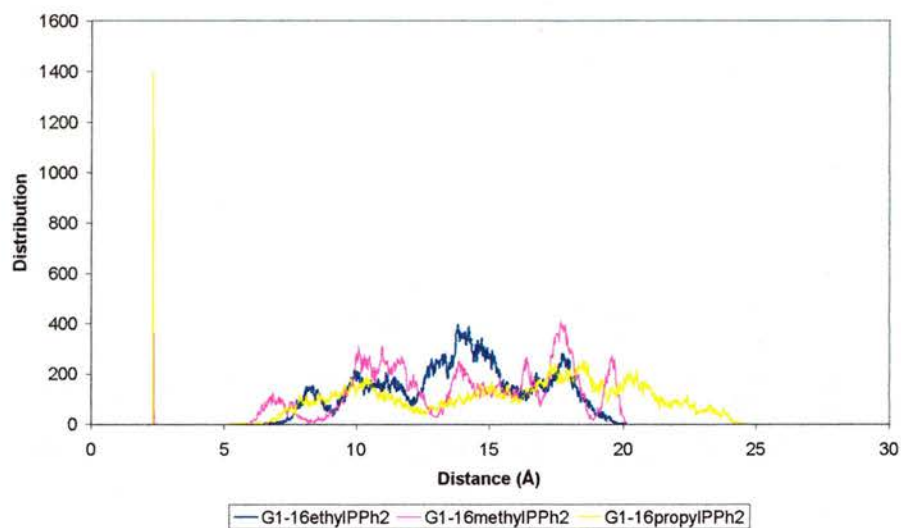
Figure 5.34: P-Rh distances calculated for each dendrimer complex, large peak between 0 and 5 Å corresponds to P-Rh that are bound together and has been scaled down by a factor of ten

While figures 5.33 and 5.34 relate to the dendrimer structure with rhodium in bidentate co-ordination, what happens when the rhodium is only co-ordinated to one phosphine? It has been proposed that some of the success of these dendrimers as catalysts is due to the fact that if the rhodium becomes unbound from a phosphine site, there are many more sites around to 'catch' the complex[14]. Figure 5.35 shows G1-16ethylPPh$_2$ with the rhodium bound only to one phosphorus. The distribution of distances shows that 5 Å is the closest most phosphines will go to the rhodium, although compared to figure 5.34, the distribution has shifted down to 5 Å slightly, most likely due to the phosphorus on the same branch as the Rh-P.
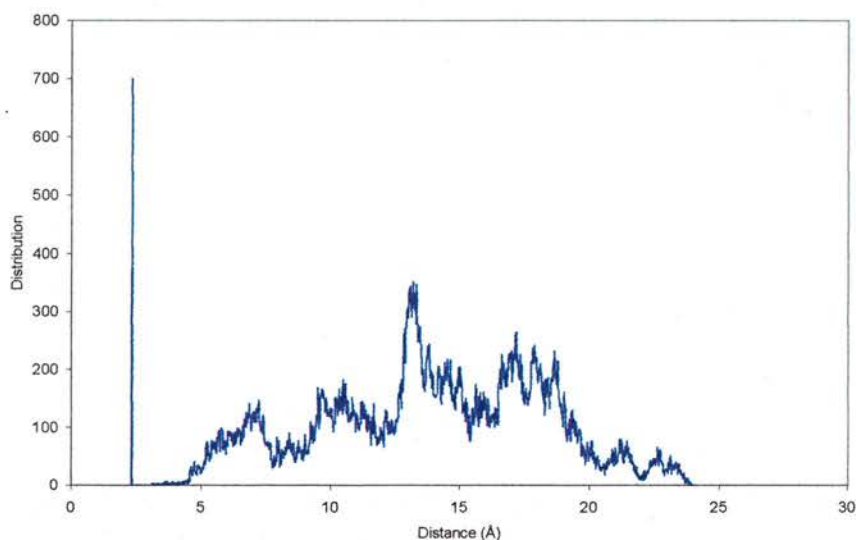
Figure 5.35: G1-16ethylPPh$_2$ complex, phosphorus rhodium distances with only one phosphorus bound to the rhodium. Large peak between 0 and 5 Å corresponds to P-Rh that are bound together and has been scaled down by a factor of ten.

Figure 5.35 also shows that there is an increase in the maximum P-P distance when only one phosphorus atom is bound to the rhodium. The large distribution at around 15 Å in figure 5.34 has been replaced with a broader distribution around 15 – 20 Å in figure 5.35, which is of similar magnitude.

5.3 Conclusions

Sufficient parameters were added to the MM+ force field in Hyperchem to permit the calculation of the bite angle for three dendrimers and three model compounds. From this it was determined that the bite angle of the dendrimer that showed high catalytic selectivity, G1-16ethylPPh$_2$ was approximately 128 ° and the closest to the value of 120 ° thought to indicate diequatorial binding that favours linear products. G1-16methylPPh$_2$ was found to have a lower bite angle indicating that it may prefer axial-equatorial binding and G1-16propylPPh$_2$ has a larger bite angle and the greatest flexibility range.

Visual inspection of the simulations of the dendrimers indicated that the rhodium centre used for bite angle twisted into the interior of the dendrimer, not sufficiently to be called back folded, but enough to occupy a space that a bulkier complex could not. To overcome this the rhodium complex was modelled using restraints to eliminate the need for parameters and resulted in a significant increase in PRhP angle for G1-16methylPPh$_2$. A significant decrease in flexibility was found for G1-16methylPPh$_2$ and G1-16ethylPPh$_2$ indicating that the large complex influenced the PRhP angle in some way. This decrease in flexibility was shown by an increase in the minimum accessible bite angle, which is most likely due to enforcing diequatorial binding at the rhodium complex.

5.4 References

1. C. A. Tolman, *Chem. Rev*, 1977, **77**, 312.

2. C. P. Casey and G. T. Whiteker, *Isr. J. Chem.*, 1990, **30**, 299.

3. C. P. Casey, G. T. Whiteker, M. G. Melville, L. M. Petrovich, J. A. Gavney and D. R. Powell, *J. Am. Chem. Soc.*, 1992, **114**, 5535.

4. N. S. Imyanitov, *Kordinats Khim* , 1985, **11**.

5. D. White, B. C. Tavener, P. G. L. Leach and N. J. Coville, *J. Organomet. Chem.*, 1994, **478**, 205.

6. Y. Koide, S. G. Bott and A. R. Barron, *Organometallics*, 1996, **15**, 2213.

7. K. Angermund, W. Baumann, E. Dinjus, R. Fornika, H. Gorls, M. Kessler, C. Kruger, W. Leitner and F. Lutz, *Chem. Eur. J.*, 1997, **3**, 755.

8. T. L. Brown and K. J. Lee, *Coord. Chem. Rev.*, 1993, **128**, 89.

9. J. J. Carbo, F. Maseras, C. Bo and P. W. N. M. Van Leeuwen, *J. Am. Chem. Soc.*, 2001, **123**, 7630.

10. C. R. Landis and J. Uddin, *J. Chem. Soc., Dalton Trans.*, 2002, 729.

11. L. A. Van Der Veen, M. D. K. Boele, F. R. Bregman, P. C. J. Kamer, P. W. N. M. Van Leeuwen, K. Goubitz, J. Fraanje, H. Schenk and C. Bo, *J. Am. Chem. Soc.*, 1998, **120**, 11616.

12. M. Kranenburg, Y. E. M. Vanderburgt, P. C. J. Kamer, P. W. N. M. Van Leeuwen, K. Goubitz and J. Fraanje, *Organometallics*, 1995, **14**, 3081.

13. D. Gleich, R. Schmid and W. A. Herrmann, *Organometallics*, 1998, **17**, 4828.

14. L. Ropartz, K. J. Haxton, D. F. Foster, R. E. Morris, A. M. Z. Slawin and D. J. Cole-Hamilton, *J. Chem. Soc., Dalton Trans.*, 2002, 4323.

Chapter 6. Synthesis of Polyhedral Oligomeric Silsesquioxanes

6.1 Introduction

Small POSS molecules with 8 functional groups have been widely reported by a number of research groups. They have been synthesised by several routes including hydrolytic condensation, hydrosilation and various functional group transformations. Dittmar *et al.*[1] and Feher *et al.*[2-15] have reported the synthesis of several new POSS molecules through a variety of routes.

R = Cl, SH; R' = Me, Et
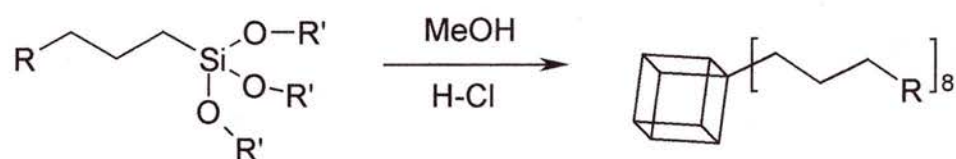
Figure 6.1: Condensation of POSS cubes as attempted by Dittmar *et al.*[1].

Feher's work has produced similar results for different functional groups including aminopropyl POSS, p-chlorophenyl POSS and others. For all the variety of POSS cores reported in the literature only four have been used as dendrimer cores: H_8T_8, vinyl POSS[16-20], aminopropylPOSS[12] and diphenylphosphinoethylPOSS[21-23].

For the purpose of this project a functionalised POSS cube will be any molecule in which the number of terminal groups is less than or equal to eight, a dendrimer will be any molecule in which the number of terminal groups is 14 or more.
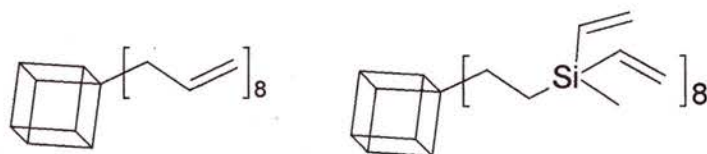
Figure 6.2: Allyl functionalised POSS cube and first generation POSS dendrimer functionalised with 16 vinyl groups.

A variety of routes to functional POSS cubes have been investigated for use as

dendrimer cores and metal organic framework building blocks. This work has been

attempted through condensation, hydrosilation and functional group transformation.

POSS dendrimers have a large number of terminal groups in a few generations and it

would be possible to sacrifice some of these terminal groups to add different

functionality into the molecule. For example, the addition of small fluorous

ponytails to one corner and ligating groups to the other seven would modify the

solubility properties of the resulting molecule. It has been reported by Feher *et al.*

that it is possible to use 1 molar equivalent of triflic acid to hydrate one corner of the

vinyl POSS creating an alcohol group[13].

The opportunity to make mixed silsesquioxanes was taken, using a silsesquioxane

that is known to form the octamer, vinyl POSS, and attempting to add (without going

down Feher's route of corner capping[6,7]) one corner of another silane.
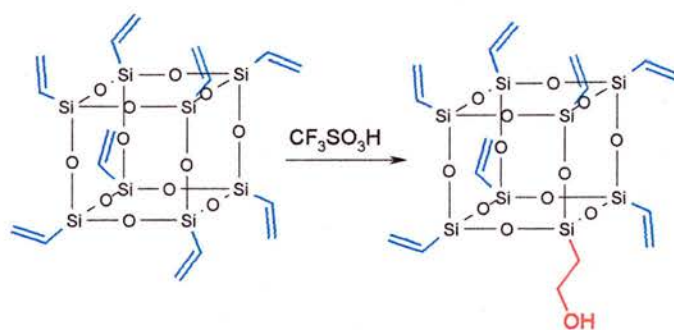
Figure 6.3: Reaction of vinyl POSS with triflic acid, hydrating one vinyl group, as reported by Feher *et al.* [13]

The incorporation of CF_3 groups was considered with catalysis in mind, both for use

with fluorous solvents (proof of concept) and for making POSS cubes where one

fluorous group could be added and 7 ligating groups (from the vinyl POSS). This

would provide an example of incorporating functional groups to alter solubility into

POSS dendrimer catalysts.

A POSS molecule, R_6T_6 with propyl anisole functional groups was recently reported

by Bassindale *et al.* through the non-hydrolytic condensation of appropriate

trichlorosilanes[24]. Anisole groups are useful synthetic precursors to phenols and for dendrimer synthesis, a phenol functionalised POSS would be extremely useful. Dittmar *et al.* had reported the synthesis of the R_8T_8 version of the propyl anisole POSS by hydrosilation of allylanisole to H_8T_8[1]. The phenyl rings and methoxy substituents made this a likely candidate for condensation and crystallisation and so hydrolytic condensation of trichlorosilylpropylanisole was attempted to try to obtain a crystalline product. Trichlorosilylpropylanisole had been previously reported by Schenning *et al.* as an intermediate for the synthesis of insulated molecular wires[25]. The demethylation of allyl anisole was also reported using boron tribromide in reasonable yields by both Schenning[25] and Agharahimi[26].

A closely related compound was also considered as a suitable dendrimer core - dimethoxyallylbenzene. Dimethoxyallylbenzene was hydrosilated to trichlorosilane to attempt to condense a dimethoxybenzene POSS cube, suitable for conversion to a biphenol. After formation of the biphenol, it was envisaged that Fréchet wedge type dendrimers could be synthesised divergently from this cube.

The acetoacetonate POSS offered another route to a carboxylic acid functionalised molecule, both for use as a dendrimer core (through esterifcation) and for modular materials. A propyl alcohol terminated POSS was investigated both for a dendrimer core and for synthesis of modular materials through its oxidation to a carboxylic acid. The oxidation of POSS molecules requires careful control of the reaction conditions to ensure that the silicon oxygen framework remains intact.

6.2 Results and Discussion

Several approaches were taken to the synthesis of POSS molecules, involving condensation and hydrosilation to produce a range of suitable compounds as dendrimer cores.
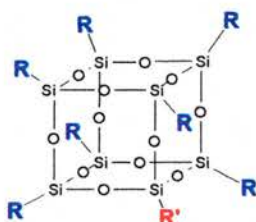
Figure 6.4: Schematic representation of $R_7R'T_8$.

Method (compound number)	Expected Product		Obtained Product
	R	R'	
Condensation $*_1(1)$	$CHCH_2$	$= R$	Vinyl POSS[27,28]
Condensation $*_1 *_3(2)$	H	$= R$	H_8T_8[29,30]
Condensation $*_3 (3)$	$C_3H_6NH_2$	$= R$	Semicrystalline[12]
Condensation $*_1 (4)$	C_2H_4CN	$= R$	Gel
Condensation $*_1 (5)$	$C_2H_4CF_3$	$= R$	Gel[31]
Condensation $*_1 (6)$	C_3H_6Br	$= R$	Crystals[23,32]
Condensation $*_2 (6)$	C_3H_6Br	$= R$	Gel[23,32]
Condensation $*_1 (7)$	$C_2H_4COOCH_3$	$= R$	Gel
Condensation $*_2 (7)$	$C_2H_4COOCH_3$	$= R$	Gel
Condensation $*_1 (8)$	$CHCH_2$	C_2H_4CN	Vinyl POSS
Condensation $*_1 (9)$	$CHCH_2$	$C_2H_4CF_3$	Vinyl POSS
Condensation $*_1 (10)$	$CHCH_2$	$C_2H_4COOCH_3$	Vinyl POSS
Condensation $*_2 (11)$	$C_3H_6C_6H_3(OCH_3)_2$	$= R$	Gel
Condensation $*_2 (12)$	$C_3H_6C_6H_4OCH_3$	$= R$	Crystals and gel
Hydrosilation to H_8T_8 (12)	$C_3H_6C_6H_4OCH_3$	$= R$	Solid product[1]
Demethylation (13)	$C_3H_6C_6H_4OH$	$= R$	No product
Hydrosilation to H_8T_8 (14)	C_3H_6OH	$= R$	Solid product[15]
Oxidation (15)	$C_2H_4CO_2H$	$= R$	No product

Table 6.1: Reactions attempted during project. $*_1$ reaction was carried out using commercially available trichlorosilane derivatives, $*_2$ reaction was carried out by synthesising the relevant trichlorosilane. $*_3$ reaction was carried out using commercially available triethoxysilane derivatives.

The synthesis of vinyl POSS (**1**) and H_8T_8 (**2**) proceeded well according to literature methods. H_8T_8 was synthesised with minimal $H_{10}T_{10}$ following the route of Agaskar *et al.* and recrystallised[29]. Prompt removal of crystals formed in this reaction was necessary to prevent polymerisation of the reaction mixture. The small scale of these reactions and the predicted low yields meant that great care had to be taken while working up reaction mixtures. In particular, concentrating mixtures on a rotary evaporator caused polymerisation due to the combined heat and low pressure if too much solvent was removed. This was especially apparent in H_8T_8 synthesis when concentrating the solution containing the product prior to crystallisation. This led either to polymerisation of the product or poor crystals that were more readily polymerised when used in other reactions.

AminopropylPOSS (**3**) proved to be difficult to synthesise and handle. It was largely down to luck whether crystals were formed or not and until a batch had produced some crystals there was no way to seed the reaction. This was a very time consuming reaction, often sitting for three months with no solid product. The solids obtained in this reaction, while partially crystalline, appeared to have some amorphous material present. An attempt to recrystallise this mixture of the octahydrochloride salt led to its break-up. An alternative method of synthesis, usually used to produce phenyl POSS was attempted for aminopropylPOSS[33]. The method was modified by the addition of hydrochloric acid to hydrolyse the triethoxysilane before reflux in toluene with benzyltrimethylammoniumhydroxide. Benzyltrimethylammoniumhydroxide is often used to cleave POSS cubes and open one corner and react to form the silicate cube. A polymer was formed, perhaps due to the heat used to remove the toluene or the reaction conditions in general. It is well known in reactions to form silicate cages that the ratios of reactants are critical, as well as the conditions[34]. It is also likely that the hydrochloric acid protonated the

primary amine groups and then reacted with the trimethylbenzylammonium hydroxide although no trimethylbenzylammonium chloride precipitated. The hydrolysis of aminopropyltriethoxysilane causes additional problems due in part to the reaction amines with silicon-chlorides.

Attempts to synthesise other silsesquioxanes by condensation of various monomers were less successful with gels being formed in two cases (NCC_3H_6-, **4** and $F_3CC_2H_4$-, **5**). A small quantity of cubic crystals was obtained in a yellow oil following work up of the condensation of $CH_3CO_2C_2H_4$- (**7**). It was not possible to separate them from the oil and attempts to wash them resulted in their dissolution.

Br-propyl POSS (**6**) was synthesised successfully in a low yields by condensation and confirmed by ^{1}H NMR. The attempt to prepare the same product by hydrosilation of allylbromide to trichlorosilane and subsequent condensation resulted in the formation of a black gel-like precipitate that was insoluble in most common organic solvents. Commercially available trichlorosilanes generally gave the best results in condensation. This is because it is of higher purity than those trichlorosilane derivatives synthesised through hydrosilation of trichlorosilane to an unsaturated molecule.

Several attempts were made to condense silsesquioxanes with different substituents at the corners. A 1:7 ratio of $RSiCl_3$ to $CH_2CHSiCl_3$ was used and in several cases, crystals were formed (summary of products in table 6.1). These were found to be vinyl POSS crystals by 1H NMR. The kinetics of the vinyl POSS condensation is slow (at least 6 weeks for a modest yield) but it may be the case that the condensation of other silanes is even slower meaning that the vinyl silane will react first and exclusively. This could be potentially overcome by adding the other silane partially hydrolysed at the start of the reaction and attempting to create POSS cubes with other ratios of substituents such as 1:1 or 1:3.
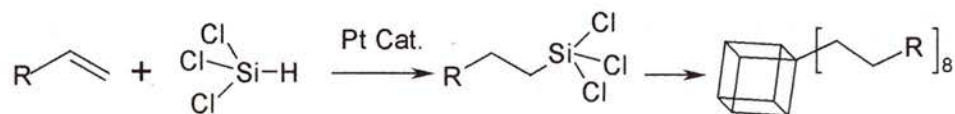
Figure 6.5: Synthesis of trichlorosilane derivatives suitable for condensation into POSS species, conditions for condensation vary.

The synthesis of trichloro-[3-(3,4-dimethoxyphenyl)-propylsilane (**11**) and its condensation was unsuccessful due, mainly, to the difficulties in purifying the trichlorosilane formed. While trichlorosilane used in the reaction is very volatile, and can be used as the solvent as well as a reactant, it is extremely important to ensure that it is removed from the product before hydrolysis. Again the conditions for hydrolysis and condensation are extremely important and clearly in this reaction, they were not correct. It may be that acetone is not a suitable solvent or that a different method of condensation (for example with $FeCl_3$ or by the phenyl POSS route) should be used. Alternatively, the reaction may not have been left for long enough before work up, as the kinetics of this condensation may have been very slow. Dittmar *et al.* reported reasonable success with methanol/hydrochloric acid and chloropropyltrialkoxysilane, left for 5 weeks to condense, indicating that methanol may be a potentially useful solvent for this reaction.

As was the case in all the condensation reactions, the duration of the reactions was so long that there was little opportunity to repeat experiments.

A single crystal structure was obtained for propylanisole POSS (**12**), synthesised from the conversion of allyl anisole to trichloro- [3-(4-methoxyphenyl)-propyl]-silane and condensation. This reaction illustrates the time scales of these reactions perfectly as it was left to stand for five months, concentrated and then left to stand for a further 6 weeks enabling crystals to form. A second attempt at this reaction was only left for 14 weeks and resulted in a gel being formed. In the second attempt, a vast excess of trichlorosilane was used to form trichloro- [3-(4-methoxyphenyl)-propyl]-silane to ensure that the reaction was nearly quantitative. It may be that the

excess trichlorosilane was not fully removed from the product before the

condensation reaction was started. The reaction to form propylanisolePOSS can be

carried out very successfully by hydrosilation to H_8T_8 in good yields offering a

viable alternative route to larger quantities for further reaction.
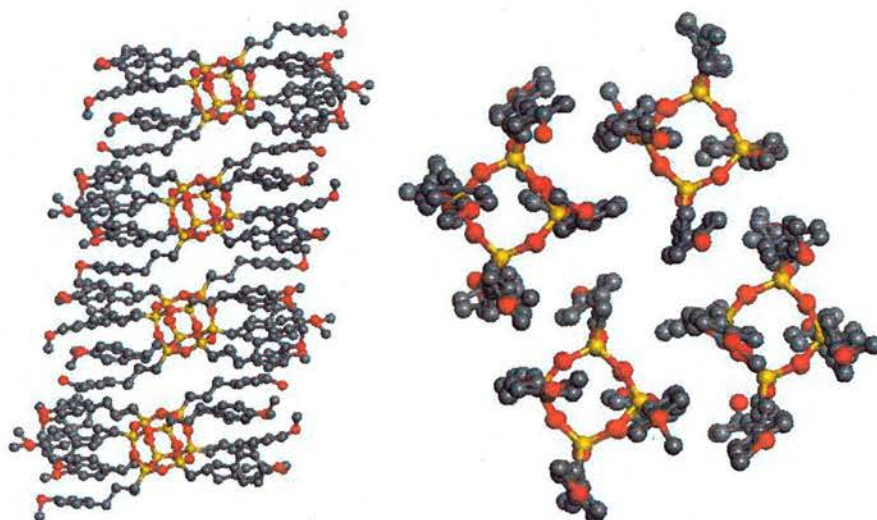
Figure 6.6: Crystal structure of Allylanisole POSS, **12**.

The crystals obtained were of sufficient size to be analysed on a laboratory based

diffractometer. The orientation of the POSS molecules in the structure indicates that

there may be some liquid crystalline character. Instead of the branches expanding

from the core forming globular molecules, they form cylindrical molecules.

Differential Scanning Calorimetry analysis was carried out to investigate this further

but revealed no obvious phase changes around the melting point of the sample.

Liquid crystalline behaviour can be determined by observing the melting and cooling

of the sample using a polarising optical microscope but requires experience of the

various types of liquid crystal phases.

223

Identification code	KHRM1, **12**	
Empirical formula	$C_{80} H_{104} O_{20} Si_8$	
Formula weight	1610.35	
Temperature	125(2) K	
Wavelength	0.71073 Å	
Crystal System	Triclinic,	
Space Group	P-1	
Unit cell dimensions	a = 18.4836(18) Å	alpha = 95.239(2) °
	b = 20.0019(19) Å	beta = 106.811(2) °
	c = 23.506(2) Å	gamma = 98.328(2) °
Volume	8149.4(14) Å^3	
Z, Calculated density	4, 1.313 Mg.m^{-3}	
Absorption coefficient	0.202 mm^{-1}	
F(000)	3424	
Crystal size	0.7 x 0.5 x 0.5	
Theta range for data collection	1.57 to 25.43 °	
Limiting indices	-22<=h<=22, -24<=k<=22, -28<=l<=25	
Reflections collected / unique	49188 / 29298 [R(int) = 0.1203]	
Completeness to theta = 25.43	97.2 %	
Absorption correction	None	
Refinement method	Full-matrix least-squares on F^2	
Data / restraints / parameters	29298 / 0 / 841	
Goodness-of-fit on F^2	3.330	
Final R indices [I>2sigma(I)]	R1 = 0.3202, wR2 = 0.6314	
R indices (all data)	R1 = 0.4462, wR2 = 0.6795	
Largest diff. peak and hole	3.172 and -1.356 e.Å^{-3}	

Table 6.2: Crystal data and structure refinement for KHRM1, compound **12**.

The initial crystal structure obtained gave a poor refinement and attempts to rerun the sample lead to worse results indicating that some degradation of the crystals was occurring over time.

The single crystal x-ray diffraction and refinement were carried out by Prof. Alex Slawin.

The synthetic utility of propyl anisole POSS came from the potential to convert the anisole group to a phenol group (**13**), making it a useful core for dendrimer synthesis. This conversion was attempted by using boron tribromide at low temperatures. The resulting solution was concentrated but no product was obtained on evaporation of

the solvent. This may be due to several reasons – poor extraction of the product or reactants from the reaction mixture, poor solubility of the octaphenol in dichloromethane or the POSS cube itself may have been broken up during the reaction, resulting in an insoluble (in DCM) product or water soluble product. This reaction was not attempted again because, as a core for Fréchet wedge type dendrons, it was felt that Fréchet wedge type dendrimers did not offer the properties required of a dendrimer catalyst and so the work was not pursued (Chapter 7). The same is true of the condensation of dimethoxyallyl benzene.

Allylalcohol POSS (**14**) was readily synthesised by hydrosilation of allyl alcohol to H_8T_8. This reaction was carried out using ether as a co-solvent with a large excess of allyl alcohol. This meant that the product formed was insoluble in the solvent mixture and precipitated from the solution. A similar approach was used for the hydrosilation of allyl anisole to H_8T_8. As carboxylic acids are useful precursors for metal organic frameworks (Chapter 8), an attempt was made to oxidise the propylalcohol POSS (**14**) to an octa-ethanoic acid POSS (**15**). This was carried out using aqueous sodium hydroxide and potassium permanganate. No products were extracted successfully, and the starting material was not retrieved. The oxidation of the alcohol groups required mild conditions if possible to avoid break up of the POSS cube and in this case, the sodium hydroxide was clearly too strong a base and caused cleavage of the siloxane links.

6.3 Experimental Details

Synthesis of Vinyl POSS, 1[27,28]
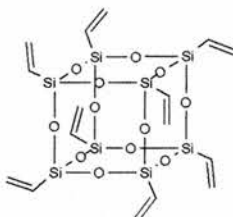
Vinyl POSS was synthesised by the literature method. Full details can be found in appendix 2.

Synthesis of H-POSS, H_8T_8, 2[29,30]
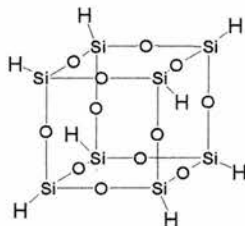
A mixture of anhydrous iron (III) chloride (50 g), concentrated hydrochloric acid (20 cm^3, 37 % aqueous solution), methanol (40 cm^3), hexane (350 cm^3) and toluene (50 cm^3) were stirred together forming a biphasic mixture. A solution of trichlorosilane (20 cm^3, 0.198 moles) in hexane (150 cm^3) was added drop-wise via tubing pump over several hours, the rate of addition was approximately 0.5 cm^3/min. The solution was stirred overnight. The organic layer was decanted, added to a mixture of anhydrous potassium carbonate (14 g) and anhydrous calcium chloride (10 g). The aqueous layer was extracted with a further portion of hexane (100 cm^3) and this added to the organic mixture. This was then allowed to stir for 6 hours before being filtered to remove the drying agents. The resulting solution was concentrated under reduced pressure until a white solid started precipitating. Additional hexane was added to redissolve this solid and the mixture cooled to –30°C to allow crystals to

form. The crystals were filtered from solution and rinsed with a small volume of cold hexane, yield 2.02 g, 19.2 %.

^{1}H NMR (300 MHz, CDCl$_3$) δ_H: 4.2 (s, 8H, HSi)

The reaction can be repeated by reusing the iron chloride mixture. Fresh hydrochloric acid and organic solvents were added and the reaction carried out as before. This reaction has been repeated using the same iron chloride up to four times without any significant drop in yields. For the final reaction, the biphasic mixture is filtered into a separating funnel and extracted with hexane. The aqueous layer is discarded and the organic layer treated as normal.

The crude H$_8$T$_8$ was recrystallised to ensure greater purity, removing any residual H$_{10}$T$_{10}$ and other hexane soluble fractions. Whilst it was expected that the mixture crystallising from the toluene hexane mixture was fairly pure, recrystallisation was useful in the cases where the crystals were small or poorly defined. Crude H$_8$T$_8$ was added to a small volume of boiling hexane and toluene added drop-wise until all of the crude H$_8$T$_8$ had dissolved. Colourless needle-like crystals formed on standing and were filtered off. A second crop was obtained from the filtrate but this was found to be impure.

Pure Product, First Crop NMR: ^{1}H NMR (300 MHz, CDCl$_3$) δ_H: 4.2 (s, 8H)

The analytical data was in agreement with the literature[29].

Synthesis of Aminopropyl POSS, 3[12]
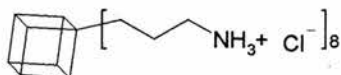
Method 1: as per Feher et al.[12]

Crude aminopropylPOSS was synthesised by literature methods. Full details can be found in appendix 2.

Method 2: Method of producing phenyl POSS[33 35]

Aminopropyltriethoxysilane was added slowly to a vigorously stirred mixture of toluene (200 cm^3) and concentrated hydrochloric acid (75 cm^3, 37 % aqueous solution). This mixture was stirred overnight to allow conversion of the amine to its hydrochloride salt and hydrolysis of the triethoxysilane. The toluene layer was separated, washed with brine and reduced by half in volume. Benzytrimethylammoniumhydroxide (40 % in methanol, 10 cm^3) was added and the mixture refluxed for 3 days. After this time, the volatiles were removed under reduced pressure yielding a small quantity of polymer. It is thought that the heat used to remove the toluene caused the silane to polymerise, forming an insoluble gel.

Attempted synthesis of Butyronitrile POSS from NCC$_3$H$_6$SiCl$_3$, 4
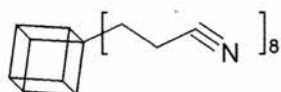
4-Trichlorosilanyl-butyronitrile (10 cm^3, 9.99 mmol) was added drop-wise to a mixture of acetone (375 cm^3) and water (112.5 cm^3 water). The mixture was stirred for 2 months without any product forming. The volume was reduced by half and allowed to stand for a further 2 months resulting in a gel being formed. The gel was insoluble in common organic solvents and was not characterised.

Attempted synthesis of 3,3,3-trifluoropropyl POSS, 5[31]
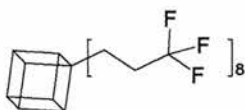
Trichloro- (2,2,2-trifluoropropyl)-silane (1.63 cm^3, 1 mmol) was added drop-wise to a mixture of acetone (37.5 cm^3) and water (11.3 cm^3). The mixture was stirred for 2 months without any product forming. The volume was reduced by half and allowed

to stand for a further 2 months resulting in a gel being formed. The gel was insoluble in common organic solvents and was not characterised.

Synthesis of Bromopropyl POSS, 6[23,36]
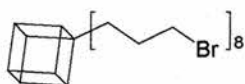
Method 1:

(3-bromopropyl)-trichlorosilane (1.60 cm^3, 0.010 mol) was added drop-wise to a mixture of acetone (37.5 cm^3) and water (11.3 cm^3). The mixture was stirred for 6 weeks and found to be biphasic. The lower layer (approx. 2 cm^3) was extracted and left to stand overnight. Crystals were formed and filtered from solution. The volume of the upper layer was reduced by half and left to stand resulting in the formation of crystals.

^{1}H NMR (300 MHz, CDCl$_3$) δ_H: 0.75 (16 H, t, SiCH_2), 1.8 (16 H, m, CH$_2$CH_2), 3.35 (16 H, t, CHBr), The above data is in agreement with the literature[23,36]

Method 2:

Trichlorosilane (35.34 cm^3, 0.35 mol) was added drop-wise to a mixture of allylbromide (28.17 cm^3, 0.3255 mol), dry ether (20 cm^3) and Karstedt's catalyst (0.2 cm^3, 0.1M solution in xylenes). The mixture refluxed for 30 minutes with the heat from the exothermic reaction. The reaction was stirred for 4 hours before the volatiles were removed under reduced pressure and transferred to a solution of aqueous acetone (500 cm^3 acetone, 30 cm^3 water). The mixture was allowed to stir. A black residue formed overtime which, once filtered, proved to be insoluble in common organic solvents. Organic solvents such as DMF and ether caused the solid to swell indicating that it was most likely polymeric.

Attempted synthesis of Ethylacetate POSS, 7

Method 1:
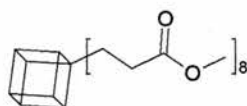
3-Trichlorosilanyl-propionic acid methyl ester (1.74 cm^3, 9.99 mmol) was added

drop-wise to a mixture of acetone (37.5 cm^3) and water (11.3 cm^3). The mixture was

stirred for 6 weeks before being extracted with DCM, saturated brine solution, and

water. The combined organic layers were dried with anhydrous magnesium sulfate

and concentrated under reduced pressure. A small quantity of cubic crystals formed

in a yellow gel but dissolved during attempts to wash them with a small volume of

cold DCM. The solvent was allowed to evaporate slowly at room temperature but

recrystallisation did not occur and a yellow gel formed.

Method 2:

Trichlorosilane (35.33 cm^3, 0.35 mol) was added drop-wise to a mixture of

allylacetate (35.12 cm^3, 0.3255 mol), dry ether (50 cm^3) and Karstedt's catalyst (0.2

cm^3, 0.1 M solution in xylenes). The mixture refluxed for 30 minutes with heat from

the exothermic reaction. The reaction was stirred overnight, filtered through a pad of

celite, the volatiles removed under reduced pressure before being transferred to a

solution of aqueous acetone (500 cm^3 acetone, 30 cm^3 water). The mixture was

allowed to stir at room temperature but after 6 weeks, a yellow gel had formed

creating a biphasic system. The gel was insoluble in common organic solvents and

not analysed further.

Attempted synthesis of Butyronitrile₁Vinyl₇POSS, 8
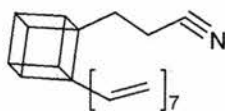
4-Trichlorosilanyl-butyronitrile (7.78 cm³, 0.050 mol) and trichlorovinylsilane (44.51 cm³, 0.352 mol) were added drop-wise to a mixture of acetone (1500 cm³) and water (450 cm³). The mixture was stirred for 6 weeks during which time a white crystalline precipitate formed. The precipitate was filtered off and found to be vinyl POSS by ¹H NMR. The remaining acetone mixture was extracted with DCM, washed with water and saturated brine, dried with anhydrous magnesium sulfate and concentrated under reduced pressure. Large colourless crystals formed and these were filtered from solution, again found to be vinyl POSS by ¹H NMR. The NMR data is in agreement with literature values for vinyl POSS[27]

Attempted synthesis of 3,3,3-trifluoropropyl₁Vinyl₇ POSS, 9
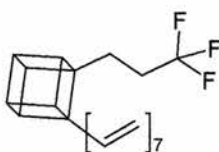
Trichloro- (3,3,3-trifluoropropyl)-silane (2.77 cm³, 0.017mol) and trichlorovinylsilane (14.89 cm³, 0.118 mol) were added drop-wise to a mixture of acetone (500 cm³) and water (150 cm³). The mixture was stirred for 6 weeks during which time a white crystalline precipitate formed. The precipitate was filtered off and found to be vinyl POSS by ¹H NMR.

¹H NMR (300 MHz, CDCl₃) δ_H: 5.8 – 6.2 (m, vinyl protons, 24H); ¹³C NMR (75 MHz, CDCl₃) δ_C: 128.69 ($=CH_2$), 136.99 ($CH=$)

The NMR data is in agreement with literature values for vinyl POSS[27]

Attempted synthesis of Ethylacetate₁Vinyl₇POSS, 10
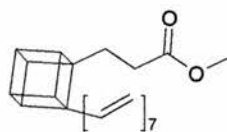
3-Trichlorosilanyl-propionic acid methyl ester (2.69 cm^3, 0.0154 mol) and

trichlorovinylsilane (15 cm^3, 0.118 mol) were added drop-wise to a mixture of

acetone (500 cm^3) and water (150 cm^3). The mixture was stirred for 6 weeks during

which time a white crystalline precipitate formed. The precipitate was filtered off

and found vinyl POSS by ^{1}H NMR. The remaining acetone mixture was extracted

with DCM, washed with water and saturated brine, dried with anhydrous magnesium

sulfate and concentrated under reduced pressure.

First Crop: ^{1}H NMR (300MHz, CDCl₃) δ$_H$: 5.8 – 6.2 (m, 24 H, vinyl protons); ^{13}C

NMR (75 MHz, CDCl₃) δ$_C$: 129.09 (=CH₂), 137.41 (CH=)

Second crop: ^{1}H NMR –signals too small to integrate, but approximately the same as

the first crop. The NMR data is in agreement with literature values for vinyl POSS[27]

Attempted synthesis of Trichloro- [3-(3,4-dimethoxyphenyl)-propyl] silane and

condensation, 11
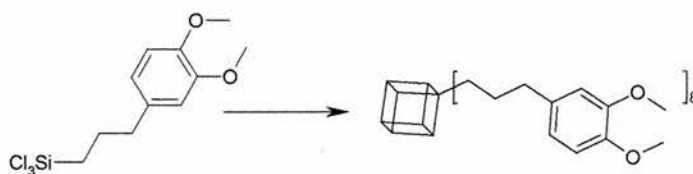
Trichlorosilane (40 cm^3, 0.396 mol) was added drop-wise to a mixture of allyl

dimethoxybenzene (56 cm^3, 0.3255 mol), dry ether (20 cm^3) and Karstedt's catalyst

(0.2 cm^3, 0.1 M solution in xylenes). The mixture was initially yellow but turned

dark green then blue whilst refluxing due to the exothermic reaction. The refluxing

was maintained for 30 minutes before the mixture was stirred overnight. Two small

flakes of triphenylphosphine were added to the now purple mixture to convert the

catalyst to a less reactive form, causing the solution to turn yellow. The mixture was filtered through celite, and the volatiles removed under reduced pressure. The resulting red liquid was added drop-wise via cannular to THF (500 cm^3) and water (30 cm^3, degassed) and allowed to stir for 2 months. The reaction mixture changed from clear to yellow, becoming biphasic but no crystals formed. The mixture was separated; the aqueous acetone phase discarded and an attempt made to dissolve the silane-containing phase. A variety of organic solvents were tried without success.

Synthesis of propylanisole POSS, 12
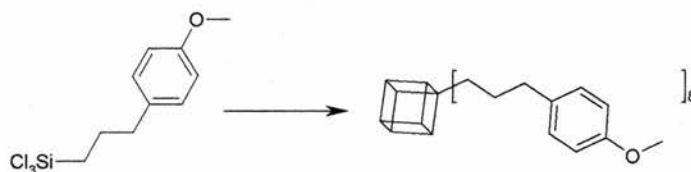
Method 1:synthesis and condensation of trichloro- [3-(4-methoxyphenyl)-propyl]-silane[24,25]

1-allyl-4-methoxybenzene (5.18 cm^3, 0.0337 mol) is dissolved in dry ether (20 cm^3) before Karstedt's Catalyst (0.2 cm^3, 0.1M solution in xylenes) was added. Trichlorosilane (4.55 cm^3, 0.045 mol) is added slowly, drop-wise causing the solution to reflux gently and turn green. Reflux was maintained for 6 hours before the solution allowed to cool and stir overnight. The solvent and excess silane was removed under reduced pressure and the resulting red residue dissolved in acetone (200 cm^3). Water (10 cm^3) was added drop-wise over 30 minutes and the mixture stirred for an additional 3 hours before being left to stand for 5 months. The mixture now dark in colour was concentrated under reduced pressure, reducing the volume by approximately half. The mixture was allowed to stand, open for 6 weeks and the resultant colourless crystals filtered and washed with a small volume of cold acetone. A second crop was obtained by concentrating the filtrate and allowing it to stand.

Mpt: 132 – 136 °C; ^{1}H NMR (CDCl$_3$, 300 MHz) δ_H: 0.55 (16 H, t, C*H$_2$*Si), 1.6 (16 H, quintet, C*H$_2$*CH$_2$Si), 2.12 (Acetone), 2.5 (16 H, t, C-C*H$_2$*), 3.7 (24 H, s, OC*H$_3$*), 6.7 (16 H, d, C*H*, arom), 6.95 (16 H, d, C*H*, arom); ^{13}C NMR (CDCl$_3$, 75 MHz) δ_C: 11.66 (*C*H$_2$Si), 24.99 (*C*H$_2$CH$_2$), 30.93 (Acetone), 37.89 (*C*-CH$_2$), 113.68 (O-*C*H$_3$), 129.28 (*C*H, arom), 129.28 (*C*H, arom), 134.42 (*C*, arom), 157.68 (*C*, arom); CHN Elemental Analysis Found: C 60.75; H, 6.43. Calc. for C$_{80}$H$_{104}$O$_{20}$Si$_8$: C, 59.67, H, 6.51. The above data are in agreement with literature[1]. The crystals obtained were analysed by single crystal x-ray diffraction.

Attempt 2:[25]

1-allyl-4-methoxybenzene (50 cm^3, 0.3255 mol) was dissolved in dry ether (50 cm^3) before Karstedt's Catalyst (0.2 cm^3, 0.1 M solution in xylenes) was added. Trichlorosilane (90.8 cm^3, 0.9 mol, large excess) is added slowly, drop-wise causing the solution to reflux. Reflux was maintained for 30 minutes before a further portion of trichlorosilane (20 cm^3, 0.198 mol) was added to compensate for losses due to reflux. The solution was then allowed to cool and stir for three days. The mixture was filtered through a pad of celite before the solvent and excess silane was removed under reduced pressure. The resulting liquid was transferred via cannular to a stirred mixture of acetone (1500 cm^3) and water (450 cm^3). The pale yellow mixture was left to stir. After 10 weeks, a small quantity of solution (approx. 100 cm^3) was removed and the organics extracted with toluene, washed with water and dried with anhydrous magnesium sulfate. The resulting mixture was concentrated under reduced pressure and allowed to stand, causing a gel to form. The remainder of the mixture was stirred for 14 weeks in total and resulted in a gel forming. Attempts to dissolve the gel in various solvents and leave to crystallise failed to produce any crystalline product.

Method 2: Hydrosilation of 1- allyl-4-methoxybenzene to H_8T_8.

H_8T_8 (0.1 g, 0.24 mmol) was dissolved in dry ether (30 cm^3) and 1-allyl-4-methoxybenzene (1.85 g, 12.5 mmol) was added. The resulting mixture was stirred and Karstedt's catalyst (0.3 cm^3, 0.1M solution in xylenes) was added. After 2 hours, a white precipitate started to form. The mixture was stirred for 18 hours in total. The white precipitate was filtered from the mixture, 0.27 g, 71 % yield Mpt: 134 – 138 °C; ^{1}H NMR (300 MHz, CDCl$_3$) δ_H: 0.6 (16 H, t, C*H*$_2$Si), 1.65 (16 H, quintet, C*H*$_2$CH$_2$Si), 2.55 (16 H, t, C-C*H*$_2$), 3.8 (24 H, s, OC*H*$_3$), 6.75 (16 H, d, C*H*, arom), 7.05 (16 H, d, C*H*, arom). The analytical data is in agreement with the literature[1].

Attempted synthesis of phenolpropyl POSS, 13
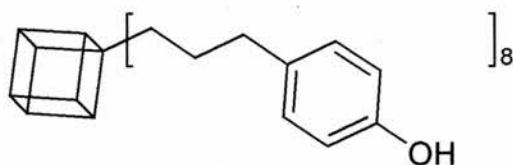
Propyl anisole POSS (0.26 g, 0.16 mmol) was dissolved in DCM (20 cm^3) and cooled to –78 ° C. Boron tribromide (16 cm^3, 1 M in DCM, 1.6 mmol,) was added and the mixture allowed to warm to room temperature and stir for 1 hour. The mixture was poured into sodium thiosulfate solution (0.2 M, 50 cm^3), extracted with DCM (3 x 50 cm^3), dried over anhydrous magnesium sulfate and concentrated under reduced pressure. The resulting concentrated solution was placed in the freezer to see if crystals formed. No solid product was obtained however as evaporation of the solvent left a small quantity of yellow gel, which was insoluble in common organic solvents

Synthesis of Allyl alcohol POSS, 14[15]
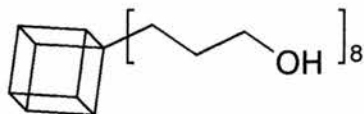
H_8T_8 (0.67 g, 1.55 mmol) was dissolved in a mixture of dry ether (20 cm^3) and allyl

alcohol (20 cm^3). Kharstedt's catalyst (0.2 cm^3, 0.1 M solution in xylenes) was

added slowly and the mixture was stirred for 30 minutes before being refluxed for 6

hours, cooled and stirred at room temperature over night. After 1 hour of refluxing a

white precipitate starts to form and after the reaction is complete, it was filtered from

solution to leave amber liquid. The amber liquid was concentrated under reduced

pressure leaving an orange oil. Diethyl ether was added to the oil, causing a white

precipitate to form. The first precipitate gave 0.94 g, 68 % yield.

^{1}H NMR (300 MHz, CDCl$_3$) δ_H: 0.6 (16H, t, SiCH_2), 1.6 (16H, m, CH$_2$CH_2), 3.4

(16H, t, CH_2OH), 4.9 (8H, s, broad, OH). The above data is in agreement with

literature[5]

Attempted oxidation of Alcohol POSS, 15[32]
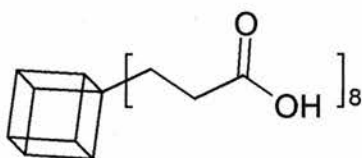
A solution of sodium hydroxide was prepared by dissolving sodium hydroxide

pellets (3 g, 0.075 mol) in deionised water (50 cm^3) and chilled to 4 °C before use. A

solution of potassium permanganate was prepared by dissolving potassium

permanganate (10 g, 0.063 mol) in water (150 cm^3) and chilled to 4 °C before use.

Propyl alcohol cube (0.4 g, 0.45 mmol) was added to sodium hydroxide solution (3

cm^3 of above solution, 3.6 mmol) and cooled in an ice bath. Potassium

permanganate solution (25 cm^3 of above solution, 10.8 mmol) was added slowly over

15 minutes. The mixture was stirred for 1 hour in the ice bath then stirred for 2 hours while warming to room temperature. Sodium metabisulfite was added to destroy the excess potassium permanganate (slow addition with stirring until the solution became totally decolourised).

The first attempt to extract the product was made by using DCM. The organic layer was extracted with DCM, acidified with dilute hydrochloric acid and this aqueous layer extracted with further portions of DCM. The solvent was removed under reduced pressure but no product was obtained.

The second attempt to retrieve a product was made by acidifying the aqueous layer, extracted with DCM and concentrated under reduced pressure, again yielding no product.

The third attempt to retrieve a product was made by extracting the aqueous layer (now highly acidic) with chloroform. The chloroform extract was concentrated under reduced pressure and yielded a very small quantity of cubic crystals.

A further attempt was made to recover some product by concentrating the aqueous layer under reduced pressure to give a solid residue. Chloroform was added to the residue, which appeared to be partly soluble. The chloroform was separated from the solids, the solids washed with further portions of chloroform and the combined organic extracts concentrated under reduced pressure but again no product was recovered.

6.4 Conclusions and Further Work

Vinyl and hydrido POSS have been synthesised successfully for use as dendrimer cores. Condensation of bromopropylPOSS was also successful using commercially available bromopropyltrichlorosilane. Attempts to create multiple functionalised POSS molecules resulted in vinyl POSS being formed preferentially perhaps due to different reaction rates of the silanes used. The synthesis of aminopropylPOSS was unsuccessful due to difficulties in obtaining a crystalline product. Work on this amine was not pursued further due to time constraints, following difficulties with synthesis but it remains a useful synthetic building block for POSS materials despite the problems discussed.

The preparation of trichlorosilanes from allylbromide and allylacetate and subsequent condensation produced gels despite the reactants being in similar ratios to the reaction of commercially available monomers. This was thought to be due to the difficulties in purifying the functionalised trichlorosilanes produced.

A propylanisole functionalised POSS cube was successfully synthesised through condensation of a trichlorosilyl monomer and through hydrosilation of propylanisole to H_8T_8. The single crystal structure was obtained from the condensation reaction and found to have some similar characteristics to liquid crystal molecules. Attempts to convert the anisole groups to phenol groups were unsuccessful most likely due to the reaction conditions cleaving the siloxane linkages in the POSS cube.

Allylalcohol was successfully hydrosilated to H_8T_8 but attempts to oxidise this to the acid failed, again due to the reaction conditions breaking up the POSS cube.

Chapter 6. *Synthesis of Polyhedral Oligomeric Silsesquioxanes*

6.5 Reference List

1. U. Dittmar, B. J. Hendan, U. Florke and H. C. Marsmann, *J. Organomet. Chem.*, 1995, **489**, 185.

2. F. J. Feher and R. L. Blanski, *J. Chem. Soc., Chem. Commun.*, 1990, 1614.

3. F. J. Feher and R. L. Blanski, *Makromol. Chem., Macromol. Symp.*, 1993, **66**, 95.

4. F. J. Feher and T. A. Budzichowski, *J. Organomet. Chem.*, 1989, **373**, 153.

5. F. J. Feher and T. A. Budzichowski, *J. Organomet. Chem.*, 1989, **379**, 33.

6. F. J. Feher, F. Nguyen, D. Soulivong and J. W. Ziller, *Chem. Commun.*, 1999, 1705.

7. F. J. Feher and S. H. Phillips, *J. Organomet. Chem.*, 1996, **521**, 401.

8. F. J. Feher, J. J. Schwab, S. H. Phillips, A. Eklund and E. Martinez, *Organometallics*, 1995, **14**, 4452.

9. F. J. Feher, D. Soulivong and A. G. Eklund, *Chem. Commun.*, 1998, 399.

10. F. J. Feher, D. Soulivong, A. G. Eklund and K. D. Wyndham, *Chem. Commun.*, 1997, 1185.

11. F. J. Feher, K. J. Weller and J. J. Schwab, *Organometallics*, 1995, **14**, 2009.

12. F. J. Feher and K. D. Wyndham, *Chem. Commun.*, 1998, 323.

13. F. J. Feher, K. D. Wyndham, R. K. Baldwin, D. Soulivong, J. D. Lichtenhan and J. W. Ziller, *Chem. Commun.*, 1999, 1289.

14. F. J. Feher, K. D. Wyndham, M. A. Scialdone and Y. Hamuro, *Chem. Commun.*, 1998, 1469.

15. F. J. Feher, K. D. Wyndham, D. Soulivong and F. Nguyen, *J. Chem. Soc., Dalton Trans.*, 1999, 1491.

16. P. I. Coupar, P. A. Jaffres and R. E. Morris, *J. Chem. Soc., Dalton Trans.*, 1999, 2183.

17. P. A. Jaffres and R. E. Morris, *J. Chem. Soc., Dalton Trans.*, 1998, 2767.

18. L. Ropartz, D. F. Foster, R. E. Morris, A. M. Z. Slawin and D. J. Cole-Hamilton, *J. Chem. Soc., Dalton Trans.*, 2002, 1997.

19. L. Ropartz, K. J. Haxton, D. F. Foster, R. E. Morris, A. M. Z. Slawin and D. J. Cole-Hamilton, *J. Chem. Soc., Dalton Trans.*, 2002, 4323.

20. X. J. Zhang, K. J. Haxton, L. Ropartz, D. J. Cole-Hamilton and R. E. Morris, *J. Chem. Soc., Dalton Trans.*, 2001, 3261.

21. B. Hong, T. P. S. Thoms, H. J. Murfee and M. J. Lebrun, *Inorg. Chem.*, 1997, **36**, 6146.

22. H. J. Murfee, T. P. S. Thoms, J. Greaves and B. Hong, *Inorg. Chem.*, 2000, **39**, 5209.

23. S. Lucke and K. Stoppek-Langner, *Appl. Surf. Sci.*, 1999, **145**, 713.

24. A. R. Bassindale, I. A. Mackinnon, M. G. Maesano and P. G. Taylor, *Chem. Commun.*, 2003, 1382.

25. A. P. H. J. Schenning, J. D. Arndt, M. Ito, A. Stoddart, M. Schreiber, P. Siemsen, R. E. Martin, C. Boudon, J. P. Gisselbrecht, M. Gross, V. Gramlich and F. Diederich, *Helv. Chim. Acta*, 2001, **84**, 296.

26. M. R. Agharahimi and N. A. Lebel, *J. Org. Chem.*, 1995, **60**, 1856.

27. C. Bonhomme, P. Toledano, J. Maquet, J. Livage and L. Bonhommecoury, *J. Chem. Soc., Dalton Trans.*, 1997, 1617.

28. T. N. Martynova and T. I. Chupakhina, *J. Organomet. Chem.*, 1988, **345**, 11.

29. P. A. Agaskar, *Inorg. Chem.*, 1991, **30**, 2707.

30. M. D. Nyman, S. B. Desu and C. H. Peng, *Chem. Mater.*, 1993, **5**, 1636.

31. V. I. Lavrentev and V. B. Durasov, *Zh. Obshch. Khim+.*, 1992, **62**, 2722.

32. R. Benkeser and E. Bennett, *J. Am. Chem. Soc.*, 1958, **80**, 5414.

33. J. Choi, A. F. Yee and R. M. Laine, *Macromolecules*, 2003, **36**, 5666.

34.   I. Hasegawa and S. Sakka, *ACS Symp. Ser.*, 1989, **398**, 140.

35.   R. Tamaki, Y. Tanaka, M. Z. Asuncion, J. W. Choi and R. M. Laine, *J. Am. Chem. Soc.*, 2001, **123**, 12416.

36.   S. Lucke, K. Stoppek-Langner, J. Kuchinke and B. Krebs, *J. Organomet. Chem.*, 1999, **584**, 11.

Chapter 7. Convergent Synthesis of POSS Dendrimers

7.1 Introduction

There are many reports in the literature of functionalised POSS molecules but fewer examples of POSS or silicate dendrimers. Muller and Edelmann [1] reported carbosilane dendrimers based on a TMA silicate core that was functionalised through chlorosilation. Chlorodimethylvinylsilane was used, allowing for the introduction of olefinic functional groups and subsequent hydrosilation reactions resulted in a second-generation dendrimer with 24 terminal vinyl groups being characterised. A similar family of dendrimers was reported by Jaffrès and Morris including examples of 24 and 72 terminal vinyl groups [2]. These dendrimers were synthesised divergently from vinyl POSS by exhaustive hydrosilation and Grignard reactions. Coupar went on to show that vinyl POSS could be functionalised with silanol groups, reporting dendrimers with 16 terminal OH groups [3]. This work was further expanded by Zhang *et al.* where a series of alcohol terminated dendrimers were produced [4]. The molecular modelling of this series is discussed in Chapter 3. Similar techniques were used by Ropartz *et al.* to produce the first example of a POSS dendrimer catalyst by reacting terminal vinyl groups with phosphines to form terminal ligating groups [5-9]. This work is discussed in more detail in chapters 4 and 5. Feher and Wyndham reported amine and ester functionalised POSS molecules as potential cores for dendrimers and exploited the reaction of methyl acrylate with amines to produce PAMAM dendrimers divergently [10].

While the vast majority of POSS dendrimers have been synthesised divergently there have been a few examples of convergent synthesis. Hong *et al.* reported the use of a phosphine octasilsesquioxane core for dendrimers functionalising the surface with

small dendrons prepared from 3,5-dihydroxybenzylalcohol and terpyridine functionalised benzyl bromides as terminal units (figure 7.1)[11,12]. These were converted to photo- and redox- active organometallic moieties by complexation to ruthenium-bipyridine complexes.

3,4-dihydroxybenzylalcohol
Repeat Unit

Terpyridine functionalised
benzyl bromide
Terminal Group

Diphenylphosphinoethyl POSS
Core
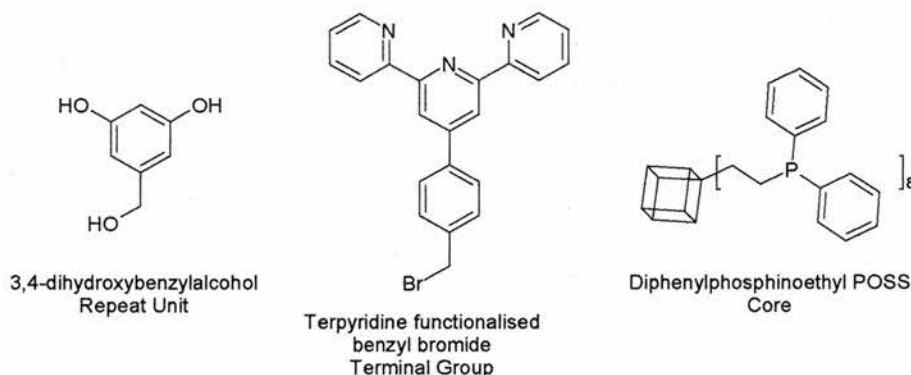
Figure 7.1: Three components used to convergently synthesise POSS dendrimers, adapted from Hong *et al.* [11,12]

Saez *et al.* reported liquid crystal POSS dendrimers synthesised convergently due to both the size of the branches and the nature of the reactions again by hydrosilation to $Q_8M_8{}^H$ [13,14].

Convergent synthesis is advantageous over divergent synthesis because it allows low yielding or different chemical reactions to be used. For instance, a reaction that gives typically 35 % yields would not be suitable for divergent synthesis because at higher generations, the molecules would become increasingly impure. A reaction that gives greater than 90 % yields would be perfect for divergent synthesis only if the reaction was suitable for the core. An example of this is PAMAM dendrimers. If an amine core is used such as ammonia, diaminoalkane or aminopropylPOSS, divergent synthesis is high yielding but if a core such as H_8T_8 is desired, convergent means are used. Similarly for Fréchet type wedges, the reactions to form the branches give good yields but not good enough for divergent synthesis. The other main advantage comes when purifying the final product. With a high yielding reaction to attach the branches to the core it is likely that the only defects within the

products will be molecules missing an entire branch and so will be easier to purify. The reaction is only required to work on a small number of sites. Compare this to divergent synthesis when a reaction is required to take place at a very large number of sites resulting in a number of defects which are harder to purify because they are only small deviations from the perfect structure[15].

7.2 Synthesis of Fréchet type Dendrimers

7.2.1 Introduction

Hawker and Fréchet developed the concept of convergent dendrimer synthesis based around an AB$_2$ monomer 3,5-dihydroxybenzylalcohol as an alternative to iterative divergent procedures[16-19].

X = H, F, Cl, Br
Y = OH, Br, CHO
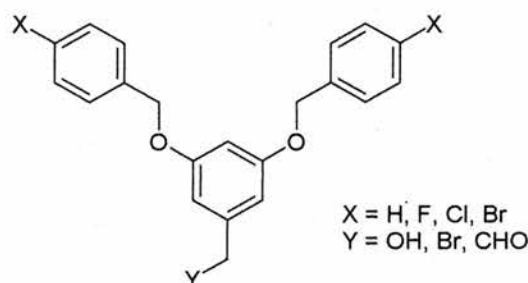
Figure 7.2: First generation Fréchet Type Wedge with a variety different 'roots' (Y) and 'tips' (X)

Essentially synthesis begins with the periphery of the molecule through selecting benzylbromide groups to react with 3,5-dihydroxybenzylalcohol forming first generation branches. Conversion of the benzylalcohol group to benzyl bromide facilitates synthesis of second and subsequent generations by allowing reaction with further molecules of 3,5-dihydroxybenzylalcohol. Ultimately large branches with functionalised benzene peripheries and benzylalcohol roots are produced.

X = H, F, Cl, Br
Y = OH, Br, CHO
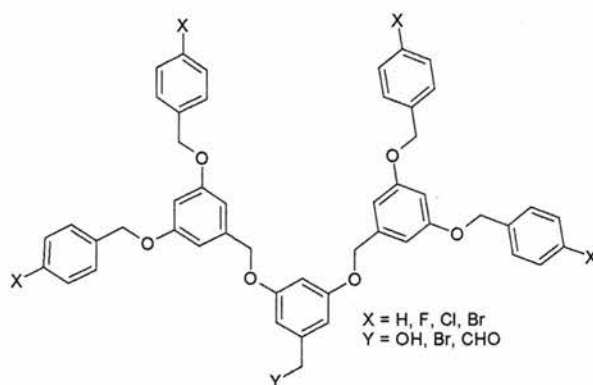
Figure 7.3: Second-Generation Fréchet Type Wedge with functionality as above.

The final synthetic step involves the attachment of the branches to the core. The ease of converting the benzylalcohol groups to benzylbromides has been exploited to great effect creating many dendrimers with Fréchet Wedges.

First generation Fréchet dendrons were synthesised with bromobenzene terminal groups and various attempts were made to attach these to the POSS core by the addition of groups capable of undergoing hydrosilation. Attempts were made to circumvent some of the difficulties encountered by using allyl functionalised benzenes such as 3,4-dimethoxyallylbenzene. Demethylation of methylethers has been widely reported in the literature, mainly in natural product synthesis. Coolen *et al.* reported yields of 37 % for the demethylation of 4-allyl-2methoxy phenol by stepwise reaction with sodium hydride and lithiumdiphenylphosphide[20]. Bhatt *et al.* reported the use of sodium iodide and silicon tetrachloride for demethylation[21]. Through conversion of the methoxy groups to phenol groups, Fréchet type dendrons could be synthesised with hydrosilatable groups already attached.

7.2.2 Results and Discussion

7.2.2.1 Synthetic Strategy
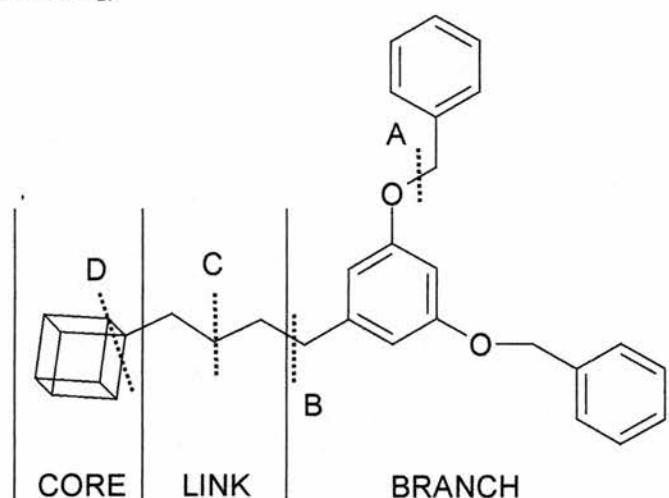
Figure 7.4: Schematic representation of first generation Fréchet type POSS dendrimer with four potential disconnections marked.

Figure 7.4 shows a general representation of a POSS dendrimer with several potential disconnections marked. When considering the synthesis of large macromolecules it is important to look at all possible ways of assembling the various component parts. In the case of Fréchet type dendrimers synthesised convergently, the two main components are the POSS core and the branch; the difficulty comes in linking the two in a suitable manner. Most of the synthetic routes use hydrosilation at some stage to functionalise the components. Disconnection **C** offers the most likely route, it being the disconnection between the POSS core and a branch with a reactive root. Disconnection **B** refers to a functionalised POSS core and minimal functionality on the branch while disconnection **A** involves the creation of a POSS core with phenol groups, forming the Fréchet wedge in the final step, a divergent route. Total convergent synthesis could be achieved with disconnection **D** that would involve the creation of a trichloro- or triethoxy- silane branch for condensation. This was not attempted for these branches due to the difficulties with POSS condensations for larger substituents discussed in detail in Chapter 6.

Divergent synthesis of these dendrimers, disconnection A was attempted using 3,4-dimethoxyallylbenzene. Suitable allyl or vinyl benzenes with 3,5- hydroxy or methoxy groups could not be found. The essential reaction step to the success of this reaction was the removal of the methoxy groups to form a diol. This was attempted several times but despite ^{1}H NMR of the crude product indicating that demethylation had occurred, the product could not be isolated from by-products. It would be difficult to hydrosilate 2-hydroxyl, 1-allyl phenol to H_8T_8 due to side reactions from the phenolic groups.

	Branch	Reagent	Cube	Disconnection	Ref.
i.	R-OH	Acryloyl chloride, Base	H_8T_8 or $Q_8M_8{}^H$	C	
ii.	R-OH	Pentenoyl chloride, Base	H_8T_8 or $Q_8M_8{}^H$	C	
iii.	R-OH	Allyl bromide, Base	H_8T_8 or $Q_8M_8{}^H$	C	[22]
iv.	R-MgBr or R-Li	Chlorodimethylsilane	Vi_8T_8 or $Q_8M_8{}^{Vi}$	C	
v.	R-MgBr or R-Li	Chlorodimethylvinylsilane	H_8T_8 or $Q_8M_8{}^H$	C	
vi.	R-Si-H	Conversion to Si-Cl	TMA Silicate	B	
vii.	R- Br	Grignard Formation	TMA Silicate	B	
viii.	R-Br	Grignard Formation	$(CH_3O)_8Si_8O_{12}$	B	
ix.	R-Br	Grignard Formation	Cl_8T_8	B	[23]
x.	R-OH	Base	$(BrCH_2CH_2CH_2)_8 Si_8O_{12}$	B	
xi.	R-Br	Base	$(HOCH_2CH_2CH_2)_8 Si_8O_{12}$	B	
xii.	R(C=O)H		$(HOCH_2CH_2CH_2)_8 Si_8O_{12}$	B	
xiii.	R-Br		$(Ph_2PCH_2CH_2)_8 Si_8O_{12}$	B	[12 24,25]
xiv.	R-OH	Base (Et$_2$NOH)	H_8T_8 or $Q_8M_8{}^H$	B	[26]

Table 7.1: Disconnections B and C and potential synthetic routes towards them.

The order of the reactions is very important to maximise the yield obtained. For instance, hydrosilation of 3,4-dimethoxyallylbenzene to H_8T_8 followed by demethylation then reaction with benzylbromides would be lower yielding than demethylation of 3,4-dimethoxyallylbenzene, reaction with benzylbromides then

hydrosilation to H_8T_8. Additionally the reactants required to demethylate may cause cleavage of the POSS core, making the first route yet more unattractive.

7.2.2.2 Synthesis of branches based on 3,5-dihydroxybenzene derivatives

The synthesis of **16** and its conversion to new compounds **18** and **19** were very successful. Preparation of compound **17** was less straightforward most likely due to the silyl ether linkage's susceptibility to hydrolysis. ^{1}H NMR of the crude reaction products revealed that the reaction had been at least partially successful but all attempts at isolation failed.
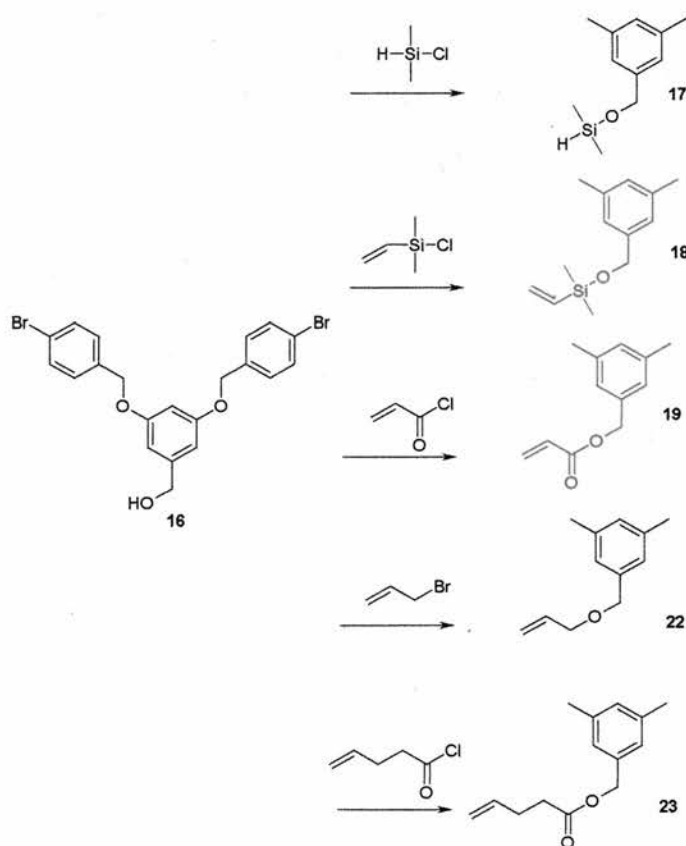
Figure 7.5: Attempted functionalisation of compound **16**. Compounds in red were successfully synthesised. The bromobenzyloxy groups have been omitted from the compounds **17 – 19**, **22**, **23** for clarity. Componds **18** and **19** are new.

At this point, it was decided to use chlorodimethylvinylsilane instead of chlorodimethylsilane and perhaps the greater size of this led to the isolation of compound **18**. Hydrosilation of compound **18** to H_8T_8 was unsuccessful despite a

variety of methods being attempted. The main products were compound **16** and an

insoluble polymeric substance. This implies that hydrosilation was taking place

followed by break-up of the silyl ether linkage leading to the formation of a POSS

polymer (figure 7.6).
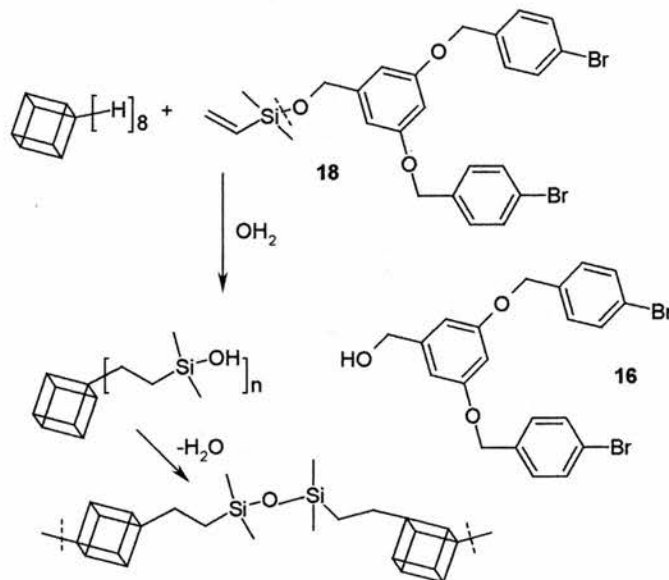
Figure 7.6: Possible fate of the hydrosilation products of H_8T_8 and dendrons.

The use of Speier's catalyst may have facilitated the cleavage of the silyl ether due to

its acidity but Karstedt's catalyst gave little reaction under similar reaction

conditions. The reaction scheme depicted in figure 7.6 would require water to be

present within the reaction mixture and as every effort was made to exclude water

from the reaction it is not unreasonable to conclude that the product may have been

formed and hydrolysed on work-up. This does not explain the failure of Karstedt's

catalysts to catalyse the reaction but it would have been unlikely to yield an isolated

product.

Compound **19** was synthesised through reaction of compound **16** and

acryloylchloride. This allowed a vinyl group to be added to the branch forming a

vinyl ester rather than a silyl ether. Hydrosilation of compound **19** and H_8T_8 proved

difficult, possibly due to electronic reasons.

The introduction of a terminal vinyl group was then attempted through etherification with the attempted synthesis of compound **22**. The reaction conditions for this were unsuccessful most likely due to solubility issues with the aqueous bases. It might be possible to synthesise this product using a strong base such as sodium hydride[22]. The failure of this reaction meant that the two synthetic routes involving alcohols and allyl bromides were not attempted, (from table 7.1, **x – xii**). It was believed that a base strong enough to deprotonate the alcohol would lead to the cube breaking up.
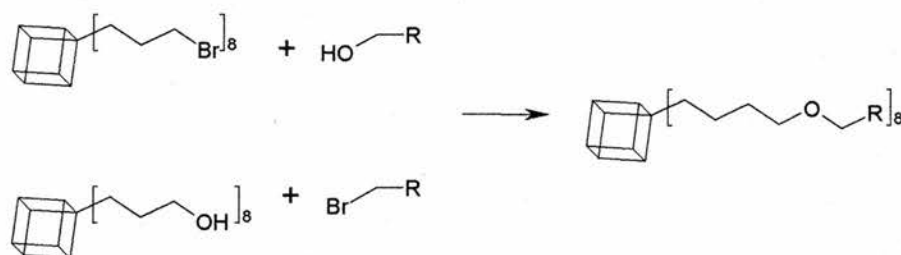
Figure 7.7: Synthetic route towards dendrimer, R is Fréchet type wedge (table 7.1, **x – xii**).

As the synthesis of compound **19** (acryloylchloride) was successful but the hydrosilation failed, an attempt was made to form an ester linkage with more atoms between the ester and the vinyl group. This lead to the attempted synthesis of compound **23** from compound **16** and pentenoylchloride. Unfortunately, this reaction was unsuccessful maybe due to the less reactive acid chloride. In any case, this would have created a very long flexible branch that may not have been particularly desirable for catalysts.

At this point the aim of hydrosilating a direct derivative of compound **16** onto a POSS core was abandoned and attempts made to exploit the reaction converting the benzyl alcohol group into a benzyl bromide, mainly used for creating larger generation branches. As it was likely that this would be used in a Grignard reaction, a branch without terminal Br groups was synthesised, compound **25**. The competing reaction of benzyl bromide and bromobenzenes would have created additional impurities[27]. Although benzyl bromides were believed to react faster than

bromobenzenes, for the purpose of trying the reaction compound **25** was prepared.

Previous attempts to convert compound **16** into the bromide form had failed

(compound **24**), thought to be due to the age of the CBr_4 being used despite being

recrystallised from methanol before use. This reaction was later carried out

successfully with CBr_4 and compound **25**.
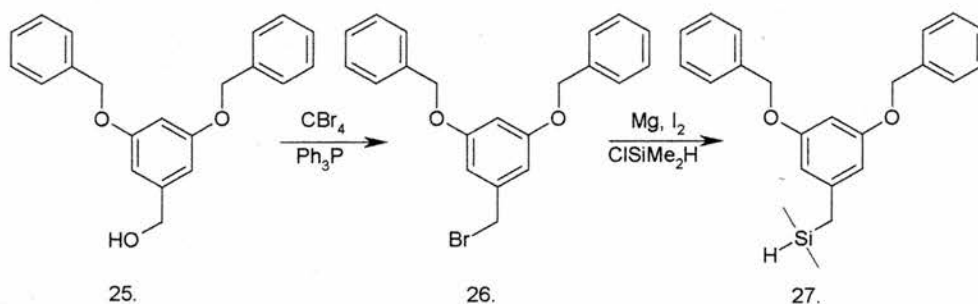
Figure 7.8: Attempted synthesis of compound **27**.

Compound **26** was synthesised in a two step reaction by firstly preparing the benzyl

alcohol (compound **25**) and using that without further purification to form the benzyl

bromide form, compound **26**. This was successfully achieved and a pure sample of

compound **26** obtained. A larger excess of reagents was used for the second step of

the reaction. Compound **26** was used to attempt to prepare a Grignard reagent and

react that with chlorodimethylsilane. It was planned that this (compound **27**) would

be hydrosilated to vinyl POSS. The Grignard reaction proved to be difficult and

resulted in a wide range of products including some caused by water being present

(potentially from incomplete reaction with the chlorosilane and the water from the

work up) and also from oxygen being present.

7.2.2.3 Synthesis of branches based on 3,4-dimethoxybenzene derivatives

Following the many difficulties in modifying the Fréchet wedge dendrons a search

for aromatic molecules possessing suitable functionality was carried out. Substituted

benzene compounds of the general form 3,5-dimethoxy-1-allyl or vinyl benzene or 1-

hydroxyl-3-allyl or vinyl phenol were extremely desirable starting points but neither were commercially available.
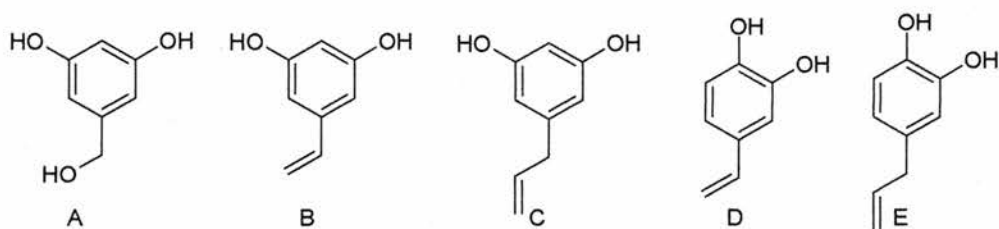
Figure 7.9: Various 1,3,5- and 1,3,4- substituted benzenes suitable for reaction to form Fréchet type dendrons. Molecule A is 3,5-dihydroxybenzylalcohol, discussed above, while B - E offer both necessary phenol groups for reaction, and hydrosilatable groups. Synthetic routes to C and E (**24**) were reported by Coolen et al.[20].

Dittmar *et al.* reported the synthesis of propylanisole POSS by hydrosilation of allyl anisole (1-allyl-4-methoxybenzene) onto H_8T_8[28]. This was simply accomplished, both by hydrosilation and condensation (Chapter 6) and provided a starting point for branches based around 3,4-dimethoxy allyl benzene. The success of reactions of this type depended on two main reactions being efficient. Firstly hydrosilation to the POSS core of the alkenyl group and secondly deprotection of the molecule to give phenols. 3,4-dimethoxylallylbenzene was commercially available and demethylation of 3,4- disubstituted benzenes was not reported to be difficult, using borontribromide. Demethylation of 4-methoxy allyl benzene was attempted first and gave a small isolated yield of 4-allyl phenol (**28**). ^{1}H NMR of the crude product showed that the reaction had been successful but subsequent attempts to purify it were only moderately successful

^{1}H and ^{13}C NMR of both the crude and purified versions of compound **29** (4-allylbenzene-1, 2-diol) revealed no organic impurities, and was carried out with different concentrations of BBr$_3$ because of two proposed mechanisms for the reaction (figure 7.10).
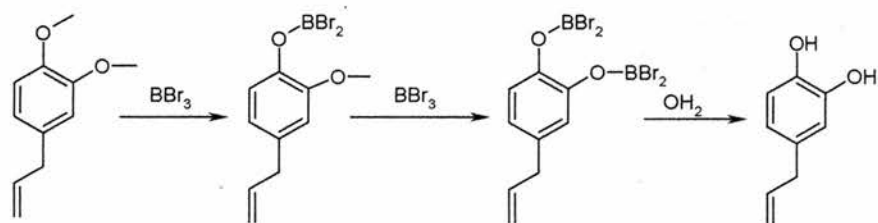
Mechanism 1: two step reaction with two moles of boron tribromide.
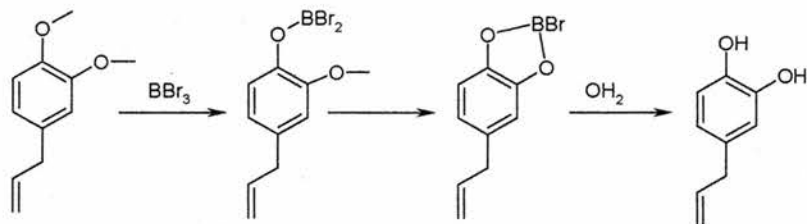
Mechanism 2: reaction with one mole of boron tribromide forming a cyclic boron species.

Figure 7.10: Two proposed mechanisms for the reaction of boron tribromide with 4-allyl-1, 2-dimethoxy benzene producing compound **29**.

The reaction using 3 molar equivalents of BBr$_3$ was just as successful as the reaction with 1.2 molar equivalents showing that the reaction can go via the cyclic intermediate proposed in mechanism 2. Using a smaller quantity of BBr$_3$ might lead to fewer impurities. The desired product was reported as a white solid and the product obtained a purple oil that could not easily be purified further. ^{1}H and ^{13}C NMR of the crude product revealed that acetone was present in stoichiometric quantities and care was take in latter attempts to avoid any acetone contamination during the reaction.

An alternate method of demethylation of 3,4- and 3,5- dimethoxy allyl benzene derivatives was reported by Coolen *et al.* using either sodium hydride and lithiumdiphenylphosphide or aluminium and carbondisulfide[20]. The yields were moderate, with 37 % for the 3,4- dialcohol, and, because 3,5-dimethoxyallylbenzene had to be synthesised from 3,5-dimethoxychlorobenzene, approximately 40 % across two steps for the 3,5- dialcohol.
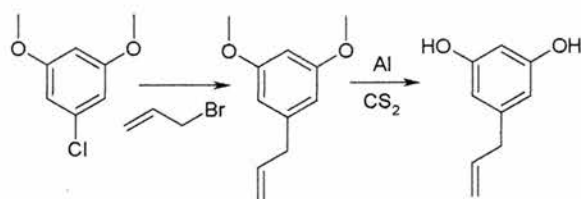
Figure 7.11: Synthesis of 3,5-dimethoxyallylbenzene and demethylation[20].

At this point, it was felt that Fréchet wedge chemistry did not offer some of the

desired properties required. As these molecules were to be used as ligands, at some

point a ligating group would have to be added. This would be most likely after

attachment to the POSS core due to the need for Pt catalysis. The bromobenzene

terminal groups on the Fréchet wedge were not felt to be reactive enough under

suitable conditions for this goal to be achieved. Beerens *et al.* had reported the

synthesis of carbosilane dendrimers through reaction of 1,4-dibromobenzene with

chlorosilanes, and further functionalised at four terminal bromobenzene site with

diphenylphosphine units in good yield (97%) using n-butyllithium and

chlorodiphenylphosphine[29]. Butyllithium has been used to open the ring of a

siloxane and so may not be suitable for use on the POSS cube[30].
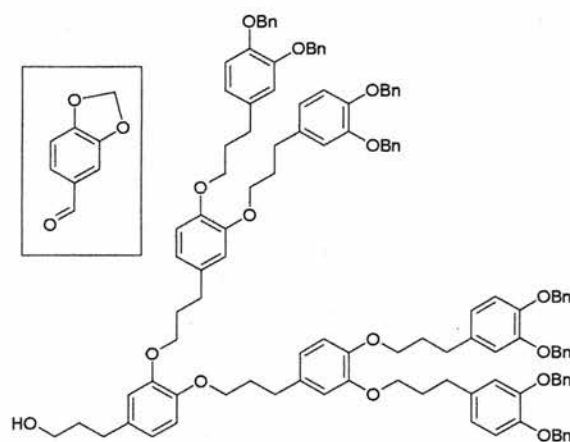
Figure 7.12: Dendrons reported by Zhou *et al.*[31], inset 3,4-methylene-dioxybenzaldehyde starting
material.

Subsequently Zhou *et al.* have reported the synthesis of polyether dendrimers from

3,4-methylene-dioxybenzaldehyde using phosphorus pentachloride as a

demethylating agent[31]. These were made with propyl alcohol roots, following

reaction of the aldehyde group (figure 7.12).

7.2.3 Experimental Detail

7.2.3.1 Branches based on 3,5-dihydroxy benzyl alcohol

Synthesis of [3,4-Bis- (4-bromobenzyloxy)-phenyl] methanol, 16[32,33]
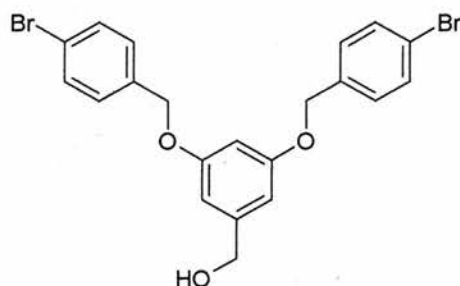
Compound **16** was synthesised sucessfully by literature methods. Full synthetic details can be found in appendix 2.

Synthesis of [3,5-Bis- (4-bromo-benzyloxy)-benzyloxy)-dimethyl-silane], 17
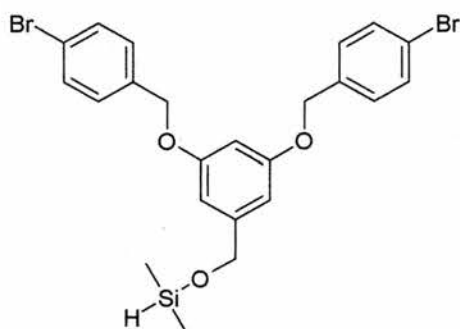
Method 1:

16 (1.967 g, 4.8 mmol) was dissolved in ether (35 cm^3) by warming in a water bath. **16** was found to have poor solubility in ether and precipitated on cooling to 0 °C. Freshly distilled triethylamine (0.5 g, 5 mmol) was added followed by drop-wise addition of chlorodimethylsilane (0.47 g, 5 mmol). The poor solubility of compound 16 limited any possible reaction and subsequent work-up recovered the unchanged starting material.

Method 2:

16 (1.967 g, 4.18 mmol) and freshly distilled triethylamine (1.0 cm^3, 10 mmol) were dissolved in dry THF (30 cm^3) and the solution cooled to 0 °C. No precipitation was

observed. Chlorodimethylsilane (0.47 g, 5 mmol) was added drop-wise and the

mixture warmed to room temperature. The reaction was monitored using TLC and

NMR and after 18 hours additional chlorodimethylsilane (0.1 cm^3, 0.6 mmol) was

added and left for 24 hours at which time ^{1}H NMR indicated that the reaction was

complete.

^{1}H NMR (300MHz, CDCl$_3$); δ_H 0.25 (6 H, d, $J = 2.5$Hz, Si(CH_3)$_2$), 4.66 (2 H, s,

ArCH_2OSi), 4.70 (1 H, septet, $J = 2.6$Hz, SiH), 4.99 (4 H, s, ArCH_2O), 6.46 (1 H, m,

ArH), 6.57 (2 H, m, ArH), 7.28 (4 H, d, $J = 8.5$ Hz, ArH), 7.50 (4 H, d, $J = 8.5$ Hz,

ArH)

The resulting mixture was hydrolysed with water and extracted with ether. The

aqueous layer was further extracted with three more portions of ether and then the

combined organic layers were washed with brine and dried with anhydrous

magnesium sulfate. The solvent was evaporated off under reduced pressure leaving a

cream solid. The product was purified by flash chromatography using ether as the

elutant. NMR of the purified product revealed only **16** was present.

Method 3:

16 (2.08 g, 4.6 mmol), triethylamine (0.96 cm^3, 7 mmol) and a catalytic amount of

dimethylaminopyridine (DMAP) were dissolved in dry THF (30 cm^3) and the

solution cooled to 0 °C. No precipitation was observed. Chlorodimethylsilane (0.59

cm^3, 4.6 mmol) was added drop-wise while stirring and the mixture allowed to warm

to room temperature and stir overnight. The products were worked up as per method

2 and an attempt was made to recrystalise the product from methanol, giving a white

solid. ^{1}H NMR of the products indicated the presence of **16** alone.

Synthesis of 3,5-Bis- (4-bromo-benzyloxy)-benzyloxy]-dimethyl vinyl silane, 18
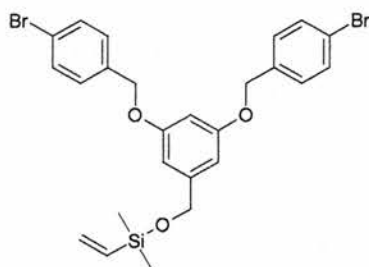
16 (3.426 g, 7.7 mmol) was dissolved in dry THF (50 cm^3) under argon.

Triethylamine (1.92 cm^3, 14 mmol) and a catalytic amount of DMAP were added and

the mixture cooled to 0 °C in an ice bath. Chlorodimethylvinylsilane (0.93 g, 7.7

mmol) was added drop-wise and a white precipitate formed immediately. The

mixture was stirred under argon at room temperature for 24 hours. The reaction

mixture was hydrolysed with water and extracted with ether. The aqueous layer was

further extracted with three portions of ether and the combined organic layer washed

with brine and dried with anhydrous magnesium sulfate. The solvent was evaporated

off under reduced pressure leaving yellow oil which formed a cream precipitate on

cooling, yield 4.11 g, 95 %.

R$_F$ (ether) 0.75; Mpt: 48 °C; ^{1}H NMR (300 MHz, CDCl$_3$); δ 0.21(6 H, s, Si (CH_3)$_2$),

4.62 (2 H, s, ArCH_2CO$_2$), 4.98 (4 H, s, ArOCH_2Ar), 5.80 (1 H, m, vinyl), 6.08 (2 H,

m, vinyl), 6.45 (1H, t, ^4J = 2 Hz, ArH), 6.56 (2 H, d, ^4J = 2 Hz, ArH), 7.28 (4 H, d, J

= 8 Hz, ArH), 7.50 (4 H, d, J = 8 Hz, ArH); ^{13}C NMR (75 MHz, CDCl$_3$): δ -2.16 (2

C, Si (CH_3)$_2$), 64.50 (ArCH_2CO$_2$), 69.15 (2 C, ArCH2O), 100.74 (arom CH), 105.34

(2 C, arom CH), 121.72 (2 C, arom CBr), 128.93 (4 C, arom CH), 131.57 (4 C, arom

CH), 133.47 (HC=CH$_2$), 135,82 (2 C, aromCCH$_2$), 136.88 (arom CCH$_2$), 143.48

(HC=CH$_2$), 159.52 (2 C, aromCOCH$_2$); FTIR cm^{-1} 2955, s, (SiO), 1586, m, (C=C),

1151, 1059, 1001, 832, 798; CHN Elemental Analysis Found: C 53.60; H, 3.75.

Calc. for C$_{25}$H$_{26}$Br$_2$O$_3$Si: C, 53.39; H, 4.66; Mass spectrum (EI): *m/z* 564 (8, M$^+$ (2

^{81}Br)), 562 (12, M$^+$ (^{79}Br + ^{81}Br)), 560 (7, M$^+$ (2 ^{79}Br)), 171 (98), 169 (100) and 90 (17).

Synthesis of Acrylic acid 3,5-bis- (4-bromo-benzyloxy)-benzyl ester, 19
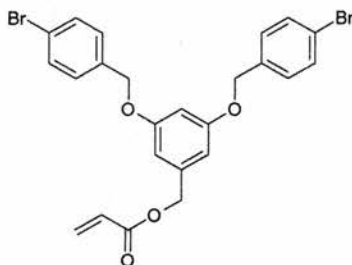
16 (2. 4g, 5 mmol) and triethylamine (0.76 g, 7.5 mmol) were dissolved in dry ether (50 cm^3) and cooled to 0 °C. Acryloylchloride (0.68 g, 7.5 mmol) was added drop-wise and the mixture warmed to room temperature and stirred continuously. A white precipitate was formed almost instantly. The reaction progress was followed by ^{1}H NMR and after 1 hour appeared to have gone to completion. The product was extracted with ether and water, the organic phase dried with anhydrous magnesium sulfate and evaporated to dryness under reduced pressure. Extraction of the product with water and ether formed an emulsion, which after several attempts at extraction with ether, DCM and brine gave a yield of 2.55 g, 96 %.

^{1}H NMR (300 MHz, CDCl$_3$): δ 4.98 (4 H, s, ArOCH_2Ar), 5.12 (2 H, s, ArCH_2CO$_2$), 5.87 (1H, d, J = 10 Hz, vinyl), 6.17 (1 H, m, vinyl), 6.24 (1 H, m, vinyl), 6.51 (1 H, s, ArH), 6.59 (2 H, s, ArH), 7.28 (4 H, d, J = 8 Hz, ArH), 7.50 (4 H, d, J = 8 Hz, ArH); ^{13}C NMR (75 MHz, CDCl$_3$): δ 65.88 (ArCH_2CO$_2$), 69.23 (2 C, ArCH_2O), 101.71 (aromCH), 107.06 (2 C, arom CH), 121.82 (2 C, arom CBr), 128.01 (HC=CH$_2$), 128.92 (4 C, arom CH), 131.13 (HC=CH$_2$), 131.56 (4 C, arom CH), 135.55 (2 C, arom CCH$_2$), 138.21 (arom CCH$_2$), 159.65 (2 C, arom COCH$_2$). 165.72 (CHCO$_2$); FTIR cm^{-1} 2728, m, (CH), 1722, s, (C=O), 1601, s, (C=C), 1398, s, (C-O), 1281, 1267, 1204, 1165, 1064, 1035; CHN Elemental Analysis Found: C 52.94; H,

3.78. Calc. for $C_{25}H_{26}Br_2O_3Si$: C, 54.16; H, 3.79; Mass spectrum (EI): *m/z* 534 (5, M^+ (2 ^{81}Br)), 532 (10, M^+ ($^{79}Br + ^{81}Br$)), 530 (5, M^+ (2 ^{79}Br)), 171 (98), 169 (100) and 90 (19).

Attempted synthesis of Fréchet Wedge Dendrimer I, 20
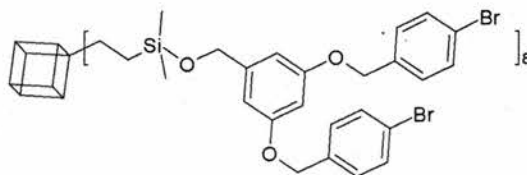
Method 1:

18 (1.006 g, 1.8 mmol) and H_8T_8 (0.079 g 0.18 mmol) were dissolved in dry THF (50 cm^3) and Karstedt's catalyst (0.1 cm^3, 0.1 M solution in xylenes) added. The mixture was heated at reflux for 48 hours. ^1H NMR of the mixture revealed incomplete reaction and that the majority of the product was unchanged starting material, **18**.

Method 2:

18 (0.503 g, 0.9 mmol) and H_8T_8 (0.038 g 0.09 mmol) were dissolved in dry toluene (50 cm^3) and Speier's catalyst (0.1 cm^3, 0.01 M in propan-2-ol solution) added. The mixture was heated at reflux for 48 hours. ^1H NMR revealed that some of the silyl ether had been hydrolysed to **16**.

Method 3:

18 (1.006 g, 1.8 mmol) and H_8T_8 (0.079 g, 0.18 mmol) were dissolved in dry toluene (50 cm^3) and Karstedt's catalyst (0.1 cm^3, 0.1 M solution in xylenes) added. The mixture was stirred at room temperature for 24 hours. ^1H NMR of the mixture revealed incomplete reaction and the majority of the product was found 18.

Method 4:

18 (0.503 g, 0.9 mmol) and H_8T_8 (0.038 g, 0.09 mmol) were dissolved in dry toluene (50 cm^3), cooled to 0 °C and Speier's catalyst (0.1 cm^3, 0.01 M in propan-2-ol solution) added. The mixture was stirred at room temperature for 48 hours, during

which time a further portion of Speier's catalyst (0.1 cm^3, 0.01 M in propan-2-ol solution) was added. ^{1}H NMR revealed that the signals for the vinyl group on **18** had reduced and the signal for the hydrogen on the POSS core had disappeared seemingly implying complete reaction. It was also noted that a substantial fraction of the products consisted of an insoluble polymer like gel. No structural information was obtained for this product. The reaction was halted by adding water and extracting the organic products with DCM. The organic layer was dried with anhydrous magnesium sulfate and evaporated to dryness under reduced pressure. A white solid was obtained which was determined to be **16** by ^{1}H NMR.

Attempted synthesis of Fréchet Wedge Dendrimer II, 21
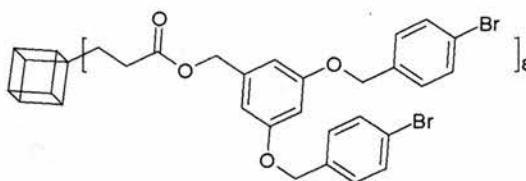
19 (0.543 g, 1 mmol) and H$_8$T$_8$ (0.046 g, 0.1 mmol) were dissolved in dry toluene (20 cm^3). Speier's catalyst (0.1 cm^3, 0.01 M in propan-2-ol solution) was added drop-wise and the mixture left to stir for six hours. NMR was used to follow the progress of the reaction. After 6 hours an additional volume of Speier's catalyst (0.1 cm^3, 0.01 M in propan-2-ol solution) was added and the mixture heated at reflux for 48 hours. The reaction was halted by adding water and extracting the organic products with DCM. The organic layer was dried with anhydrous magnesium sulfate and evaporated to dryness under reduced pressure. A white solid was obtained which was determined to be **19** by ^{1}H NMR.

Attempted synthesis of [1-allyloxy methyl-3, 5-bis- (4-bromo-benzyloxy)-benzene], 22
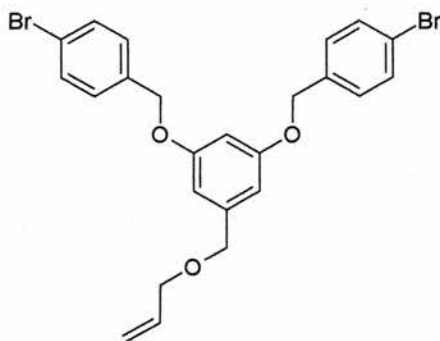
Method 1[34]:

Sodium hydroxide (0.22 g, 5.56 mmol in 20 cm^3 water) was added to solution of **16** (1.178 g, 2.46 mmol) in THF (50 cm^3). Benzyltriethylammoniumchloride (0.1 g, phase transfer catalyst) and the mixture stirred vigorously by mechanical means. 3-chloropropene (30 cm^3, 7.4 mmol) was added drop-wise and the mixture stirred at ether (3 x 30 cm^3), washed with 1 M hydrochloric acid (30 cm^3), saturated sodium hydrogen carbonate (30 cm^3) and dried with anhydrous magnesium sulfate. The solvent was removed under reduced pressure leaving a yellow liquid. A white solid precipitated from the concentrated solution, which was found to be compound **16** by ^{1}H NMR.

A second attempt at this reaction, leaving the mixture stirring for 5 days and adding extra sodium hydroxide after 24 hours also resulted in no apparent reaction.

Method 2:

A solution of **16** (0.504 g, 1.05 mmol) in dry ether (25 cm^3) was stirred mechanically under argon. 3-chloropropene (0.097 g, 1.3 mmol) was added followed by freshly distilled triethylamine (0.131 g 1.3 mmol). The mixture was stirred at room temperature for 24 hours. The reaction was quenched by the addition of water and the organic layer extracted with ether (3 x 10 cm^3). The combined organic extracts were dried with anhydrous magnesium sulfate and the excess solvent evaporated off

leaving a yellow liquid and cream coloured precipitate. ^{1}H NMR of the product

revealed that the yellow liquid was unreacted 3-chloropropene and the cream

coloured precipitate was unreacted **16**.

Attempted synthesis of [pent-4-enoic acid 3,5-bis- (4-bromo-benzyloxy)-benzyl

ester], 23
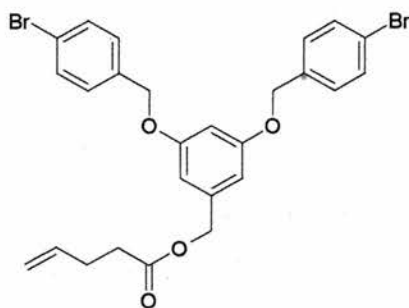
16 (0.48 g, 1 mmol) was dissolved in dry toluene (50 cm^3) and the mixture cooled to

0°C in an ice bath, whilst being continuously stirred. Freshly distilled triethylamine

(0.19 cm^3, 1.3 mmol) was added drop-wise and the mixture stirred for five minutes.

Pent-4-enoyl chloride (0.14 cm^3, 1.3 mmol) was added drop-wise and a white

precipitate formed instantaneously. The mixture was allowed to warm to room

temperature and stir for one hour. The reaction was halted by the addition of water

(50 cm^3) causing the precipitate to disappear. The organic layer was extracted DCM

(2 x 30 cm^3) and washed with saturated brine solution. The organic phase was

separated and the aqueous layers extracted with further portions of DCM (2 x 30

cm^3). The combined organic extracts were dried with anhydrous magnesium sulfate

and the solvent removed under reduced pressure leaving a yellow oil with a small

amount of white precipitate. ^{1}H NMR of the crude product revealed that the yellow

oil was pentenoic acid and the white precipitate was most likely residual magnesium

sulfate.

Attempted synthesis of [1,3-Bis- (4-bromo-benzyloxy)-5-bromomethyl-benzene],

24
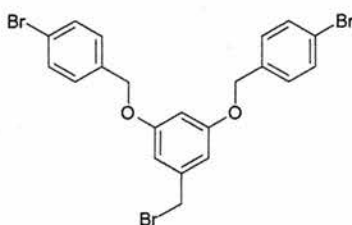
16 (1.07 g, 2.24 mmol), carbon tetrabromide (0.93 g, 2.8 mmol, recrystallised from

methanol) and triphenylphosphine (0.98 g, 2.80 mmol) were dissolved in dry THF

(50 cm^3). The mixture was stirred for 30 minutes. The organic phase was extracted

with DCM (3 x 50 cm^3) and washed with water. The combined organic phases were

dried with anhydrous sodium carbonate and the solvent removed under reduced

pressure leaving yellow oil with some yellow needle like crystals. TLC (1:3 hexane:

DCM) and showed a possible product, along with spots correlating with all reactants.

The compound was purified by a short silica gel column using the same solvent

mixture as the TLC however there was no product. The column produced

approximately 50 mg in total of a mixture of reactants and possible product but not

enough to be characterised. The starting compound, **16** was not recovered

successfully.

Attempted synthesis of an Si-H terminated branch in three steps, 25, 26 and 27
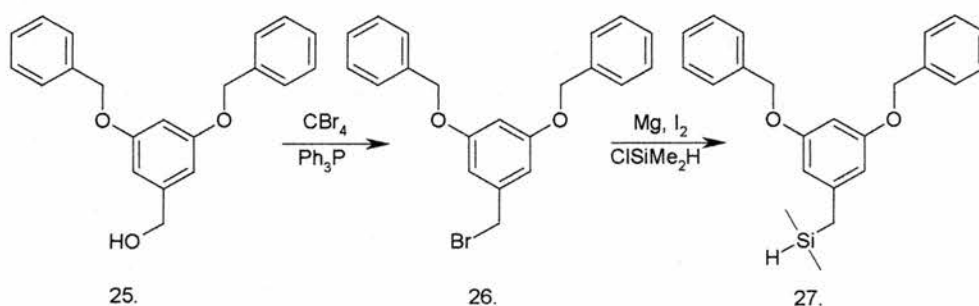
Step 1: Synthesis of benzylbromide branches, 25

Benzyl bromide (8.68 cm³, 73 mmol), potassium carbonate (10 g, 73 moles), 3,5-dihydroxybenzylalcohol (5 g, 35.6 mmol) and a catalytic amount of 18-crown-6 (1.88 g, 7.1 mmol) were dissolved in acetone (200 cm³). This mixture was refluxed for three days. After cooling the solvent was removed under reduced pressure, the residue dissolved in ether and washed with water. The organic layer was dried over anhydrous magnesium sulfate and concentrated.

As 5 g of 3,5-dihydroxybenzylalcohol is used, it is calculated that for 100 % yield 13.65 g of product would be obtained. The next step of the reaction is calculated on this basis.

*Step 2: Synthesis of bromide, **26***

The crude product, **25** is dissolved in dry THF along with carbon tetrabromide (14.76 g, 44.5 mmol) and triphenylphosphine (14.52 g, 44.5 mmol). This mixture was stirred for 1 hour before being concentrated under reduced pressure. The branches were purified by a short silica gel column, eluted initially with 1:3 hexane: DCM, followed by DCM then ether: DCM, 19:1. A pure sample was obtained, 8.16 g, 59.5 % over two steps.

¹H NMR (300 MHz, CDCl₃) δ$_H$: 4.52 (2 H, s, CH_2Br), 5.18 (4 H, s, ArCH_2OAr), 6.75 (1 H, m, ArH), 6.80 (2 H, m, ArH), 7.4 – 7.65 (10 H, m, Ar-H)

*Step 3: Grignard Reaction, **27***

26 (1.33 g, 4.3 mmol) was dissolved in dry THF and added slowly to a suspension of Mg (0.12 g, 5 mmol) and I₂ (single crystal). The mixture was refluxed gently for 8 hours and stirred at room temperature overnight by which point it had turned black. Chlorodimethylsilane (0.76 g, 8 mmol) was added slowly and the reaction refluxed for a further 6 hours and allowed to stir overnight at room temperature. Water was added to the reaction followed by DCM. The organic layers were separated and dried with anhydrous magnesium sulfate before being concentrated under reduced

pressure to give a pale brown waxy solid. The product was purified by a short silica

gel column with ethyl acetate in petroleum ether. There was very little product

retrieved from the column, despite changing the solvent from 40 % ethyl acetate in

petroleum ether through to pure ethyl acetate.

^{1}H NMR of the products obtained indicated a number of products including

unreacted **26**, and several impurities. No sample of the desired product was

obtained.

7.2.3.2 Branches based on 3,4-dimethoxy allyl benzene

Synthesis of 4-allyl phenol, 28
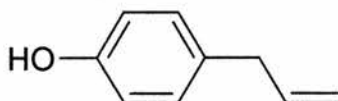
1-allyl-4-methoxy benzene (5.0 cm^3, 32.6 mmol) was added to dry degassed DCM

(100 cm^3). The mixture was stirred and cooled to −78 °C. Boron tribromide (35 cm^3,

35 mmol, solution 1 M in DCM) was added drop-wise. The reaction mixture was

stirred continuously and allowed to warm to room temperature for 1 hour. The

reaction was then cooled in an ice/water bath before being quenched by the addition

of water (30 cm^3). The organic layer (now purple) was separated and the aqueous

layer extracted with DCM (3 x 30 cm^3). The combined organic extracts were washed

with saturated brine solution, dried with anhydrous magnesium sulfate and the

solvent removed under reduced pressure. The product was brown oil that gave no

separation in TLC with a variety of solvents. ^{1}H NMR of the crude product showed

that the methoxy peak had disappeared and there was now an OH peak present. A

small silica column using DCM as an elutant purified the product was moderately

successful and produced a small quantity of pure 4-allyl phenol as a pale brown clear

liquid. NMR: ^{1}H NMR (300 MHz , CDCl$_3$) δ$_H$: 7.2 (d, J = 8.4 Hz, 2 H, Ar-*H*), 6.8

(d, J = 8.4 Hz, 2 H, Ar-*H*), 6.0 (m, 1H, C*H*=CH$_2$), 5.1 (m, 2 H, CH=C*H$_2$*), 4.9 (broad,

s, 1 H, O*H*), 3.4 (d, J = 6.6 Hz, 2 H, -C*H$_2$*-CH=); ^{13}C NMR (CDCl$_3$, 70 MHz) δ$_C$:

153.59, 132.311, 130.44, 130.20, 115.49, 115.295, 39.296. The above data are in

agreement with the literature[35].

Attempted synthesis of 4-allyl-benzene-1, 2-diol, 29
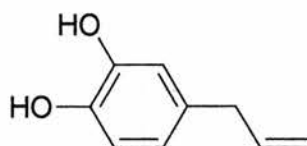
4-allyl-1, 2-dimethoxybenzene (5 cm^3, 16.3 mmol) was dissolved in dry DCM (50

cm^3) and the mixture cooled to –78 °C. Boron tribromide (50 cm^3, 50 mmol, 1 M in

DCM) was added drop-wise and the mixture allowed to warm to room temperature

and stir until it turned dark (approximately 4 hours). The reaction was quenched by

slowly pouring the mixture into iced water, and extracting the organic phase with

further portions of DCM (3 x 50 cm^3). This was then dried with anhydrous

magnesium sulfate and evaporated to dryness under reduced pressure. The crude

product was viscous purple oil. All glassware was rinsed with DCM and thoroughly

dried before use to avoid any contamination from acetone.

The crude product, 4-allyl benzene-1, 2-diol was purified shaking the purple oil with

hexane, forming a biphasic system of the oil and hexane and pipetting the hexane off.

The hexane solution was evaporated to dryness under reduced pressure, causing a

white waxy solid to form.

^{1}H NMR (300 MHz, CDCl$_3$) δ$_H$: 6.8 (d, 1 H, Ar-*H*), 6.75 (d, 1 H Ar-*H*), 6.7 (m, 1H

Ar-*H*), 6.6 (broad, s, 1 H, O*H*), 5.9 (m, 1 H, C*H*=CH$_2$), 5.1 (m, 2 H, CH=C*H$_2$*), 3.2

(d, 2 H, -C*H$_2$*-CH=)

The data agrees with literature[36].

This reaction was repeated using 4-allyl-1, 2-dimethoxybenzene (5 cm^3, 16.3 mmol) and boron tribromide (20 cm^3, 20 mmol, 1 M in DCM). The above method was followed and gave a purple oil product, which NMR revealed to be identical to above.

7.2.4 Conclusions and Further Work

The successful synthesis of three new compounds has been achieved, however attempts to synthesise Fréchet type POSS dendrimers are disappointing. From the experiments conducted it appears that attachment of this kind of dendron through hydrosilation reactions is a difficult process where the hardest part is functionalising the Fréchet type dendrons with suitable groups. While the use of 1-allyl, 3,4-dimethoxy benzene looked like a convenient way of circumventing this problem, converting the dimethoxy groups to phenols proved more difficult than expected. With additional difficulties foreseen further down the line when functionalising these molecules with ligating groups for use as catalysts, it was decided to stop pursuing this line of research.

These dendrimers were being investigated as new dendrimer architectures for catalysis and as such the addition of groups such as diphenylphosphine to the periphery would have created problems either through low yield or through reaction with platinum hydrosilation catalysts. This does not mean these systems could not be investigated further for other applications that do not involve such sensitive groups. For example, polyfluoroenes[37] and other light emitting polymers could be attached to the periphery of these dendrimers through reactions such as Suzuki coupling with the bromobenzene.

7.3 Synthesis of PAMAM Dendrimers

7.3.1 Introduction

Poly (amidoamine) dendrimers (PAMAM dendrimers) were the first dendrimers to be synthesised and have subsequently become the most studied family of dendrimers having been well characterised and developed commercially. PAMAM dendrimers are synthesised divergently through sequential Michael type addition of α,β-unsaturated carbonyl compounds (methyl acrylate and related compounds) to primary amines followed by amidation of the esters.

First generation, NH₂ Terminated
G1-1,2-diaminoethane-4NH₂

Second Generation COOMe Terminated
G2-1,2-diaminoethane-8COOMe
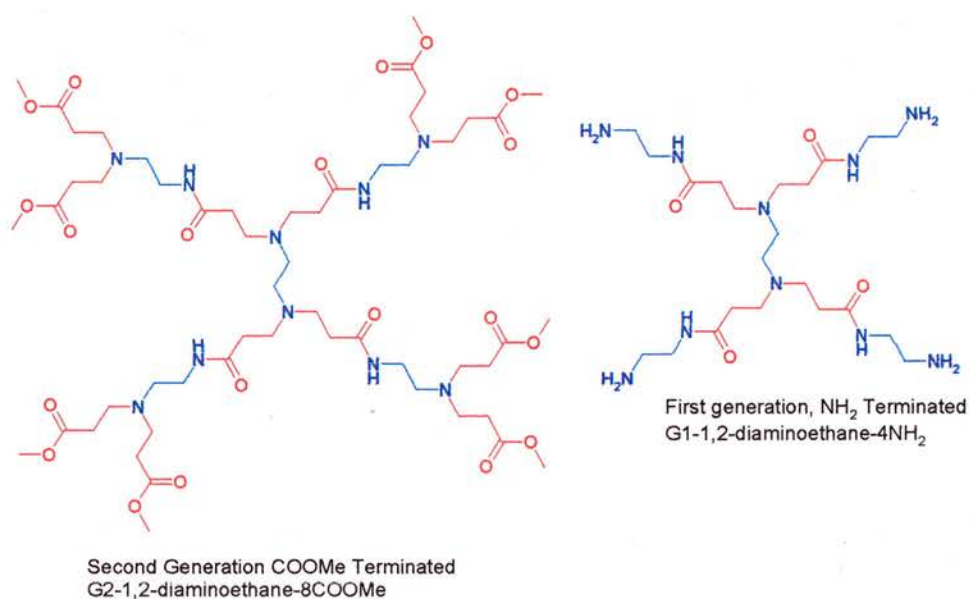
Figure 7.13: PAMAM dendrimers with 1,2-diaminoethane cores, methyl acrylate units in red, diamino ethane units in blue.

The ease of synthesis and the commercial availability has lead to PAMAM dendrimers being widely exploited for applications as varied as catalysis, host-guest systems (including chelating to metal ions)[38], organic-inorganic hybrid materials and biological applications such as drug delivery and biomimicry[39]. The commercial potential of any PAMAM system is greater than other dendrimers due to the ease and reproducibility of the synthetic procedures and the ease of functionalising the terminal ester/amine groups for many applications. The notation Gx-Y-nZ refers to

the generation (x), the core or root (Y) and the number (n) and nature of the terminal groups (Z).

Feher *et al.* reported the synthesis of octaaminopropyl POSS and its subsequent transformation into G1-POSS-16COOMe and G1-POSS-16NH$_2$ first generation PAMAM dendrimers through divergent synthesis[10]. OctaaminopropylPOSS proved to be highly unstable and relatively difficult to handle making it less attractive as a dendrimer core. There have been a number of reports of less ordered PAMAM-Silica dendrimers such as those reported by Alper *et al.* [40-42]. A heterogeneous catalysis system was created through reaction of commercially available aminopropylsilica gel with 1,2-diaminoethane and methyl acrylate to create four generations of amine terminated PAMAM branches anchored on the gel (G0 – gel itself, G3 – third generation branch).
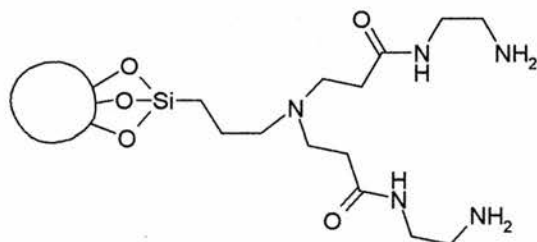
Figure 7.14: G1 PAMAM dendrons immobilised on silica gel, G1-silica-2NH$_2$. Circles represent silica gel[40,42,43].

These dendrimers were then functionalised with diphenylphosphine units and complexed to palladium for the carbonylation of iodobenzene. Gong *et al.* used similar reactions to functionalise third generation amine terminated PAMAM dendrimers with diphenylphosphinomethane groups for ligands in the rhodium catalysed hydroformylation of oct-1-ene and styrene[44]. Interestingly, up to half the terminal amine groups were functionalised in this manner, the other half were given sulfonic acid groups to make the molecules water soluble. In this way, these ligands were used in a two-phase reaction system that operated under mild conditions.

PAMAM dendrimers were completely immobilised on silica surfaces by Chung *et al.* and used for the enantioselective addition of diethylzinc to benzaldehyde[45]. The immobilised dendrimers were further functionalised with a long alkyl spacer and a chiral auxiliary molecule and it was this combination that was found to improve the conversion, selectivity and enantioselectivity of the reaction.

From these few examples it is possible to see that PAMAM dendrimers have great potential as catalysts through the ease of reaction with ligating groups to create functional molecules and in their potential to have additional groups to impart other properties. Of most interest to this project are the PAMAM dendrons synthesised from aminopropyl silica gel. This heterogeneous system did not produce high l: b ratios for the hydroformylation of oct-1-ene although a preference for the linear isomer was shown. The most obvious homogeneous catalyst equivalents of these PAMAM dendrimers would be those with POSS cores, highly ordered silica particles of precisely defined size. It is possible that this well-defined size and density of terminal groups will influence the selectivity of subsequent catalysts prepared from such species. By preparing such molecules convergently there is far greater scope for the incorporation of different branches to modify the conditions under which the ligand performs, for example water or fluorous phase soluble groups for biphasic reaction systems or bulkier groups to facilitate better removal of the ligand.

One example could be found for the reaction of allyl amine and an acrylate ester in the literature by Miyahara *et al.*[46].

3,7-diazabicyclo[3.3.1]nonane
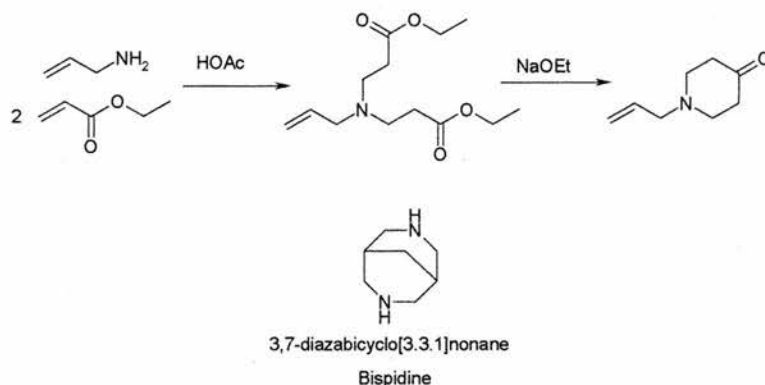
Bispidine

Figure 7.15: Synthesis of ethyl PAMAM branch and its subsequent conversions to allylpiperdin-4-one and Bispidine. Adapted from Miyahara *et al.*[46].

The synthesis and characterisation of bis (carbethoxyethyl) allylamine was reported from allyl amine and ethyl acrylate by reflux with an acetic acid catalyst (figure 7.15). This was converted to 1-allylpiperdin-4-one a precursor for the synthesis of Bispidine, (3,7-diazabicyclo-[3.3.1] nonane).

The addition reaction of glycidol and aminopropyltriethoxysilane and hydrolytic condensation of the product, N,N-di(2,3-dihydroxypropyl)aminopropyltriethoxysilane were studied by Mori *et al.* (figure 7.16)[47]. In a similar way to that attempted in this project, aminopropyltriethoxysilane was functionalised and aqueous hydrofluoric acid used to facilitate condensation.
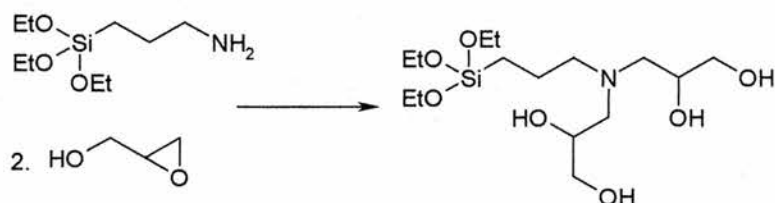
Figure 7.16: Addition reaction to triethoxysilane, as carried out by Mori *et al.* [47].

The reaction was allowed to run for two hours before work-up. MALDI-TOF mass spectrometry was carried out to gain some understanding of the various species produced and a variety of silicon-oxygen structures were thought to have been formed, including linear chains, ladders, and partial and complete cages. Various molecular ions were recognised including one corresponding to the T8 cage.

References for Chapter 7 begin on page 295

A recent and interesting combination of POSS/silicate and PAMAM dendrimer chemistry was reported by Dvornic *et al.*[48]. PAMAM dendrimers were functionalised with POSS cubes connected through one corner (figure 7.17).
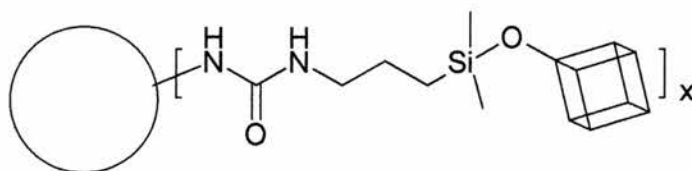
Figure 7.17: PAMAM-POSS/Silicate hybrid material synthesised by Dvornic *et al.* PAMAM dendrimer represented by a circle, x = number of terminal groups, from 16 (G2) to 128 (G5).

POSS cubes with one isocyanatopropyl corner were attached to terminal amine groups of G2 – G5 PAMAM dendrimers in close to quantitative yields for G2 (16NH$_2$). The degree of substitution of the terminal amines was good (approx. 82 %) for all bar G5 despite the size of the POSS species. These molecules represent the first POSS dendrimers in which the role of the POSS has been reversed, creating dendrimers with POSS and PAMAM physical properties.

The main goal of this section is to synthesise PAMAM-POSS dendrimers through a convergent route. This will be attempted in two main ways. Firstly, PAMAM dendrons will be prepared using allyl amine as a suitable starting material and once prepared will be attached to H$_8$T$_8$ via hydrosilation. The second approach involves the preparation of branches that can undergo condensation reactions. To this end aminopropyltriethoxysilane will be used and reacted to produce branches of various generations that can be condensed. These routes will also eliminate the difficulties in handling aminopropylPOSS and the hydrosilation method would allow the incorporation of other branches to the dendrimer.

7.3.2 Results and Discussion

7.3.2.1 Synthetic Strategy
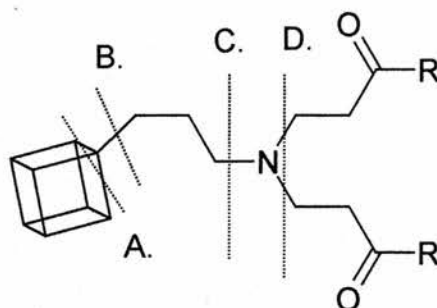
Figure 7.17: Schematic representation of PAMAM-POSS dendrimer. R represents branches of varying generation.

Several possible synthetic routes towards PAMAM-POSS dendrimers are described in figure 7.18 and table 7.2. Approaches based on disconnections A and B have been used here while Feher *et al.* have reported success using the method described by disconnection D[10]. Disconnection C gives a route that is, as yet, untried.

Disconnection	Precursors	Process	Ref.
A	$Cl_3SiC_3H_6N(C_2H_4COR)_2$, $(C_2H_4O)_3SiC_3H_6N(C_2H_4COR)_2$	Condensation, total convergent growth	
B	$CH_2CHCH_2N(C_2H_4COR)_2$, H_8T_8	Hydrosilation, convergent growth	
C	BromopropylPOSS, $HN(C_2H_4COR)_2$	Convergent Growth	
D	Amine POSS, methyl acrylate, 1,2-diaminoethane	Addition, divergent growth	10

Table 7.2: Disconnections shown in figure 7.17 and synthetic routes towards PAMAM-POSS dendrimer, attempted or proposed.

7.3.2.2 Synthesis of branches based on allyl amine derivatives
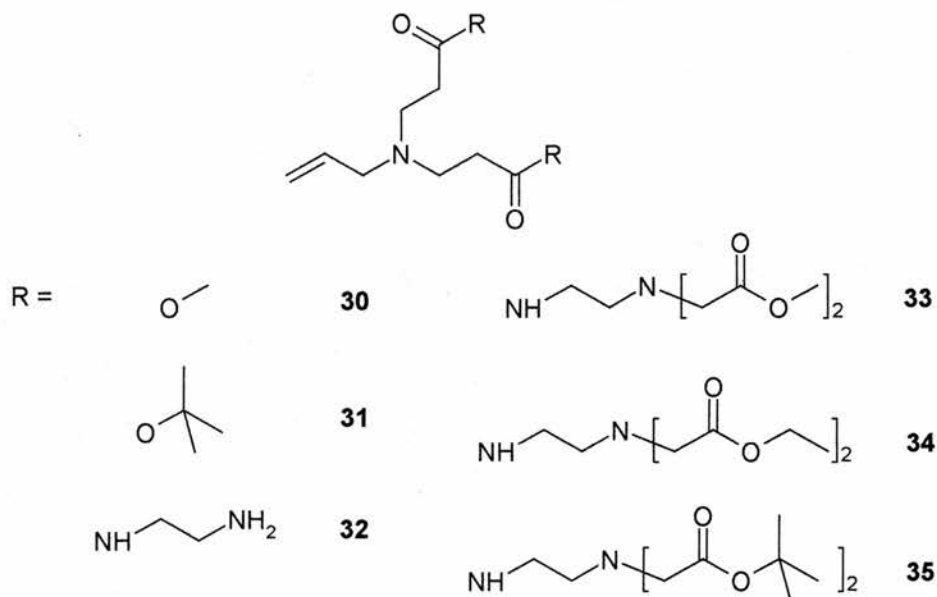
Figure 7.19: New compounds **30 - 35**

The synthesis of several dendritic branches based on allyl amine was achieved

initially creating 6 new compounds (**30 - 35**). The reactions to produce these

branches were high yielding under mild conditions and appeared to proceed without

any major side reactions due to the careful execution of this work. The only issue

with PAMAM dendrimer synthesis, and the main ways of producing impurities, are

incomplete reaction and poor removal of excess reagents. Fortunately, incomplete

reaction can be easily detected by NMR for low generations and was not a major

issue here as no dendrons above G2 were synthesised. Removal of the excess

reagents is extremely important because while precursors such as methyl acrylate and

1,2-diaminoethane are relatively volatile, small first generation dendrimers are not.

Incomplete removal of excess methyl acrylate would lead to it reacting with 1,2-

diaminoethane in the next reaction step competing with the desired reaction and also

creating large impurities. It is possible to detect such impurities by NMR, which

would manifest themselves as additional or overlapping signals in regions of the

spectra where sharp signals were expected for the branches.

Characterisation by NMR is not a simple matter for dendrimers, in particular second generation and above as there are a large number of atoms in similar environments creating many signals, some overlapping. In order to make sense of this more advanced NMR correlation experiments were run. ^{1}H-^{13}C and ^{1}H-^{1}H correlation spectroscopy (COSY) experiments were used with the correlation between atoms assisting in the assignment. The area relating to NCH$_2$CH$_2$CO is particularly difficult to interpret beyond the first generation as it contains signals corresponding to G1and G2. Many of the peaks in NMR spectra have been very generally assigned because of this.

The most common impurities in the NMR spectra were due to hydrogen bonding to the dendrons. For example, unreacted 1,2-diaminoethane hydrogen bonds strongly to first generation branches making purification slightly more difficult (compounds **32** and **36**, amine terminated branches). This is a known issue with PAMAM dendrimers and butanol was added to replace the diamine at hydrogen bonding sites. This of course means that butanol will always be present in samples creating errors in CHN elemental analysis and extra signals in NMR spectra. The solvent methanol was also present in the purified samples due to the extreme difficulties in removing it from the products.

Other acrylates (ethyl acrylate and t-butyl acrylate) were used to see if the hydrogen bonding problems could be eliminated. It was hoped that terminating the molecules with t-butyl acrylate would inhibit hydrogen bonding to the molecule through the bulk of the t-butyl groups. In addition, groups such as these can be removed under different reaction conditions, offering more versatile routes for synthesis.

The length of time for complete reaction increased with generation and addition of 1,2-diaminoethane was always slower than addition of methyl acrylate. In case of

incomplete reaction the product was merely redissolved in methanol and additional

reactants added.

The attempt to add acrylic acid directly onto allyl amine created mixed results. It

seems that Michael addition of the double bond competes with reaction of the acid

and amine creating a range of products. This was attempted to investigate whether it

would be possible to avoid oxidising the methyl ester at the end of the reaction, if

acidic groups were required at the periphery. The oxidation of the methyl ester was

also attempted but resulted in no product for analysis, perhaps due to the reaction
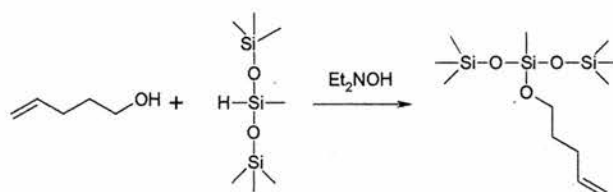
conditions.

Figure 7.20: Base catalysed reaction of alcohol, ROH with Si-H, as detailed by Bassindale *et al.* [26]

Hydrosilation of the dendrimer branches, particularly G1-allyl-2COOMe proved to

be far from simple. Various conditions were attempted and these were selected to try

to promote the α-addition to H_8T_8. Initial attempts created insoluble polymer-like

products that seemed to be forming before any catalyst was added. It is possible that

a reaction pursued by Bassindale *et al.* is responsible for this (figure 7.20)[26]. It is

possible for Si-H species to react with alcohols to form Si-O-R in the presence of

base and in the case of these reactions, the branches themselves could be catalysing

the addition of the solvent (isopropanol) or impurities (methanol or butanol) to H_8T_8

creating highly polymerisable moieties, particularly if methanol is added.
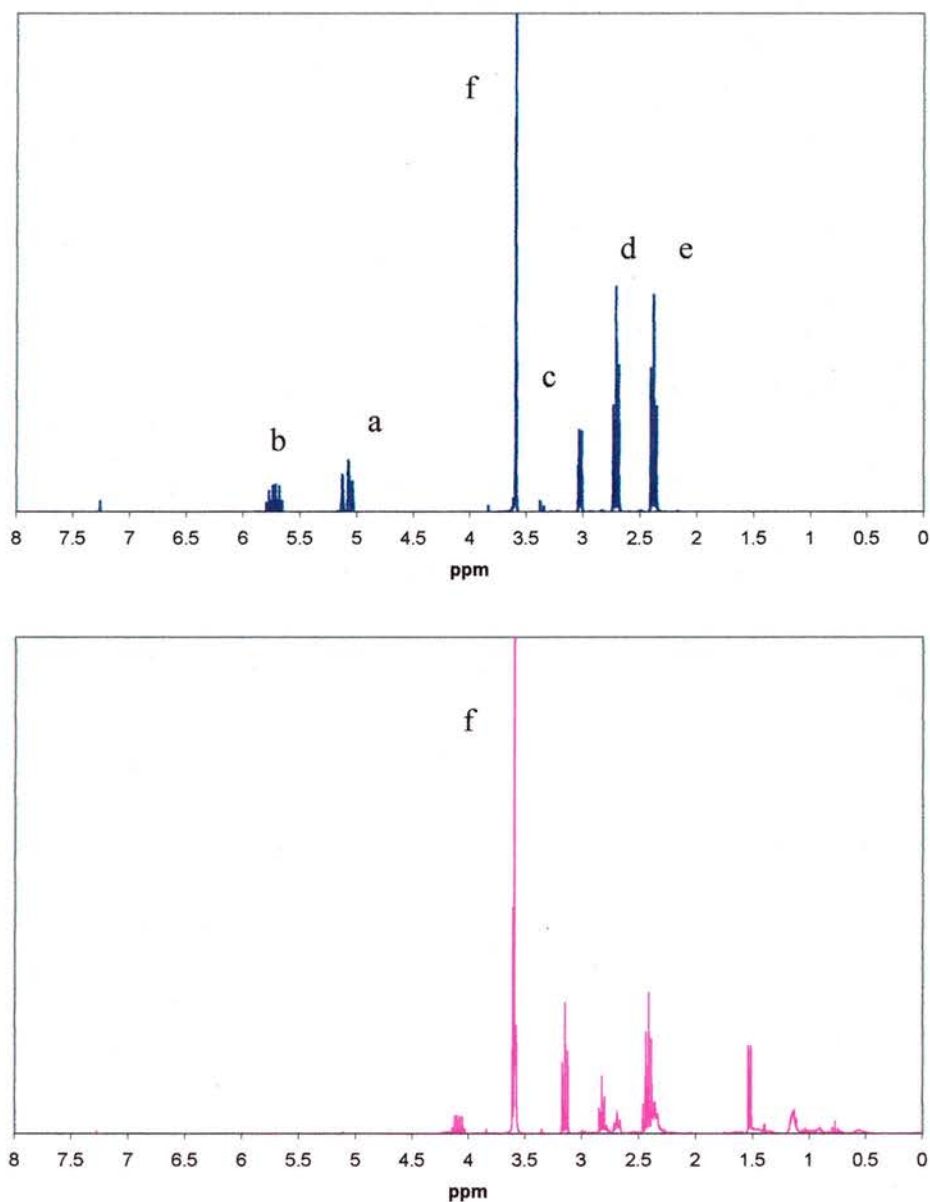
Figure 7.21: ^{1}H NMR spectra of G1-allyl-2COOMe (top, blue) and attempted hydrosilation of G1-allyl-2COOMe to H_8T_8 (bottom, pink). Integration has been omitted for clarity.

When hydrosilation of G1-allyl-2COOMe did not result in a polymer, the products were extremely difficult to separate from the excess reactants. Figure 7.21 shows the proton NMR of G1-allyl-2COOMe, fully assigned (key in figure 7.22) and the proton NMR of the crude product of hydrosilation.
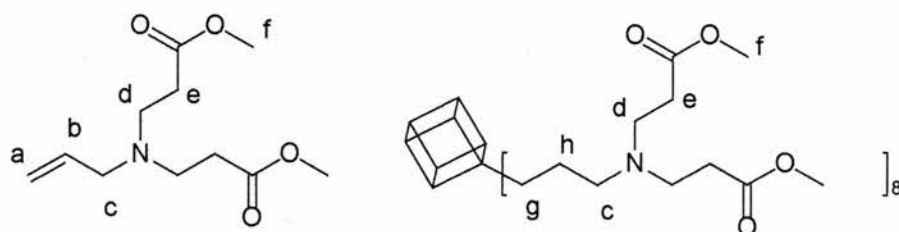
Figure 7.22: G1-allyl-2COOMe and G1-POSS-16COOMe, lettering refers to NMR signals in figure 7.21.

The peaks **a** and **b** have disappeared, indicating that the double bond has been removed, and the doublet corresponding to **c** is no longer present. The main peak that remains identical between the two spectra is **f**, that of the OCH_3 terminal group. The signals between 0.5 and 3.5 ppm in the lower spectrum appear to loosely correspond with those reported by Feher for this molecule, synthesised by divergent means from aminopropylPOSS[10].

Assignment	Feher(ppm)
c	2.40
d	2.40
e	2.71
f	3.61
g	0.593
h	1.51

Table 7.3: ^{1}H NMR Assignment for G1-POSS-16COOMe by Feher *et al*[10]

Signals corresponding to **c**, **d** and f can be identified in figure 7.21, indicating that OCH_3, CH_2N and NCH_2 groups appear to be present. There is no clear peak for **e** corresponding to CH_2CO, and the peaks for **g** and **h** are ambiguous perhaps indicating that α and β addition has occurred. All attempts to purify this product resulted in no product being obtained, indicating that it must be retained on the celite pad used to remove the platinum catalyst. Attempts to hydrosilate G1-allyl-$2NH_2$ to H_8T_8 produced a polymer gel. This may have been due to the mechanism described above, base catalysed addition of alcohols to H-Si or may be due to base catalysed cleavage of Si-O-Si bonds creating a random polymer. Base catalysed cleavage of

aminopropylPOSS by the NH_2 groups was reported to be one of the main routes of decomposition of aminopropylPOSS at room temperature[10]. If this is the case, terminal amine POSS dendrimers would have to be prepared divergently and at subzero temperatures. Due to time constraints, this work was not successfully completed.

Calculation of the yield for compounds **31** and **33** was difficult due to the presence of butanol within the branches and so when reacted further, the number of moles used is calculated on the basis of a pure sample and quoted as approximately *x* moles. The yields of subsequent products are quoted as masses only due to this.

7.3.2.3 Synthesis of branches based on aminopropyltriethoxysilane derivatives

Synthesis of branches based on aminopropyltriethoxysilane produced two new PAMAM species, compounds **41** and **42**. The reactions of acrylates and aminopropyltriethoxysilane were as straightforward and high yielding as the allyl amine equivalents and purification was simply a matter of removing the unreacted acrylates. Condensation of these molecules proved to be more complicated. The difficulties surrounding the condensation of aminopropyltriethoxysilane were discussed in Chapter 6, where the major problem was encouraging the products to crystallise from solution. This was also an issue with these condensations and because this work was attempted within the last six months of this project, it was felt that the reactions should be left for as long as possible in the hope that a solid product would be produced. There are several ways in which these reactions might be analysed further. Firstly, by working up the reactions by removing the methanol (likely to produce a gel) and washing the product thoroughly to remove excess acid. Secondly, by using MALDI-TOF mass spectrometry to determine the masses of products present and identify the species (similar to the method of Mori *et al.*[47]).

Thirdly, to attempt to obtain a solid or crystalline product using a variety of techniques thought to promote solid formation such as those detailed by Dittmar *et al.* [28]. Extreme care must be taken to avoid the irreversible formation of gels, particularly during the work up where high temperatures may be involved.

7.3.3 Experimental Details

7.3.3.1 Branches based on allyl amine

Synthesis of 3-[allyl- (2-methoxycarbonyl-ethyl)-amino]-propionic acid methyl ester, G1-allyl-2COOMe, 30
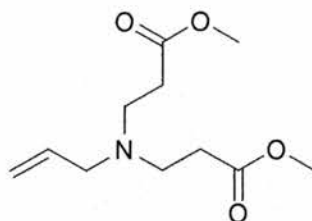
Methyl acrylate (11.25 cm^3, 0.125 mol) was added to a solution of allyl amine (3.5 cm^3, 0.0466 mol) in methanol (20 cm^3) and stirred overnight. The solvent and excess methyl acrylate were removed under reduced pressure leaving the product, **30**, a colourless oil, 10.25 g, 96 %.

^{1}H NMR (300 MHz, CDCl$_3$) δ: 2.3 (4H, t, N-C*H*$_2$), 2.7 (4H, t, C*H*$_2$-CO), 3.1 (6H, s, OC*H*$_3$), 5.1 (2H, t, C*H*$_2$=CH), 5.7 (1H, m, CH$_2$=C*H*); ^{13}C NMR (CDCl$_3$, 70 MHz): 32.76 (*C*HCOO), 49.20 (N-CH$_2$), 51.74 (OCH$_3$), 57.23 (CH$_2$N), 117.71 (H$_2$*C*=C), 135.65 (CH$_2$=*C*H), 173.14 (*C*=O); CHN Elemental Analysis: Found C 57.73, H 9.06, N 6.83; Calculated for C$_{11}$H$_{19}$NO$_4$: C 57.63, H 8.35, N 6.11.

Synthesis of 3-[allyl- (2-tert-butoxycarbonylethyl)-amino]-propionic acid tertbutyl ester, G1-allyl-2COO^{t}Bu, 31
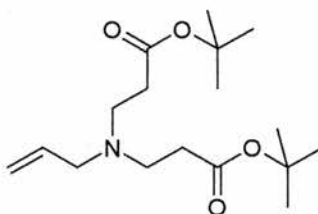
Allyl amine (15.02 g, 0.263 moles) was added to a stirred solution of t-butyl acrylate (83 g, 0.684 moles) and methanol (84.83 g). The mixture was stirred overnight and

the methanol and excess t-butyl acrylate removed under reduced pressure. The

product, **31**, was a colourless oil, 73.95 g, 91 % yield.

^{1}H NMR (300 MHz, CDCl$_3$) δ: 1.3 (18H, s, CC*H$_3$*),2.25 (4H, t, N-C*H$_2$*), 2.7 (4H, t,

C*H$_2$*-CO), 5.1 (2H, t, C*H$_2$*=CH), 5.7 (1H, m, CH$_2$=C*H*); ^{13}C NMR (CDCl$_3$, 70 MHz):

28.45 (6C, C*C*H$_3$). 32.76 (*C*HCOO), 49.20 (N-CH$_2$), 51.74 (O*C*C), 57.23 (CH$_2$N),

117.71 (H$_2$*C*=C), 135.65 (CH$_2$=*C*H), 173.14 (*C*=O);

Synthesis of 3-[allyl –[2-(2-amino-ethylcarbamoyl)-ethyl]-amino}-N- (2-amino-ethyl)-propionamide, G1-allyl-2NH$_2$, 32
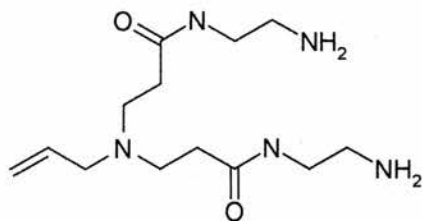
Ethane-1, 2-diamine (10 g, 0.166 mol) was added to a solution of **30** (10 g, 0.0436

mol) in methanol (50 cm^3) and stirred overnight. The solvent and excess amine was

removed under reduced pressure to leave colourless oil. ^{1}H NMR revealed that the

reaction was incomplete and that there was ethane-1, 2-diamine remaining within the

oil. The partially reacted product (9 g) was dissolved in methanol (50 cm^3) and a

further portion of ethane-1, 2-diamine (10 g, 0.166 mol) was added. This mixture

was left to stir for five days and worked up as previously leaving a clear oil. ^{1}H

NMR revealed that while the reaction was now complete, there was still ethane-1, 2-

diamine trapped within the oil. The product was dissolved in butan-1-ol in order to

displace the amine from the oil and the solvent removed under reduced pressure.

This was repeated until ^{1}H NMR indicated that no free amine was present in the

product, however butan-1-ol remained trapped making accurate calculation of the

yield impossible.

^{1}H NMR (CDCl$_3$, 300 MHz) δ_H: 2.2 (4H, t, NCH_2), 2.5 (4H, t, CH_2C=O), 2.5 (4H, m, CH_2NH$_2$), 2.9 (2H, d, CH_2N), 3.1 (4H, q, NHCH_2), 4.9 (2H, m, H_2C=), 5.6 (1H, m, =CH), 7.6 (2H, m, NHCH$_2$); ^{13}C NMR (CDCl$_3$, 70 MHz) δ_C: 34 (2C, NCH$_2$), 41 (2C, CH$_2$C=O), 42 (2C, NHCH$_2$), 45 (2C, CH$_2$NH$_2$), 49 (2C, CH$_2$N), 57 (=CHCH$_2$N), 118 ($H_2$$C$=), 134 (=$C$H), 173 (2C, C=O); CHN Elemental Analysis Found: C 55.00, H 11.27, N 19.57; Calculated for C$_{13}$H$_{27}$N$_5$O$_2$: C 54.71, H 9.54, N 24.

Additional signals were found in the NMR spectra corresponding to butan-1ol in quantitative amounts: ^{1}H NMR δ_H: 0.75 (3H, t, CH_3), 1.18 (2H, m, CH$_3$CH_2), 1.35 (2H, m, CH_2CH$_2$OH), 1.9 (1H, s, broad, OH), 3.38 (2H, t, CH_2OH); ^{13}C NMR δ_C: 13.92 (CH$_2$OH), 19.09 (CH$_2$CH$_2$OH), 34.89 (CH$_3$$CH_2$), 62.30 ($CH_3$).

3-[(2-{3-[allyl- (2-{2-[bis- (2-methoxycarbonyl-ethyl)-amino]-ethylcarbamoyl}-ethyl)-amino]-propionylamino}-ethyl)-(2-methoxycarbonyl-ethyl)-amino]-propionic acid methyl ester, G2-allyl-4COOMe, 33
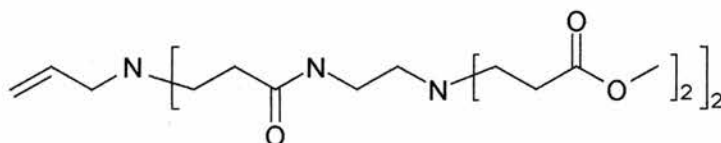
Methyl acrylate (16 cm^3, 0.178 mol) was added to a solution of **32** (10 g, approx. 0.0350 mol) in methanol (50 cm^3) and stirred overnight. The solvent and excess methyl acrylate were removed under reduced pressure leaving the product, **33**, colourless oil, yield: 20.5 g

^{1}H NMR (CDCl$_3$, 300 MHz), δ_H: 2.34 (12 H, m, NCH_2), 2.45 (4H, t, CH$_2$CH_2N), 2.7 (12H, m, CH_2O), 3.1 (2H, d, CHCH_2N), 3.2 (4H, q, NHCH_2), 3.6 (12H, s, OCH_3), 5.05 (2H, t, CH_2CH), 6.75 (1H, m, CH$_2$CH), 7.1 (2H, m, NH); ^{13}C NMR (CDCl$_3$, 70 MHz), δ_C: 32 (2C, CH$_2$CON), 33 (4C, NCH$_2$$CH_2$COO), 37 (2C, CONH$CH_2$), 49.5 (2C, N$CH_2$), 50 (4H, CH$_2$CO), 51.5 (4C, OCH$_3$), 52 (2C, CH$_2$N), 59(CH$_2$N), 118

(CH_2=), 135 (=CH), 172 (2C, C=O), 173 (4C, C=O); CHN Elemental Analysis

Found: C 54.02, H 8.80, N 11.47; Calculated for $C_{29}H_{51}N_5O_{10}$: C 55.31, H 8.16, N

11.12.

3-[(2-{3-[allyl- (2-{2-[bis- (2-ethoxycarbonyl-ethyl)-amino]-ethylcarbamoyl}-ethyl)-amino]-propionylamino}-ethyl)-(2-ethoxycarbonyl-ethyl)-amino]-propionic acid ethyl ester, G2-allyl-4COOEt, 34

Ethyl acrylate (2.94 g, 0.035 mol) was added to a solution of 31 (2.0 g, approx. 7

mmol) in methanol (100 cm³) and stirred overnight. The solvent and excess ethyl

acrylate were removed under reduced pressure leaving the product, **34**, colourless oil,

yield: 3.75 g

^{1}H NMR (300 MHz, CDCl$_3$), δ_H: 1.2 (12H, t, CH$_2$CH_3), 2.25 (12H, m, NCH_2), 2.45

(4H, t, CH$_2$CH_2N), 2.7 (12H, m, CH_2CO), 3.1 (2H, d, CHCH_2N), 3.25 (4H, t,

NHCH_2), 4.1 (8H, q, OCH_2), 5.1 (2H, t, CH_2CH), 5.75 (1H, m, CH$_2$CH), 7.2 (2H, br

s, NH); ^{13}C NMR (CDCl$_3$, 70 MHz), δ_C: 14.5 (4C, CH$_3$), 33.1 (2C, CH$_2$CON), 33.8

(4C, NCH$_2$$CH_2$COO), 37.4 (2C, CONH$CH_2$), 48.9 (2C, N$CH_2$), 49.5 (4H, CH$_2$CO),

50.0 (4C, OCH$_3$), 52.6 (2C, CH$_2$N), 60.62 (CH$_2$N), 118.3 (CH$_2$=), 134.8 (=CH),

172.8 (2C, C=O), 172.9 (4C, C=O);

3-[(2-{3-[allyl- (2-{2-[bis- (2-tert-butoxycarbonyl-ethyl)-amino]-

ethylcarbamoyl}-ethyl)-amino]-propionylamino}-ethyl)-(2-tert-butoxycarbonyl-

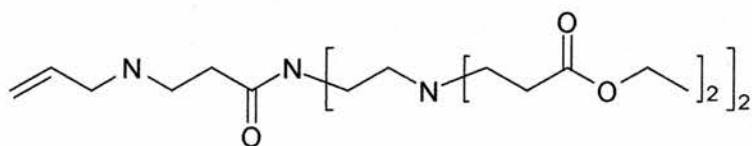**ethyl)-amino]-propionic acid tert-butyl ester, G2-allyl-4COO^tBu, 35**
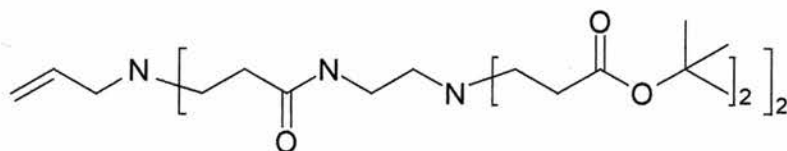
Tertiary-butyl acrylate (5.13 g, 0.04 mol) was added to a solution of 31 (2.1 g, 7.36

mmol) in methanol (100 cm^3) and stirred overnight. The solvent and excess t-butyl

acrylate were removed under reduced pressure leaving the product, **35**, colourless oil,

yield: 5.3 g,

^{1}H NMR (300 MHz, CDCl$_3$), δ_H: 1.35 (36H, s, C (CH_3)$_3$), 2.25 (12H, m, NCH_2),

2.45 (4H, t, CH$_2$CH_2N), 2.65 (12H, m, CH$_2$CO), 3.15 (2H, d, CHCH_2N), 3.3 (4H, t,

NHCH_2), 5.1 (2H, t, CH_2CH), 5.75 (1H, m, CH$_2$CH); ^{13}C NMR (70 MHz, CDCl$_3$,),

δ_C: 28.45 (12 C, CCH$_3$), 34.1(4C, NCH$_2$CH$_2$COO), 34.2 (2C, CH$_2$CON), 37.63 (2C,

CONHCH$_2$), 49.5 (2C, NCH$_2$), 50.2 (4H, CH$_2$CO), 53.5 (2C, CH$_2$N), 57.5 (CH$_2$N),

119 (CH$_2$=), 131 (4C, CC) 134(=CH), 172.1 (2C, C=O), 172.5 (4C, C=O).

Attempted synthesis of G1-allyl-2COOH, 36
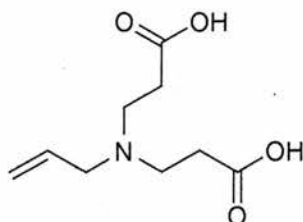
Method 1: - direct addition of acrylic acid

Allylamine (5 g, 0.088 mol) was dissolved in methanol (50 cm^3). Acrylic acid

(13.69 g, 0.19 mol) was added slowly resulting in an exothermic reaction being

observed. The reaction was stirred for 24 hours at room temperature and the

volatiles were removed under reduced pressure leaving a colourless oil.

References for Chapter 7 begin on page 295

^{1}H NMR showed many overlapping signals that was too complicated to be interpreted accurately.

Method 2:

30 (5 g, 0.0218 moles) was dissolved in methanol (50 cm^3). Aqueous sodium hydroxide (22 cm^3, 2 M solution) was added drop-wise resulting in an exothermic reaction. The mixture was stirred vigorously for three hours. Saturated sodium hydrogen carbonate solution was added followed by chloroform. The organic layer was extracted and concentrated under reduced pressure. A white precipitate was formed but gave no signal in ^{1}H NMR. The aqueous layer was extracted with ethyl acetate and the combined ethyl acetate layers dried over anhydrous magnesium sulfate. Removal of the volatiles left nothing to analyse.

Attempted synthesis of G1-POSS-16COOMe dendrimer by Condensation, 37
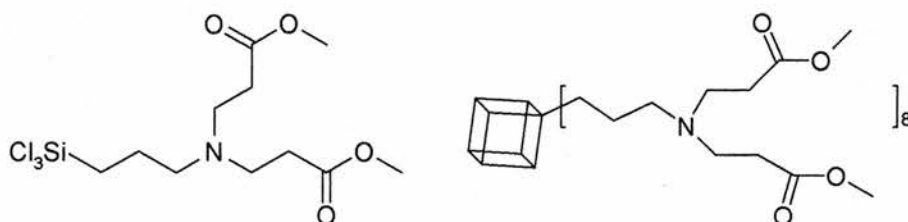
30 (0.0377 mol, 7.726 g) was dissolved in dry propan-2-ol (40 cm^3) and Karstedt's catalyst was added (0.2 cm^3, 0.1 M solution in xylenes). Trichlorosilane (4.55 cm^3, 6.10 g, 0.045 mol) was added slowly, the mixture refluxed for 6 hours before the solution allowed to cool and stir overnight. The solvent and excess silane was removed under reduced pressure and the resulting yellow oil dissolved in acetone (200 cm^3). Water (10 cm^3) was added drop-wise over 30 minutes, the mixture stoppered and left to stir. White solids were observed forming in the flask but these dissolved upon agitation. The kinetics of reaction are likely to be very slow and so this reaction has been left to stand for as long as possible.

Attempted synthesis of G1-POSS-16COOMe by Hydrosilation, 37
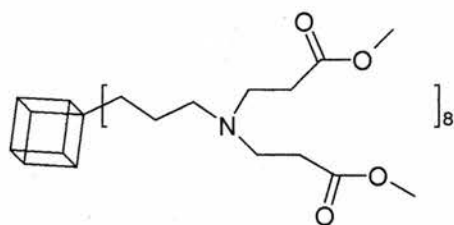
Method 1:

H_8T_8 (0.53 g, 1.25 mmol) was dissolved in isopropanol (30 cm^3). **30** (4.2 g, 18.3 mmol) was dissolved in isopropanol (10 cm^3) and added drop-wise via syringe. After addition of **30** was complete, Karstedt's catalyst (0.2 cm^3, 0.1 M solution in xylenes) was added. The mixture was refluxed for eight hours and allowed to cool and stir overnight. One flake of triphenylphosphine was added to deactivate the catalyst and the reaction mixture poured on to a small pad of celite. The celite pad was washed with copious amounts of isopropanol followed by DCM but no product was retrieved. ^{1}H NMR of the crude product was carried out. NMR DATA

Method 2[49]:

30 (1.38 g, 6.00 mmol) was dissolved in toluene (20 cm^3) and Karstedt catalyst (0.1 cm^3, 0.1 M solution in xylenes) added. The solution was gently aerated via syringe for 1 minute. H_8T_8 (0.25 g, 0.59 mmol) was dissolved in toluene (20 cm^3) and added in small portions over four hours. The reaction mixture was stirred at room temperature for 72 hours. One flake of triphenylphosphine was added to deactivate the catalyst and the solvent removed under reduced pressure. ^{1}H NMR of the crude product indicated no reaction had occurred.

Attempted synthesis of G1-POSS-16NH₂ dendrimer, 38
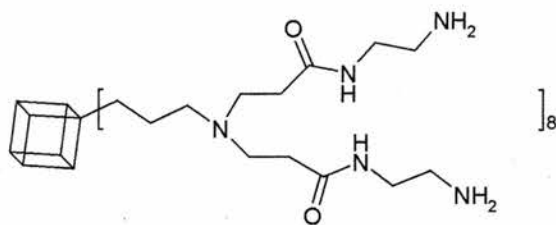
Method 1:

H_8T_8 (0.5 g, 1.18 mmol) and **31** (3.37 g, approx. 11.8 mmol) were dissolved in

isopropanol (50 cm³). Karstedt's catalyst was added (0.2 cm³, 0.1 M in xylenes) and

the mixture stirred overnight before being refluxed for 8 hours. A further portion of

Karstedt's catalyst (0.2 cm³, 0.1 M solution in xylenes) was added and the mixture

again stirred overnight, refluxed for 8 hours and allowed to cool to room temperature

leaving a yellow solution with some solid material present. One flake of

triphenylphosphine was added to neutralise the catalyst and the reaction mixture

decanted on to a small pad of celite. The celite was washed with copious amounts of

isopropanol and when that yielded no product, large volumes of DCM were used

which was also unsuccessful. A small quantity of material was isolated from the

reaction flask, which was insoluble in common organic solvents and looked like a

polymer gel.

Method 2:

H_8T_8 (0.5 g, 1.18 mmol) and **31** (3.37 g, approx. 11.8 mmol) were dissolved in

isopropanol (50 cm³). Speier's catalyst was added (0.2 cm³, 0.01 M solution in

propan-2-ol) and the mixture stirred at room temperature for 3 days. At this point,

the mixture had obviously formed a polymer gel, which was insoluble in DCM,

methanol and DMF. No further analysis could be attempted.

Attempted synthesis of G2-POSS-32COOMe Dendrimer, 39
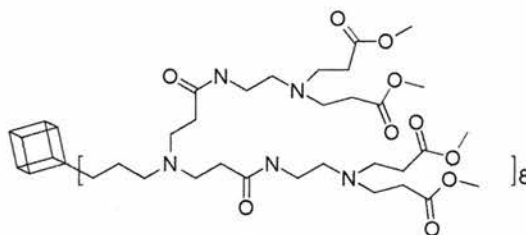
H_8T_8 (0.432 g, 0.686 mmol) and **33** (5.8 g, 9.2 mmol) were added to isopropanol (50 cm^3) and stirred for 1 hour. The reactants appeared to have dissolved successfully and Karstedt catalyst (0.3 cm^3, 0.1 M solution in xylenes) was added drop-wise via syringe. The mixture was heated to reflux for 6 hours, stirred at room temperature overnight, heated to reflux for 8 hours and again stirred at room temperature overnight by which point a solid was visible in the bottom of the flask. The reaction mixture was decanted from this product, loaded onto a short silica column, and eluted with isopropanol. The product appeared to stick on the column and an attempt was made to flush the column through with DCM, which was also unsuccessful. The solids left in the reaction flask were insoluble in a variety of solvents and appeared polymeric in nature.

Synthesis of G1-triethoxysilane-2COOMe, 40
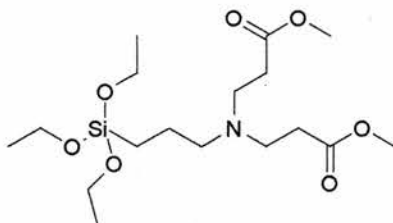
Aminopropyltriethoxysilane (15 cm^3, 0.0641 mol) was added drop-wise to a mixture of methanol (100 cm^3) and methyl acrylate (12 cm^3, 0.13 mol). The mixture was stirred overnight then the volatiles were removed under reduced pressure to give a clear liquid, yield: 23.21 g, 92 %

^{1}H NMR (CDCl$_3$, 300 MHz) δ$_H$: 0.4 (t, 2H, SiC*H$_2$*), 1.05 (t, 9H, C*H$_3$*CH$_2$), 1.35 (quin, 2H, SiCH$_2$C*H$_2$*), 2.2 (t, 2H C*H$_2$*N), 2.25 (t, 4H, NC*H$_2$*), 2.6 (t, 4H, C*H$_2$*CO), 3.55 (s, 6H, OC*H$_3$*), 3.75 (q, 6H, C*H$_2$*O); ^{13}C NMR (CDCl$_3$, 75 MHz,) δ$_C$: 7.92 (Si*C*H$_2$), 18.50 (*C*H$_3$CH$_2$O), 20.56 (SiCH$_2$*C*H$_2$), 32.82 (N*C*H$_2$), 49.52 (*C*H$_2$CO), 51.60 (O*C*H$_3$), 56.79 (*C*H$_2$N), 58.56 (*C*H$_2$O), 173.71 (*C*=O);

FTIR cm^{-1} 2974, s, (SiO); 2810, s, (CH$_2$); 2750, m, (NCH$_2$); 1740 (C=O, s),1450; s, 790, s, (Si-O);

Attempted synthesis of G1-POSS-16COOMe, 37
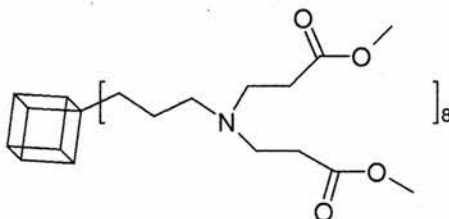
40 (20 g, 0.051 mol) was dissolved in ethanol (250 cm^3). Concentrated hydrochloric acid (20 cm^3, 37 % aqueous solution) was added drop-wise over one hour. The mixture was stirred at room temperature for one month left to stand at –30 °C for 8 weeks. No solid formed but the mixture became biphasic with a white lower layer

believed to be the silane and a clear yellow upper layer. The mixture was then

warmed to room temperature and stirred vigorously for a further 2 months.

Synthesis of G1-triethoxysilane-2COO^{t}Bu, 41
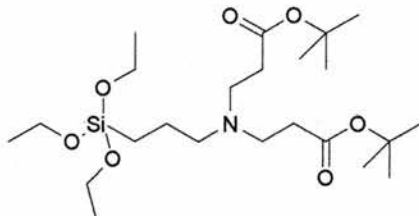
Aminopropyltriethoxysilane (15 cm^3, 0.0641 mol) was added drop-wise to a mixture

of methanol (100 cm^3) and tertiary butyl acrylate (19 cm^3, 0.13 mol). The mixture

was stirred overnight then the volatiles were removed under reduced pressure to give

a clear liquid, yield 27.95 g, 91.3 %.

^{1}H NMR (CDCl$_3$, 300 MHz) δ_H: 0.45 (t, 2H, SiCH_2), 1.05 (t, 9H, CH_3CH$_2$), 1.3 (s,

12H, C (CH_3)$_3$), 1.4 (quin, 2H, SiCH$_2$CH_2), 2.25 (t, 4H, NCH_2), 2.3 (t, 2H CH_2N),

2.65 (t, 4H, CH_2CO), 3.8 (q, 6H, CH_2O); ^{13}C NMR (CDCl$_3$, 75 MHz) δ_C: 7.92

(SiCH$_2$), 18.59 (CH$_3$CH$_2$O), 20.88 (SiCH$_2$$CH_2$), 28.37 (C$CH_3$), 34.13 (N$CH_2$), 49.68

(CH$_2$CO), 56.91 (CH$_2$N), 58.57 (CH$_2$O), 80.36 (CCH$_3$), 172.34 (C=O).

FTIR cm^{-1} 2970, s, (CH$_2$); 2750, m, (NCH$_2$);1740,s, (C=O); 790 (Si-O, s);

Attempted synthesis of G1-POSS-16COO^{t}Bu, 42

41 (26.71 g, 0.0559 mol) was dissolved in methanol (260 cm^3). Concentrated hydrochloric acid (20 cm^3, 37 % aqueous solution) was added drop-wise during which an exothermic reaction was observed and the mixture left to stir at room temperature for one month. The reaction vessel was then transferred to the freezer and allowed to stand for a further 8 weeks but no crystallisation was observed. The reaction was then warmed to room temperature and stirred vigorously for a further 2 months during which time no crystallisation was observed.

Synthesis of various PAMAM dendrons was very successful using allylamine and aminopropyltriethoxysilane as starting points. This led to the formation of several new compounds. Initial attempts at hydrosilation were moderately successful with crude product NMR revealing some reaction had taken place. More work is required to perfect the reaction conditions and the purification techniques, particularly of the G2-PAMAM branches. Possible routes for the failure of some of the hydrosilation reactions were identified, mainly to do with the action of bases on the POSS cube or promoting the addition of alcohols to Si-H.

Characterisation of all molecules produced was attempted although this was made difficult by the similar signals of G2 branches in ^{1}H and ^{13}C NMR and the presence of impurities such as methanol, 1,2-diaminoethane and butanol. These are known difficulties with the synthesis of dendrimers, particularly PAMAM dendrimers. The synthesis of branches from aminopropyltriethoxysilane was also successful but as yet there are no results from the condensation reactions because of the long time scales of these reactions.

7.4 Conclusions and Further Work

The attempted convergent synthesis of POSS dendrimers has been moderately
successful with several new dendritic branches being synthesised. Unfortunately
attaching the branches was not as straight forward as envisioned and often resulted in
polymeric products.

Fréchet type dendrons were initially thought to offer good potential as catalytic
supports but with further consideration of the reactions required, it was not thought
possible to attach PPh$_2$ units to the terminal bromobenzyl groups. The route of using
a benzene derivative that already possessed hydrosilatable functional groups held
much promise but the difficulties of converting the methoxy group to phenol groups
meant that this work was unsuccessful.

PAMAM dendrimers offered more promise as they were chosen based on several
reports of having diphenylphosphine terminated branches, used as homogeneous and
heterogeneous catalysts. Synthesis of various branches was reasonably successful
but hydrosilation to H$_8$T$_8$ has yet to yield definitive results. The reaction conditions
are highly critical and would require much more work to perfect them.

Condensation of triethoxysilane PAMAM derivatives offers an interesting route to
convergent synthesis forming the POSS core in the final reactive step. The time
scales of such reactions may be long but may also offer a means to circumnavigate
the unstable nature of aminopropylPOSS in both its octahydrochloride and free
amine form.

7.5 References

1. E. Muller and F. T. Edelmann, *Main Group Metal Chemistry*, 1999, **22**, 485.

2. P. A. Jaffres and R. E. Morris, *J. Chem. Soc., Dalton Trans.*, 1998, 2767.

3. P. I. Coupar, P. A. Jaffres and R. E. Morris, *J. Chem. Soc., Dalton Trans.*, 1999, 2183.

4. X. J. Zhang, K. J. Haxton, L. Ropartz, D. J. Cole-Hamilton and R. E. Morris, *J. Chem. Soc., Dalton Trans.*, 2001, 3261.

5. L. Ropartz, D. F. Foster, R. E. Morris, A. M. Z. Slawin and D. J. Cole-Hamilton, *J. Chem. Soc., Dalton Trans.*, 2002, 1997.

6. L. Ropartz, K. J. Haxton, D. F. Foster, R. E. Morris, A. M. Z. Slawin and D. J. Cole-Hamilton, *J. Chem. Soc., Dalton Trans.*, 2002, 4323.

7. L. Ropartz, R. E. Morris, D. F. Foster and D. J. Cole-Hamilton, *Chem. Commun.*, 2001, 361.

8. L. Ropartz, R. E. Morris, D. F. Foster and D. J. Cole-Hamilton, *J Mol Catal A-Chem*, 2002, **182**, 99.

9. L. Ropartz, R. E. Morris, G. P. Schwarz, D. F. Foster and D. J. Cole-Hamilton, *Inorg Chem Commun*, 2000, **3**, 714.

10. F. J. Feher and K. D. Wyndham, *Chem. Commun.*, 1998, 323.

11. B. Hong, T. P. S. Thoms, H. J. Murfee and M. J. Lebrun, *Inorg. Chem.*, 1997, **36**, 6146.

12. H. J. Murfee, T. P. S. Thoms, J. Greaves and B. Hong, *Inorg. Chem.*, 2000, **39**, 5209.

13. I. M. Saez and J. W. Goodby, *J. Mater. Chem.*, 2001, **11**, 2845.

14. I. M. Saez, J. W. Goodby and R. M. Richardson, *Chem. Eur. J.*, 2001, 7, 2758.

15. S. Grayson and J. Frechet, *Chem. Rev*, 2001, **101**, 3819.

16. J. M. J. Frechet and C. J. Hawker, *React Funct Polym*, 1995, **26**, 127.

17. J. M. J. Frechet, C. J. Hawker, I. Gitsov and J. W. Leon, *J. Macromol. Sci., Chem.*, 1996, **A33**, 1399.

18. J. M. J. Frechet, C. J. Hawker and K. L. Wooley, *J. Macromol. Sci., Chem.*, 1994, **A31** , 1627.

19. C. J. Hawker, K. L. Wooley and J. M. J. Frechet, *J. Chem. Soc., Chem. Commun.*, 1994, 925.

20. Coolen Hkac, J. A. M. Meeuwis, Vanleeuwen Pwnm and R. J. M. Nolte, *J. Am. Chem. Soc.*, 1995, **117**, 11906.

21. M. V. Bhatt and S. S. Elmorey, *Synthesis-Stuttgart*, 1982, 1048.

22. X. Camps, H. Schonberger and A. Hirsch, *Chem. Eur. J.*, 1997, **3**, 561.

23. V. W. Day, W. G. Klemperer, V. V. Mainz and D. M. Millar, *J. Am. Chem. Soc.*, 1985, **107**, 8262.

24. S. Lucke and K. Stoppek-Langner, *Appl. Surf. Sci.*, 1999, **145**, 713.

25. S. Lucke, K. Stoppek-Langner, J. Kuchinke and B. Krebs, *J. Organomet. Chem.*, 1999, **584**, 11.

26. A. R. Bassindale and T. Gentle, *J. Organomet. Chem.*, 1996, **521**, 391.

27. E. C. Taylor, R. P. Chaudhuri and S. E. Watson, *Tetrahedron*, 1999, **55**, 1631.

28. U. Dittmar, B. J. Hendan, U. Florke and H. C. Marsmann, *J. Organomet. Chem.*, 1995, **489**, 185.

29. H. I. Beerens, P. Wijkens, J. T. H. B. Jastrzebski, F. Verpoort, L. Verdonck and G. Van Koten, *J. Organomet. Chem.*, 2000, **603**, 244.

30. A. R. Bassindale and T. E. Gentle, *J. Mater. Chem.*, 1993, **3**, 1319.

31. Z. L. Zhou, F. Wang and X. P. Cao, *Chinese Journal of Chemistry*, 2003, **21**, 1636.

32. C. J. Hawker and J. M. J. Frechet, *J. Am. Chem. Soc.*, 1990, **112**, 7638.

33. C. Hawker and J. M. J. Frechet, *J. Chem. Soc., Chem. Commun.*, 1990, 1010.

34. B. Jursic, *Tetrahedron*, 1988, **44**, 6677.

35. A. P. H. J. Schenning, J. D. Arndt, M. Ito, A. Stoddart, M. Schreiber, P. Siemsen, R. E. Martin, C. Boudon, J. P. Gisselbrecht, M. Gross, V. Gramlich and F. Diederich, *Helv. Chim. Acta*, 2001, **84**, 296.

36. A. Ozanne, L. Pouysegu, D. Depernet, B. Francois and S. Quideau, *Org Lett*, 2003, **5**, 2903.

37. S. Setayesh, A. C. Grimsdale, T. Weil, V. Enkelmann, K. Mullen, F. Meghdadi, E. J. W. List and G. Leising, *J. Am. Chem. Soc.*, 2001, **123**, 946.

38. M. S. Diallo, L. Balogh, A. Shafagati, J. H. Johnson, W. A. Goddard and D. A. Tomalia, *Environ. Sci. Technol.*, 1999, **33**, 820.

39. R. Esfand and D. A. Tomalia, *Drug Discovery Today*, 2001, **6**, 427.

40. H. Alper, *Abstr. Pap. Am. Chem. S*, 2001, **221**, 4-INOR.

41. R. O. R. Costa, W. L. Vasconcelos, R. Tamaki and R. M. Laine, *Macromolecules*, 2001, **34**, 5398.

42. S. M. Lu and H. Alper, *J. Am. Chem. Soc.*, 2003, **125**, 13126.

43. H. Alper, P. Arya, S. C. Bourque, G. R. Jefferson and L. E. Manzer, *Can J Chem*, 2000, **78**, 920.

44. A. J. Gong, Q. H. Fan, Y. M. Chen, H. W. Liu, C. F. Chen and F. Xi, *J Mol Catal A-Chem*, 2000, **159**, 225.

45. Y. M. Chung and H. K. Rhee, *Catal. Lett.*, 2002, **82**, 249.

46. Y. Miyahara, K. Goto and T. Inazu, *Synthesis-Stuttgart*, 2001, 364.

47. H. Mori, M. G. Lanzendorfer, A. H. E. Muller and J. E. Klee, *Macromolecules*, 2004, **37**, 5228.

48. P. R. Dvornic, C. H. Thompson, S. E. Keinath and E. J. Hill, *Macromolecules*, 2004, Advance Article.

49. G. H. Mehl and J. W. Goodby, *Angew. Chem., Int. Ed. Engl.*, 1996, **35**, 2641.

References for Chapter 7 begin on page 295

Chapter 8. Synthesis of Silicates

8.1 Introduction

Tetramethylammoniumsilicate (TMAsilicate) has been widely synthesised and characterised by many researchers. It has also been used to form $Q_8M_8^H$ and $Q_8M_8^{Vi}$, direct analogues of H_8T_8 and Vinyl POSS and used in a similar manner. There are fewer reports of silicate cubes functionalised with larger organosilicon derivatives, or other species. $Q_8M_8^H$ has been used as an alternative to H_8T_8 for the synthesis of dendrimers including dendritic liquid crystals[1,2] and vinyl POSS equivalent has been also reported as a core for divergent synthesis of a ferrocene terminated dendrimer[3].

One aim of this work is to investigate the synthesis of silicate cubes and derivatives to assess if they are viable alternatives to H_8T_8 and vinyl POSS for dendrimer cores, and to see if reaction of these cubes with other chlorosilanes can lead to more unusual cores.

Figure 8.1: Metal Organic Framework precursors synthesised from vinyl POSS and TMAsilicate illustrating the more rigid structure produced by the use of TMAsilicate. G is a generic substituent

Metal organic frameworks can be synthesised using di-, tri- and even tetra-functionalised molecules such as benzene dicarboxylic acids but the essential feature is the rigidity of the species used. Reliance on hydrosilation to attach suitable groups to vinyl or H_8T_8 inevitably creates a minimum of a flexible ethyl link between cube and group (figure 8.1). A functionalised silicate could be a route around this problem, creating a shorter, more rigid link like Si-O-Si. The

second aim of this work is to assess the feasibility of functionalising TMAsilicate

with large chlorosilanes such as those derived from bromobenzaldehyde.

Finally, the reactivity of the silicate anion is investigated through preliminary

studies into reactions with chlorodiphenylphosphine. Again, this was to produce a

rigid building block for synthesis of extended networks, or as an alternative to

octa(diphenylphosphinoethyl)$_8$T$_8$ as a dendrimer core[4].

8.2 Silicate Synthesis

8.2.1 Introduction

Silsesquioxanes such as H$_8$T$_8$ or vinyl POSS are obtained in low yields from long

synthetic processes. More rapid synthesis of a suitable POSS-like molecule with

either vinyl or proton groups capable of undergoing hydrosilation in higher yields

is a desirable goal. Q$_8$M$_8$^{H} and Q$_8$M$_8$^{Vi} can be used in a similar manner to the

octahydrido and octavinyl POSS and participate in hydrosilation reactions. The

main advantage of these molecules is typical yields over two reaction steps is in

the region of 80 %, when compared to 20 % for silsesquioxanes[5].

TMAsilicate is also investigated for metal-organic framework synthesis (section

8.3). To this end, the reaction of TMAsilicate with larger chlorosilanes were

investigated. Bulky substituents such as phenyl groups were chosen for this work

as one potential target for MOF synthesis are derivatives of benzaldehyde. An

attempt was made to synthesise both di- and tri- phenyl functionalised

octasilicates. Divergent dendrimer synthesis has begun from vinyl POSS and

branch points (increased multiplicity of terminal groups) added through

hydrosilation of chlorosilanes. The reaction of chlorotrivinylsilane and TMA

silicate was attempted to create a core with far more reactive groups that are closer to the cubic core than could be achieved using POSS chemistry.

8.2.2 Results and Discussion

TMA silicate (TMAsilicate, **43**) was synthesised simply from a silicon source and TMA hydroxide. This reaction could be carried out in two ways. The first through reaction of tetraethoxysilane and TMA hydroxide[6], and the second by reflux of silicic acid and TMA hydroxide[3]. The first method was used because it was more straightforward. This was reasonably successful although it was not possible to record accurate yields due to the various crystal forms. The molecular mass of the silicate cage and counter ions is 1137.85 gmol[-1], but is usually found as a hydrate[7].

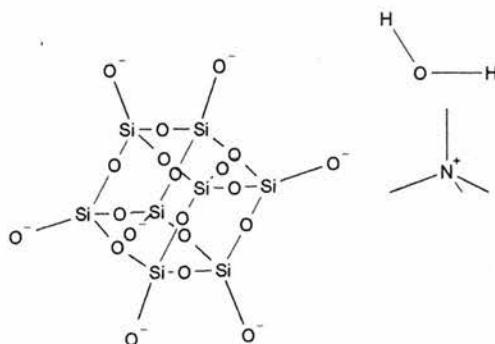**Figure 8.2:** Tetramethylammoniumsilicate with only one TMA counter ion and one water molecule for clarity.

Three crystal structures have been reported to date containing 67, 69 or 116 water molecules making the molecular masses vary from 2344.86 g/mol to 3956.84 g/mol[6,7]. Once the solution containing the product was concentrated, crystals formed readily although for some reactions the solution was required.

$$\text{a.} \quad [Si_8O_{20}]^{8-} + (8+x)\,R_3SiCl \rightarrow Si_8O_{20}\,(SiR_3)_8 + x/2\,R_3SiOSiR_3$$

$$\text{b.} \quad 8[NCH_3)_4]^- + (8+x)R_3SiCl \rightarrow 8N(CH_3)_4Cl + xHCl$$
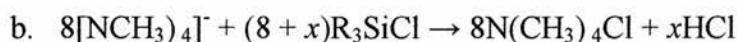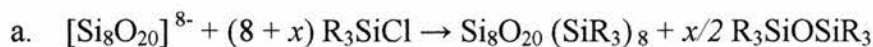
Figure 8.3: Two equations showing general reaction of the silicate cube (a) and side reaction of the tetramethylammonia cation (b). An excess of chlorosilane is generally used and forms a disiloxane when the reaction is quenched with water, along with hydrochloric acid.

TMAsilicate can be readily functionalised by reaction with chlorosilanes and a large excess must be used to ensure complete reaction at the silicate sites. The water molecules present within the crystal structures cause some issues with these types of reactions, as chlorosilanes tend to react with water to form disiloxane species. Indeed water is added to quench the reaction deliberately to remove any unreacted chlorosilanes. The TMAsilicate solution is sometimes used for these reactions allowing the quantity of water present to be calculated. In the case of trimethylchlorosilane and dimethylchlorosilane, the disiloxanes formed are liquids and easily separated from the required product but in the case of triphenylchlorosilane, the corresponding disiloxane is a solid and may even be formed preferentially over reaction with the silicate. In all attempts to make $Q_8M_8{}^{Ph3}$ (**49**) it was not possible to separate the disiloxane from the octamer. XRD found the sample to be the disiloxane although ^1H-^{29}Si Cross Polarisation Magic Angle Spinning NMR indicated the presence of Q silicons (silicate). It has been reported that the octamers have lower solubility than other related species and so crystallise selectively or are left behind during recrystallisation. This has not been found to happen with this reaction.

The synthesis of Q_8M_8 (**44**) proceeded well and was carried out to perfect conditions for reactions of other chlorosilanes and TMASi and to produce a crystalline solid for use as a solid state NMR standard.

$Q_8M_8{}^H$ (**45**) was synthesised as an alternative to H_8T_8. The synthetic procedure was reported to be quicker and higher yielding than H_8T_8 without the chance of

forming an $H_{10}T_{10}$ equivalent. This was not found to be the case as it was difficult to calculate how much chlorodimethylsilane was required for the reaction, due to the inexact mass of TMASi being used. Despite a solid product being produced by reactions, it was difficult to separate TMA chloride from the other products.
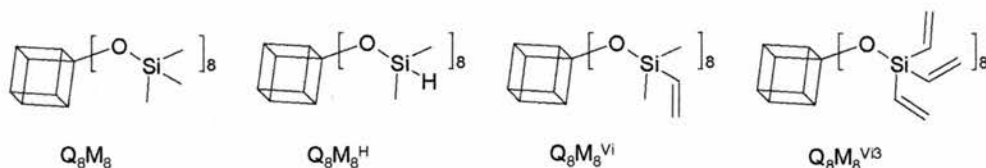
Figure 8.4: Structures of several TMAsilicate derivatives synthesised.

Attempts to synthesise $Q_8M_8^{Vi3}$ (**47**) were unsuccessful. The desired product could not be separated from the corresponding disiloxane and TMA chloride. A similar outcome was found for $Q_8M_8^{Ph2}$ (**48**).

The synthesis of $Q_8M_8^{Vi}$ (**46**) was also found to be harder than suggested by literature and while a solid product was obtained, all attempts to recrystallise it failed and nothing useable could be obtained. No further attempts were made to synthesise this because of the ease synthesising Vinyl POSS and the purity in which it is obtained.

8.2.3 Experimental Details

Typical Synthesis of octakis (tetramethylammonium) pentacyclo

[9.5.1.13,9.15,15.17,13] octasiloxane-1, 3,5,7,9,11,13,15-octakis (yloxide)

hydrate, TMAsilicate, 43
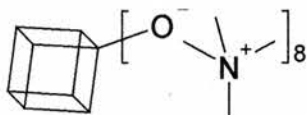
A mixture of TMAhydroxide (23 g), tetraethoxysilane (23 g), methanol (100 cm^3)

and water (20 cm^3) was allowed to stir for 24 hours. The mixture was

concentrated and allowed to stand. The crystals that formed were filtered out and

used as is, or dried in the oven before use. This method was scaled up as

appropriate. No yield can be measured due to three known crystal forms of

TMAsilicate each having a variable quantity of water trapped within the

structure[7].

Synthesis of Q$_8$M$_8$, 44[8]
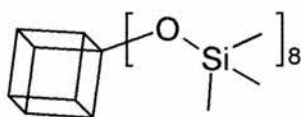
Method 1:

Tetramethylammoniumsilicate (60 g, freshly made, not dried) was dissolved in

DMF (200 cm^3) and hexane (150 cm^3). Chlorotrimethylsilane (50 cm^3, large

excess) was added drop-wise and the resulting mixture stirred overnight before

being cooled in an ice water bath and water added drop-wise. The organic layers

were separated and the aqueous layer further extracted with ether. The combined

organic extracts were dried over magnesium sulfate, concentrated and left to stand

to allow crystallisation to take place. The crystals were filtered off and washed

with a small portion of acetonitrile. A second crop was also filtered off.

Mpt: 284 – 286 °C; ^{1}H NMR (300 MHz, CDCl$_3$) δ_H: 0.1 (s, 72H, CH_3Si); ^{29}Si

NMR (solid state) δ_{Si}: two peaks around 12 (*Si*Me$_3$), four peaks in the range of –

108 to -110 (*Si*O$_4$)

The above data are in agreement with the literature[8,9]

Method 2:

Hydrochloric acid (20 cm^3, 37 % aqueous solution) was added to propan-2-ol (40

cm^3) which was added slowly to hexamethyldisiloxane (35 cm^3) and water (18

cm^3). The resulting mixture was stirred for 15 minutes before TMA silicate (5 g,

fresh) was added in small portions over 30 minutes and the resulting mixture

allowed to stir overnight. Water was added to quench the reaction and the organic

layers extracted with ether, dried over magnesium sulfate and concentrated before

being allowed to stand to allow crystallisation to take place. The crystals were

filtered off and washed with cold acetonitrile. ^{1}H NMR revealed them to be

Q$_8$M$_8$, **44**.

Synthesis of Q$_8$M$_8$^{H}, 45[8]
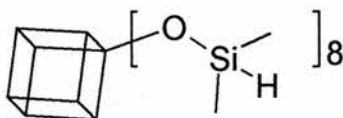
Method 1:

TMAsilicate (5 g, freshly synthesised) was dissolved in DMF (200 cm^3) and

pentane (100 cm^3). Chlorodimethylsilane (15 cm^3, large excess) was added drop-

wise and the mixture stirred overnight. Water was added to hydrolyse any

remaining chlorodimethylsilane and the organic layer extracted with ether. The

combined organic extracts were dried with magnesium sulfate and concentrated

before being left to stand to complete crystallisation. A small quantity of crystalline material was produced, filtered from solution and washed with cold acetonitrile.

Method 2

TMAsilicate (4.65 g, synthesised and dried overnight in oven) was dissolved in propan-2-ol (200 cm^3) under argon. Chlorodimethylsilane (10 cm^3) was added slowly and the mixture stirred for two hours, with argon purge before being stoppered and allowed to stir overnight. Water was added drop-wise and the organic layer extracted with ether, dried with magnesium sulfate and concentrated. A small quantity of semi-crystalline solid was produced.

^{1}H NMR: (300 MHz, CDCl$_3$) δ_H: 0.2 (s, 48 H, Si-CH_3), 4.75 (s, 1 H, Si-H)

The above data is in agreement with literature[8].

Synthesis of Q$_8$M$_8$^{Vi}, 46[8]
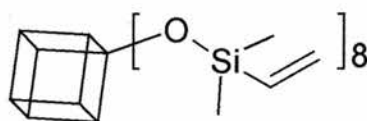
A solution of hydrochloric acid (10 g, 37 % aqueous solution) in propan-2-ol (40 cm^3) was prepared. TMAsilicate (2 g, as synthesised), propan-2-ol (50 cm^3) and chlorodimethylvinylsilane (5 g) was stirred until the solids had dissolved. Hydrochloric acid solution was added slowly and the resulting mixture allowed to stir for 2 hours. Water was added to hydrolyse any residual chlorosilane and a precipitate formed. The precipitate was partitioned between water and ether, the ether extracts dried with magnesium sulfate and concentrated. The concentrate was allowed to stand to allow crystallisation to take place.

^{1}H NMR (300 MHz, CDCl$_3$) δ_H: 0.1 (s, 48H, SiCH_3), 5.5 (d, 8H, =CH_2), 5.7 (d, 8H, =CH_2), 5.9 (t, 8H, CH=). The above data is in agreement with the literature[8].

Synthesis of $Q_8M_8^{Vi3}$, 47
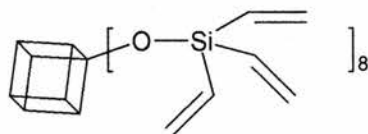
TMAsilicate (2 g, as synthesised), propan-2-ol (50 cm^3) and chlorotrivinylsilane (5 g, 0.034 mol, excess) were stirred together until the solids had dissolved. Hydrochloric acid solution (4 cm^3, as synthesised for **46**) was added slowly drop-wise and the resulting mixture allowed to stir overnight. Water was added to hydrolyse any residual chlorosilane and a precipitate formed. The precipitate was partitioned between water and ether, the ether extracts dried with magnesium sulfate and concentrated. The concentrate was allowed to stand to allow crystallisation to take place. No crystallisation occurred and a gel formed that polymerised over time.

Synthesis of $Q_8M_8^{Ph2}$, 48
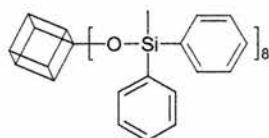
TMAsilicate (2.72 g, freshly made) was dissolved in DMF (200 cm^3) and hexane (100 cm^3). Chlorodiphenylmethylsilane (5 g, 0.0215 mol) was added in small portions and the resulting mixture stirred overnight. Water was added and the organic layers extracted with ether, dried over anhydrous magnesium sulfate, concentrated and allowed to stand. A semi-crystalline solid formed upon evaporation of the residual solvent.

Mpt: 32 – 36 °C (reported for dimer, 47- 50 °C [10]); ^{1}H NMR (300 MHz, CDCl$_3$)

δ_H: 0.45 (s, 3H, Si-CH_3); 7.2 – 7.3 (m, 6H, Ar-*H*); 7.4 (m, 4H, Ar-*H*)

Synthesis of $Q_8M_8^{Ph3}$, 49
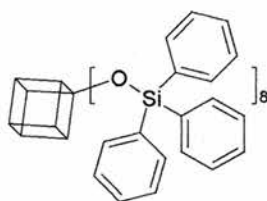
Method 1:

TMA Silicate (15.43 g, freshly made) was dissolved in DMF (250 cm^3) and hexane (100 cm^3). Chlorotriphenylsilane (14 g, large excess) was added and the mixture stirred overnight. Water was added and the organic layer separated. The aqueous layer was further extracted with ether and the combined organic extracts dried with magnesium sulfate before being concentrated, allowed to crystallise and filtered. A small portion of the crystals were recrystallised in acetonitrile and DCM.

Analysis of single crystals by single crystal xray diffraction at Daresbury indicated that the crystals were hexaphenyldisiloxane (M_2^{Ph3}), the dimer[11]. ^{1}H-^{29}Si Cross Polarisation Magic Angle Spinning NMR indicated the presence of a Q silicon signal in the region of -100 ppm in addition to a large signal for the M silicons of the dimer. It is not known whether this Q silicon signal was due to compound **49** being successfully synthesised or due to the presence of unreacted TMAsilicate (**45**). Mpt: 218 – 220 °C, literature melting point of dimer 226 °C[11].

^{1}H NMR (300 MHz, CDCl$_3$) δ_H: 7.3 (m, 3H, arom C-*H*), 7.6 (m, 2H, arom Si-C-C-*H*).

Method 2:

TMA silicate (2 g, as synthesised), propan-2-ol (50 cm^3) and chlorotriphenylsilane (3 g) was stirred until the solids had dissolved. Hydrochloric acid (4 cm^3, solution as per **46**) was added slowly drop-wise and the resulting mixture allowed to stir overnight. Water was added to hydrolyse any residual chlorotriphenylsilane and a

precipitate formed. The precipitate was partitioned between water and ether, the ether extracts dried with magnesium sulfate and concentrated. The concentrate was allowed to stand to allow crystallisation to take place. A small quantity of crystals formed, were filtered form solution and allowed to dry in air.

^{1}H NMR (CDCl$_3$, 300 MHz) δ_H: 7.0 – 7.4 (m, arom-*H*, 15H)

8.2.4 Conclusions

TMA silicate was successfully synthesised according to literature methods and used to produce Q_8M_8, $Q_8M_8^H$ and $Q_8M_8^{Vi}$, however the latter two were in low yields due to difficulties in obtaining a solid product. It was not felt that these molecules were a viable alternative to H_8T_8 and vinyl POSS and this work was not pursued.

The synthesis of $Q_8M_8^{Ph3}$ or $Q_8M_8^{Ph2}$ was of limited success due to difficulties in separating the disiloxane dimers from any octamers produced. The notion that the octamers should be less soluble did not seem to apply. It is possible that ^1H – 29Si CP MAS confirmed the existence of $Q_8M_8^{Ph3}$ through location of a Q silicon signal but despite a crystalline product, no single crystals of the octamer could be isolated for structural elucidation. It was not possible to isolate any samples of the octamer for analysis. $Q_8M_8^{Vi3}$ was also unsuccessful perhaps due to the bulky trivinyl substituents preferentially forming the corresponding disiloxane.

Initial studies into the attachment of larger groups to TMAsilicate have not been successful, but at the same time, following literature procedures for the synthesis of $Q_8M_8^H$ and $Q_8M_8^{Vi}$ have also proved difficult. If the reaction conditions could be optimised for the smaller chlorosilane reactions, it might be possible to be more successful with the larger ones such as chlorotriphenylsilane.

8.3 Metal Organic Frameworks

8.3.1 Introduction

Metal Organic Frameworks or Co-ordination Polymers are versatile materials usually made by careful design of ligating species, metal salts, and control of conditions such as temperature, pressure and solvents. These materials have many uses, including storage of gases, catalysis and others directly relating to their structure. Ideal organic precursors include iminodiacetic acid, and other amines or carboxylic acids. The metal salts most often complex with the carboxylic acid groups and the frameworks can include guest species such as solvent molecules or templating species. It is not always possible to remove the guest species without collapsing the structure.
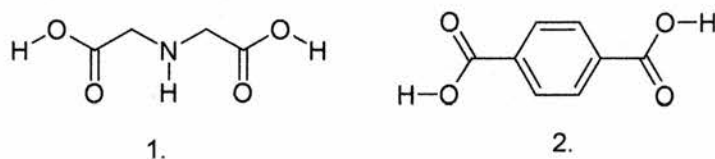
Figure 8.4: 1: iminodiacetic acid, 2: terephthalic acid. Building blocks for metal organic frameworks.

Metal Organic Frameworks incorporating POSS molecules offer a route to creating reticular structures from large precursors with multiple reactive sites. Ideally, the rigid structure of the POSS cube should be extended by rigid groups like phenylcarboxylic acids or amines. Long aliphatic chains are perceived to be less able to form ordered structures. To that end, attempts have been made to synthesise POSS cubes with aldehyde, carboxylic acid or diphenylphosphine functional groups. TMAsilicate has been chosen for this work as the Si-O-Si linkage formed through reaction with chlorosilanes is more rigid and shorter than the CH_2CH_2Si linkage formed by hydrosilation to H_8T_8 or vinyl POSS.

8.3.2 Carboxylic Acid Building Blocks

8.3.2.1 Introduction

Aldehyde and Carboxylic Acid functional groups are largely interchangeable but are quite difficult to incorporate into POSS molecules. A carboxylic acid functionalised POSS was a desirable synthetic target to create a rigid molecule with carboxylic acid functionality suitable for the synthesis of metal organic frameworks. Aldehydes and acids are difficult to hydrosilate directly to H_8T_8 for electronic reasons as short distances between the double bond and the carbonyl lead to competing O silylation, while long distances lead to less rigid structures that are less desirable. Fortunately the synthetic utility of aldehydes is widely exploited and many ways to protect them have been devised. The most rigid aldehyde is benzaldehyde and this is readily protected by reaction with ethylene glycol to form a dioxolane protecting group. Previous work has shown that it is possible to use bromobenzaldehyde to form a dioxolane, add an Si-H through Grignard chemistry then attach to the vinyl POSS through hydrosilation. This created a flexible POSS cube[12].
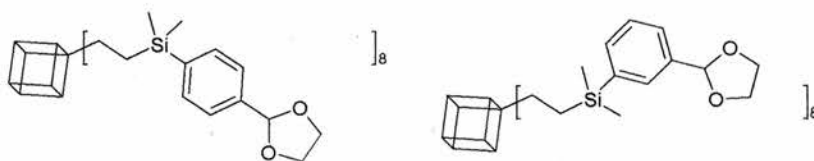
Figure 8.5: Protected benzaldehyde groups attached to POSS cubes through hydrosilation as reported by Manson *et al.* [12]. Starting materials are 4- or 3- bromobenzaldehyde.

Several approaches to attaching benzaldehyde group to the POSS cube are attempted. The reaction of TMAsilicate with chlorosilanes is exploited by attempting to functionalise the dioxolane with Si-Cl. This has been attempted either through conversion of Si-H to Si-Cl species or reaction with dichlorodimethylsilane or silicon tetrachloride followed by condensation.

8.3.2.2 Results and Discussion

Synthesis of the dioxolane (**50**) proceeded well from bromobenzaldehyde and it was found to crystallise in cold conditions. A similar molecule was commercially available and that was used for many reactions. Whereas the dioxolane would be converted directly to the aldehyde then acid, the commercially available dioxolane could be converted to the methyl ester, then aldehyde or acid (figure 8.6).
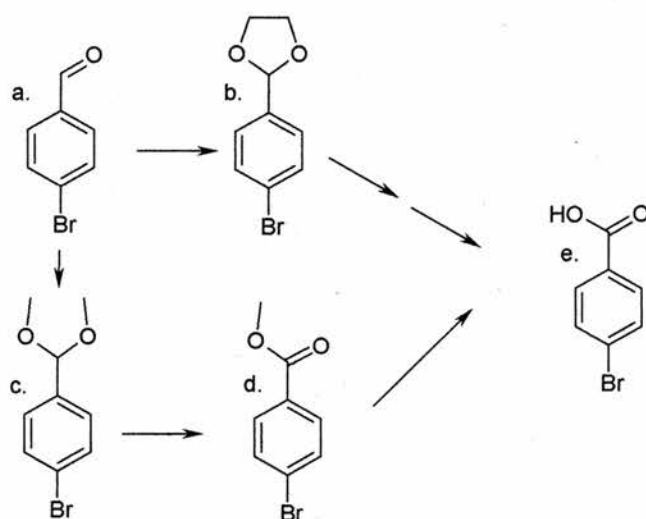
Figure 8.6: 4-Bromobenzaldehyde (a) and related structures 2-(4-bromophenyl)-[1,3]-dioxolane, **50** (b), commercially available 4-bromobenzene dimethylacetal (c) and partially oxidised derivative (d), and 4-bromobenzoic acid (d).

Three clear routes to the synthesis of benzaldehyde POSS cubes were attempted. Two utilised the reaction of chlorosilanes and TMAsilicate, and the third used condensation of trichlorosilanes. The protected benzaldehyde was formed into a Grignard reagent; RMgBr then reacted with a chlorosilane of some description. The reaction was found to go very rapidly if the magnesium was heated under argon first, often refluxing (in THF) under its own steam. The Grignard reagent was then used to react with chlorodimethylsilane resulting in the successful synthesis of **51** and **52**.

X = H (**51**), Cl   X = H (**52**), Cl
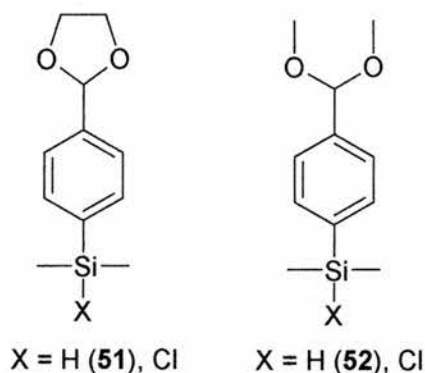
Figure 8.7: Compounds **51** and **52** and related chlorosilanes.

The attempted conversion of the terminal Si-H bond to Si-Cl by a variety of routes proved less than straightforward[13-18]. In order to characterise the products of such reactions, water was added to quench the reactions to form the corresponding disiloxane if the chlorosilane had formed. These reactions were to find a viable route for conversion of the Si-H to Si-Cl bond. ^{1}H NMR of the products of these reactions generally showed that the protecting groups were being partially removed by the chlorinating agents (particularly thionyl chloride[17]).
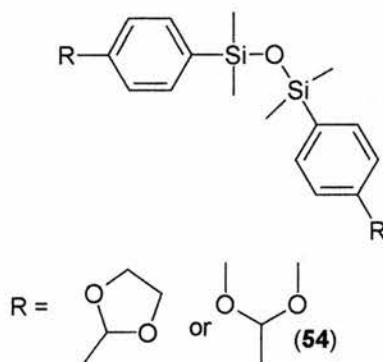
Figure 8.8: Disiloxane produced by reaction of water and chlorosilane (**54**).

This was not believed to be a great issue as the aldehyde or acid would not interfere with reaction of the chlorosilane with TMAsilicate. This work was moderately successful and N-chlorosuccinimide was found to be the best Si-H chlorinating agent that also caused minimal oxidation of the protecting group[16]. The chlorination reactions were carried out on smaller molecules to test the efficiency of the reactions and this lead to the successful conversion of triethoxysilane to chlorotriethoxysilane (**53**) using copper chloride and

diisopropylethylamine[13]. The same reagents had little effect on compound **51** and other routes were found.

The second route to a Si-Cl terminated species was done with careful addition of the Grignard reagent to dichlorodimethylsilane. Addition of this to TMAsilicate was unsuccessful most probably due to the water present in TMAsilicate forming the disiloxane preferentially. In all of the reactions of chlorosilanes with TMAsilicate there seems to be little incentive for the chlorosilane to react with the TMAsilicate unless it is in very large excess. A very large excess of compounds such as **51** and **52** results in a very low overall yield. This work was not pursued further for this reason.

Preparation of a trichlorosilane derivative of 4-bromobenzene dimethylacetal was attempted by reaction of RMgBr with silicon tetrachloride (**58**). As one molar equivalent of Grignard had to be added to silicon tetrachloride, initial attempts involved transferring the Grignard by cannular to a solution of silicon tetrachloride in THF. The unreacted magnesium and viscosity of the Grignard reagent caused the cannular to block and so a dilute silicon tetrachloride solution was added to the Grignard (made highly dilute by adding more THF). This problem was overcome on subsequent attempts by using a larger volume of THF to facilitate transfer by cannular. Trichlorosilanes are susceptible to water so these compounds have to be handled cautiously. Removal of the solvent and excess trichlorosilane was carried out on a rotary evaporator purged with nitrogen with the water bath at 60 °C to ensure that all unreacted silicon tetrachloride was removed. Condensation of this product (attempted synthesis of **58**) was attempted by both the slow hydrolytic condensation at room temperature similar to that used to synthesise vinyl POSS and by the method used to synthesise phenyl POSS[19,20]. The latter is known to produce crystals after several days of refluxing and the

presence of viscous oil implied that a gel had formed. This could have been due to excess silicon tetrachloride being present or simply that the ratios of reactants were incorrect. The slow condensation route was allowed to stir for 6 weeks and attempts were made to filter out the small quantity of solid formed. This solid was most likely a small quantity of magnesium chloride left over residue from the Grignard reaction, as it was insoluble in organic solvents. The remainder of the reaction formed a gel on concentrating, probably due to the low pressure and higher temperatures (30 °C) used. Formation of a gel is assumed to be an irreversible process of polymerisation and no further analysis was carried out on those products.

8.3.2.3 Experimental Details

Synthesis of 2-(4-bromophenyl)-[1,3]-dioxolane, 50[12]
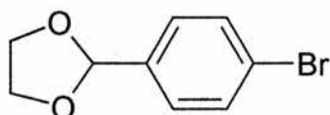
Bromobenzaldehyde (25 g, 0.135 mol), ethane-1, 2-diol (12 g, 0.19 mol), p-toluenesulfonic acid (0.4 g, 2.1 mmol) and Toluene (200 cm^3) was refluxed under Dean and Stark conditions for 2 hours until the point that no more water was produced. The toluene was removed under reduced pressure, the residue partitioned with ether and aqueous sodium hydrogen carbonate solution. The aqueous layer was further extracted with ether and the organic layers combined, washed with brine and dried over magnesium sulfate. The mixture was concentrated and left to stand allowing the product to crystallise. The crystals were filtered and washed with a small volume of cold ether.

Mpt 37 °C; ^{1}H NMR (300 MHz, CDCl$_3$): δ_H: 3.9 – 4.1 (4H, m, OCH_2); 5.7 (1H, s, OCHO); 7.2 (2H, d, Ar-H); 7.4 (2H, d, Ar-H); ^{13}C NMR (75 MHz, CDCl$_3$) δ_C: 65.711 (OCH_2); 103.430 (ArCHO); 123.641 (Ar-C-CHO or Ar-Br); 128.594 (ArC); 131.899 (ArC); 137.391 (Ar-C-CHO or ArC-Br)

The above data is corresponds to that reported in the literature[12].

Synthesis of (4-[1,3]-dioxolan-2-yl-phenyl)-dimethylsilane, 51[12]
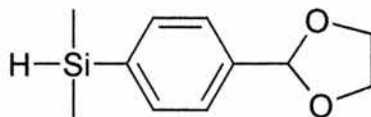
Dry THF (40 cm^3) was added to a mixture of magnesium powder (1.61 g, 0.066 mol), **50** (6 g, 0.026 mol) and iodine (single crystal). The reaction was heated to reflux until it had turned black (approx. 1 hour). After cooling to room

temperature, additional THF (20 cm³) and chlorodimethylsilane (4 cm³, 0.036

mol) was added slowly. The reaction was refluxed for a further 4 hours and

allowed to stir at room temperature overnight. The reaction was quenched by the

addition of water, extracted with ether, washed with dilute aqueous hydrochloric

acid, sodium hydrogen carbonate solution and dried with anhydrous magnesium

sulfate. The volatiles were removed under reduced pressure. The product was

purified by distillation at reduced pressure to give a colourless oil. Yield (1.24 g,

23 %)

¹H NMR (300 MHz, CDCl₃) δ_H: 0.4 (6H, d, SiCH₃), 4.1 (4H, m, OCH₂CH₂O),

4.4 (1 H, m, Si-*H*), 5.8 (1 H, s, OC*H*O), 7.4 – 7.6 (4 H, m, arom *H*). The NMR

data is in agreement with the literature[12]

Synthesis of (4-dimethoxymethyl-phenyl)-dimethylsilane, 52
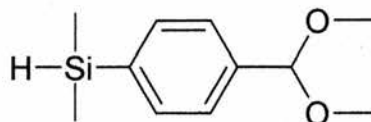
Dry THF (40 cm³) was added to a mixture of magnesium powder (0.7 g, 0.029

mol), 4-bromobenzaldehyde dimethylacetal (2.9 cm³, 0.016 mol) and iodine

(single crystal). The reaction was heated to reflux until it had turned black

(approx. 30 min). After cooling to room temperature, additional THF (20 cm³)

and chlorodimethylsilane (2.5 cm³, 0.023 mol) was added slowly. The reaction

was refluxed for a further 4 hours and allowed to stir at room temperature

overnight. The reaction was quenched by the addition of water, extracted with

ether, washed with dilute aqueous hydrochloric acid, sodium hydrogen carbonate

solution and dried with anhydrous magnesium sulfate. The volatiles were

removed under reduced pressure.

^{1}H NMR (300 MHz, CDCl$_3$) δ$_H$: 0.2 (6H, s, Si-CH_3); 3.2 (6H, s, OCH_3); 4.3 (1H, m, Si-H); 5.3 (1H , s, OCHO); 7.3 (2H, d, ArH); 7.4 (2H, d, ArH).

Synthesis of chlorotriethoxysilane, 53[13,21,22]
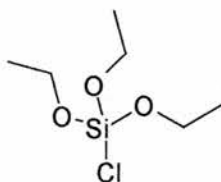
Cupric chloride (8.4 g, 84.8 mmol) and 20 cm^3 dry acetonitrile cooled to 0 °C in an ice bath. Diisopropylethylamine (12 cm^3, 67 mmol) was slowly added and allowed to warm to room temperature. Triethyoxysilane was slowly added (0.4 g, 39.2 mmol solution in 10 cm^3 acetonitrile) and the reaction heated to 80 °C overnight. The reaction was allowed to cool and pentane added to extract the products. The pentane was removed and distilled to leave the products.

Starting Material

^{1}H NMR (300 MHz, CDCl$_3$) δ$_H$: 1.1 (9H, t, CH_3), 3.7 (6H, q, CH_2), 4.1 (1H, s, Si-H)

Product

^{1}H NMR (300 MHz, CDCl$_3$) δ$_H$: 1.2 (9H, t, CH_3), 3.8 (6H, m, CH_2),

Attempted synthesis of 1,3-Bis- (4-dimethoxymethyl-phenyl)-1,1,3,3-tetramethyldisiloxane, 54
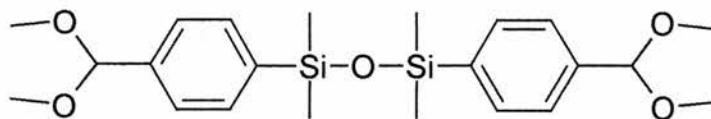
Method 1[15]:

52 (1 g, 4.88 mmol) was dissolved in dry hexane (20 cm^3) and stirred under constant argon purge. SnCl$_4$ (1.71 cm^3, 14.6 mmol) was added slowly and the

mixture allowed to stir for 1 hour. A white precipitate was formed and filtered off. The filtrate was concentrated under reduced pressure. Water was added in an attempt to form the disiloxane, the organic component was extracted with DCM, washed with brine and the volatiles removed under reduced pressure. The product was obtained as a milky liquid that formed a white precipitate on addition to NMR solvents, making NMR analysis impossible.

Method 2: Sulfuryl Chloride[18]

Sulfurylchloride (2.8 cm^3, 0.035 mol) was dissolved in DCM (600 cm^3) and added slowly to a solution of **52** (5.5 g, 0.027 mol) in DCM (100 cm^3) cooled to 0 °C. The reaction was allowed to warm to room temperature and stir overnight with an argon purge to remove the gases produced. The solvent was removed under reduced pressure and the residue analysed by ^{1}H NMR.

Method 3: Thionyl chloride[17]

51 (1 g, 5.03 mmol) and thionyl chloride (0.721 cm^3, 10 mmol) were refluxed together for 3 hours at 90 °C with a continuous argon purge to remove gases formed. The remaineder of the volatiles were removed under reduced pressure and the residue analysed by ^{1}H NMR.

Method 4: N-Chlorosuccinamide[16]

52 (1g, 5.03 mmol) was dissolved in dry DCM (20 cm^3). N-chlorosuccinamide (1.5 g, 11 mmol) was added and the mixture stirred at room temperature for 48 hours. Water was added to quench the reaction, and the organic layer extracted with DCM and dried with anhydrous magnesium sulfate. The volatiles were removed under reduced pressure.

^{1}H NMR (300 MHz, CDCl$_3$) δ_H: 0.2 (6H, s, Si-CH_3); 3.2 (6H, s, OCH_3); 5.3 (1H, s, OCHO); 7.3 (2H, d, ArH); 7.4 (2H, d, ArH).

Attempted synthesis of Cl₈T₈, 55[17]

H_8T_8 (0.71 g, 1.64 mmol) was placed into a flask under argon and $SOCl_2$ (4 cm^3, 54.8 mmol) added slowly. H_8T_8 partially dissolved but no reaction was observed. A small portion of the mixture was removed for analysis by ^{1}H NMR and it was determined that no discernible reaction had occurred.

^{1}H NMR (300 MHz, CDCl₃) δ_H: 4.2 (9H, s, Si-*H*); 4.3 (10H, s, Si-*H*)

corresponding to a near 50:50 mix of H_8T_8 and $H_{10}T_{10}$, as was found in the original sample of H_8T_8 used for this reaction.

Attempted chlorination of TMA Silicate, 56[23]

TMA Silicate (1.2 g) measured into flask under argon and $SOCl_2$ (6 cm^3, 0.082 mol) added slowly. Effervescence was observed and the reaction flask turned cool to touch.

Attempted synthesis of Octa- (4-[1,3]-dioxolan-2-yl-phenyl)-dimethylsiloxyoctasilicate, 57
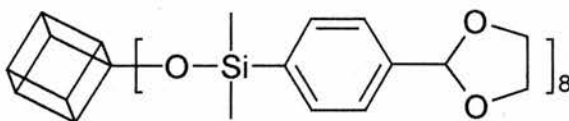
Method 1:

51 (6.0 g, 26.2 mmol) was dissolved THF (60 cm^3), and added to magnesium (1.278 g, 52.29 mmol) (previously heated under argon to 100 °C for 30 minutes), iodine and dichlorodimethylsilane (14.92 cm^3, 131 mmol) in THF 10 cm^3. The mixture was stirred for 2 hours at 50 °C during which time it turned black. The solvent was removed along with excess silane under reduced pressure, washed with dry THF (20 cm^3) and that evaporated to ensure all unreacted dichlorodimethylsilane had been removed. The residue was dissolved in THF (20

cm^3) and transferred via cannular to a clean dry flask. TMAsilicate (2 g) in DMF (50 cm^3) was added and a precipitate formed after 3 hours of stirring. This was filtered from the solution, and attempts made to dissolve it in dichloromethane. Only a small quantity of the precipitate was soluble in dichloromethane and it was most likely that this was TMAChloride.

Water was added to the reaction and a second precipitate formed. This was filtered and attempts made to dissolve it in dichloromethane. The precipitate was found to be insoluble in dichloromethane and so the solution was heated to boiling and boiling methanol added to try and dissolve the product. This was unsuccessful. Other solvents were tried without success.

Method 2:

Magnesium (1.5 g, 0.062 mol), iodine (1 crystal) and **50** (10 g, 0.043 mol) were stirred under argon. Dry THF (30 cm^3) was added and the mixture refluxed for 1 hour, until the solution had turned black. The reaction was allowed to cool to room temperature and dichloromethylsilane (5.2 cm^3, 0.05 mol) was added drop-wise. The reaction was refluxed for 4 hours and allowed to stir overnight at room temperature. The mixture was filtered to remove unreacted magnesium powder before being distilled to remove the THF and excess silane. The residue was dissolved in dry hexane (100 cm^3) and added to a solution of fresh TMA silicate (2.28 g) in DMF (200 cm^3). The biphasic system was stirred vigorously overnight before being quenched with water (200 cm^3) and extracted with ether. The ether layer was washed with brine and dried with anhydrous magnesium sulfate. The volatiles were removed under reduced pressure leaving a small quantity of yellow oil. ^{1}H NMR revealed a small quantity of **50** and various other solvents indicating that no product was recovered.

Attempted synthesis of dioxolane POSS, 58
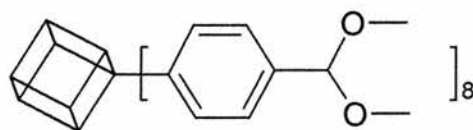
Magnesium powder (1.58 g, 0.065 mol) was heated to 100 °C under continuous argon purge for 30 minutes. The magnesium was allowed to cool and dry THF (20 cm^3) and iodine was added. 4-bromobenzene dimethylacetal (10 cm^3, 0.0598 mol) was added drop-wise. The mixture was refluxed for 5 hours until it had turned black. After cooling to room temperature an additional portion of THF (50 cm^3) was added to dilute the Grignard reagent (50 cm^3) a large excess of silicon tetrachloride (15 cm^3, 0.131 mol in 50 cm^3 THF.) was added drop-wise. The reaction was heated to reflux for a further 2 hours and stirred overnight. The resulting mixture was filtered to remove unreacted magnesium and concentrated under reduced pressure to remove the volatiles. The residue was dissolved in acetone (200 cm^3) and water was added very slowly (20 cm^3). The mixture was allowed to stir for 6 weeks during which time the solution turned black and a white precipitate formed. The white precipitate was found to be insoluble in organic solvents, implying that it might have been magnesium chloride. The acetone was removed under reduced pressure causing a gel to form that was insoluble in common organic solvents.

Method 2

Preparation of Grignard

Magnesium powder (2.19 g, 0.095 mmol) was weighed in to a flask equipped with a condenser and heated under constant argon purge to 100 °C to ensure the glassware was dry and activate the magnesium powder. The flask was cooled and dry THF (35 cm^3) was added. A crystal of iodine was dissolved in dry THF (5

cm^3) and the resulting solution added to the magnesium suspension. 4-bromobenzene dimethylacetal (15 cm^3, 0.090 mol) was added slowly and an exothermic reaction was observed, causing the mixture to reflux. The reflux was maintained for 30 minutes and then for an additional 3 hours by which point the reaction mixture had turned dark. The reaction cooled and the Grignard-THF solution transferred via cannular to a solution of silicon tetrachloride (15 cm^3, 0.118 mol) in THF (60 cm^3). The magnesium was washed with several 20 cm^3 portions of THF until the washings were virtually colourless, indicating that all the Grignard reagent had been transferred to the silicon tetrachloride solution. After stirring for 30 minutes, the volatiles were removed under reduced pressure leaving amber solid.

Preparation of POSS

Toluene (160 cm^3) was added to the amber solid, followed by deionised water (100 cm^3) creating a biphasic system. The aqueous layer was pale yellow and contained a white precipitate while the organic layer was orange in colour. The mixture was stirred overnight. The organics were extracted with DCM and concentrated under reduced pressure. A solid formed at this point, thought to be inorganic salts and so was filtered from the mixture. Benzyl trimethylammonium hydroxide was added (40 cm^3 of 40 % solution in MeOH) and the mixture set to reflux. Addition of the base solution caused the mixture to turn from yellow to red and this changed to purple upon heating. The mixture was then refluxed for 8 in every 24 hours resulting in a biphasic system of a yellow upper layer and dark red lower layer.

The yellow layer was decanted and left to slowly evaporate. The lower layer was found to be viscous oil that was insoluble in other solvents, even when heated.

8.3.3 Diphenylphosphine Building Blocks

8.3.3.1 Introduction

Phosphine functionalised POSS cubes have a use as a dendrimer core[24,25] and are generally synthesised through a radical reaction of diaryl or dialkyl phosphine and vinyl or allyl POSS[4,26]. These molecules, although small, have a degree of flexibility in their arms that makes them less appealing as building blocks for metal organic framework synthesis. The reaction of Si-O⁻ and chlorodiarylphosphine derivatives has been reported by Glidewell[27] and was thought to be a useful way to functionalise TMAsilicate to produce an octaphosphine POSS cube suchas $(Ph_2P)_8Si_8O_{20}$.

Metal organic frameworks with phosphorus have been reported using silver salts . There are also many classes of metal phosphorus frameworks such as AlPOs (aluminium phosphates), GaPOs (Gallium phospates) and various metal phosphates, usually derived from a phosphorus acid such as phosphoric or dialkylphosphinic acid. The small molecule created by the reaction of chlorodiphenylphosphine and TMAsilicate was also regarded as a useful core for Fréchet wedge dendrons, offering a variation on those used by Hong *et al.*[24,25].

8.3.3.2 Results and Discussion
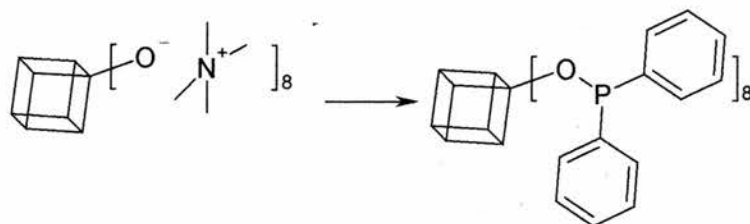
Figure 8.9: Reaction of TMAsilicate and Chlorodiphenylphosphine – desired product.

The synthesis of TMAsilicate and reaction with chlorodiphenylphosphine proved

to be very difficult to accomplish. The reaction was carried out at room

temperature under conditions used to synthesis Q_8M_8 as there are very few reports

in literature of any similar reactions. Glidewell reported reaction of $K^+[OSiPh_3]^-$

with $ClPPh_2$ at room temperature in toluene or light petroleum producing

$Ph_2POSiPh_3$, as well as the corresponding $Na^+[OSiMe_3]^-$ derivative[27]. The

reactions were carried out over an hour and precipitated KCl and NaCl was

removed before the solvents being evaporated to yield the products. The products

were found to give ^{31}P chemical shifts in the region of +26 to +28 p.p.m.
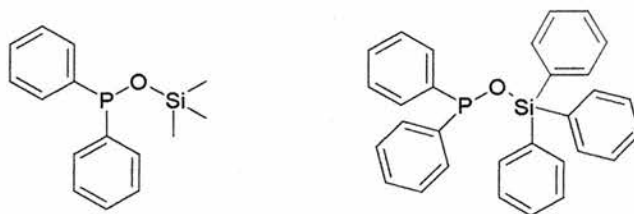
Figure 8.10: Products of the reaction of $Na^+[OSiMe_3]^-$ and $K^+[OSiPh_3]^-$ with
chlorodiphenylphosphine as reported by Glidewell *et al.* [27].

There are a number of explanations for the poor success of this reaction using

TMAsilicate. Firstly, it is difficult to get a sample of TMAsilicate that is dry.

Freshly made TMAsilicate is very wet when crystalline and drying in an oven

often appears to result in the cube decomposing or rearranging. This is not

completely unexpected, as tetramethyammonium hydroxide has been used as base

to open one corner of a silsesquioxane cube[28]. TMAsilicate bought from Aldrich,

whilst appearing drier than freshly made still had an indeterminate quantity of water present.

Water is a greater issue for this synthesis than for that of Q_8M_8 and derivatives or for carboxylic acid derivatives. This is because in the former case, most methodologies take into account the large quantity of water in TMAsilicate. For the latter, the work did not progress well enough for the water content of TMAsilicate to become a real issue.

TMAsilicate is soluble in a very limited range of solvents – isopropanol, DMF, methanol and so finding a suitable solvent mixture for this reaction is very difficult. The problem with this synthesis may not lie so much with formation of the product but rather with extracting it. Both methods for this reaction produce white precipitates when chlorodiphenylphosphine is added to TMAsilicate-solvent solution. When synthesising other TMAsilicate derivatives this precipitate is generally TMAchloride and it is easily filtered out. TMAchloride is of limited solubility in solvents making further analysis difficult. In the reactions below it was assumed that the white precipitate was TMAchloride. The difficulties then lie in retrieving the product. Proton NMR is virtually useless as any products have signals in the aromatic region, which overlap greatly making them indistinguishable. In method 1 using THF as a solvent, the volatile parts are evaporated and a waxy white solid is left. The vast majority of this was found to be insoluble in ether and believed to be an ether insoluble diphosphine dimer appearing in phosphorus NMR as a double doublet 40 and –20 ppm. This double doublet is greatly reduced after the product has been washed with ether and the ether insoluble portions removed. Octasilsesquioxane derivatives are known to be less soluble in organic solvents than decasilsesquioxanes and related species, one property that makes their synthesis easier but here it could be complicating things.

If the octamer is formed, it may be present in the ether insoluble solids and cannot be separated from the dimer.
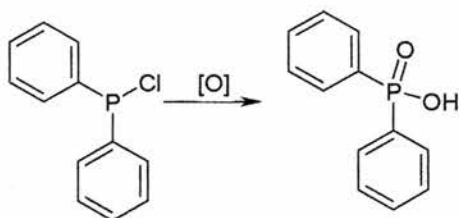
Figure 8.11: Oxidation of chlorodiphenylphosphine to diphenylphosphinic acid.

Chlorodiphenylphosphine is both air and moisture sensitive, forming among other things, diphenylphosphinic acid. It is possible, therefore, that the chlorodiphenylphosphine has reacted with the water present from the TMAsilicate or from air when left to oxidise to form diphenylphosphinic acid and this could be the main product of this reaction. In any case, to what ever extent the reaction of chlorodiphenylphosphine and TMAsilicate was sucessful, no octa-(diphenylphosphine)octasilicate was isolated by NMR techniques, although the ^{31}P NMR spectra implied that a species corresponding to Si-O-P(O) may be present[29].

It was decided to attempt to crystallise the phosphine mixture to gain more appreciation for the species contained within. A number of experiments were carried out at both room temperature through slow evaporation and at high temperature and pressure within autoclaves.

Several crystalline products were obtained from this work. **60F** produced clear crystals that were on the borderline of size for a laboratory based single crystal x-ray diffractometer. X-ray diffraction was attempted and while the crystals were found to diffract, no pattern could be obtained due to the crystal size. The crystals were then sent to Daresbury for analysis but no suitable crystals could be found for analysis. **60B, 61C, 62D** and **63E** all produced a crystalline product but the crystals were large and highly intergrown and have not yet been characterised.

The reaction of cobalt chloride hydrate with the phosphine solution at 150 °C in an autoclave yielded a substantial quantity of dark blue needle like crystals that were almost fibrous in appearance. No suitable crystals could be found for x-ray analysis

Reaction of the phosphine solution and copper sulfate provided the most insightful results with a quantity of blue crystals similar in colour to copper sulfate being produced at room temperature on slow evaporation of the solvent, methanol. Unlike copper sulfate these crystals (**64B**) were insoluble in water and were sent to Daresbury for single crystal x-ray analysis.

The structure consists of chains of square planar copper bound to four oxygen molecules bridged by diphenylphosphino units
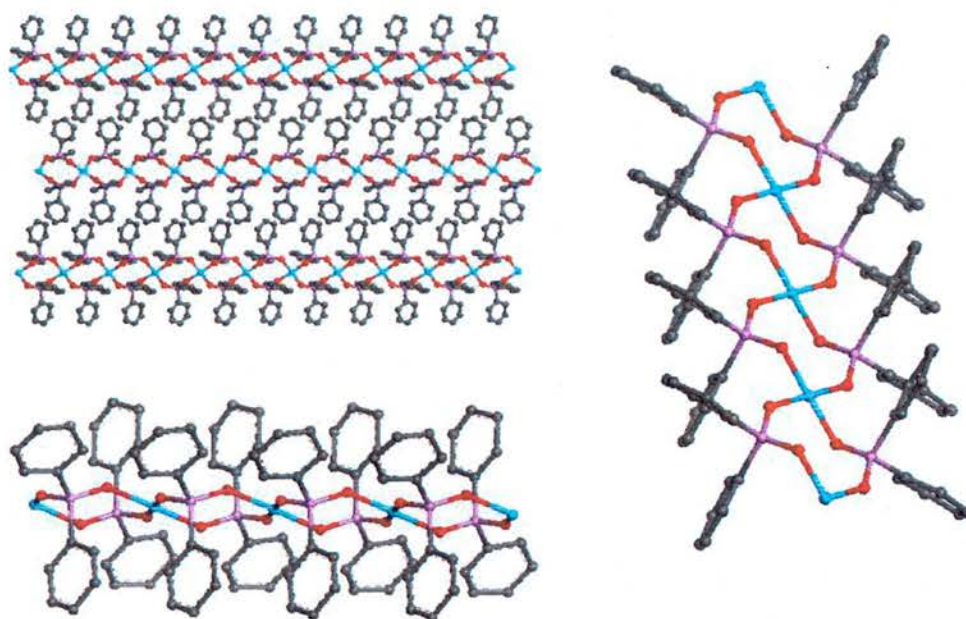
Figure 8.12: Copper phosphonate crystal structure. Grey – carbon, Red – oxygen, Purple – phosphorus and blue – copper.

Figure 8.12 shows various views of the crystal structure with the phenyl rings either axial or equatorial to the plane of the copper. Despite the twists and bends in the structure created by the oxygen and phosphorus bonds, the copper is flat. Unfortunately this is not a new structure having been reported in 1988 by Bino *et*

al. [30]. It is an example of a copper phosphonate structure and is generally

synthesised by reaction of copper sulfate with diphenylphosphinic acid in ethanol.

The copper phosphonate precipitates from solution on standing at room

temperature.

Identification code	stan244, **64e**	
Empirical formula	$C16 H14 Cu O4 P2$	
Formula weight	451.93	
Temperature	150 (2) K	
Wavelength	0.68800 Å	
Crystal system	Monoclinic	
Space group	Cc	
Unit cell dimensions	a = 16.519(3) Å	alpha = 90 °
	b = 5.0541(10) Å	beta = 96.27(3) °
	c = 25.460(5) Å	gamma = 90 °
Volume	2112.9 (7) Å^3	
Z, Calculated density	4, 1.421 Mgm^{-3}	
Absorption coefficient	1.163 mm^{-1}	
F(000)	916	
Crystal size	0.1 x 0.05 x 0.03 mm	
Theta range for data collection	3.12 to 29.43 °	
Limiting indices	-23<=h<=23, -7<=k<=7, -36<=l<=36	
Reflections collected / unique	11253 / 6130 [R(int) = 0.0211]	
Completeness to theta = 29.43	98.2 %	
Absorption correction	None	
Refinement method	Full-matrix least-squares on F^2	
Data / restraints / parameters	6130 / 2 / 353	
Goodness-of-fit on F^2	1.083	
Final R indices [I>2sigma(I)]	R1 = 0.0342, wR2 = 0.1014	
R indices (all data)	R1 = 0.0466, wR2 = 0.1104	
Absolute structure parameter	0.48(3)	
Largest diff. peak and hole	0.697 and -0.460 e.Å^{-3}	

Table 8.1: Crystal data and structure refinement for stan244, **64e**.

A related structure was also reported with DMF coordinated to the copper centres,

alternating position down the chain (above or below the plane of the copper[31].

Bino *et al.* also reported a similar structure containing manganese[30-32].

The diphenylphosphinic acid needed to participate in this reaction is most likely created through oxidation, either by water from TMAsilicate or oxygen and moisture in air, of chlorodiphenylphosphine. Unfortunately, the silicate cube was not present in the crystal structure making it harder to understand the fate of that species.

8.3.3.3 Experimental Details

Attempted synthesis of octadiphenylphosphino-octasilicate, 59
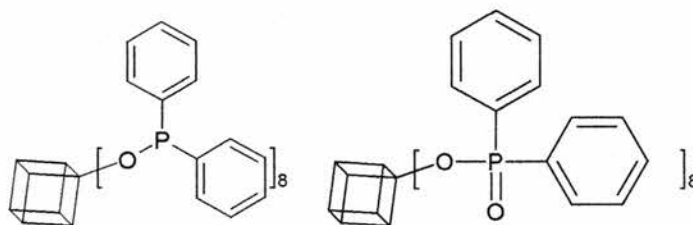
Method 1:

TMAsilicate (2 g, dried) was dissolved in THF (40 cm^3) and stirred rapidly for 10 minutes. Triethylamine (3 cm^3, 0.022 mol) was added slowly and the mixture stirred for a further 5 minutes. Chlorodiphenylphosphine (5 cm^3, 0.028 mol) was added slowly and an exothermic reaction was observed while a white precipitate formed. An additional portion of THF (10 cm^3) was added to facilitate stirring and the mixture was filtered after 1 hour. The solvent was removed leaving a waxy white solid. The white precipitate was believed to be TMAchloride. ^{31}P NMR of this waxy solid showed a double doublet corresponding to a bis-diphosphine compound and so the solid was dissolved in ether to remove this dimer, known to be insoluble in ether. The mixture was filtered and the ether evapourated leaving a yellow oil.

Method 2:

TMAsilicate (5 g, bought) was dissolved in a mixture of DMF (50 cm^3) and hexane (15 cm^3) and stirred vigorously with argon gas bubbling through. Chlorodiphenylphosphine (9 cm^3, 0.050 mol) was added slowly and the mixture stirred for 1 hour during which time a white precipitate formed. The solvents were separated and the hexane layer concentrated under reduced pressure. The residue was partially redissolved in ether, decanted and concentrated to leave a yellow oil which was left to oxidise in air.

NMR data for diphenylphosphinic acid: source – Aldrich library of NMR data

^{1}H NMR δ_H: 7.5 (m, 4H, Arom C-*H*), 7.7 (m, 6H, Arom C-*H*)

^{13}C NMR δ_C: 135.68, 133.89, 131.25, 131.22, 130.81, 130.68, 128.31, 128,14 (m, Arom C)

^{31}P NMR δ_P: 21.2, 25.2, 27.5, 32.5, 41.2

Wozniak *et al.* reported 31P NMR for $Ph_3SiOP(O)Ph_2$ at 21.2 ppm for, and $Ph_3SiOPPh_2$ at 94.1 ppm, implying that the signal at 21.2 in the 31P NMR spectra may correspond to and Si-O-P(O)Ph$_2$ species, such as the desired product[29].

Synthesis of Metal Organic Frameworks with Silver Triflate, 60

	Silver Triflate	TMA Silicate	Dpp Cube	Solvent	Product
A	Spatula tip	N/a	Small mass	Ether	
B	Spatula tip	N/a	Small mass	MeOH/Et$_2$O 1:1	Crystalline
C	Spatula tip	N/a	Small mass	MeCN/Et$_2$O 1:1	
D	Spatula tip	N/a	Small mass	MeCN/Et$_2$O 1:4	
E	Spatula tip	N/a	Filtrate	MeOH	
F	Spatula tip	N/a	Oxidised remains	MeOH	Crystals
G	Spatula tip	N/a	Old	MeOH	

The above reactions were allowed to stand in air and evaporate slowly.

General Procedure for synthesis of metal organic frameworks with Cu, Co and Ni salts at room temperature

59 was prepared by method 2. The yellow oil produced was dissolved in methanol (50 cm^3) and used in small portions in each reaction (5 cm^3 portions, designated A in tables).

Synthesis of Metal Organic Frameworks with Nickel salts, 61

	Metal	Mass	Solvent	Cube	Solvent	Product
A	$NiSO_4$	ST	MeOH	A	MeOH	Gel
B	$NiCl_2$	ST	H2O	A	MeOH	Gel
C	$NiCl_2$	ST	MeOH	A	MeOH	Crystals
D	$NiSO_4$	ST	H2O	A	MeOH	Gel
E	$NiCl_2$	ST	MeOH/H_2O	A	MeOH	Gel

ST – spatula tip

The above reactions were allowed to stand at room temperature and evaporate slowly.

Synthesis of Metal Organic Frameworks with Cobalt salts, 62

	Metal	Mass	Solvent	Cube	Solvent	Product
A	$CoCl_2$	ST	MeOH	A	MeOH	Gel
B	$CoCl_2$	ST	H_2O	A	MeOH	Gel
C	$CoSO_4$	ST	H_2O	A	MeOH	Gel
D	$CoSO_4$	ST	MeOH	A	MeOH	Crystals
E	$CoCl_2$	ST	MeOH/H_2O	A	MeOH	Gel

The above reactions were allowed to stand at room temperature and evaporate slowly.

	Metal	Mass	Water	Cube	Methanol	Time	Temp.	Product
F	$CoCl_2$	0.3 g	2 g	1.06 g	5 g	18 hr	150 °C	Blue needle crystals
G	$CoCl_2$	0.3 g	2 g	0 g	5 g	18 hr	150 °C	Pink solution

The above reactants were mixed in teflon lined autoclave and heated.

Synthesis of Metal Organic Frameworks with Copper salts, 63

	Metal	Mass	Solvent	Cube	Solvent	Product
b	$CuCl_2$	ST	MeOH	A	MeOH	Gel
e*	$CuSO_4$	ST	MeOH	A	MeOH	Crystals
h	$CuCl_2$	ST	H_2O	A	MeOH	Gel
k	$CuSO_4$	ST	H_2O	A	MeOH	Gel
o	$CuCl_2$	ST	MeOH/H_2O	A	MeOH	Gel

The above reactions were allowed to stand at room temperature and evaporate slowly.

Synthesis of Copper Phosphonate, 64

59 (4.08 g) was dissolved in methanol (66 g) and portioned into 10 cm^3 aliquots.

To each portion was added a metal salt (0.2 g) dissolved in methanol (5 g) and the

mixture allowed to stand, at room temperature and open to air for 2 weeks.

Crystals were found to have formed in reaction B that looked very much like

small copper sulfate crystals. Reaction B was filtered, and a small quantity of the

crystals tested for water solubility. As the crystals did not dissolve in water, it

was concluded that they were not copper sulfate and sent for single crystal x-ray

analysis. The other metal salts and ligand formed gels on standing from which no

solid products were obtained.

	Metal	Mass	Cube Solution	Methanol	Product
A	AgOTf	0.2 g	10 cm^3	5 g	Gel
B	CuSO$_4$	0.2 g	10 cm^3	5 g	Blue crystals
C	NiCl$_2$	0.2 g	10 cm^3	5 g	Gel
D	Co(NO$_3$)$_2$	0.2 g	10 cm^3	5 g	Gel

8.3.4 Conclusions

Attempts to synthesise metal organic framework building blocks with carboxylic acid and diphenylphosphine groups were largely unsuccessful. This is mainly down to difficulties in attaching these groups to the silicate cube in a way that creates the most rigid unit possible. Various methods to attach a benzoic acid derivative were tried, largely without success due to difficulties in forming an Si-Cl bond and the hazards of working with TMAsilicate and its unknown water quantity. The diphenylphosphine work was similarly unsuccessful but did yield several crystalline samples, believed to be various metal phosphonates following single crystal analysis of a copper form. ^{31}P NMR may indicate the possible presence of the phosphine cube but a sample could not be isolated for analysis.

8.4 Conclusions and Further Work

Preliminary investigations into the use of TMAsilicate derivatives as for new dendrimer cores and building blocks for metal organic frameworks have been largely unsuccessful. This is due to the difficulties in using TMAsilicate in conjunction with moisture sensitive species such as chlorosilanes and chlorophosphines. One single crystal structure was obtained from this work and several other crystalline samples are pending analysis. TMAsilicate does not appear to be a useful synthetic intermediate beyond that which is already published – $Q_8M_8^H$ and $Q_8M_8^{Vi}$. This is unfortunate as TRASilicate versions of D3R and D5R have been reported and could lead to interesting materials. The Q_6M_6 and $Q_{10}M_{10}$ have also been reported so possibly these molecules could provide alternative cores for dendrimers synthesised divergently or convergently if the H or Vinyl form could be synthesised.

8.5 References

1. I. M. Saez and J. W. Goodby, *J. Mater. Chem.*, 2001, **11**, 2845.

2. I. M. Saez, J. W. Goodby and R. M. Richardson, *Chem. Eur. J.*, 2001, **7**, 2758.

3. C. M. Casado, I. Cuadrado, M. Moran, B. Alonso, B. Garcia, B. Gonzalez and J. Losada, *Coord. Chem. Rev.*, 1999, **186**, 53.

4. S. Lucke and K. Stoppek-Langner, *Appl. Surf. Sci.*, 1999, **145**, 713.

5. P. G. Harrison, *J. Organomet. Chem.*, 1997, **542**, 141.

6. M. Wiebcke and D. Hoebbel, *J. Chem. Soc., Dalton Trans.*, 1992, 2451.

7. D. Hoebbel and W. Wieker, *Z. Anorg. Allg. Chem.*, 1971, **384**, 43.

8. N. Auner, B. Ziemer, B. Herrschaft, W. Ziche, P. John and J. Weis, *Eur. J. Inorg. Chem.*, 1999, 1087.

9. M. Backer, A. R. Grimmer, N. Auner, P. John and J. Weis, *Solid State Nucl Mag*, 1997, **9**, 241.

10. F. S. Kipping, *J. Chem. Soc.*, 1927, 105.

11. E. G. Rochow and K. G. Ingold, *J. Am. Chem. Soc.*, 1954, **76**, 4852.

12. B. W. Manson, J. J. Morrison, P. I. Coupar, P. A. Jaffres and R. E. Morris, *J. Chem. Soc., Dalton Trans.*, 2001, 1123.

13. R. A. Gossage, E. Munoz-Martinez and G. Van Koten, *Tetrahedron Lett.*, 1998, **39**, 2397.

14. R. J. P. Corriu, M. Granier and G. F. Lanneau, *J. Organomet. Chem.*, 1998, **562**, 79.

15. R. Hager, O. Steigelmann, G. Muller and H. Schmidbaur, *Chem. Ber.*, 1989, **122**, 2115.

16. N. Auner, R. Probst, F. Hahn and E. Herdtweck, *J. Organomet. Chem.*, 1993, **459**, 25.

17. V. I. Zhun, A. B. Zhun, S. D. Vlasenko, L. A. Belorusskaya, E. A. Chernyshev and V. D.

Sheludyakov, *Zh. Obshch. Khim+.*, 1982, **52**, 2565.

18. J. D. Buynak, J. B. Strickland, G. W. Lamb, D. Khasnis, S. Modi, D. Williams and H. M. Zhang, *J. Org. Chem.*, 1991, **56**, 7076.

19. J. W. Choi, R. Tamaki, S. G. Kim and R. M. Laine, *Chem. Mater.*, 2003, **15**, 3365.

20. J. Choi, A. F. Yee and R. M. Laine, *Macromolecules*, 2003, **36**, 5666.

21. M. E. Havill, I. Joffe and H. W. Post, *J. Org. Chem.*, 1948, **13**, 282.

22. I. Joffe and H. W. Post, *J. Org. Chem.*, 1949, **14**, 424.

23. P. D. Lickiss and K. M. Stubbs, *J. Organomet. Chem.*, 1991, **421**, 171.

24. B. Hong, T. P. S. Thoms, H. J. Murfee and M. J. Lebrun, *Inorg. Chem.*, 1997, **36**, 6146.

25. H. J. Murfee, T. P. S. Thoms, J. Greaves and B. Hong, *Inorg. Chem.*, 2000, **39**, 5209.

26. S. Lucke, K. Stoppek-Langner, J. Kuchinke and B. Krebs, *J. Organomet. Chem.*, 1999, **584**, 11.

27. I. Ferguson and C. Glidewell, *J. Chem. Soc., Dalton Trans.*, 1971, 2071.

28. F. J. Feher, R. Terroba and J. W. Ziller, *Chem. Commun.*, 1999, 2153.

29. L. Wozniak, M. Cypryk and J. Chojnowski, *Tetrahedron*, 1989, **45**, 4403.

30. P. Betz and A. Bino, *Inorg. Chim. Acta*, 1988, **145**, 11.

31. P. Betz and A. Bino, *Inorg. Chim. Acta*, 1988, **149**, 171.

32. P. Betz and A. Bino, *Inorg. Chim. Acta*, 1988, **147**, 109.

Chapter 9. Conclusions and Further work

9.1 Conclusions and Further Work: Computational Work

9.1.1 Dendritic Alcohols

The molecular modelling studies into three dendritic alcohols were very successful and the use of the different solvent conditions gave useful insight into the change in shape experienced by dendrimers in solvents of varying polarity. It was found that the effects of the solvent are greater for the molecules with fewer terminal groups, implying that the steric effects of dendrimers with large numbers of terminal groups outweigh the influence of the solvent as calculated here. No significant folding back of the dendrimer branches was noticed, due at least in part, to the short length of the branches and the limited flexibility in such short arms. This in turn implied that there was not sufficient steric strain within the molecule to cause back folding and no terminal groups approached within 2.5 Å of the core. It is likely that all the terminal groups are on the surface of the dendrimer and would be able to participate in further reactions.

9.1.2 Dendritic Diphenylphosphines

The modelling of the diphenylphosphine dendrimers provided valuable insight into the effects of varying the generation, solvent, branch composition and temperature on the structure. No folding back of branches was observed and this was due to the large size of the diphenylphosphine terminal groups. In general, the dendrimers grow smaller when heated, more spherical if a CH_2 in the branch

is replaced with an oxygen and increasing the generation leads to a decrease in available space per terminal group, resulting in a close packed state. This may also explain the difficulties in synthesising some molecules with a large number of terminal groups.

This molecular modelling study could be extended by modelling G2-propyl - 48PPh$_2$ as this was not modelled due to its size. It would also be interesting to attempt to model a dendrimer with a molecular volume of 150 Å^3 and 24 terminal groups. Synthesis of dendrimers with 24 terminal groups resulted in incomplete coverage of the molecular surface and if such a dendrimer could be modelled, it would be useful to see if it could then be synthesised. This would expand the modelling as a useful molecular design tool, predicting which dendrimers could be synthesised fully, and which would possess too much steric strain for complete reaction.

9.1.3 Bite Angle and Complex

Parameters were successfully added and modified in the MM+ forcefield of the Hyperchem computer program and used to calculate the bite angle of three dendrimers, three model compounds and a series of test compounds, at a variety of temperatures and for a minimum energy structure. For dendrimers it was felt that the minimum energy bite angle did not give a true representation of the molecule as it was extremely difficult to find a minimum energy structure for such a large species. The dynamic bite angle was calculated at a variety of temperatures and gave the flexibility range. G1-16ethylPPh$_2$ was found to have a

bite angle closest to 120 °, which is thought to promote diequatorial binding at a metal centre, and influence the selectivity of reactions such as hydroformylation. Visual inspection of the dendrimer structure showed that the rhodium centre as added for the bite angle calculation was curling into the interior. As this would not be possible for a metal complex to adopt such a configuration, a metal complex was also modelled using restraints to fix the geometry. From this, the complex bite angle was calculated and the effects of the complex on the rest of the dendrimer structure was assessed.

This work could be carried further using combined quantum mechanics/molecular mechanics methods to model transition states with QM methods, and the bulk of the dendrimer with molecular mechanics methods. The dendrimer could also be modelled with a variety of potential intermediates by molecular mechanics methods using restraints similar to those used for the complex. This would allow the effect of various intermediates on the dendrimer structure to be measured to examine its influence.

9.2 Conclusions and Further Work: Synthesis

9.2.1 Convergent Dendrimer Synthesis

The synthesis of several new dendrimer branches was completed successfully but it was not possible to attach them to the POSS core. The Fréchet wedge type dendrons were extremely difficult to functionalise with suitable groups while the PAMAM dendrons were very simply synthesised. Preliminary experiments showed that hydrosilation of allyl terminated PAMAM branches was occurring and further work is required to perfect the reaction conditions. These dendrimers will also be convenient to turn into ligands through the addition of groups such as diphenylphosphine, as reported by several research groups.

Attempts to synthesise PAMAM dendrimers by a totally convergent method were slow and at the point of writing, no solid had formed. Such condensation reactions are very slow and the reactions should be left for as long as necessary to see if any solid product forms. The best possible case for these molecules would be the production of crystals, leading, potentially, to a single crystal structure, of which few are reported in literature.

In general, convergent POSS dendrimer synthesis is less easy to accomplish than divergent synthesis.

9.2.2 POSS and Silicates

The synthesis of a variety of POSS and silicate cubes were attempted, leading to two single crystal structures of which one had been previously reported. BromopropylPOSS was also successfully synthesised by condensation although

attempts to condense POSS cubes with a variety of functional groups generally lead to gels being formed. Synthesis of mixed POSS cubes led to either gels or vinyl POSS being formed exclusively due to different rates of reaction. Various silicates were found to be far harder to synthesise than expected, such as $Q_8M_8^H$ and due to this were not considered to be viable alternatives to H_8T_8 as dendrimer cores.

Attempts to synthesis a benzoic acid functionalised POSS or silicate cube were unsuccessful. This was mainly due to difficulties in synthesising appropriate chlorosilanes and problems with reaction with TMAsilicate. It may be possible to synthesis shorter species with appropriate functional groups by the routes described below.

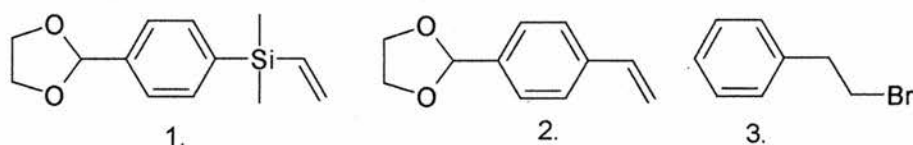**Figure 9.1:** Three rigid disubstituted benzene molecules. 1 is a derivative of those discussed above, 2 is a styrene derivative that can be synthesised from 3 following the method of Matveentseva[1]

Molecules 1 and 2 above can be attached to H_8T_8 (1 is the vinyl silane version of those discussed above). 2 is advantageous because there is one fewer atom in the potential link between POSS and benzene ring.

9.3 Publications

Work from this thesis has been published in three journal articles:

1. X. J. Zhang, K. J. Haxton, L. Ropartz, D. J. Cole-Hamilton and R. E. Morris, *J. Chem. Soc., Dalton Trans.*, 2001, 3261.

2. L. Ropartz, K. J. Haxton, D. F. Foster, R. E. Morris, A. M. Z. Slawin and D. J. Cole-Hamilton, *J. Chem. Soc., Dalton Trans.*, 2002, 4323.

3. K. J. Haxton, D. J. Cole-Hamilton and R. E. Morris, *J. Chem. Soc., Dalton Trans.*, 2004, 1665.

9.4 References

1. M. S. Matveentseva, Z. I. Buloichik, A. M. Lazareva, L. R. Uvarova and I. P. Zyatkov, *Zh. Org. Khim.*, 1984, **20**, 814.

Appendix 1: Abbreviations and Definitions

Nuclear Magnetic Resonance

d	Doublet
Hz	Hertz
J	Coupling constant in Hertz
m	Multiplet
MHz	Megahertz
NMR	Nuclear Magnetic Resonance
CP	Cross Polarisation
MAS	Magic Angle Spinning
COSY	Correlation Spectroscopy
ppm	Parts Per Million
s	Singlet
t	Triplet
δ	Chemical Shift in Parts per Million

Mass Spectrometry

MALDI-TOF	Matrix Assisted Laser Desorption Ionisation – Time Of Flight
EI	Electrospray Ionisation
M/z	Mass to Charge Ratio
M+	Molecular Ion
MS	Mass Spectrometry

Infra-Red and Ultra Violet Spectroscopy

FTIR	Fourier Transform Infra Red Spectroscopy
m	Medium

s	Strong
UV	Ultra Violet Spectroscopy
vs	Very Strong
vw	Very Weak
w	Weak
υ_{max}	Infra-red Adsorption Frequency

X-Ray Diffraction

scXRD	Single Crystal X-Ray Diffraction
XRD	X-Ray Diffraction

Other Techniques

CHN	Carbon Hydrogen Nitrogen Elemental Analysis
DSC	Differential Scanning Calorimetry

Computational Techniques

General Definitions

CVFF	Consistent Valence Force Field
DFT	Density Functional Theory
MM+	Molecular Mechanics Plus Force Field
MM2	Molecular Mechanics 2 Force Field
NPT	Constant Number, Pressure, Temperature
NVE	Constant Number, Volume, Energy
NVT	Constant Number, Volume, Temperature
PCFF	Polymer Consistent Force Field
RMS	Root Mean Square

| UFF | Universal Force Field |

Analysis

PCF	Pair Correlation Function
Rg	Radii of Gyration
A.R.	Aspect Ratio
Ix	Moment of Inertia with respect to the x-axis
M	Mass
Iy	Moment of Inertia with respect to the y-axis
Iz	Moment of Inertia with respect to the z-axis
Ir	Moment of Inertia

Synthesis

General Definitions

Hr	Hour
M	Moles per litre
Min	Minute
mmol	millimoles
mol	moles
POSS	Polyhedral Oligomeric Silsesquioxane
RT	Room Temperature

Chemicals

| DCM | Dichloromethane |
| DMF | Dimethylformamide |
| H_8T_8 | Hydrido Polyhedral Oligomeric Silsesquioxane |

Karstedt's Catalyst	Platinum (0)-1,3-divinyl-1,1,3,3-tetramethyldisiloxane, solution in xylenes
Speier's Catalyst	Hexachloroplatinic Acid, solution in propan-2-ol
THF	Tetrahydrofuran
TMAS	TetraMethylAmmonium Silicate
Vinyl POSS	Octavinyl Polyhedral Oligomeric Silsesquioxane

Appendix 2: General Synthetic Methods

**Synthesis of Vinyl POSS, 1[1,2]**
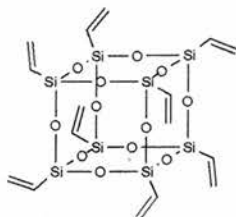
Vinyltrichlorosilane (50 cm^3, 0.377 mol) was added drop-wise to a mixture of

acetone (1500 cm^3) and water (450 cm^3). The mixture was stirred for 6 weeks during

which time white crystals formed. The crystals were removed by filtration and

washed with a small volume of cold acetone. Yield 9.02 g, 30 %

^{1}H NMR (300 MHz, CDCl$_3$) δ_H: 5.8 – 6.1 (24 H, m, C*H*C*H$_2$*)

^{13}C NMR (75 MHz, CDCl$_3$) δ_C: 129.1 (=*C*H$_2$), 137.5 (*C*H=)

The analytical data are in agreement with the literature[1].

**Synthesis of Aminopropyl POSS, 3[3]**
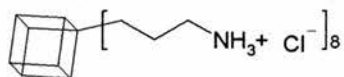
Method 1: as per Feher et al.[3]

Concentrated hydrochloric acid (134 cm^3, 33 % in H$_2$O,) was added slowly over 4

hours to a mixture of aminopropyltriethoxysilane (100 cm^3, 0.427 mol) and methanol

(1800 cm^3). This mixture was stirred for up to 3 months, removing precipitated

product by filtration at regular intervals and using a little of the product to seed the

next batch.

The crude amine POSS was recrystallised with boiling methanol and filtered while hot to give an insoluble fraction and a methanol soluble fraction. The methanol soluble fraction had the solvent removed under reduced pressure and was then dissolved in the minimum volume of boiling methanol and allowed to stand and crystallise.

Synthesis of [3,4-Bis- (4-bromobenzyloxy)-phenyl] methanol, 16[4,5]
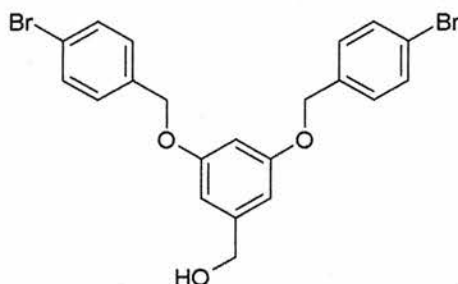
Bromobenzylbromide (5.75 g, 23 mmol), 3,5-dihydroxybenzyl alcohol (1.54 g, 11 mmol), potassium carbonate (3.04 g, 33 mmol) and 18-crown-6 (0.58 g, 2.2 mmol) were dissolved in dry acetone (30 cm^3) and heated at reflux under argon for 48 hours. The resulting pale beige mixture was cooled and evaporated to dryness. The solid residue was dissolved in DCM (100 cm^3) and washed with water (100 cm^3). The aqueous layer was extracted with DCM (3 x 50 cm^3) and the combined organic extracts dried with anhydrous magnesium sulfate. The solvent was removed under reduced pressure leaving a pale waxy solid. The crude product was purified using flash chromatography with 1:19 ethyl acetate: DCM to give a white solid, yield 4.20 g, 80 %.

R_F (1:19 ethyl acetate: DCM) 0.35; ^{1}H NMR (300 MHz, CDCl$_3$): δ_H 1.62 (1 H, m, CH$_2$O*H*), 4.65 (2 H, s, C*H$_2$*OH), 5.00 (4 H, s, ArC*H$_2$*OAr), 6.55 (1 H, m, Ar*H*), 6.60 (2 H, m, Ar*H*), 7.25 (4 H, d, J = 8.5 Hz Ar*H*), 7.55 (4 H, d, J = 8.5 Hz Ar*H*); ^{13}C NMR (75 MHz, CDCl$_3$): δ_C 44.8 (*C*H$_2$Ar), 63.0 (*C*H$_2$OH), 69.29 (2 C, O*C*H$_2$Ar),

105.33 (2 C, arom CH), 121.8 (2 C, arom CBr), 129.7 (4 C, arom CH), 131.6 (4 C, arom CH), 135.7 (2 C, arom C), 141.2 (arom C), 158.14 (2 C, arom CO).

The above data are in agreement with the literature[4-6].

References

1. C. Bonhomme, P. Toledano, J. Maquet, J. Livage and L. Bonhommecoury, *J. Chem. Soc., Dalton Trans.*, 1997, 1617.

2. T. N. Martynova and T. I. Chupakhina, *J. Organomet. Chem.*, 1988, **345**, 11.

3. F. J. Feher and K. D. Wyndham, *Chem. Commun.*, 1998, 323.

4. C. J. Hawker and J. M. J. Frechet, *J. Am. Chem. Soc.*, 1990, **112**, 7638.

5. C. Hawker and J. M. J. Frechet, *J. Chem. Soc., Chem. Commun.*, 1990, 1010.

6. K. L. Wooley, C. J. Hawker and J. M. J. Frechet, *J. Chem. Soc. Perkin Trans. 1*, 1991, 1059.